FOCUS ON MECHANICAL FAILURES:

MECHANISMS AND DETECTION

Proceedings of the 45th Meeting
of the
Mechanical Failures Prevention Group

Annapolis, Maryland

April 9-11, 1991

Compiled by
Henry C. Pusey
and
Sallie C. Pusey

A Publication of the

Vibration Institute

A NOT-FOR-PROFIT CORPORATION

Special Notice

TABLE OF CONTENTS

VALVE DIAGNOSTICS

SYSTEMS FAILURE ANALYSES - CASE HISTORIES

APPENDIX

PREFACE

The 45th Meeting of the Mechanical Failures Prevention Group(MFPG) was sponsored by the Office of Naval Research(ONR), the David Taylor Research Center(DTRC), the Naval Civil Engineering Laboratory (NCEL) and the Vibration Institute. The conference was held April 9-11, 1991 at the Holiday Inn Hotel and Conference Center in Annapolis, Maryland. Meeting management, program coordination, exhibit scheduling and proceedings compilation were by the Vibration Institute. A technical tour of selected facilities at DTRC, Annapolis was arranged by DTRC's **Christopher Nemarich**. MFPG Council Chairman, **Henry R. Hegner** of ECO, Inc. chaired an active 16-person Technical Program Planning Committee; a high quality selection of proposed papers and the Committee's hard work resulted in an excellent program. Henry R. Hegner chaired the Opening Session. Other session chairmen are identified on the section title pages in these proceedings.

It is appropriate to recognize four distinguished invited speakers whose papers do not appear in these proceedings. **Captain Clark Graham**, Commander of the David Taylor Research Center presented the Keynote Address. **Mr. Allan C. Brown** from the United Kingdom's Bristow Helicopter, Ltd. presented a paper on "*The Development to Production of an Integrated Health and Usage Monitoring System for Helicopters.*" Our first Plenary Speaker, **Mr. Henry K. Whitesel** of DTRC, discussed the applications of "*Fiber Optic Sensors for Shipboard Machinery Monitoring and Damage.*" The final Plenary Lecturer, **Senior Special Agent William A. Tobin**, explored the fascinating world of "*Forensic Metallurgy in the FBI.*" Special thanks are also due to **LCDR James Taylor** and **Dick Fairman** for organizing a panel session on Expert Systems Applications, and to **John S. Mitchell** of Bruel and Kjaer Instruments, Inc. for conducting a workshop on Predictive Maintenance.

The Mechanical Failures Prevention Group was organized in 1967 under the sponsorship of the Office of Naval Research to focus on mechanical failure technology. Improved reliability, greater safety and economic savings were among the obvious goals to be achieved through a better understanding of mechanical failures. The original objectives continue to form the basis for the activities of the current technical committees. These committees and their distinguished chairmen are as follows:

Detection, Diagnosis and Prognosis
Chairman: Dr. Howard A. Gaberson, Naval Civil Engineering Laboratory

Failure Mechanisms
Chairman: Dr. MarjorieAnne E. Natishan, David Taylor Research Center

Materials Durability Evaluation
Chairman: Dr. Sudhamay Basu, The Scientex Corporation

Machinery Durability
Chairman: Professor Reginald G. Mitchiner, Virginia Polytechnic Institute and State University

Those interested in working on any of these committees should contact the appropriate chairman. Your contributions will be most welcome.

As our society becomes more and more mechanized, as demands on performance become more exacting, and as our technology becomes increasingly complex, each mechanical failure reaches greater significance. In terms of the economy of the country, mechanical failures represent a cost of billions of dollars every year to industry, the government, and the general public. Improved public safety, an area of paramount concern, may be achieved by a higher

level of understanding of the mechanical failure process coupled with innovative techniques for failure avoidance, especially when using new or emerging materials in the design of structures and equipment.

The problems relating to mechanical failure prevention are complex and extensive. It is the goal of the Mechanical Failures Prevention Group to provide an effective mechanism for the coordination of efforts to apply our technological expertise to prevent, control, and avoid such failures. All MFPG conferences are planned with this goal in mind. On behalf of the Technical Program Planning Committee, I hope that this 45th Meeting has made a positive contribution to the achievement of this goal.

On behalf of Dr.Eshleman and the Vibration Institute, I want to thank our co-sponsors and the MFPG Council for inviting us to participate in the organization of the 45th MFPG Meeting. We fully expect that this series of conferences will continue to provide a common meeting ground for those who have mechanical failure problems and those who are engaged in failure avoidance technology.

Henry C. Pusey
General Chairman, MFPG '91

FEATURED PAPERS

Opening Session, Plenary

Chairman: Henry R. Hegner
ECO, Inc.

SAFETY ISSUES ARISING FROM THE METALLURGICAL INVESTIGATION INTO THE DC-10 AIRPLANE ENGINE FAN DISK SEPARATION SIOUX CITY, IOWA

James F. Wildey, II
National Transportation Safety Board
Washington, DC 20594

ABSTRACT: The separation of the engine fan disk was the result of a fatigue crack that initiated at a nitrogen-stabilized hard alpha defect in the bore of the disk. Details of the metallurgical examination will be discussed. Also, the quality assurance procedures associated with the production of titanium billets, issues concerning the design and certification criteria of engine components, and the adequacy of engine manufacturers' and airline operators' inspection programs and techniques will be addressed.

KEY WORDS: Damage tolerance; engine certification; fatigue cracking; fracture mechanics; hard alpha inclusions; human factors; inspections; titanium

BACKGROUND: On July, 19, 1989, a United Airlines McDonnell Douglas DC-10 airplane experienced an uncontained failure of the tail-mounted General Electric CF6-6 engine while cruising at 37,000 feet altitude. The separation, fragmentation, and forceful discharge of fan rotor parts from the forward section of the engine led to the loss of all three hydraulic systems that powered the airplane's flight controls. The flight crew experienced severe difficulties controlling the airplane and were able to maintain only partial control by manipulating the thrust settings for the two wing-mounted engines, which continued to operate normally throughout the accident sequence. Although the airplane was capable of flying in this manner, there was insufficient control to allow for a successful runway landing. As a result, the airplane crashed during an emergency landing at the Sioux Gateway Airport, Sioux City, Iowa. Of the 296 people on the airplane, 112 were fatally injured.

During reconstruction of the airplane and engine after the accident, it was apparent that the fan disk had burst apart, sending shrapnel-like pieces of the fan blades into the horizontal stabilizer, where hydraulic lines to the control surfaces in the tail were severed. Figure 1 shows a cut-away view of the CF6-6 engine, with a dashed line around the components lost in flight. Pieces of the fan disk from the forward section of the failed engine were not recovered from the Iowa corn fields until mid-October, about 3 months after the accident. Initial examination of the fan disk revealed that its separation was a result of a fatigue crack.

As a result its investigation of this accident, the National Transportation Safety Board determined that the probable cause of the accident was:

[T]he inadequate consideration given to human factors limitations in the inspection and quality control procedures used by United Airlines' engine overhaul facility which resulted in the failure to detect a fatigue crack originating from a previously undetected metallurgical defect located in a critical area of the stage 1 fan disk that was manufactured by General Electric Aircraft Engines. The subsequent catastrophic disintegration of the disk resulted in the liberation of debris in a pattern of distribution and with energy levels that exceeded the level of protection provided by design features of the hydraulic systems that operate the DC-10's flight controls.

LOADING OF THE FAN DISK: The fan disk from the CF6-6 engine is the largest rotating engine component, weighing 370 pounds, and having a diameter of 32 inches. Figure 2 shows a cross section through one side of the disk and the adjacent engine components. The rim of the disk holds 38 fan blades, each about 28 inches in length. The overall diameter of the fan rotor assembly (disk and blades) is a little over 7 feet. The total assembly weighs over 800 pounds and rotates at a maximum of about 3,500 RPM.

The primary loads on the stage 1 fan disk are radial outboard loads in the dovetail slots. These loads arise from the disk holding the fan blades against centrifugal forces during rotation of the assembly. The radial loading imposed by the fan blades results in radial stresses in the disk rim and circumferential (hoop) loading that is maximum at the forward corner of the bore inside diameter surface.

EXAMINATION OF THE DISK: The disk contained two principal fracture paths which resulted in about one third of the rim separating from the remainder of the disk. One of the fracture areas progressed largely circumferentially through the web, and the other was on a near-radial plane, progressing through the bore, web, disk arm, and rim. The near-radial fracture is approximated by the cross-hatched region shown in figure 2. Features on the circumferential fracture were typical of an overstress separation stemming from multiple origin areas in the radius between the disk arm and the web. The near-radial fracture also contained overstress features over most of its surface. However, on this break the overstress features stemmed from a preexisting fatigue crack region in the bore of the disk.

Fractographic, metallographic, and chemical analysis examinations of the fatigue region revealed that the fatigue crack initiated from a metallurgical anomaly that was located on the inside diameter surface of the bore approximately in the center of the fatigue region, 0.86 inch from the forward corner of the bore. The core of the defect contained only alpha phase (as opposed to the 50-50 mixture of alpha and transformed beta phases expected for normal microstructure) with an elevated hardness level and excessive nitrogen. A defect of this type is referred to as a nitrogen-stabilized, hard alpha inclusion, since the nitrogen stabilizes the alpha phase and causes the increase in hardness. Enriched alpha microstructure (with greater than 50% alpha phase) associated with the defect extended significantly beyond

the area containing only stabilized alpha structure, gradually blending into the normal microstructure.

A portion of the fatigue crack surface around the origin area was slightly discolored, even after extensive cleaning. The fractographic examination revealed that there was no abrupt change in the topography at the boundary of the discolored region that would account for the apparent difference in color. A later section of this paper contains a discussion of the probable mechanism that created this discoloration.

The total number of fatigue striations was estimated using scanning electron microscopy. This analysis established that fatigue cracking started very early in the life of the disk.

ULTRASONIC, MACROETCH, AND EDDY CURRENT INSPECTIONS: During the original manufacturing process for the separated fan disk, General Electric performed an immersion ultrasonic inspection and a surface macroetch inspection of the part while it was in an intermediate machined shape. Neither of these inspections resulted in rejection of the disk.

An ultrasonic inspection is capable of detecting subsurface defects such as cracks or voids. However, hard alpha structure is not readily detectable with ultrasonic means unless, as is often the case, it is associated with cracking or voids. For the accident disk, the fact that the defect (subsurface at the time of the ultrasonic inspection) was not detected suggests that there were insufficient cracks or voids in the defect to reject the part. After the Sioux City accident, General Electric developed intricate contact and immersion ultrasonic inspection programs that were used to inspect the disks in the remaining CF6-6 engine fleet. These inspection programs were quickly implemented and revealed that several additional disks contained hard alpha defects. However, the defects in these disks were in locations where the stress levels, combined with the size of the defects, did not generate cracking that extended outside of the defect area. Hard alpha has a very low fracture toughness and tends to crack under relatively minor loads.

The Safety Board believed that the ultrasonic inspections of in-service fan disks were necessary and were the proper inspections for the detection of subsurface defects. However, because the ultrasonic inspections could not detect small but potentially critical surface cracks in the forward corner of the inside diameter surface of the bore, the Safety Board recommended that an alternate inspection method be developed and required for this area. General Electric developed an eddy current inspection of the bore that met the Safety Board's concern. The eddy current inspection became a part of the maintenance manual for the CF6-6 engine, and, as explained in the next section, is required to be performed every time the fan disk is separated from the fan section for any reason.

The other inspection performed on the intermediate shape of the disk during original manufacturing was a macroetch inspection. This inspection is designed to detect surface material defects such as

hard alpha, segregation, and overheated areas. In the area of the inside diameter surface of the bore, there was only 0.15 inch between the etched surface of the intermediate shape and the final shape of the disk. It is likely that the altered microstructure associated with the core of the defect extended primarily in the direction of the forging grain flow, which is parallel to the surface at the defect location. If this is true, there may have been no rejectable microstructure on the etched surface.

However, the Safety Board concluded that the hard alpha defect would have been detectable if the final shape of the disk had been macroetch inspected. For this reason, the Board recommended that manufacturers be required to perform a surface macroetch inspection of the final shape of all critical titanium alloy engine components.

FLUORESCENT PENETRANT INSPECTIONS OF THE SEPARATED DISK: The General Electric maintenance manual for the CF6-6 engine suggests that detailed inspections be performed on the fan disk from one of these engines every time the disk is disassembled from the fan module for any reason. This manual, with slight modification, was incorporated into the United Airlines, FAA-approved, maintenance program, thereby making the GE-recommended inspection criteria mandatory. During its life, the accident disk was disassembled from the fan module a total of six times. The primary inspection performed by United during each of these shop visits was a fluorescent penetrant inspection (FPI).

The last time that the accident disk was separated from the fan module was only 760 cycles before the accident. The FPI inspection performed by United at this time did not detect any defects in the disk, which was then returned to operation as serviceable. In attempting to determine the size of the crack at the time of this inspection, it was suggested that the discolored portion of the fatigue crack was created during an alkaline cleaning that the United process specifications require for the disk in preparation for the FPI inspection. This alkaline cleaning removes possible foreign material and enhances the detectability of cracks. Because there was no topographic reason for the discoloration, and because are no operational environments or conditions that could create such a discoloration, it was reasonable to conclude that the discoloration marked the size of the crack at the time of the most recent inspection before the accident.

Fracture mechanics evaluations of the disk were also performed by General Electric and United, using various mechanical properties data, surface correction factors, and loading spectra. The evaluation judged most realistic by the Safety Board indicated that the surface length of the crack at the time of the inspection 760 cycles before the accident was 0.498 inch, very close to the actual surface length of the discolored area (0.472 inch).

In searching for a reason to explain how an inspector could miss a crack of this size, many avenues were explored. The design and operation of the disk do not give rise to bulk residual compressive stresses that could physically close a crack and make it undetectable. Nor should the presence of shot peening (if done prior

to cracking) significantly reduce the probability of detection of a crack of this size. Fluorescent penetrant inspection has long been a standard industry inspection for a wide variety of components, including shot peened titanium components. For these reasons, the Safety Board concluded that the failure to detect the crack was not a result of the technical limitations of the inspection process. However, the investigation disclosed that the FPI inspection of the disk, like any manual inspection process, is far from foolproof.

INSPECTION LIMITATIONS: All inspection processes have both technical and human factors limitations. Even under ideal circumstances, there will be flaws in a component that are small enough to avoid detection with any given inspection method. For flaws larger than this minimum detectable size, it is possible to develop probability of detection information for each flaw size.

In order to maximize the probability that a detectable defect is actually detected, a large variety of factors must be controlled during the inspection process. For example, during an FPI inspection, each of the many processing steps must be performed correctly in order to assure the most accurate inspection. The various inspection materials must be kept within cleanliness limits and changed when required. Inspection equipment must be properly calibrated and kept in good repair. The inspection area needs to be clean and well lit. And procedural documentation must ensure that process control is maintained.

For inspection of the CF6-6 engine fan disk, additional problems are caused by the size and weight of the component. During the FPI inspection of a disk, it is suspended by a sheathed cable. The cable passes through the disk's center hole and presses against the bore. During application of the fluorescent penetrant solution, the disk needs to be manually rotated to allow the penetrant to have access to the area previously covered by the sheath. The disk should be similarly rotated as the excess penetrant fluid is washed from the disk and again when the developer powder is applied after drying. As the disk is inspected for indications, the inspector must ensure that all areas of the disk are examined in great detail.

Also inherent in any inspection are human factors limitations that should be considered. If the inspector is not well rested or is not motivated to find defects, the probability of detection can be degraded. Also, a difficult vigilance problem arises if certain components or certain portions of components are never found to contain a defect indication. It is a natural tendency for an inspector to pay more attention to components or portions of components that have had histories of indications and less attention to those with no previous indications. In the case of the separated CF6-6 engine fan disk, the fatigue crack was located on the inside surface of the disk bore, an area that had never before been found to contain a crack. In addition, each disk usually contains a large number of indications associated with the wear coatings in the dovetail slots at the rim of the disk. Under these conditions, it is possible that an inspector's attention could be diverted away from the bore area and toward the rim area.

As a result of the findings regarding the potential problems associated with nondestructive inspections, the Safety Board recommended that the Federal Aviation Administration:

> Intensify research in the nondestructive inspection field to identify emerging technologies that can serve to simplify, automate, or otherwise improve the reliability of the inspection process. Such research should encourage the development and implementation of redundant ("second set of eyes") inspection oversight for critical part inspections, such as for engine rotating components.

CERTIFICATION REQUIREMENTS FOR ENGINE COMPONENTS: The fact that a critical, high-energy, engine component catastrophically ruptured before reaching its life limit raised questions concerning the methods used to certificate engine components. The process of certificating engine components has changed little since the late 1960's, when the CF6-6 engine components were approved for operation. The engine manufacturer develops component designs, uses analytical methods (supported by limited testing) to determine stress levels, and, applying the expected load spectrum, calculates a fatigue life to the initiation of a detectable fatigue crack using inferior fatigue properties for the component material. The FAA sets the life limit for the component at one third of the manufacturer's calculated life to initiation, thereby providing an additional safety margin. As service time on a component accumulates, the FAA can extend or reduce the life limit, based on additional information such as recalculations of the stress levels, failure history, and operating experience.

For the CF6-6 engine fan disk, the calculated life to initiation of a fatigue crack was 54,000 cycles. Therefore, the FAA assigned a life limit of one third of this value, 18,000 cycles. The disk involved in the Sioux City accident separated after reaching 15,503 cycles.

One of the assumptions underlying the current engine component certification process is that the component material, after passing the various manufacturing inspections, is free of defects that would significantly reduce the fatigue properties of the part. Because of this assumption, there are no specific intervals during which engine components must be inspected. However, the separation of the disk involved in the Sioux City accident shows that this assumption is not always correct. To date, manufacturers have considered in-service inspections of commercial engines at specific intervals as unnecessary and overly burdensome, citing the current inspection programs as giving an adequate margin of safety. Instead, they are continually working to reduce the probability that a component could pass the manufacturing inspections and still contain a significant defect.

The separated fan disk was made from Ti-6Al-4V, a titanium alloy containing 6% aluminum and 4% vanadium. As processing of titanium has developed, more and more process requirements have been added to eliminate as many potential sources of problems as is possible. For example, when titanium material for the separated disk was produced

in 1970, process specifications required double vacuum melting of the titanium ingot and contact ultrasonic inspection of the billet. Recycled material was allowed. The current process specifications require triple vacuum melting and an immersion ultrasonic inspection of the billet. Recycled material cannot be used, and a large number of welding and cleanliness controls have been added. Also, manufacturers are considering changing the melting process to an electron beam or plasma arc hearth melting procedure (plus a vacuum arc melting step) in order to allow further opportunity for defects such as hard alpha anomalies to dissolve into the molten pool.

DAMAGE TOLERANCE FOR ENGINES: Because it is not possible for the manufacturing process to give complete assurance that components are defect free, engine manufacturers have been investigating the possibility that engine components could be inspected at specific hard intervals during their life so as to ensure that an undetected defect does not cause a failure. The method used to develop these hard inspections limits is referred to as damage tolerance. Since about 1978, the structure of all major jet transport airplanes has been maintained and inspected under the damage tolerance philosophy. Also, some military engines are purchased and maintained under a program that incorporates many aspects of the damage tolerance philosophy.

Using the damage tolerance method of determining inspection intervals involves several steps. First, an inspection method is chosen, and the maximum undetectable defect size for the inspection method is determined. Next, the stress level in critical areas of the component is generated, along with the anticipated load spectrum for the component. Then, it is assumed that the largest undetectable defect actually exists in the component, and a fracture mechanics evaluation is performed to estimate the number of stress cycles required to fail the part under the anticipated load spectrum. Finally, the number of cycles to failure is divided by two and the component is inspected at that interval to ensure two opportunities to detect a fatigue crack growing from the defect. If the inspection frequency is unacceptably high, a more sensitive inspection method can be used, or the chosen method can be improved in order to detect a smaller defect.

The Safety Board has recommended to the Federal Aviation Administration that steps be taken to try to extend the safety benefits afforded by damage tolerance inspections to the critical components in transport airplane jet engines. However, we at the Safety Board recognize that if damage tolerance inspections were required tomorrow for critical engine components, the inspection methods currently available would necessitate inspections at such frequent intervals that there would be a huge economic burden. Large numbers of engines would not be able to be used because of insufficient inspection capacity. In order for damage tolerance to be applied to engine components, inspection methods that detect smaller defects with a much higher degree of reliability should be developed. In most currently available inspection methods, a wide variability in detection arises from the human factors problems associated with the inspection. Research into individual inspection

problems has shown that while automated inspection systems do not always detect defects as small as those detected by a human inspector, the reliability of an automated system can be significantly better at detecting larger defects. Therefore, the greatest improvements in the near future may come from the development of automated inspection systems for a wider variety of components.

CONCLUSION: The type of fan disk separation involved in the Sioux City accident is extremely rare, and air travel remains one of the safest modes of transportation. However, improvements in maintenance practices and inspection procedures should further reduce the likelihood of such an event happening again. Furthermore, it is hoped that hydraulic control system design improvements, brought about as a result of the Sioux City accident, will make future airplanes less susceptible to crippling damage in the event that a similar separation does occur.

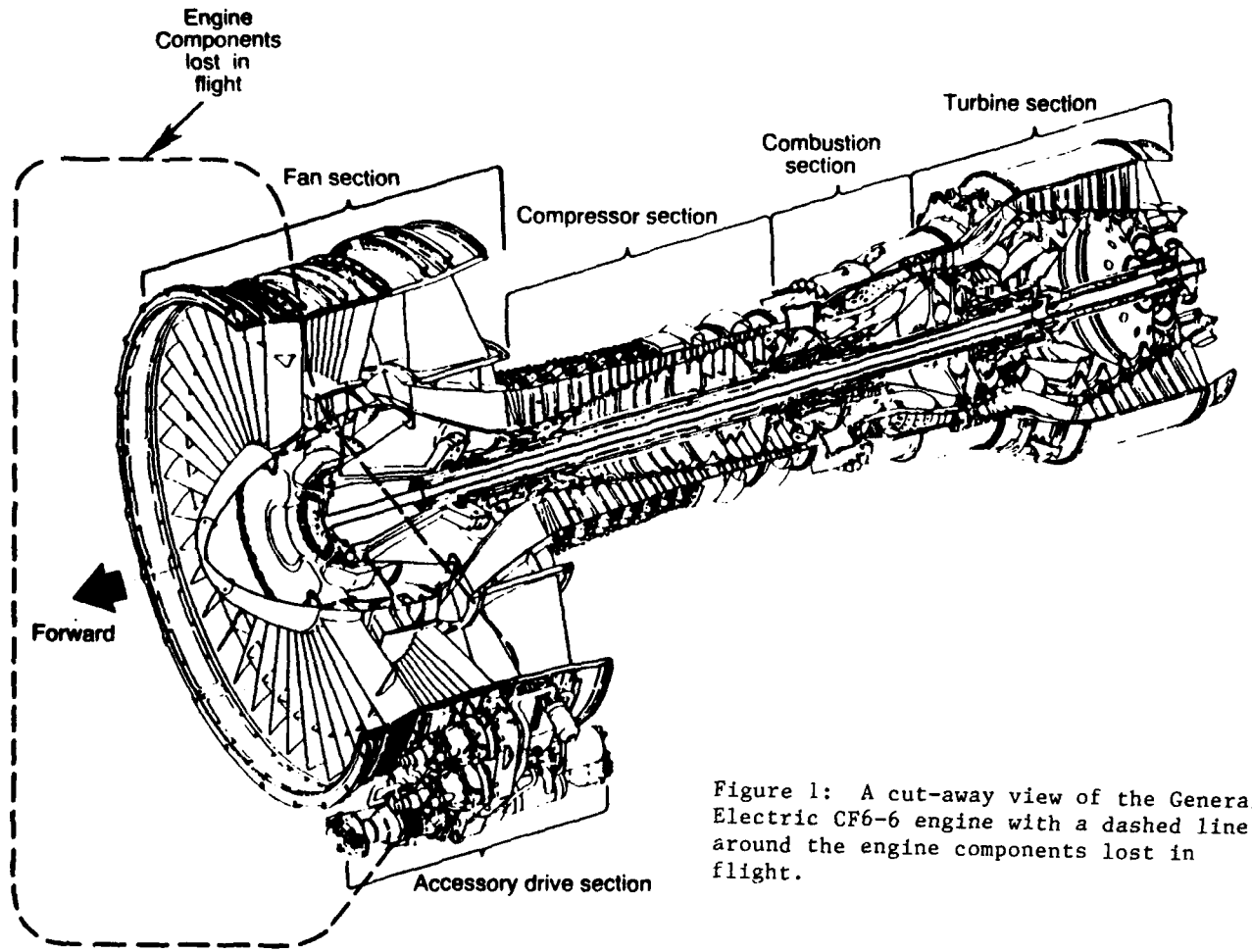

Figure 1: A cut-away view of the General Electric CF6-6 engine with a dashed line around the engine components lost in flight.

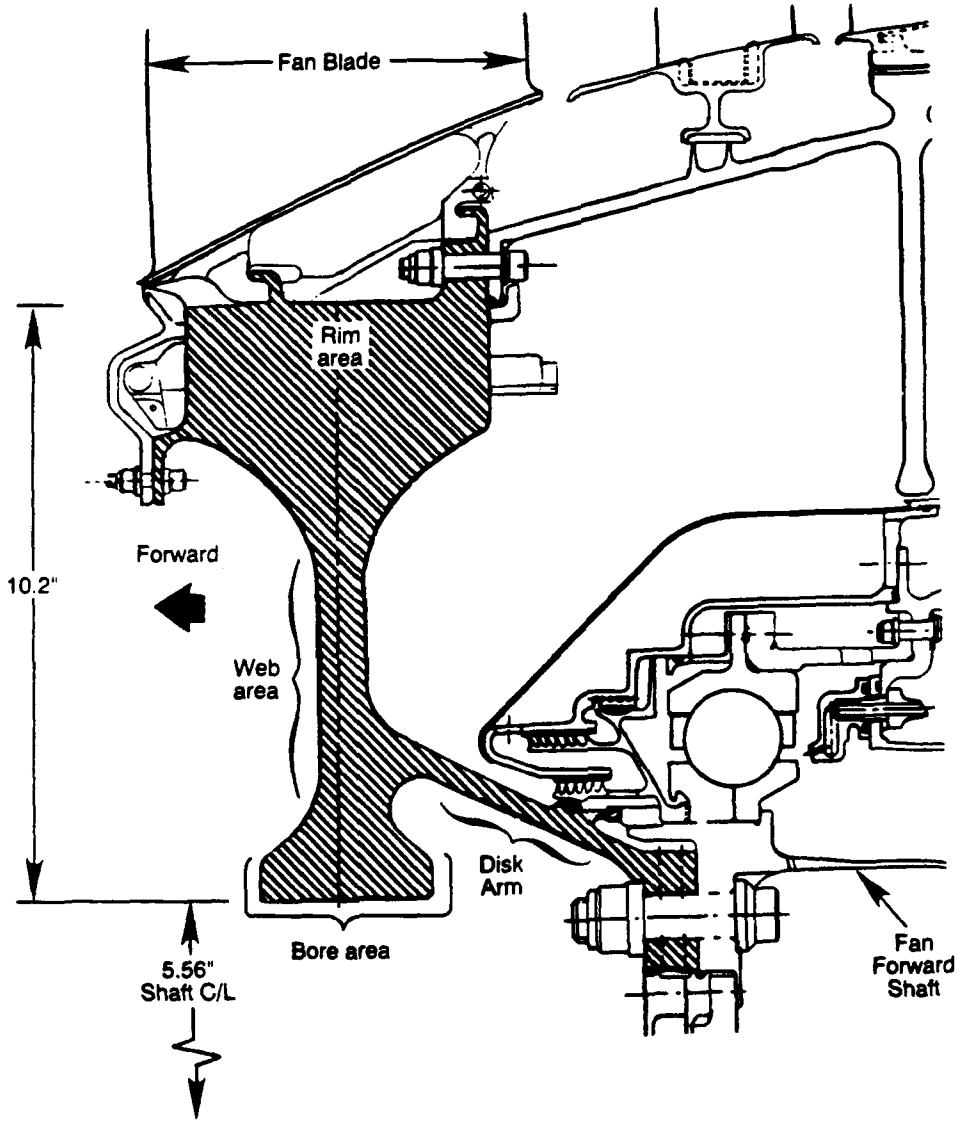

Figure 2: Cross section through one side of the fan disk (cross hatched component) and adjacent engine components.

CONDITION BASED MAINTENANCE IN THE ROYAL NAVY

Commander William N Watson Royal Navy
Ministry of Defence
DGME/ME433
Room 5 Block B
Foxhill
Bath BA1 5AB
England

Abstract: The Royal Navy introduced a policy of Maintenance by Condition into its Surface Fleet in 1980 and subsequently into the Submarine Flotilla. The aim of this paper is to examine the progress over the years since the introduction of this policy, to describe the various trials carried out and underway, and finally to suggest the possible way ahead. It will list, and describe briefly some of the more significant projects being undertaken by the various specialist sections. It will look at the new techniques being considered for future use and development, and at the way in which they can be integrated into a comprehensive maintenance management system. Finally it will consider the probable cost savings and potential cost effectiveness of condition based maintenance and condition monitoring.

Key Words: Condition based maintenance; Condition monitoring; Cost effectiveness; Diesels; Gas turbines; Maintenance management systems; Marine propulsion equipment; Royal Navy; Warships.

INTRODUCTION: The subject of condition based maintenance is one which is receiving a great deal of attention throughout all branches of engineering in the Royal Navy. It is seen by Headquarters as offering significant savings in manpower and maintenance costs. This interest at high level has led to the establishment of a Condition Based Maintenance and Condition Monitoring Cell within Director General Marine Engineering's (DGME) organisation. This cell acts as the focal point for condition based maintenance and the choice and development of condition monitoring techniques throughout the Sea Systems Controllerate covering all areas including weapon systems. In all areas of Marine Engineering design techniques for condition monitoring, and its close relation engine health monitoring, are under active development.

The Royal Navy had for many years been among the World leaders in the design and use of Preventative Maintenance when in 1980 it declared that its maintenance policy was to be "Maintenance by Condition". This decision was based on the belief that availability would be increased through the reduction in programmed alongside maintenance periods. Cost savings would be achieved by the reduction of manpower and material intensive maintenance routines on healthy equipment. The policy would be based on the following principles:

a. The maximum use of condition based maintenance

b. Critical examination of maintenance requirements against operational requirements

c. Overhaul and repair action was to be taken at the lowest sensible level

Each equipment was to be maintained according to one of three categories:

a. Time and occasion - where legal, defect history or access considerations determine it should remain as Preventative Maintenance

b. Monitored Wear-out - those equipments where condition monitoring is achievable and practical

c. Natural Wear-out - those less important, less expensive, equipments which can be allowed to run to failure.

The condition monitoring which was introduced as a result of this new policy relied mainly on vibration analysis with only limited use of other techniques. Unfortunately the Engineer was not given adequate instrumentation to determine the condition of his machinery. That which was supplied was manpower intensive, inaccurate and gave little perceived gain - hence its relegation to the back of the Engine Room cupboard. Nor was the Engineer able to feel confident that a failure following his professionally considered decision to omit or postpone a maintenance routine would be understood by an Authority who did not appreciate the nuances of the new policy. Hence Preventative Maintenance remained in use in its pre-condition monitoring form. By 1983 it was clear that the policy was not working and a committee (the Naval Equipment Condition Monitoring Committee (NECMC)) was formed, consisting of senior representatives of MOD Headquarters, Design staffs, Operating Authorities, Research Establishments etc, in an attempt to put more drive and purpose into the introduction of the policy into the present and future Fleet. The result of the studies instituted by this committee led to the introduction into the Fleet of improved monitoring equipment. In conjunction with this came the start of the principle on which all todays work is based - that of putting the ability to determine the true condition of his machinery into the hands of the ship's Engineer Officer and in reducing his reliance on shore based specialist teams such as the Fleet Vibration Analysis Unit (FVAU), the Fleet Gas Turbine Team or the Fleet Diesel Team.

The improved monitoring equipment, which was introduced by the NECMC in the mid 1980's, has allowed Commander in Chief Fleet's Engineering Staff, as the Maintenance Authority, to develop new procedures for the routine collection and analysis of vibration data by the Ship's Staff. The FVAU, which has sections in each major base, is responsible for the overall supervision of the vibration monitoring programme throughout the Fleet. Every ship and submarine carries a number of hand-held analogue overall vibration meters and a portable spectral analyser together with a technician trained in its use and in vibration analysis. As each ship is either accepted into service or completes a refit documentation is supplied by the FVAU which specifies which equipments are to be monitored and at what periodicity, the specified

measuring points for each machine, the alert and alarm limits of overall vibration and the action to be taken should those limits be exceeded. The FVAU carry out a full analysis of all machinery to determine its condition and to set baseline overall vibration levels before handing the operation of the system to the ship. Ship's Staff take overall vibration readings, and in some cases process parameters, on each machine at regular intervals, usually monthly, and record them manually on a trend graph. If the prescribed limits are exceeded the vibration specialist is informed and he will then carry out a full spectral analysis to establish the severity of the fault and to determine the maintenance action required or the revision of the monitoring procedure that may be necessary. Should the onboard specialist not be able to resolve the problem he will call upon the services of the FVAU who have more sophisticated equipment and a deeper specialist knowledge. The Engineer Officer is thus able to base some of his maintenance decisions on condition monitoring information. However the system is clearly more manpower intensive than is desirable and would lend itself to computerisation.

The NECMC also introduced a number of trials in an attempt to speed up the introduction of the policy and to increase confidence in its effectiveness Fleetwide.

The major trial, **the Condition Monitoring Trial**, which was set up with the objectives of assessing the ability of condition monitoring techniques to predict failure of engineering systems and to evaluate the potential for cost savings over a period of three years, has recently completed its report stage.

This trial was carried out on four submarines and three surface ships and used hand held electronic data collectors to gather data - principally vibration but also some process parameters - from a limited number of equipments. This data was used in conjunction with computer programs which allowed the onset of faults to be detected, their progress to be trended, and thus time to failure to be predicted. The data was collected at regular intervals and sent to an engineering consultancy, YARD in Glasgow, where it was analysed and the ships informed of their findings. At the same time Engineer Officers were encouraged to use the data for their own assessment before sending it off and most did. YARD also produced a global data base and analysed the overall performance of the equipment prior to commencing the report write-up. A number of successful predictions were made, cost benefits were obtained and the aims of the trial achieved.

The Submariners were so impressed with the results of the trial that they commissioned a survey, to a closely defined user requirement, of all available data collectors and software with the aim of determining the best package for RN use. The selected equipment is now being used to extend the CM Trial in a further five Submarines. Although the condition monitoring available is limited, in the main, to vibration analysis there is a clear commitment to replace preventative maintenance with condition based maintenance where at all possible and the Maintenance Management System is being progressively modified following properly constituted engineering audits.

The ships and submarines involved in the earlier trial have retained their trials fit, albeit less capable than todays more sophisticated equipment, and the scope of their data collection has been extended, with all data now being retained and analysed onboard. There is only limited support being provided by the Shore Authorities in both the new trials and Ship's Staff are expected to make their own decisions as to the condition of their machinery and to undertake maintenance accordingly.

The Infra-red Trial arose out of the CM Trial and consists of surveying the electrical equipment of a ship with a hand held Infra-red camera at regular intervals. The intention was to trend the results but this proved to be impractical for a number of reasons - not least the weight and complexity of the camera. However it was shown that the procedure was of value as a fault detection process and would lead to greatly increased electrical safety if properly used. Despite the advantages demonstrated it was felt that the technique did not at present lend itself to use by ship's staff and should be limited to use by a shore support team on an opportunity basis. Further trials using a much smaller, lighter British made camera with some novel coincident natural picture recording capabilities are to be carried out in the near future and these may lead to more regular shipboard use of this technique.

The Watchkeeping data trial now running in two ships is probably one of our most successful to date. In it the paper based watchkeeping data system is replaced by electronic data gatherers and computers. The data is collected on a modified Psion data gatherer to a predetermined route and uploaded to a PC in the machinery control room. The Chief of the Watch is automatically informed of any readings which are in alert or alarm. He can then trend these parameters over the last 48 hours and can, if he wishes, compare them simultaneously and graphically with a predetermined list of up to five other parameters which have been selected as giving the best indication of the health of the given machine. Every 24 hours the days readings are transferred to an administrative PC, compressed to one typical figure for the day and stored for long term trending. All reports such as the machinery status reports, fuel reports etc are capable of automatic generation. Algorithms are being developed using the watchkeeping data which will automatically create and trend new parameters indicative of a machines performance - both for short-term and long-term use. The trial is being enhanced by the electronic collection of vibration data which will be compared with the long term trended data provided by the watchkeeping parameters. It is the intention to install the system in all Type 42 Destroyers starting in early 1991. This, together with Closed Circuit Television, is expected to reduce the watchkeeping workload to such an extent that it will generate a saving of two mechanics from the ships' complement.

RESEARCH AND DEVELOPMENT: In the specialist equipment sections a large amount of work has been carried out on devising ways of determining the condition of major equipments. Much of this work has been aimed at engine health monitoring which is closely related to condition monitoring and has a read across in many cases.

Diesels: The development of condition monitoring in diesels is a rapidly expanding subject. The majority of the research is also being

carried out at the Marine Engines Section, Royal Aircraft Establishment, Pyestock (RAE) although a significant amount has been undertaken by the Fleet Vibration Analysis Unit and the Fleet Diesel Team - particularly with regard to Torsional Vibration Analysis. Some of the techniques under review are:

Vibration Analysis: The FVAU surveys combined with ship's staff Vibration Monitoring records are proving valuable tools despite the difficulties inherent in a reciprocating engine. Defects are being detected early enough to enable corrective action to be taken. Torsional vibration techniques are proving their worth as is damper fluid sampling. Research is being carried out into the use of laser doppler vibrometers for the determination of torsional vibration and for some of the linear vibration recording such as that connected with injector/cylinder condition. There is a great deal to be gained from these techniques but the complex analysis required will preclude their introduction to the Fleet for some time.

Lubricating Oil Sampling: Improved test kits using modern technology have been introduced with the aim of limiting oil changes to condition or major overhaul only.

Injector Performance: Devices for determining injector performance externally are becoming available and trials are being carried out to determine their worth.

Blowby Meters: A Cusson's Blowby meter has been successfully proved at RAE and a trial at sea is being undertaken to determine the operating parameters associated with the meter.

System Identification and Related Techniques: Changes in engine condition tend to have a greater influence on the transient response of parameters than on their steady state values. If it were possible, therefore, to plot the response of a given set of parameters during a given change in load, then any variation in the shape of that plot in subsequent load changes must indicate a change in condition of the engine. Research by RAE in conjunction with Cambridge Consultants Ltd modelled the response of an engine using System Identification to determine transfer functions of selected sub-processes and pattern recognition techniques to detect change in condition and identify faults. Initial studies used computer simultations of a diesel engine to show the feasibility of this approach and it was subsequently confirmed on a small diesel engine. The technique is directly transferable to gas turbines and studies are now underway on the Spey.

Turbocharger Performance: Trials to date, using run-down times, have provided little evidence of condition, reducing performance or impending failure. However, engineering commonsense suggests that the performance of such a vital part of the engine should give some indication of condition. Experience with System Identification (see above) suggests that the analysis of transients should provide the necessary information using combinations of input/output conditions (temperature, pressure and speed). Trials are being undertaken at RAE.

Engine Condition Monitoring System: This system determines the condition of the in-cylinder components using inferred cylinder

pressure diagram analysis. A computer program derives the cylinder pressure using data from strain gauged bolts and washers and is also capable of monitoring other parameters. The object is to provide a computerised system which monitors parameters and compares them with baseline models. The sensitivity to small changes in certain parameters is detected by a computerised databank containing a complex map of acceptable conditions. The system is presently being validated on Valenta and Ventura engines at Pyestock. It will shortly be combined with DEIMOS, an AI Knowledge Based condition monitoring and fault diagnosis system the development of which is being funded by a consortium from Industry and the Royal Navy, which will analyse the out-of-tolerance parameters and provide a diagnosis of fault condition to the operator.

Consumption Monitoring: The accurate determination of fuel and oil usage trends can give a good indication of engine condition. A number of devices capable of monitoring oil usage are being investigated.

Gas Turbines: A substantial amount of engine health and condition monitoring is already carried out on propulsion gas turbines and has been instrumental in producing a significant extension in engine life between overhauls. Performance monitoring is carried out at regular intervals. Run down times are recorded and trended. Magnetic plugs are inspected and the debris analysed, quantified and trended leading to full SOAP procedures if necessary. Periodic internal optical inspections using flexible endoscopes are undertaken by ships' staff with more detailed inspections being undertaken by the Fleet Gas Turbine Team to determine life remaining.

The development of condition monitoring techniques for gas turbines is a fast moving and ever increasing area of activity. The majority of the research is being carried out by the Marine Engines Section, RAE Pyestock, in conjunction with the Rolls Royce Spey development programme:

Gas Path Analysis: This involves the detection of debris in the gas stream using electrostatic probes to monitor the health of the gas path. Results to date on the Exhaust Debris Monitoring System have been very encouraging and the trial is continuing. A trial has recently commenced of an Intake Debris Monitoring System to assess the level of debris ingested by engines in service. The technique measures the changes in the electrostatic charges held by particles in the gas stream, either as "events" or as a continuous change in signal level. Trials have shown that a number of possible faults each exhibit a particular "event" pattern, some of these faults are:

Blade seal rubs
Hot gas/carbon erosion of HP blades and Inlet Guide Vanes
Erosion by ingested debris (particularly when linked to Intake Debris Monitoring)
Corrosion by ingested salts, and sulphur and vanadium within fuel
Combustion/combustor faults
Spalling of Combustor/blade/vane coatings
Blade failures
Changes in engine performance

An outline specification for an on-line monitor is being produced. It is considered that this technique has much potential.

Vibration Analysis: RAE, working in conjunction with Naval Air Materials Laboratory, Fleetlands, has tailored the advanced vibration analysis package developed by Messrs Stuart Hughes Ltd to model the Spey engine. The engine is monitored by seven accelerometers and the tape recorded data is analysed regularly using advanced signal processing techniques. The onset of bearing, gearing and blade problems can be detected and monitored - allowing time to engine removal to be predicted. A bearing defect was detected early in the last series of engine trials and was monitored throughout. The fact that it showed only a very gradual deterioration allowed the trial to continue with confidence.

Visual Techniques: Optical inspection programmes for the Spey on trial have been developed using a miniaturised video camera at the end of a flexible probe which generates a high quality image for display on a monitor or for video recording. The image can be digitised and printed as hard copy. Images can be compared at intervals and measurements recorded thus providing trend information for, say, crack propagation or corrosion/erosion.

On-line Oil Debris Monitors: Two on-line debris monitors are being trialled. This technique determines the onset and progress of bearing and gearing defects by measuring the particulate contamination of the oil return. This work is also pertinent to, and being trialled on, Diesels. Regrettably little success has yet been achieved.

System Identification and Related Techniques: This technique, which has been carried over from diesel research work, has much potential and a number of studies have been included in the Spey development programme.

Machinery Management: The integration of data from many sources, both on and off-line, is necessary to detect changes in engine condition and to diagnose faults. At present this is done infrequently and using manual methods. RAE is attempting to determine the various combinations of parameters required for given faults, to develop the necessary algorithms and to achieve the necessary integration and analysis using computerised methods. An Expert System shell has been configured to demonstrate its potential as a fault diagnosis tool. Initial results are promising. Artificial Intelligence techniques being developed for diesels (eg DEIMOS) have potential applications in this field for gas turbines.

Other Equipments and Techniques: Condition monitoring techniques are now kept constantly under review and co-ordinated across the whole of the SSC by the specialist group. New equipments and procedures are being developed at a rate with which it is difficult to keep up. Engineering designers, equipment manufacturers, and universities are constantly searching for new methods to develop, either in new fields or to enhance existing practices. The Royal Navy is about to investigate a number of these with the intention of including them in the range of techniques in Service use, concentrating initially on

those which can be used by the ship's staff in the course of their normal work. Some of the techniques under consideration are:

Oil Analysis: This will play a more effective and comprehensive role in the future. Ferrography, Fourier Transform Infra-red and on-line debris monitoring, in conjunction with an expanded SOAP programme will offer a wealth of information to the Engineer Officer as well as improving the management of oil products.

Electrical Monitoring: Until recently this has been limited to process parameters, automatic test equipment (fault finding) and performance. A number of techniques are becoming available in commercial form, of which Current Monitoring shows the most promise and is being trialled. Axial flux analysis, cooling gas analysis, and speed fluctuation analysis together with vibration analysis techniques are under active research and development fuelled by the increased industrial use of robots. These techniques will also allow the expansion of condition monitoring into the weapon engineering field in which its use has been limited.

Acoustic Emission: Until recently this had been limited by the cost and complexity of its sensors and the interpretation of its signals to the realms of non-destructive testing. Research into its use in Gas Turbines has led to the development of cheap and simple sensors and we currently have a number under evaluation in RNEC Manadon. Trials of its ability to detect the early onset of cavitation in large volume low pressure pumps is underway at the Admiralty Research Establishment Haslar. It would appear that the technique has much potential and we hope to commence trials at sea in the near future.

Performance Monitoring: In addition to the work being carried out in the Watchkeeping Trial we are intending to develop computer models of major equipments in which actual performance can be trended against predicted to give condition. Models for Diesels and Gas Turbines are well advanced and others are in the pipeline. This technique is dependent on the early development of cheap accurate and reliable sensors. Some simple efficiency monitoring systems for pumps are now available and are about to be tested.

Expert Systems: Condition monitoring is an ideal subject for incorporation into expert systems. DEIMOS for diesels has already been mentioned and commercial vibration analysis programs such as AMETHYST are now available. Other techniques will not be far behind. The drive to put the best information into the hands of the Engineer Officer makes it essential that we keep this area under close review.

AREAS REQUIRING FURTHER RESEARCH: In addition to the techniques and procedures described above there are a number of areas which require further research and development before true condition monitoring can be introduced or the before the full benefits of the system can be achieved:

Prediction of Time to Failure: As more information is acquired on failure patterns for given equipments we will be able to move away from the predominately straight line prediction methods currently in use and over to the real (exponential!) world. This, in conjunction with the

evolution of computer models, will lead to increased confidence in the system and, in the long term, improved expert systems.

Data Reduction: In earlier times the procedure was to collect as much data as possible and then try and decide what it was telling you. Besides being wasteful of effort the sheer volume of data required to produce meaningful results in the complex environment of a warship quickly overloads data filing systems and excessively complicates the procedures for determining condition. This is exacerbated by the increase in techniques in use today, despite major effort to reduce the number of parameters required to describe a fault condition. There exists a need to develop techniques which will reduce the amount of data retained within the database while not losing any which is of value, to avoid overload and to enable the system to run at a reasonable speed.

Confidence: Whilst it is easy for an Engineer Officer to accept that a fault exists if his monitors tell him so, he is not so easy to convince if, just prior to an important mission, they tell him that all is well on a plant with a known poor reliability. This incredulity increases exponentially with the importance of the task. As a result he is prone to revert to Preventative Maintenance on sensitive equipment in an attempt to give some assurance that it will survive the mission. The need, therefore, is to develop confidence that the absence of indication of failure is correct and that the equipment can be relied on to fulfil its function for the requisite period. This can be achieved by a combination of deriving patterns of performance and failure modes using computer models, and the determination in practice of mean and lead times to failure of complete equipments and of their components.

THE MAINTENANCE MANAGEMENT SYSTEM: With the drive to reduce the size of ship's complements, both for existing ships and future designs, it is essential that nugatory work is eliminated and maintenance reduced to a minimum. Part of this will be achieved in new build by fitting more reliable, more automated equipment but this will also have to contain the facility for condition monitoring either on line or manually if the full benefit is to be achieved. This specification is being written in to all future equipment requirements but the real savings will be made by the introduction of a fully integrated condition monitoring system as part of a Maintenance Management System (MMS).

A significant amount of work has been, and is to be, carried out within DGME towards the establishment of condition monitoring in ships but condition monitoring cannot be taken in isolation - it is only a tool and not a means unto itself. It needs to be built into the MMS from the start in a way in which we have never attempted before. There has only recently been a move to modify the preventative maintenance based MMS to reflect the change in policy and it remains a paper based manual system. With the move to condition monitoring, together with the increase in data and its analysis, there is a need to convert to a computerised system. To some extent this will be covered by the imminent introduction of onboard computer based administration systems but there remains a need to develop an interactive system in which all the elements of the management of maintenance - stores, history,

condition monitoring etc are automatically addressed when presented with a task. This is an area ripe for the development of an expert system.

The introduction of condition monitoring to the Fleet has, of necessity, been somewhat piecemeal. New techniques have been added into the maintenance repertoire as they have become available, often without being included in the MMS until years after their introduction. In the main an equipment and not a system approach has been taken. Therefore, in conjunction with the Design Authorities, a comprehensive "engineering audit" to determine the applicability of condition monitoring to each and every individual system and equipment of a ship is to be carried out. Each will be allocated a maintenance category as described earlier. The probable fault patterns will be determined for all parts of the various systems to decide what faults are likely to occur and with what frequency, the parameter or parameters which will predict the onset (the inability to predict the onset of a fault will result in the retention of preventative maintenance), where and by what method they can be detected, and, ideally, determine the ability to, and shape of, trend to failure. It must next be decided whether the data should be collected using hard-wired or hand-held systems. For ships already in service it will generally be cost effective to collect it using hand-held DCUs and manual systems. As the cost of sensors falls and advanced multiplexing systems become available it is probable that the option to retrofit hard wire systems will become more affordable, particularly when set against manpower costs, but generally, for existing systems, manual collection of data will predominate for some years to come. With new build it should be possible to include more hard-wired and installed systems - but care will need to be taken in both cases not to increase the maintenance load by the introduction of excessive instrumentation.

When the audit is complete it will be possible for the first time to determine a truly condition based Maintenance Management System in which the criticality and maintenance requirements of each system and equipment will have been established together with the periodicity of collection of data. This will then be incorporated into a computerised Maintenance Management package. It has yet to be established whether this will be a modified commercial package or a specifically designed system. The integrated condition monitoring system designed as a result of this study will bring together all the information available on the condition of a piece of equipment, using all the condition monitoring techniques available, allowing the Engineer Officer to determine the true condition of his equipment for the first time. Armed with this information he will be able to take the correct and most effective maintenance action.

COST EFFECTIVENESS: The subject of the cost-effectiveness of condition based maintenance and condition monitoring when applied to an organisation such as the Royal Navy is a difficult one. Everyone "knows" that it will save money and men. Unfortunately a great number of exaggerated claims have been made - not least by the equipment manufacturers but also by industrial and merchant marine companies. Savings as high as 80% of maintenance costs have been quoted. Close inspection of these figures reveals that either the company did not truly know their maintenance costs or, more likely, did not have a

maintenance management system in place before the introduction of condition monitoring. By introducing any form of management system these companies would have produced substantial cost savings and been better placed to quantify expenditure.

The savings due to condition monitoring in a manufacturing company which has moved from a clearly defined and closely controlled Planned Maintenance system is thought to be in the order of seven to fifteen per cent. This comprises a combination of savings in the costs of manpower, spares, of lost production etc, as set against the cost of implementation of the system, both in the provision of hardware and software, and in the manpower to run it (training costs can be high in an organisation subject to frequent personnel changes). It would make sense therefore to predict that the RN should expect similar savings, but the calculation of these savings is not a simple matter.

The biggest single gain to be achieved from condition based maintenance and condition monitoring is the increase in availability. This is easily costed in manufacturing terms but not for a warship, not least because of its built-in redundancy (one main engine may be out but it can still fight). The Royal Navy has been running an efficient preventative MMS for many years - but cannot accurately quantify the yearly maintenance costs for an individual warship or even a system. Maintenance personnel employed in Industry rarely have any other responsibilities and reduction in maintenance load relates directly to a reduction in men in an Industrial context. This is not necessarily the case in the Royal Navy where the maintainer is also an operator, departmental manager, firefighter, trainer etc etc. Thus the savings in manpower expected by Headquarters may not be available without other changes in Service procedures and attitudes.

Where then will the Service gain? As previously stated the introduction of a condition based Maintenance Management System with the proper tools and a clear definition of requirements, responsibilities and procedures will lead to a significant increase in availability through, amongst other things, a reduction of planned down-time. The reduction in time-based maintenance will reduce the cost of Refits which will tend to be predominantly Corrective Maintenance and Capability Enhancements. There may be a small reduction in ship's complement but there will be greater savings of manpower in Fleet Maintenance Units and other shore-based support. There will be reductions in spares usage and in Depot Spare Machinery. This will lead to reductions in overhaul costs and possibly the reduction, maybe removal, of some overhaul lines and thus further reductions in support costs. This has been demonstrated using figures derived from Gas Turbine usage where it can be shown that the detection of incipient failures leading to removal and repair before catastrophic failure will result in repair costs which can be as little as one third of those of a full overhaul/rebuild. The extension of life between overhauls has already produced significant savings for Olympus and Tynes - further extensions will produce even more.

The computerisation of condition monitoring and of watchkeeping reports will lead to major improvements in the flow of Availability, Reliability and Maintenance information to Operating Authorities allowing the pin-pointing of design weakness, the correction of these

and the avoidance of similar problems in new design leading to further reductions in maintenance requirements and costs.

CONCLUSION: After a slow start condition based maintenance and condition monitoring are now making rapid progress within the Royal Navy. All indications are that the various trials and the research being undertaken will lead to the introduction of a Maintenance Management System properly configured to employ condition monitoring, and wholly computer based. There will be savings in maintenance costs, which will more than offset the cost of introducing the system, together with significant increases in availability and effectiveness.

FAILURE PREVENTION THROUGH FAILURE ANALYSIS

Dr. Robert B. Pond, Jr.

Baltimore Gas and Electric Company
1000 Brandon Shores Road
Baltimore, Maryland 21226

Abstract: This paper describes an industry approach to using failure analysis results to provide a method for failure prevention. The analysis and packaging of failure analysis results to extend the value of analysis beyond cause and blame assessment will be examined. Current trends in the use of root cause analysis are examined along with information management approaches in the utility industry.

Key Words: Failure analysis; Root cause; Expert systems; Code requirements; Documentation; Cost effectiveness.

Introduction: There are proactive trends in the power production industry in establishing and using metallurgical, nondestructive examination (NDE) and quality assurance organizations to produce power with greater safety, reliability and economy. Similar trends have been initiated and sustained in diverse industries by a wave of successive material and system failures, many of which have been evaluated in the press. Examples of these problems include Chernobyl nuclear plant melt down, the space shuttle failure, the Bopal chemical plant failure, the Ashland oil tank collapse, the Mohave fossil power plant steam pipe rupture, and the Surrey power plant feed water pipe rupture.

This paper will describe the failure analysis elements which are typical for the nuclear utility industry. Techniques and requirements for establishing cost effectiveness are discussed.

Recent failures have led to stronger regulations and controls on design, manufacture, operation and maintenance, and failure analysis. For instance, in the nuclear power industry, the most recent ASME Section XI codes for inservice inspection state:

> Prior to authorizing a repair, the owner shall evaluate the suitability of the repair, including consideration of the cause of failure. (1)

This requirement has a hidden and important implication, because repairs may be required for any nonconformance to specifications. Therefore "failure" of a component under this rule has a broader meaning than "failure" as a degradation of function of a component. Failure analysis is applied to many repairs in the nuclear industry for nonconformances to conservative acceptance criteria. This broad use of failure analysis probably is useful to the nuclear industry. Failure analysis is applied to potential as well as actual failures. This extension enhances the reliability of critical systems. The benefits and efficiency of this encompassing application of failure analysis are a function of the manner of approach to and the process of the failure analysis.

A most essential initiator for a useful failure analysis organization is a mandate and work charter from management. The charter must be established at adequately high organizational levels so that the failure analysis organization has permanence and authority. The mandate must describe adequately the responsibilities and authorities for the failure analysis program.

The requirements for a useful utility program in failure analysis are probably similar to the requirements in many industries. Any large and continuing in-house failure analysis process requires adequate personnel and equipment. These resources are often difficult to justify and obtain. Technical personnel generally must be trained specifically to do failure analysis and there are few academic programs to prepare personnel in failure analysis. (2) Analytical equipment is relatively expensive to buy and to maintain. The total overhead for a competent failure analysis organization is adequately high to make economic justification difficult. This is especially true because cost benefits of failure analysis are not immediately obvious to management and difficult to establish.

A consistent protocol of operation is needed by any engineering organization to optimize performance. A failure analysis program describes the protocol and it must document all of the important aspects of the business. These programmatic approaches to failure analysis are commonly required for many types of nuclear utility work. Program elements in the nuclear industry always include testing procedures. These test procedures for failure analysis are derived typically from ASTM or other testing standards, and special in-house tests are proceduralized as well. Personnel training and certification for testing are required, and testing documentation requirements are established in a nuclear program. The labor and other costs of meeting procedural and training needs are relatively high and the program maintenance overhead is nonnegligible.

A failure analysis program must describe the requirements for job documentation, including record and report formats, filing requirements, and control of documents. Job documentation is especially needed to provide a record system for failure analysis results, and to establish the business record of the process. A documentation system may be complex to meet program requirements, and the system maintenance may require dedicated personnel.

Responsiveness is another requirement for an effective failure analysis operation. Failure problems often need immediate resolution. The failure analysis resolutions are sometimes slowed by tendencies to overly polish reports, and to answer all questions, including the non-relevant. Extensions of analysis beyond requirements and delays in reports raise the cost of failure analysis and often degrade and may eliminate the usefulness of the process.

A common stigma of a failure analysis program is the association of blame assessment. This negative perception is difficult to dispel without a proactive commitment throughout the organization to excellence through change. Failure analysis should be one part of a process of improving business through managing change. Consequently, failure analysis must be a service business directed toward improvement as a part of a larger process and not an end in itself.

Optimizing service transcends the commonly perceived academic requirements of failure analysis and additionally requires supervisory attention to the method of business as well as to the results. Years of effort may be expended obtaining the acquaintance and trust of personnel who operate and maintain the components that fail. Likewise, careful communication to engineering and management need be cultivated to achieve consistent acceptance of results and recommendations. Many failure analysis laboratories are relatively isolated from line organizations, engineering, and management. However, good communications with these groups are imperative for access to reliable information and for failure analysis product to be accepted and used.

The product of failure analysis work is generally an engineering report containing descriptions, data, references, resolutions of failure cause, consequences of failure, generic implications, remedial actions and recommendations. The exclusion of any of these report elements may be discretionary. There are currently trends in the nuclear industry to formally specify the elements of the failure analysis. Codification of report requirements may enhance program quality and will reduce efficiency and drive up the cost of the analysis process.

General methodologies such as root cause analysis are being applied in the nuclear industry to failure analysis. Root cause analysis usually recognizes two paths to problem solution: a technical path, and a nontechnical path. [3] The nontechnical path of root cause analysis uses a question structure to generate probable cause of failure by establishing differences between faulted and unfaulted conditions. Methods for checking consistency of the results are provided in the process. The root cause methodology may be self-consistent and wrong. We have identified incorrect analyses created by applications of root cause analysis by non-technical personnel, operating past the boundaries of required technical understanding. The ready acceptance of the incorrect results as a product of an accepted process poses a danger to the utility industry. The methodologies of root cause analysis are probably helpful in the correct hands, but the use of these techniques by nontechnical personnel is not viable.

Recently, expert systems for failure analysis have been tried in the utility industry. Electric Power Research Institute (EPRI) recently issued expert system computer software for failure analysis of failed fossil plant boiler tubes. [4] First, EPRI compiled and printed an extensive, comprehensive text on causes of boiler tube failures. [5] The failure analysis text was used to generate a fault tree for the personal computer based expert failure analysis system. The fault tree was constructed to duplicate all the conditions cited for the many types of tube failures in the text. This

expert computer system appears to be most useful and easy to understand and manipulate. Baltimore Gas & Electric Co. (BG&E) failure analysis personnel reviewed and approved of the technical basis of the program. Subsequently, tests by BG&E personnel for EPRI on real boiler tube problems yielded seven discrepancies in nine trials between the computer product and laboratory failure analysis results. These disparities occurred with failure analysis engineers and technicians making data entries. Some number of incorrect analyses should be expected from any expert system in the hands of nontechnical personnel. Without an independent technical verification, the quality of the results can not be known. In current form, this expert system may provide an incorrect analysis in the guise of a highly qualified technical result. The expert system may augment failure analysis, but the expert system alone appears inferior to the capabilities of a qualified failure analysis organization.

We anticipated that the EPRI expert system provides the basis of an effective teaching tool. The fault tree questions may be used in conjunction with a slide viewer which is controlled and indexed by the computer software and provides real examples of failures. This teaching system may be modified easily to include plant specific questions and slides. (6)

One of the most important and elusive assessments of a failure analysis organization is cost effectiveness. Proper failure analysis generally directs job processes to one of many paths. Consequently, cost effectiveness may not be measured without the advantage of knowing the incurred costs of paths which would have been taken without the advantage of failure analysis. The amount of completed work may adequately indicate program cost effectiveness if the failure analysis organization is perceived as providing a service. This approach may compare average cost per failure analysis and fraction of failure analysis costs of the total job costs.

Other benefits may be derived from a failure analysis organization which has adequate flexibility. For example, BG&E's failure analysis organization is used to provide additional services in providing material selection recommendations for new and modified systems. Additionally, review of vendor process procedures, and generation of materials receipt inspection requirements and material receipt inspections are provided by our failure analysis personnel. BG&E's failure analysis organization also establishes the material critical characteristics for commercial grade dedications in nuclear applications. Technical control and monitoring of outside materials laboratories which are used by the company are provided. This failure analysis group either controls or directly provides materials research and development and special testing of materials for the company. Cathodic protection design and monitoring, corrosion testing, and coatings engineering are also areas controlled by the failure analysis personnel. These program extensions are logical and satisfy needs common to the nuclear power industry.

An example of application of utility initiative in the area of failure analysis occurred recently at Calvert Cliffs Nuclear Power Plant. On May 19, 1989, leaks were found coming from about twenty of the Inconel 600 heater sleeve penetrations in the bottom of Unit No. 2 reactor coolant system pressurizer during a refueling outage (Figure One). BG&E Co. failure analysis, non-destructive examination, and systems engineering personnel were immediately assembled to plan an approach to analyze the cause of failure. The twin, Unit No. 1 nuclear reactor, was immediately shut down by management for examination of the pressurizer. There were no leaks in the Unit No. 1 pressurizer sleeves, but the company elected to keep the Unit No. 1 plant off line in consideration of safety until a resolution of the failure analysis could be made.

Initial NDE examinations indicated that the breaches of pressure boundary were axial radial cracks in the pressurizer sleeves. The NDE examinations were directed by the failure analysis group to determine any circumferential-radial cracking which could lead to potentially catastrophic failure of the pressure boundary. It was concluded by NDE examinations that there were no such indications, either in the pressure boundary weld or in the sleeve material. This examination work was done in a radiologically contaminated and thermally hot environment.

Requests from failure analysis personnel were made for two types of samples for destructive examinations. Sleeves were selected and a request made to cut them out of the pressurizer. These sleeve samples had NDE indications and provided an advantage of being fairly easily obtained and a disadvantage that the required cuts below the attachment weld to remove these sleeves were in the locations of crack indications. Additionally, a single core sample was requested which would contain the entire sleeve, the attachment weld and an annulus of the carbon steel pressurizer head. This sample was required to complete the failure analysis. However, the damage to the pressurizer from this sample removal had to be repairable, and the field equipment for specimen removal had to be developed and qualified.

In parallel with the preparation for failure analysis, plans were being evaluated for repair for the pressurizer leaks. These evaluations included possible changes in material for the sleeve material based on projections that the failure mechanism was stress corrosion cracking.

The Nuclear Regulatory Commission issued a position that the Unit No. 1 plant could not be started unless a technical justification was made to the Commission in a document called a "Basis for Determination."

Failure Analysis personnel generated a specification for outside hot lab failure analysis work on the pressurizer specimens. The specification for the laboratory work assured a key, interactive role of BG&E personnel in the failure analysis. Proposals were reviewed and two laboratories were selected for parallel analyses. When the samples were removed, BG&E participated in the analysis at the vendors' laboratories, and critically reviewed the reports. The summary failure analysis reports were incorporated into the technical "Basis for Determination," the development of which also was controlled by the failure analysis group. (7)

The failure mode of the Inconel sleeves was found to be primary water stress corrosion cracking (PWSCC) and an important difference in manufacturing process was determined between the Unit No. 1 and Unit No. 2 pressurizers. Unit No. 2 pressurizer sleeves had been subjected to an abusive reaming operation in the location of cracking to which Unit No. 1 pressurizer sleeves were not subjected. It appears clear that reaming provided the different material behavior in the two pressurizers, the heater sleeves of which were made from the same heat of material. However, the contribution of welding stresses to PWSCC initiation could not be discounted for either Unit. BG&E failure analysis personnel are currently participants in an industry study to determine the generic implications of the BG&E pressurizer sleeve failures to all Inconel 600 penetrations of reactor coolant system boundaries. These studies are not resolved.

The "Basis for Determination" for continued operations of Unit No. 1 was submitted in September of 1989 and approved by the Nuclear Regulatory Commission. (8)

The repair plan for the Unit 2 pressurizer was also approved by the NRC and the subsequent materials processing and fabrication processes for repair were monitored and controlled by failure analysis personnel. All heater sleeves in the Unit No. 2 pressurizer were successfully replaced.

The failure analysis group and program were integral parts of the BG&E Co. team and process that resolved this complex and critical issue. The justification of a failure analysis organization and program are sometimes measured by successful responses to large industry problems which require the highest quality work in the most efficient manner.

(1) 1986 ASME Boiler and Pressure Vessel Code, Section XI, Rules for Inservice Inspection of Nuclear Power Plant Components, IWA-4130a(4).

(2) Principles of Failure Analysis, Materials Engineering Institute, American Society for Materials International, P. D. Harvey (ed.), Materials Park, Ohio (1980).

(3) Problem Solving and Decision Making, Kepner-Tregoe, Skillman, New Jersey (1987).

(4) Boiler Maintenance Workstation, EPRI GS-6584 Project 1865-7 (September 1989).

(5) Boiler Tube Failure & Correction, Prevention, and Control, EPRI GS-6467 Project 1890-7, Final Report (July 1989).

(6) Training for NDE Inspectors, Proceedings of 17th Southwest Research Institute NDE Symposium, G. P. Singh and W. R. Tweddell, San Antonio, Texas (1989).

(7) Materials Testing and Evaluation Report No. 89-30-223, Baltimore Gas and Electric Co., Baltimore Maryland (August 30, 1989).

(8) Basis for Determination, Baltimore Gas and Electric Co., Baltimore Maryland (September 18, 1989).

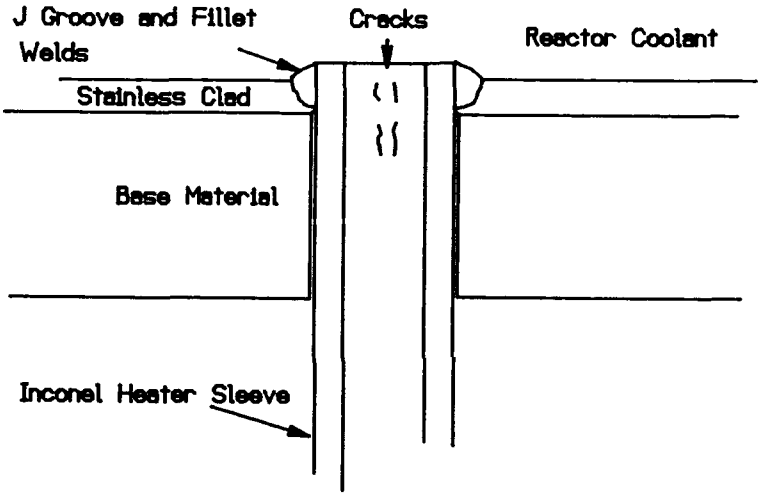

Figure One: Heater Sleeve Schematic

DETECTION, DIAGNOSIS AND PROGNOSIS

Chairman: Howard A. Gaberson
Naval Civil Engineering Laboratory

SCREW COMPRESSOR FAULT DETECTION AND DIAGNOSIS BASED ON MODELING AND ESTIMATION

C. James Li and T. Kim
Columbia University
Dept. of Mechanical Engineering
New York, NY 10027

G. W. Nickerson
David Taylor Research Center
Annapolis, MD 21402

Abstract: This paper presents a model based fault detection and identification (FDI) method for a screw compressor. Mathematic models which describe the casual relationships linking measurable system variables are derived from physical laws which govern the behavior of the compressor. These mathematical models are in the form of a system of ordinary differential equations. The parameters of the models are estimated using the least square estimators under normal and four different fault conditions. It is shown that the use of model parameters, which frequently are more directly influenced by faults, has enabled earlier and more accurate recognition of faults.

Key Words: Diagnosis; Monitoring; Modeling; Parameter estimation; Screw compressor

Introduction: To meet future naval ship missions, Hull, Mechanical and Electrical (HM&E) equipment will necessarily become increasingly complicated. Concurrently, the pressure to reduce the cost of the ship system will necessitate reduced manning and staff levels. These two driving forces work in opposition to each other and a new method of maintenance, other than planned maintenance system (PMS) for the upkeep of shipboard system machinery, must be developed.

Mechanical system condition based maintenance (CBM) has been recognized as the solution. The benefits of a CBM are improved maintenance procedures and scheduling, increased machinery operational readiness, and reduced logistics support cost. The Ship Operational Characteristics Study found that CBM on surface combatants could result in a 12% reduction in the required manning. The same study also found that CBM could allow 15% increase in the ship volume available for the combat system. A perhaps more important benefit ot a CBM system as described is the ability to provide the Commanding Officer with near-real-time readiness assessment of his/her ship system.

In a fielded system, an effective CBM system shall detect faults of a machine well before getting to the failure stage. Thus, monitoring systems must be in place to measure parameters of interest. Diagnostic algorithms must be available to convert the data obtained from the monitoring system into variables which signify the state of operation of the machine.

Whereas previous methods of condition monitoring only permitted recognition of the state of an equipment using measurable signals or their derivatives, an attempt is now being made to develop a more sensitive and reliable method by the use of model based indirect variables as well [1,2]. Previous methods can identify the chang. of the state of an

equipment only after some measurable variables have been considerably affected. The use of indirect variables, which frequently are more directly influenced by faults, is likely to enable earlier and more accurate recognition of a change of the state due to a fault. The approach is described as follows.

Measurable variables of a process are linked by causal relationships which can be described by mathematical models. For instance, best well known mathematical models are differential/difference equations. In general, these mathematical models have the following form:

$$Y = f\{U,N,\theta,X\} \qquad (1)$$

where U(t) and Y(t) are vectors of the measurable input and output variables, N generally represents a vector of nonmeasurable disturbance signals, θ is a vector of constant or slow time varying nonmeasurable process parameters, and X is a vector of partially measurable and partially nonmeasurable internal variables.

Knowing the mathematic model, indirect variables can be derived based on the following parameters:

(1) Nonmeasurable part of variables X.

(2) Nonmeasurable process parameters θ.

(3) Nonmeasurable characteristic quantities $\eta = g\{U, Y, \theta\}$.

Frequently, the basic process/equipment model can be derived from physical laws which govern the process/equipment behavior. Hence, the structure of the models is known and the parameters have to be estimated. The nonmeasurable internal variables X and process parameters θ can be obtained by state estimation and parameter estimation schemes described in ref.[3-7].

Using model based indirect variables for fault detection has the following advantages:

- The indirect variables X(t) or Θ(t) are in many cases closer to the process faults. Hence the process faults may be detected earlier and localized more precisely than just observing U and Y.
- A process fault usually causes changes of several output variables with different signs and dynamics. The model based fault detection now takes into account all these entailed changes and determines the indirect variable which has been changed directly by the fault. Hence, a more significant change in the indirect variable can be extracted and the sensitivity is improved.
- Closed loops generally compensate for changes of the outputs by changing the inputs. Therefore deviations by faults can not be found with direct measurement of outputs. Model based fault detection methods have no such limitation.
- Fewer sensors will be required. All different sensors are driven by the same dynamics of the system and are therefore functionally related. This functional redundancy can be used to achieve sensor fault tolerance or to reduce the number of sensors.

DTRC has chosen a 20Hp single screw as a test platform for this new model based fault detection and diagnosis approach. We will first illustrate the modeling of the compressor and means to estimate the parameters of the model. Then, we will present the experimental results and conclude the paper with what we have learnt from the experiments performed at our laboratories.

Modeling: The compressor system is regarded as a system consisting of a motor, an air-end, a pipe system, a radiator and oil cooler as illustrated in *Fig.1* (see Appendix for

nomenclature). A model of the compressor is obtained by combining models of these subsystems.

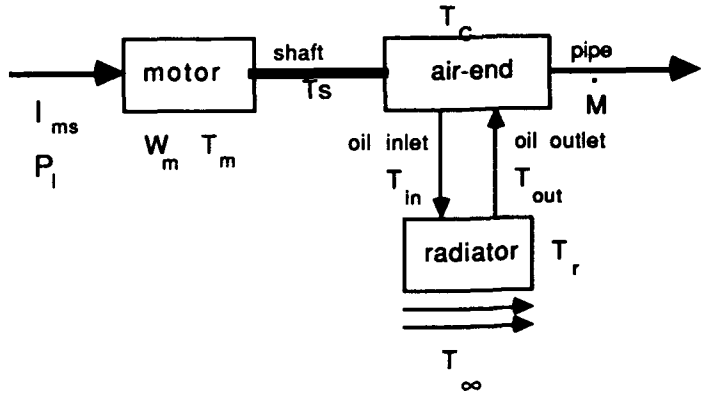

Fig. 1 A model of the compressor

Torque balance on the motor gives

$$\Theta_M \frac{dw_m}{dt} = T_M - T_{FM} - T_S \qquad (2)$$

where $T_M = C\frac{I_{ms}^2(w-w_m)}{w_m}$, $T_{FM} = C_{FM0} + C_{FM1}w_m$

Torque balance on the air-end gives

$$\Theta_C \frac{dw_m}{dt} = T_S - T_{FC} - T_C \qquad (3)$$

where $\Delta T_C = a\,\Delta w_m + b\,\Delta \dot{M} + d\,\Delta P_I$, $T_{FC} = C_{FC0} + C_{FC1}w_m$

Eq.(2) and(3) can be added together to eliminate T_S. Furthermore the equation is linearized around a steady-state equilibrium. Let us denote $\bar{w}_m$, $\bar{T}_S$, $\bar{T}_C$, $\bar{M}$, $\bar{I}_{ms}$ and $\bar{P}_I$ as values of measurable variables at the equilibrium . Then,

$$(\Theta_M+\Theta_C)\frac{dw_m}{dt} = -\left(C\frac{\bar{I}_{ms}}{\bar{w}_m^2}w + C_{FM1} + C_{FC1} + a \right)\cdot \Delta w_m - b\cdot\Delta\dot{M}$$

$$+ 2C\bar{I}_{ms}\frac{w-\bar{w}_m}{\bar{w}_m}\cdot\Delta I_{ms} - d\,\Delta P_I \qquad (4)$$

(see Appendix for details of derivations)

Pressure drop in the pipe system can be obtained from the following equation;

$$\Delta P = \Delta P_V + \Delta P_R + \Delta P_{ac} \qquad (5)$$

where $\Delta P = P_l - P_{atm}$, $\Delta P_v = C_V \frac{\dot{M}^2}{A_V}$

$\Delta P_R = C_R \dot{M}^2$, $\Delta P_{ac} = \frac{L}{A_F} \frac{d\dot{M}}{dt}$

After perturbation Eq. (5) can be written as;

$$\frac{L}{A_F} \frac{d\Delta\dot{M}}{dt} = -2\left(\frac{C_V}{A_V} + C_R\right)\bar{M} \cdot \Delta\dot{M} + \frac{L}{A_F} P_l \qquad (6)$$

Heat balance equation on the radiator gives

$$Q_r = Q_{in} - Q_{out} \qquad (7)$$

where $Q_r = \rho_r c_{pr} V_r \dot{T}_r$

$Q_{in} = \dot{m}_{oil} c_{oil} (T_{in} - T_{out})$, $Q_{out} = a_r h_r (T_r - T_\infty)$

Therefore, Eq.(7) becomes

$$\rho_r c_{pr} V_r \dot{T}_r = \dot{m}_{oil} c_{oil} (T_{in} - T_{out}) - a_r h_r (T_r - T_\infty) \qquad (8)$$

Eq.(8) and the equation formed by combining Eq.(4) and (6) give the state-space model of the compressor;

$$\frac{d}{dt}\begin{pmatrix} w_m \\ \dot{M} \end{pmatrix} = \begin{pmatrix} a_{11} & a_{12} \\ 0 & a_{22} \end{pmatrix} \cdot \begin{pmatrix} \Delta w_m \\ \Delta\dot{M} \end{pmatrix} + \begin{pmatrix} b_{11} & b_{12} \\ 0 & b_{22} \end{pmatrix} \cdot \begin{pmatrix} \Delta I_{ms} \\ \Delta P_l \end{pmatrix}$$

$$\dot{T}_r = C_1 (T_{in} - T_{out}) + C_2 (T_r - T_\infty) \qquad (9)$$

where

$$a_{11} = -\left(C \frac{\Gamma_{ms}^2}{\bar{w}_m^2} w + C_{FM1} + C_{FC1} + a \right)/(\Theta_M + \Theta_C)$$

$$a_{12} = -\, b/(\Theta_M + \Theta_C)$$

$$a_{22} = -\, 2 \frac{A_F}{L} \left(\frac{C_V}{A_V} + C_R \right) \bar{M}$$

$$b_{11} = 2C\Gamma_{ms} \frac{w - \bar{w}_m}{\bar{w}_m} /(\Theta_M + \Theta_C)$$

$$b_{12} = -\, d/(\Theta_M + \Theta_C)$$

$$b_{22} = \frac{A_F}{L}$$

$$C_1 = \dot{m}_{oil} c_{oil} / \rho_r c_{pr} V_r$$
$$C_2 = -a_r h_r / \rho_r c_{pr} V_r$$

a_{11}, a_{22} and b_{11} contain terms such as $\bar{\Gamma}_{ms}$ and $\bar{w}_m$ which change as the operating condition changes. This undesirable effect can be removed from a_{22} and b_{11} by forming two new parameters; $a'_{22} = a_{22}\bar{M}$ and $b'_{11} = b_{11}\bar{w}_m / \bar{\Gamma}_{ms}(w - \bar{w}_m)$. However, similar manipulation can not be performed with a_{11}. A qualitative analysis can be performed on these model parameters to find out which parameters of the model will be affected if a fault is present. For example, if a motor bearing becomes defective and generates larger rolling resistance than a normal one would, C_{FM1} would increase. Consequently the motor slows down and draws more current to overcome this resistance. Thus $\bar{\Gamma}_{ms}^2 / \bar{w}_m^2$ would increase. Therefore, in the case of motor bearing defect, a_{11} will change its value.

The result of the qualitative analysis is summarized in the following table.

FAULTS	AFFECTED COEFFICIENT	AFFECTED MODEL PARAMETER
MOTOR Electrical Fault	C	a_{11} b'_{11}
MOTOR Mechanical Fault (Bearing)	C_{FM1}	a_{11}
AIR-END Mechanical Fault (Bearing)	C_{FC1}	a_{11}
AIR-END ROTOR Fault	a	a_{11}
	b	a_{12}
	d	b_{12}
PIPE SYSTEM		a'_{22} b_{22}
RADIATOR Air Passage Clogging		C_1
RADIATOR Oil Passage Clogging		C_1 C_2

TABLE 1 Expected parameter changes due to different faults

Parameter estimation: Eq.(9) is a system of linear differential equations. We will need $d(w_m)/dt$, $d(\dot{M})/dt$ and $d(Tr)/dt$ to estimate the parameters of the differential equations. Numerical differentiation can be used to estimate these derivatives from w_m, $\dot{M}$ and T_r. In practice, the order of the numerical differentiation is restricted to second or third order due to the presence of measurement noise. A better alternative is to combine the numerical differentiation with filtering [5].

A very effective and well developed parameter estimation method is the Least Square(LS) method. LS method performs well when equation errors can be characterized as uncorrelated white noises. Otherwise, LS method provides biased estimates. If unbiased

estimates are desirable, modified LS method, instrumental variable method and generalized LS method and extended LS method can be used [3,6].

Experimental results: Experiments were conducted on the 20 HP single rotor screw compressor with five different conditions at two different operating pressures(75 psi and 115 psi). The five conditions include the normal condition and the following four simulated faults:

(1) Simulated friction increase by clamping the shaft
(2) Simulated worn gaterotor by changing the mesh clearance b/w the rotor and gaterotors
(3) air passage clogging in the oil cooler
(4) oil passage clogging in the oil cooler

We did not simulate all the faults listed in Table 1 because some of them, such as motor faults, can not be easily simulated or implemented.

Outputs from each transducer after appropriate signal conditioning circuits were sampled at 1KHz over a period of 1.5 second. Parameters were estimated off-line using generalized LS-method with numerical differentiation and filtering.

Table 2 presents the parameter values obtained under all the conditions. a_{12}, b_{12} and b_{22} were found to be having too large a variance after convergence. Therefore, they were excluded from the table. According to Eq.(9) a_{11}, b'_{11}, a'_{22}, C_1 and C_2 should be negative, positive, negative, positive and negative all the time. The estimates are consistent with this prediction.

	75 psi			115 psi				
	normal	friction	worn gaterotor	normal	friction	worn gaterotor	clogged air passage	clogged oil passage
a_{11}	-169.10	-209.81	-192.39	-179.35	-197.62	-226.66	-	-
b'_{11}	15.486	15.187	11.800	12.496	31.136	18.729	-	-
a'_{22}	-3.532	-2.756	-4.318	-0.125	-0.546	-3.545	-	-
C_1	0.01174(normal)						0.01266	0.00644
C_2	-0.01720(normal)						-0.01093	-0.01086

TABLE 2. Experiment result

Ideally, parameter values should not change with operating pressure of the compressor. Comparing parameter values under normal conditions at 75 psi and 115 psi, there is a noticeable amount of change in all three parameters. The change in a_{11} is only 6%, the change in b'_{11} is a moderate 20% and the change in a'_{22} is about 100%. The most significant reason for these changes is the linearization of models around an equilibrium point. One can resort to the use of nonlinear models to eliminate this. For the moment, one would hope that changes of parameters due to a fault will be more significant than changes resulted from the operating condition changes. Otherwise, a lookup table of normal parameter values vs. operating pressure should be used as a reference.

In the case of increased friction, table 1 indicates that the absolute value of a_{11} should increase since C_{FM1} and I_{MS}/W_M would increase. The experimental result shows a 24% and 10% increases of a_{11}'s absolute value at 75 psi and 115 psi respectively. In both cases, the changes of a_{11} are significantly larger than changes observed from measurable variables. In fact, motor current and rotational speed have a less than 3.4% changes at the same time. From these numbers, it is obvious that the model based approach has good sensitivity to the presence of the fault.

In the case of a worn gaterotor, table 1 indicates that the magnitude of a_{11} should increase as the "a" in equation (9) increases due to the internal leakage, a_{12} and b_{12} should change as the "b" and "d" vary. Unfortunately, we can not examine a_{12} and b_{12} due to their large estimation variances. The experimental result shows a 14% and 26% increases of a_{11}'s absolute value at 75 psi and 115 psi respectively. In both cases, the changes of a_{11} are significantly larger than changes observed from measurable variables. In fact, motor current and rotational speed have a less than 2% changes in the same period of time.

Due to the unavailability of a_{12} and b_{12}, we were not able to distinguish the gaterotor wear from the friction increase because both faults increase the magnitude of a_{11}. This problem will be resolved once a_{12} and b_{12} become available. This can be achieved through more precise models and a better measurement technique. Since neither gaterotor wear nor friction increase affects b'_{11} and a'_{22}, they should remain constant at both pressures. Experimental data shows that this is more true at 75 psi than it is at 115 psi. We also do not have enough data to compare these variations to parameter changes resulted from those faults which affect b'_{11} and a'_{22} (table 1).

When the air passage of the radiator is partially blocked, the effective surface area and radiator mass are reduced by the same ratio. Therefore, the absolute value of C_2 should remain constant. Experimental data shows that the changes of C_2 is well within the variance of the estimation. Therefore, it is consistent with the model. On the other hand, C_1 should increase significantly. However, experimental data shows a smaller increase than expected.

When the cooling oil passage is clogged, it is expected that C_1 will reduce proportionally. This is confirmed by the experimental result. C_1 changed from 0.01174 to 0.00644 while the oil flow rate was reduced by 50%. This is a very good example for the usefulness of model based approach. This example shows that through the measurement of oil temperatures which can be easily obtained using inexpensive thermocouples, one can determine the oil flow rate which is a more difficult and expensive variable to measure than temperatures.

Conclusion: We have applied model based fault detection and isolation technique to a single rotator screw compressor. It is shown that the approach has enabled the formation of indices which are frequently more sensitive than measurable variables to faults such as the gaterotor wear, friction increase, and radiator oil passage blocking. It is also found that the success of such approach depends on the precision of the model one uses. Therefore, a better modeling and parameter estimation methodology is very critical to the evolving of this relatively new approach to fault detection and isolation. It is our belief that this technique will compliment the inadequacy of existing signal processing based fault detection and isolation techniques.

References:

1. Isermann, R., "Process Fault Detection Based on Modeling and Estimation Methods -- A Survey, Automatica, Vol 20, No 4, pp387-404, 1984.
2. Geiger,G., "Fault Identification of a motor-pump system using Parameter Estimation and Pattern Classification",IFAC 9th Triennial World Congress, Budapest, Hungary, pp 1783-1788,1984.
3. Ljung, L. , Soderstrom, T. , Theory and Practice of Recursive Identification, The MIT press, Cambridge, Massachusetts, 1983.
4. Goodwin, G. C. and Sin, K. S., "Adaptive filtering, prediction and control", Prentice-Hall, Inc., Englewood Cliffs, New Jersey, 1984.
5. Young, P. C., "Parameter estimation for continuous-time models-a survey. Automatica, Vol 17, No. 23.
6. Strejc,V., "Least Square Parameter Estimation", Automatica, Vol 16, pp 535-550, 1980
7. Rao,G.P. and Sivakumad,L., "Identification of Deterministic Time-Lag Systems", IEEE Transaction of Automatic Control, AC-21,pp 527-530,1976.
8. Van Ormen Jr., H.P., "Profiles of air-end rotors",Hydraulics and Pneumatics, Mar, 1986.
9. Engelmanm,R.H.,"Static and Rotating Electromagnetic Devices",Marcel Dekker, Inc., 1982

Appendix:

nomenclature

a	air-end torque characteristic coefficient for angular velocity
a_r	surface area of radiator
A_F	sectional area of pipe
A_V	sectional area of valve
b	air-end torque characteristic coefficient for mass flowrate
C	motor characteristic coefficient($= \frac{9n}{8r_r} M_{sr}^2 \sin^2(\alpha-\beta)\ w$)
C_{FM0};C_{FM1}	motor friction coefficients
C_{FC0};C_{FC1}	air-end friction coefficients
C_{oil}	specific heat of oil
C_R	fluid resistance coefficient of pipe system
C_V	valve coefficient
c_{pr}	specific heat of radiator
h_r	convection coefficient of radiator
I_{ms}	motor stator current
L	characteristic length of pipe system
$\dot{m}_{oil}$	oil mass flowrate in the radiator
$\dot{M}$	air mass flowrate
M_{sr}	mutual inductance between stator and rotor of motor
n	number of cage in motor
P_l	air-end outlet pressure

ΔP_P	pressure drop of pipe
ΔP_R	pressure drop due to fluid resistance
ΔP_V	pressure drop due to valve
ΔP_{ac}	pressure drop due to acceleration
r_r	resistance of rotor winding
ρ_r	density of radiator material
T_M	motor torque
T_{FM}	motor friction torque
T_S	shaft torque
T_{FC}	air-end friction torque
T_C	air-end torque
T_r, T_∞	radiator and ambient temperature
T_{in}, T_{out}	oil inlet and outlet temperature
V_r	volume of radiator material
w	field rotating speed
w_m	motor speed
Θ_M, Θ_C	motor and air-end inertia

Torque balance on motor can be expressed;

$$\Theta_M \frac{dw_m}{dt} = T_M - T_{FM} - T_S \qquad (A1)$$

For the Cage Induction Motor [9], motor torque can be expressed like the following;

$$T_M = \frac{3}{4} n l_{mr} l_{ms} M_{sr} w \sin(\alpha-\beta) \frac{1}{w_m} \qquad (A2)$$

The relationship between l_{mr} and l_{ms} is

$$l_{mr} = \frac{3}{2r_r}(w-w_m) l_{ms} M_{sr} \sin(\alpha-\beta) \qquad (A3)$$

Substituting Eq.(A3) into (A2), we have

$$T_M = C \frac{l_{ms}^2 (w-w_m)}{w_m} \qquad (A4)$$

where $C = \frac{9n}{8r_r} M_{sr}^2 \sin^2(\alpha-\beta) w$

Friction force on motor T_{FM};

$$T_{FM} = C_{FM0} + C_{FM1} w_m \qquad (A5)$$

From Eq.(A1),(A4) and (A5),

$$\Theta_M \frac{dw_m}{dt} = C \frac{l_{ms}^2 (w-w_m)}{w_m} - C_{FM0} - C_{FM1} w_m - T_S \qquad (A6)$$

Small deviations around the steady-state ($\bar{w}_m$, $\bar{T}_S$, $\bar{I}_{ms}$) are considered;

$$w_m = \bar{w}_m + \Delta w_m$$

$$T_S = \bar{T}_S + \Delta T_S$$

$$I_{ms} = \bar{I}_{ms} + \Delta I_{ms}$$

After perturbation, Eq.(A6) can be expressed like the following:

$$\text{steady-state} : \quad 0 = - C_{FM0} - C_{FM1}\bar{w}_m - \bar{T}_S$$

$$\text{transient} : \quad \Theta_M \frac{dw_m}{dt} = -\left(C \frac{I_{ms}}{\bar{w}_m^2} w + C_{FM1} \right) \cdot \Delta w_m - \Delta T_S + 2C\sqrt{I_{ms}} \frac{w - \bar{w}_m}{\bar{w}_m} \cdot \Delta I_{ms} \qquad (A7)$$

Torque balance on the air-end can be expressed;

$$\Theta_C \frac{dw_m}{dt} = T_S - T_{FC} - T_C \qquad (A8)$$

This torque is a function of rotational speed, mass flowrate and discharged pressure [8]. Therefore the following equation can be obtained:

$$\Delta T_C = a \cdot \Delta w_m + b \cdot \Delta \dot{M} + d \cdot \Delta P_l$$

Air-end friction torque:

$$T_{FC} = C_{FC0} + C_{FC1} w_m$$

Substitute ΔT_C and T_{FC} into Eq.(A8) and linearize it, we have

$$\text{steady-state} : \quad 0 = \bar{T}_S - \bar{T}_C - C_{FC0} - C_{FC1}\bar{w}_m$$

$$\text{transient} : \quad \Theta_C \frac{dw_m}{dt} = \Delta T_S - (C_{FC1} + a) \cdot \Delta w_m - b \cdot \Delta \dot{M} + d \cdot \Delta P_l \qquad (A9)$$

Eq.(A7) and(A9) can be added together to eliminate T_S.

$$(\Theta_M + \Theta_C) \frac{dw_m}{dt} = -\left(C \frac{I_{ms}}{\bar{w}_m^2} w + C_{FM1} + C_{FC1} + a \right) \cdot \Delta w_m - b \cdot \Delta \dot{M} + 2C\sqrt{I_{ms}} \frac{w - \bar{w}_m}{\bar{w}_m} \cdot \Delta I_{ms} + d \cdot \Delta P_l \qquad (A10)$$

PHASE AND MAGNITUDE VIBRATION MEASUREMENTS FOR CRACKED SHAFT DETECTION

James W. Allen and James C. Robinson
Technology for Energy Corporation
10737 Lexington Drive
P.O. Box 22996
Knoxville, TN 37933-0996

Abstract: Vibration data was obtained from proximity probes mounted on large, vertical recirculation pumps under different shaft conditions: (1) cracked, (2) catastrophically cracked and (3) unknown, but probably cracked. The data consisted of the magnitude of vibration at various running speed orders, the phase relationship of vibration relative to a Keyphasor®,[1] and the magnitude of vibration at non-running speed orders. The badly cracked shaft was indicated by major changes in phase and magnitude at one and two times the running speed. Evidence of cracking for the other shaft conditions was not as clear. Analyses found that the uncertainty in the above vibration parameters can be large enough to mask it's significance and, when statistically significant data is obtainable, it can fluctuate considerably. Consequently, any analyses which rely on phase and magnitude measurements must consider the statistical uncertainty of the parameter.

Key Words: Crack growth; cracked shaft; critical speed; phase; power spectral density; pumps; spectrum; trends; uncertainty; vibration

Introduction: Cracked shafts in major pumps, turbines and other process machinery have generated a great deal of concern and investigation into methods which can be used to detect such a condition prior to catastrophic shaft failure. A key indicator of a cracked shaft includes significant changes in the magnitude and phase vector at particular orders of the running speed. For the pumps analyzed in this paper this was most notable at one times (1X) and two times (2X) the running

1 ®Keyphasor is a registered mark of Bently Nevada Corporation.

speed. Other cracked shafts have been diagnosed by changes at 3X and the vane pass speed.[2] [3] Technology for Energy Corporation (TEC) has analyzed vibration signals from large vertical pumps having shafts in various conditions. These conditions were (1) unabated propagation of an existing crack (May 11, 1989), (2) cracked, prior to unabated propagation (May 1, 1989), and (3) potentially cracked, but not certain (August 1990).

In May 1989, the shaft of large recirculation pump (B) failed when a pre-existing crack attained an unabated propagation condition. After the plant was shut down due to the inoperability of this pump, it was found that a companion recirculation pump (A) also had a cracked shaft. Fortunately signals from the proximity probes on both pumps were routed to a tape recorder before and during the failure stage. Hence signals were tape recorded prior to the B pump event for both pumps at low flow (pump operating at slow speed) and high flow (pump operating at high speed). The signals were taped for 2 hours during the event. The tape recorded signals for each pump were from a Keyphasor, a proximity probe located on the motor outboard bearing, two probes mounted on the motor inboard bearing, two probes on the pump and a probe mounted to observe axial vibration on the balance plate. In August 1990, signals were tape recorded from the A and B pump when the (new) shafts were presumably in an non-cracked condition. However, the shafts at these pumps were found to be cracked in December 1990, so their condition in August is uncertain. Proximity probe signals were recorded from the two pump sensors and a single motor inboard sensor on each pump for a period of about two hours.

Initial analyses focused on the behavior of 1X and 2X parameters on recirculation pump B prior to and including the unabated propagation stage. In the initial analysis[4] clear changes in the phase and magnitude of vibration at 1X and 2X were seen. In this paper [5] a more detailed analysis of all available data and analysis parameters was performed. The additional parameters considered were:

1. The magnitude and phase vector at most nX running speed frequencies. The primary focus was on the 1X, 2X, 3X and 5X (vane pass) orders.

---

2 D.E. Bently, A.S. Thompson, (Bently Nevada Corporation), "Detection of Cracks in Rotors", Proceedings: Third EPRI Incipient-Failure Detection Conference, (EPRI CS-5395) August 1988.

3 Stan Jenkins, (RCP Design Engineering), "A Case History of Cracked Shaft Diagnosis on a Westinghouse RCP at Three Mile Island #1", Reactor Coolant Pump, Recirculation Pump Monitoring Workshop, Toronto, Canada, March 1988.

4 James W. Allen (TEC) and Jeffrey S. Bohanick (Entergy Operations), "Cracked Shaft Diagnosis and Detection on Reactor Recirculation Pumps at Grand Gulf Nuclear Station", Nuclear Plant Journal, Volume 8 No. 3, Page 78, May-June 1990.

5 Sponsored by the Electric Power Research Institute.

2. The statistical uncertainty in the above parameters.

3. The Power Spectral Density (PSD) function calculated by nonsynchronous sampling,[6] in particular the behavior of this function between running speed frequencies and around the critical speed.

Results: The magnitude and phase vectors for the 1X, 2X, 3X and 5X running speed frequencies were determined for both pumps when the shaft was cracked and cracking unabatedly. Clear trends towards rapidly deteriorating conditions were observed in the data when the crack went into an unabated propagation stage, but *ONLY* after this condition was clearly established. Figure 1 shows the behavior of the 1X magnitude and phase before and during this event. Please note that data for time less than zero in this figure is for data taken ~10 days prior to the actual unabated propagation stage. Table 1 summarizes the changes for all 1X, 2X and 5X parameters before and after the rapid crack growth. When these parameters are compared with classical symptom charts for vibration diagnostics, they generally fit the symptoms for a cracked shaft.

Significant changes in vibration did not occur until the crack had developed to a point where failure was imminent. Obviously it would be better to diagnose a cracked shaft when cracking initially occurs and continued operation is feasible. Given a mechanism to track the degree of cracking, shaft replacement can be scheduled under non-crisis conditions. To this end, the available data was analyzed to determine if there was evidence of cracking outside the data associated with crack rapid growth.

When the data was analyzed and the classical (i.e., synchronously averaged) vibration parameters were computed, the statistical uncertainty was also calculated. The uncertainty in the vibration parameters are shown in Tables 2 and 3 for the A and B pumps respectively. The uncertainties shown were calculated from 10 individual measurements, each measurement using 5 blocks of data.

The significant observations from the data in Tables 2 and 3 are: (1) the uncertainty in the calculated 2X and 3X magnitude and phase was large except in the B pump in 1990 and when rapid crack growth was occurring, (2) the uncertainty in the 5X parameters was generally low but no different under the two shaft conditions, (3) the uncertainty in the 1X magnitude and phase was significantly higher in the A pump when the shaft was cracked in 1989 but very low for the B pump (note that the shaft in pump B was in worse condition than pump A).

---

6 Normal nX vibration parameters are determined by synchronous averaging, i.e., computation of frequency spectra are all started when the shaft is at the same physical location, usually at the Keyphasor or tachometer location.

Figure 1. RxB Pump 1X Vibration Magnitude and Phase Transition to Unabated Propagation and Propagation

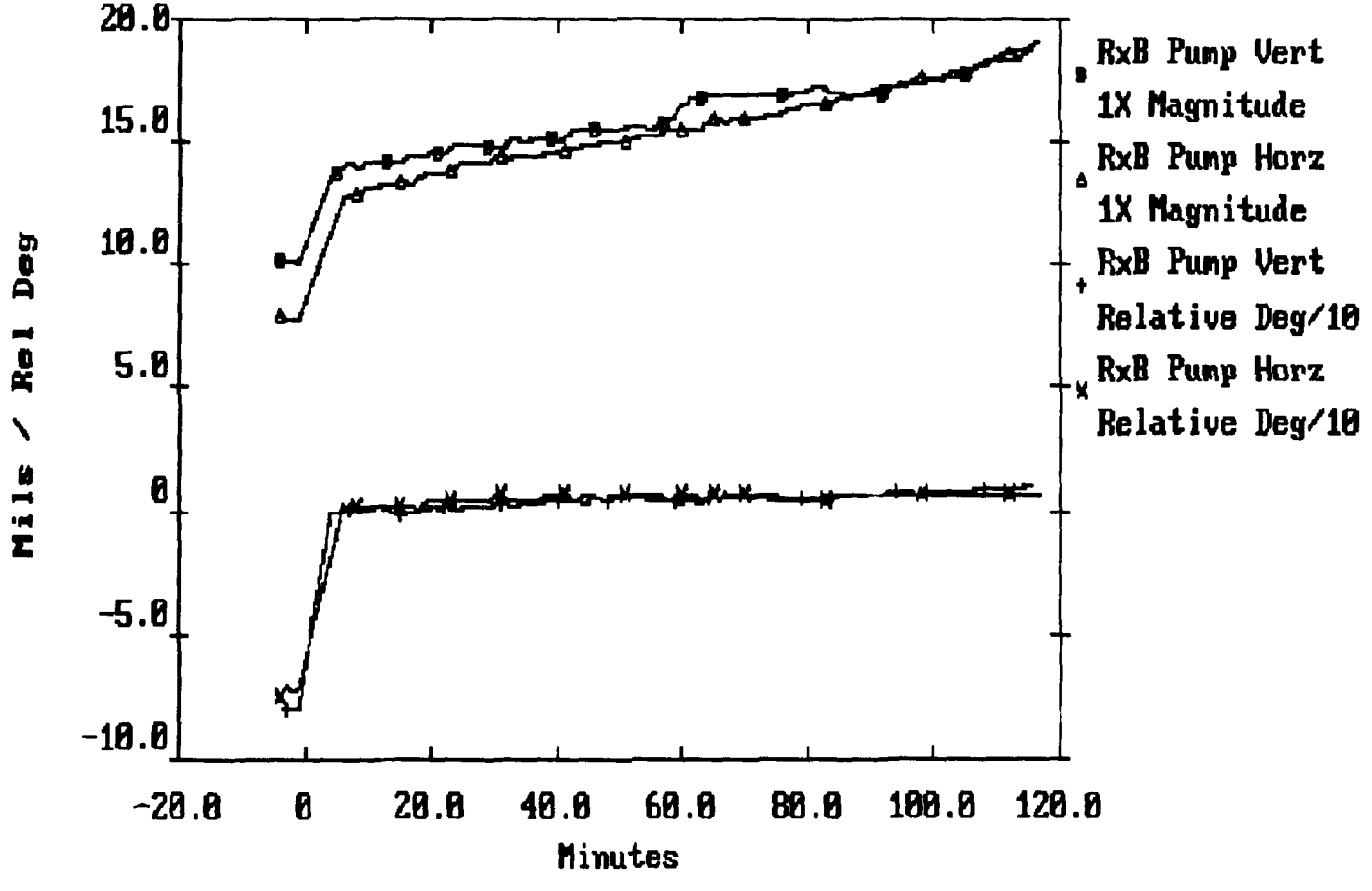

Table 1
Vibration Parameters for Shaft Before and After
Unabated Crack Propagation

Parameter[1]	Before[2]	After-Initially	After-2 Hours Later
Pump Horizontal Probe			
1X Magnitude	10.2	13.5	18.7
2X Magnitude	0.5	2.1	3.8
5X Magnitude	1.0	0.7	0.6
1X Phase	336.0	55.0	66.0
2X Phase	---	260.0	240.0
5X Phase	21.0	358.0	360.0
Pump Vertical Probe			
1X Magnitude	7.8	12.8	19.0
2X Magnitude	0.4	2.0	3.5
5X Magnitude	0.6	0.2	0.1
1X Phase	214.0	288.0	292.0
2X Phase	---	88.0	65.0
5X Phase	96.0	58.0	8.0

1. Magnitudes are in Mils, Peak-Peak. Phase values are in Degrees relative to the Keyphasor.

2. Where values are not listed, the uncertainty was too high to reliably determine a value.

Further analysis included trending the nX parameters using enough data values (or blocks) to reduce the uncertainty to a reasonable level. These results were also inconsistent, i.e., under the different cracked conditions the 1X magnitude and phase varied considerably for one of the pump probes, but not for the other companion probe located 90° away. This is shown in Figure 2 for the A pump phase at 1X.

In a paper presented at the 4th EPRI Incipient Failure Detection Conference[7] it

7 Andrew D. Dimarogonas, presented at the EPRI sponsored 4th Incipient Failure Detection Conference at Philadelphia PA, October 1990.

Table 2
Uncertainty in Vibration Parameters
Recirculation Pump A

Sensor	Parameter	Condition	1X	2X	3X	4X	5X
Pump A Vert	Magnitude (Percent)	1	11.4	15.0	28.9	9.9	1.2
		2	67.6	12.5	26.1	8.8	1.4
		3	2.1	23.5	14.1	10.0	3.2
		4	0.8	9.8	18.4	3.4	4.2
	Phase (Degrees)	1	12.6	110.0	130.0	21.8	5.1
		2	14.0	74.0	87.0	22.4	3.8
		3	3.4	53.9	59.5	11.9	3.4
		4	1.1	68.7	73.0	6.8	9.1
Pump A Horz	Magnitude	1	17.6	16.7	20.2	9.8	3.7
		2	30.4	20.0	20.6	7.2	3.8
		3	2.3	30.7	23.9	9.3	2.6
		4	0.2	9.8	22.7	3.7	8.7
	Phase	1	89.9	47.8	100.0	18.7	7.8
		2	35.0	12.0	100.6	13.4	7.2
		3	2.5	42.0	78.6	55.1	2.5
		4	1.4	20.5	75.9	7.3	7.2
Motor A IB Horz	Magnitude	1	1.6	6.5	2.5	1.5	2.8
		2	2.1	8.7	3.6	1.1	1.8
		3	2.8	17.0	14.1	0.8	1.4
		4	1.2	9.8	1.9	0.8	3.3
	Phase	1	2.9	5.8	5.3	3.2	4.4
		2	4.1	14.0	5.2	3.2	3.3
		3	7.0	38.6	16.2	2.8	2.9
		4	3.2	7.9	5.2	2.0	4.8

Conditions: 1-Cracked 1989, 2-Cracked 1989 (10 Days Later), 3-Presumed Cracked 1990, 4-Presumed Cracked 1990 (Day Later)

was stated that changes in the synchronous parameters may not occur in the shaft of a vertical pump for a circumferential crack of uniform depth. In this same paper, fairly complex models were determined to link the axial and torsional vibration modes of a shaft and their behavior under cracked conditions. It was suggested that an indication of a cracked shaft would first appear near the pump critical speed (non-running speed frequencies). To determine if such behavior was present in this data Power Spectral Densities were constructed using non-synchronous averaging techniques. Significant fluctuation between the 1X and 2X running speed

Table 3
Uncertainty in Vibration Parameters
Recirculation Pump B

Sensor	Parameter	Condition	1X	2X	3X	4X	5X
Pump B Vert	Magnitude (Percent)	1	0.8	22.4	17.6	15.6	1.1
		2	1.5	5.0	19.1	7.9	1.6
		3	0.5	3.8	8.0	15.8	3.5
		4	0.6	3.7	4.8	11.5	1.9
	Phase (Degrees)	1	1.8	52.3	21.9	53.1	2.8
		2	0.8	8.0	150.0	28.0	2.6
		3	1.0	6.0	16.8	35.8	2.8
		4	1.0	7.9	10.2	59.1	1.9
Pump B Horz	Magnitude	1	1.1	24.8	25.9	14.6	1.9
		2	1.3	2.9	19.6	34.0	7.3
		3	0.7	18.4	21.0	12.6	3.6
		4	0.6	15.4	6.4	8.3	2.4
	Phase	1	2.0	65.8	73.7	46.6	1.9
		2	1.2	5.3	9.9	8.1	10.0
		3	0.8	68.1	44.0	31.6	1.0
		4	1.2	32.2	10.6	29.4	2.7
Motor B IB Horz	Magnitude	1	0.9	4.6	2.7	0.8	1.9
		2	1.0	1.5	2.1	1.3	1.1
		3	1.4	2.5	0.7	0.6	0.8
		4	0.8	1.7	0.7	0.4	0.7
	Phase	1	2.9	6.5	3.3	1.6	3.0
		2	0.9	4.4	2.9	2.6	1.9
		3	1.7	5.1	1.5	1.0	1.1
		4	1.5	3.1	1.1	0.8	1.2

Conditions: 1-Cracked 1989, 2-Rapid Growth Crack, 3-Presumed Cracked 1990, 4-Presumed Cracked 1990 (Day Later)

frequencies was observed for the cracked shaft data on both pumps. For example, Figure 3 shows the PSD for the A pump during the 2 hour time period that the B pump was undergoing rapid crack growth. Similar behavior was also observed for the A pump in the August 1990 data set, but not in the B pump. In addition, PSDs measured the following day for pump A under presumably identical conditions did NOT show this same fluctuation.

Figure 2. RxA Pump Trend for 1X Phase
May 11, 1989 (Cracked Shaft)

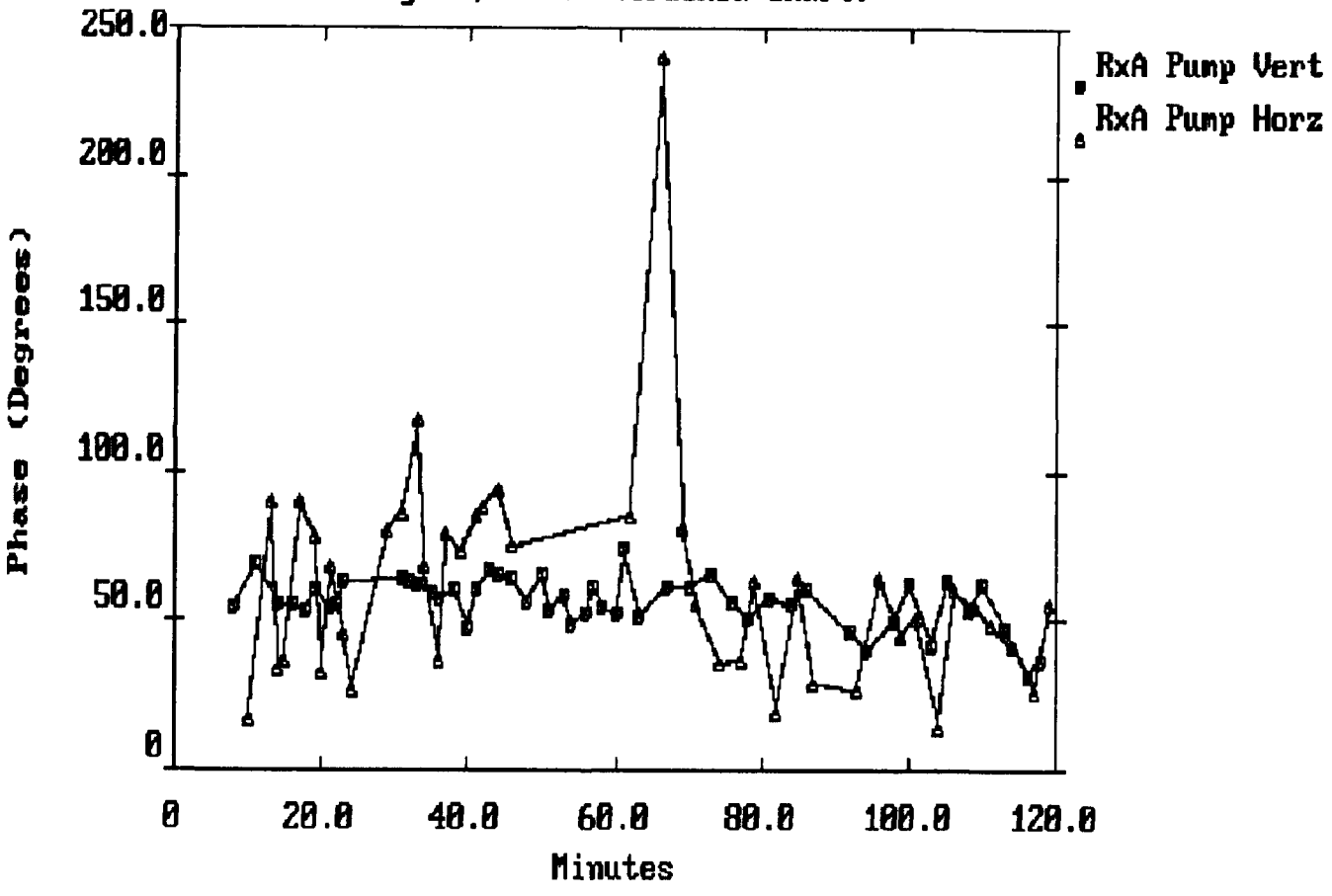

Figure 3. PSDs for Pump A Vertical Probe in August 1990 Over a Two Hour Time Period.

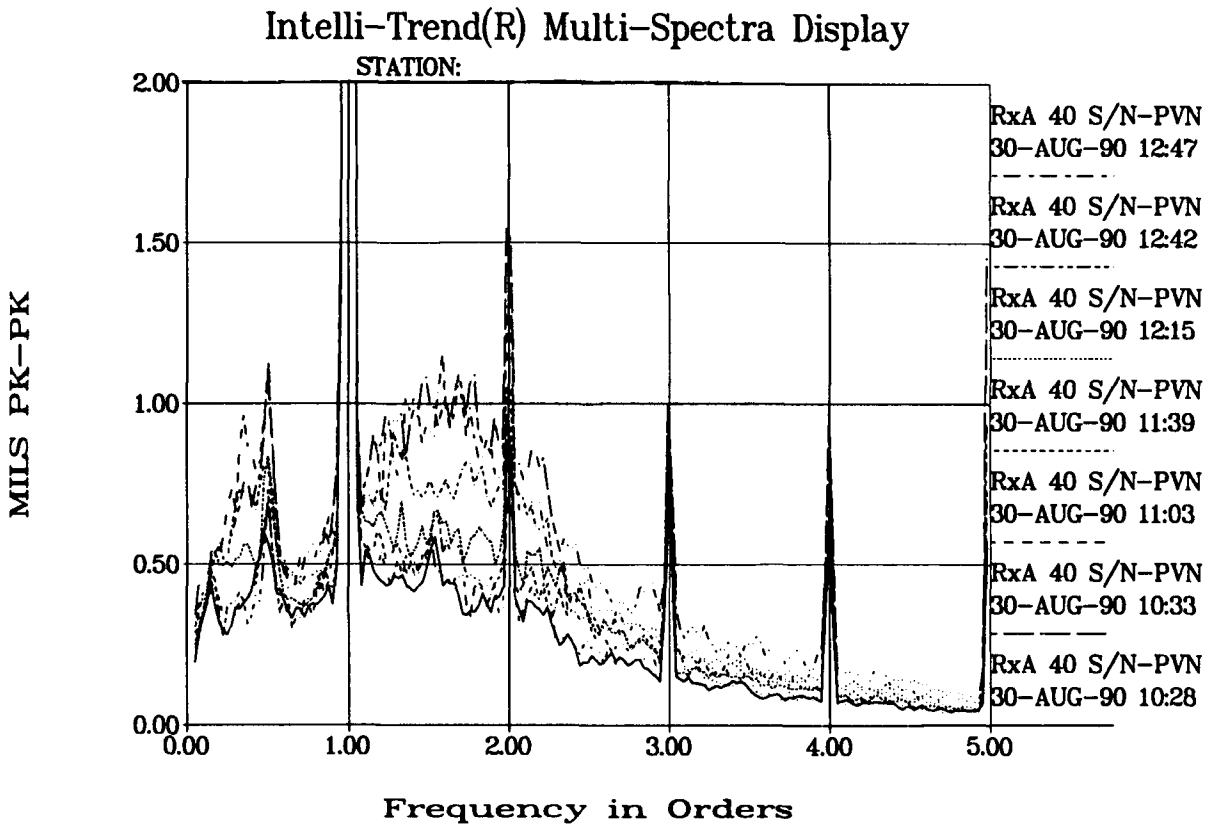

This suggests that process conditions may be the cause of such changes in the 1X-2X frequency range or could be the driving force for vibrations related to a cracked shaft.

The following general observations are made:

1. The uncertainty in vibration vectors (magnitude and phase) at running speed orders, can be large enough to mask a significant trend that could be an early indicator of a shaft crack.

2. Process conditions produce driving forces on the shaft which cause considerable fluctuation in vibration parameters even when the parameters are statistically reliable.

3. The behavior of nonsynchronous computed PSDs at non-running speed frequencies shows the same fluctuations stated above.

Conclusions:

1. Indications of a cracked shaft were NOT observed in the classical synchronous vector components of magnitude and phase at running speed orders until the crack attained an unabated propagation stage.

2. The uncertainty in the synchronous parameters should be quantified and *included in any monitoring program so accurate comparisons* between data sets can be made and potential changes in the process or the machine can be observed.

3. Vibration between 1X and 2X (where the critical speed is suspected to be) and at other nonsynchronous frequencies, had, at times, an increased magnitude. This may be an indication of a shaft crack, but the data was not conclusive.

Recommendations: Continuous monitoring is required to adequately quantify shaft behavior. Therefore a monitoring system should be capable of doing the following:

1. Calculation of classical, synchronously computed vibration vectors of magnitude and phase and their uncertainty at the running speed orders. The system should automatically trend these parameters over time at hourly intervals for later engineering observation and analysis.

2. Calculation of the signal energy and its uncertainty between running speed orders for nonsynchronously computed PSDs, again trended at least hourly. The magnitude of the fluctuations of the nonsynchronous signals should be quantified and trended.

3. Measuring the pump flow, or other condition related to flow.

PREDICTIVE/PREVENTIVE MAINTENANCE INTEGRATION AN APPROACH

Patrick P. Gehl
J B Systems, Inc.
Woodland Hills, CA 91367

Abstract: The constant furor for improved product quality and increased plant productivity demands that plant managers seek out the latest technology to keep afloat. One such technology is the integration of predictive software and maintenance management software. The combination of features found in these two software systems provides the plant manager with an extremely powerful productivity tool when properly applied. Several considerations must be evaluated, however, before such a software package should be implemented. These include the method used for data collection, the implementation steps and the operation of the combined software. Each of these considerations will be discussed on the following pages.

This review will deal only with analyzing vibration readings and not with oil analysis, temperature readings or other means of using predictive maintenance. These, however, could be included in a system using the discussed principles.

Data Collection: The goal in combining predictive and preventive maintenance techniques is to monitor the operation of a machine and perform preventive maintenance on the machine before it fails. One of the first decisions to be made by maintenance personnel is the means of monitoring to be used. The options are either continuous monitoring or manual monitoring.

Continuous monitoring has the advantages of always being current and requiring fewer labor hours after installation. The initial cost of obtaining on-line sensors and a controller and the labor for wiring the controller, however, is very high - upwards of $100,000. In addition, many of these systems require vendor supplied engineering to install.

The manual option is on the other hand, initially much less expensive; hand held or portable recorders cost under $10,000. This method does, however, require a maintenance person to "run" his route each time readings are obtained and therefore has an on-going labor cost. Manual monitoring is also extremely flexible because machines can be easily included or removed from the monitored route. With continuous monitoring, labor for wiring would be required to either add or disconnect machines.

Software is a second major consideration in combining predictive and preventive maintenance techniques. The implementor may either have software written by his data processing service or go to the market place and purchase the software. In either case, his considerations are the same. First, he must make sure that the predictive and preventive software can "talk" to each other. This simply means that the data analyzed by the predictive software can be passed on and used by the preventive software. The safest means of insuring this compatibility is to have both software segments written in the same computer language or use the same database manager and run on the same computer. If neither of these conditions are met, the likelihood of incurring operational problems is greatly increased.

Serious consideration should be given to the purchase of available software. Writing one's own software will take in excess of two or three man years and a lapse time of one year. Some excellent maintenance management packages are available for purchase; the ideal one would use the same database manager as the predictive software.

Implementation: The initial step in implementing a predictive/preventive maintenance system is to pick the plant equipment to be involved in the program. These will normally be those machines that are most critical to the plant's operation. Next, the contract or read points on each machine must be located in order to either attach the real time sensors or attach the portable data collector during the "running" of the route. The best way to locate the read points is to hire consultants, who are often available from the suppliers of the data collectors. Alternatively, the implementor can search through the machine manufacturers' literature and locate the read points, but this is an arduous task.

Upon locating the read points and either attaching the sensors to the machines and the controller or establishing the data collector contacts, the implementor must establish the signature wave from a properly operating machine. Again, this can be accomplished via consultants or from the manufacturers' literature. Once determined, this signature wave form will be used to compare against future wave readings to determine the operational state of the machine. The wave or curve is simply the vibrations picked up by the reader (on-line or portable). The vibrations are analyzed by a mathematical filter, usually a Fourier Transform, and stored in a digital format to be read by the predictive software.

It is now time for the implementor to turn his attention to the maintenance management software. This package will produce two types of work orders - preventive and corrective. For now let's only examine the preventive. The normal function of the preventive work order is to tell either a craftsman or the computer that a predetermined series of steps or procedures are to be followed. The frequency to produce these work orders is also a function of the maintenance management software.

In terms of running a predictive program, these procedures indicate that is time either for the computer to read the on-line sensor vibration data or to have a craftsman load the read route into the portable data recorder and manually collect vibration signals. This route consists of machine ID's and read points on the machines. The route is transmitted to the portable recorder by attaching a cable between it and the computer and executing a "load the route" program. Normally, several routes can be loaded into the portable recorder.

Having established his recording method, reading frequencies and the machine wave signature, the implementor is now ready to begin operation.

Operation: The Scheduler and/or Planner for the Maintenance Department initiates the first step in executing the predictive program. He does this by generating the preliminary maintenance schedule for his planning horizon. This schedule comes from the maintenance management part of the software and lists all of the tasks needed to take the vibration readings for the machines to be monitored. After sorting through the preliminary schedule, the planner

determines the actual work schedule. This schedule is in turn used by the maintenance management software to generate the work orders to the craftsmen to carry out the prescribed tasks. In general these will be preventive tasks and predictive tasks.

The predictive task or work order will instruct the craftsman to run the computer program to load the read routes into his portable data collector and proceed to collect the machine vibration readings. In practice, the craftsmen will normally only load the route into the data collector and not produce the route on hard copy. However, a properly designed predictive/ preventive package will permit him to produce the route both ways. A hard copy route should be in the form of a work order that lists the route ID, the machine ID and the read points. Figure 1 shows the form of such a work order. Only a few points are listed on the first page of what will often be a multiple page work order.

PREVENTIVE MAINTENANCE WORK ORDER

PREDICTIVE MAINTENANCE MONITORING ROUTE

Date	:	04/12/88		Work Order No.	: 500003
Page	:	1			
Asset Number	:	FAC1020S		Work Priority	: 2
Asset Code	:	15WES		Safety (Y/N)	:
Asset Desc	:	Paper Machine #2 Dryer Section			
Location	:	Pine River Pulp Mill		Orig Date	: 4/22/87
				Orig Time	: : 0
Requested By	:	PM	Fault Code: PM	Action Code: PM	
				DUE DATE	: 5/02/87
Planned By	:	DLS	LPM Date: 6/15/87	SCHED DATE	: / / 0
				SCHED TIME	: : 0

WORK REQUESTED/PROBLEM: MONTHLY MONITORING ROUTE - 85 POINTS

Support Required

ROUTE: 403M

ITEM	POINT	TRAIN	POINT ID	MEAS
1	00001	NO. 2	DRYER 10 AXIAL	IPS
2	00002	NO. 2	GEAR 11-1 AXIAL	IPS
3	00003	NO. 2	GEAR 11-2 AXIAL	IPS
4	00004	NO. 2	DRYER 11 AXIAL	IPS
5	00005	NO. 2	GEAR 11-3 AXIAL	IPS
6	00006	NO. 2	GEAR 11-4 AXIAL	IPS
7	00007	NO. 2	DRYER 12 AXIAL	IPS
8	00008	NO. 2	GEAR 13-1 AXIAL	IPS
9	00009	NO. 2	GEAR 13-2 AXIAL	IPS
10	00010	NO. 2	DRYER 13 AXIAL	IPS
11	00011	NO. 2	GEAR 13-3 AXIAL	IPS
12	00012	NO. 2	GEAR 13-4 AXIAL	IPS
13	00013	NO. 2	DRYER 14 AXIAL	IPS
14	00014	NO. 2	GEAR 15-1 AXIAL	IPS
15	00015	NO. 2	GEAR 15-2 AXIAL	IPS
16	00016	NO. 2	DRYER 15 AXIAL	IPS
17	00017	NO. 2	GEAR 15-3 AXIAL	IPS
18	00018	NO. 2	GEAR 15-4 AXIAL	IPS

STATUS CHANGES

Status: ____ Date: __/__/__ Time: __ : __ Status: __ Date: __/__/__ Time: __ : __

LABOR

EMPLOYEE #	ACTIVITY	HOURS	TYPE

Maint __/__/__ __ : __
mo day yr time

FIGURE 1

Armed with his portable recorder the craftsman begins to run his route, storing the vibration readings in the recorder. Upon completing all of his routes, the craftsman returns the portable recorder to have the readings uploaded into the predictive software program. This program analyzes the vibration recordings and compares the resulting operational curve for each machine to that of its signature curve.

This attempted comparison will produce one of three results. First, if a machine to be read was not operating, the data would not be collected and the predictive program would record this fact. Second, if the operating vibration curve is found to be within predetermined limits of the signature curve, proper machine operation would be signified. Third, if the operating vibration curve is found to be outside the predetermined safety limits the signature curve, an alarm state would be signified.

The degree to which the vibration curve is over the limit dictates in which "alarm" state the predictive software places the machine. Normally there are only two alarm states generated by a predictive maintenance program: (1) Not an emergency - corrective maintenance should be scheduled or (2) Emergency work order should be created and the machine should be taken out of service at once.

The identical analytical process is carried out by the predictive software regardless of whether the vibration readings are obtained from on-line sensors or from the portable recorder. The difference between the two processes obviously is that the on-line sensors can give a continuous state reading to the predictive software.

The predictive software generates a data file of the analytical results to be processed by the maintenance management software. This data file should consist of the work order number associated with each route, the labor hours spent running the route, the machine ID, read point ID's and alarm for each alarm state found. There is a flag set for each machine which was not operating when the reading was to be made.

The maintenance management software is now ready to examine the information passed to it by the predictive software. The function of the maintenance management software is to:

1) Close out the predictive route work order for all machines which were read and found to be operating properly.

2) Capture the labor cost associated with running the predictive route.

3) Produce an exception report for all machines not read during the route.

4) Procedure a corrective work order for all machines found to be in alarm state.

5) Automatically set the schedules for generating future predictive routes.

This combination of predictive and maintenance management software gives the user the capability of obtaining the maximum productivity from his plant's equipment.

Summary: The integration of predictive and maintenance management software, properly implemented, can provide a company with an extremely effective productivity tool. The availability of both predictive and maintenance management software makes it rather straight forward to structure such a combination. A few simple steps must be followed, however, regardless of whether the software is purchased or written in-house. These include the following:

1) Select the means of machine monitoring.

2) Choose the machines to be monitored.

3) Determine the points of the machine to be mounted.

4) Establish the frequency of the monitoring.

5) Determine the signature wave formed by the machines when operating properly.

6) Create PM type frequency tables to be used in creating work orders which instruct the craftsmen to run their read routes to collect vibration readings.

7) Begin operating the combined software system by generating the predictive work orders.

8) Assign the predictive work orders to a craftsman to run the route and collect the readings.

9) Upload the readings into the analytical software and run the predictive software to identify alarm conditions.

10) Run the management software to produce corrective

work orders for all machines in the alarm state and to close out the predictive work order for all machines. This process also captures the labor data which was collected with the vibration data.

11) Close out the work order capturing the labor and spares data after the corrective work is accomplished.

12) Continue the process for all run frequencies in the system.

These steps are depicted in Figure 2.

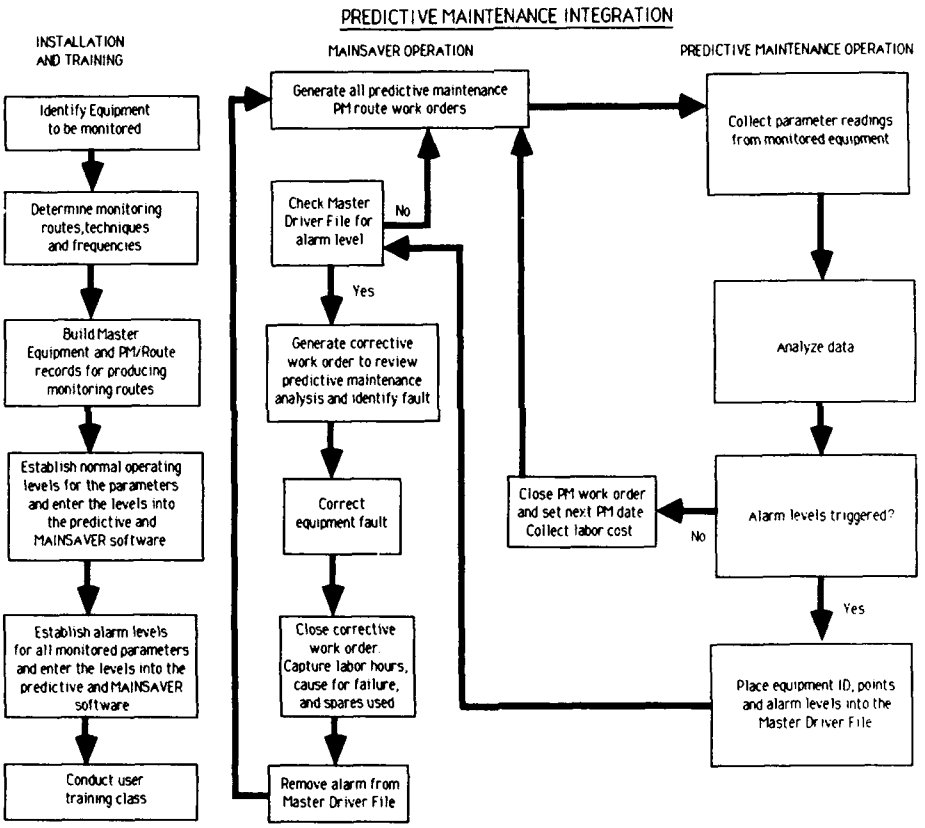

Figure 2

The logical next step to improve the combination of predictive software and maintenance management software would be to insert an "expert software package between the two software packages. With this software addition, the corrective work order could be generated with detailed instructions for repairing the machines involved.

FAILURE MECHANISMS

Chairman: M. Nabil Bassim
The University of Manitoba

FRACTOGRAPHY IN IDENTIFYING FAILURE MECHANISMS

J.I. Dickson, S. Lalonde and Li Shiqiong
Département de Génie Métallurgique
Ecole Polytechnique
P.O. 6079, Station A
Montreal, Que., Canada, H3C 3A7

Abstract: Two macrofractographic principles useful in failure analysis are presented. The first concerns the interpretation of crack splits or crack branches on the fracture surface in order to determine the crack propagation direction. It is particularly useful in analyzing gray cast iron fractures. Apparent crack splits observed on a ductile fracture are also discussed. The second principle concerns the influence of a biaxial stress on chevron patterns. It can be useful in determining fracture sequences in collapsed structures. Some microfractographic features useful in identifying fracture mechanisms are also presented. Features observed on slow crack growth regions of a galvanized structural steel bar permitted to identify the failure as produced by hydrogen-assisted cracking. The similarity between the microfractography of near-threshold fatigue cracking and transgranular stress corrosion cracking is also briefly described and discussed.

Key Words: biaxial stress; chevrons; collapsed structures; crack branching; crack splits; failure analysis; fractography; fracture mechanisms; gray cast iron; hydrogen embrittlement; stress corrosion cracking, threshold fatigue cracking

Introduction: Fractography is a very useful tool in both failure analysis and for identifying fracture mechanisms in fracture research. The basic macro-and microfractographic principles are well known and have been well documented. In the present paper, a few less well-known macrofractographic principles which have proved useful in failure analyses performed by the authors will be described. A few less well-known microfractographic features which help identify fracture mechanisms in both failure analysis and in fracture research will also be described.

Macrofractographic principles:

The Y-principle applied to crack branching (crack splits): In performing failure analysis on lamellar graphite, gray cast iron components, it is often very difficult to determine the site of fracture initiation from the lines on the fracture surface. For this material, interpreting the macroscopic river lines on the fracture surface is not very reliable. This difficulty appears to result from cracking occurring first in the relatively weak graphite phase ahead of the macroscopic crack tip. In our experience, it is much more useful to identify and to

interpret the sites at which the crack has split into two branches, even if one of these has only propagated a short distance. In such cases, employing a "Y" principle (Figure 1), whereby the crack propagates from the base of the Y towards its branches, the local crack propagation direction can be established.

In our experience, the use of this principle is very reliable for identifying the crack propagation direction at the larger crack branches or crack splits. Most large fracture surfaces of gray cast iron components present a number of crack splits or branches, which are well visible with the unaided eye (Figure 2). The smaller more microscopic branches or splits observable in a low-power optical microscope are not as reliable; nevertheless, in our experience, the large majority of these also indicate correctly the crack propagation direction. The use of this principle has proved very useful in helping to identify the approximate crack initiation site in gray cast iron components which failed producing large fracture surfaces as well as often in components which failed producing much smaller fracture surfaces. Moreover, on most of these fracture surfaces, the crack initiation site could not be correctly identified macrofractographically without using this principle.

Although we have found this same principle to also be of use in analyzing some failures of other brittle castings, it should not be considered as completely general and should not be applied blindly to all materials and all types of fractures. On ductile fracture surfaces of steel welds in H-beams, we have observed (Figure 3) quite similar macrofractographic features in which the crest of such apparent crack splits pointed systematically in the direction in which the crack was propagating, as determined from the aspect of the shear lips and from non-fractographic considerations. In this case, applying the Y principle would have systematically given an error of 180° in the crack propagation direction. These macrofractographic features on this ductile fracture surface were associated with a crack plane which was changing orientation. The observations indicated that these features could be interpreted as resulting from a segment of the crack locally resisting the change in crack plane orientation dictated by the geometry, while the crack segments to both sides followed better this change in crack orientation and then undercut the portion which had undergone less of a change in orientation. Once the cause of this fractographic feature was understood and found to give a reliable indication of the crack propagation direction, it proved useful in analyzing the detailed aspects of the fracture of other components implicated in this same failure, which was that of a strut bridge.

The influence of a biaxial stress on chevron markings: Another macrofractographic principle which proved much more useful in the study of this strut bridge failure concerns the influence of a biaxial stress state on the chevron patterns of the H-beam plates. When a large structure constructed from different beams fails producing fracture surfaces in a number of beams, it can be difficult from the fractographic evidence to determine the fracture sequence. In this case, three struts had failed on each side of the river, and the side of the bridge which failed first was clearly identifiable from the macrofractographic evi-

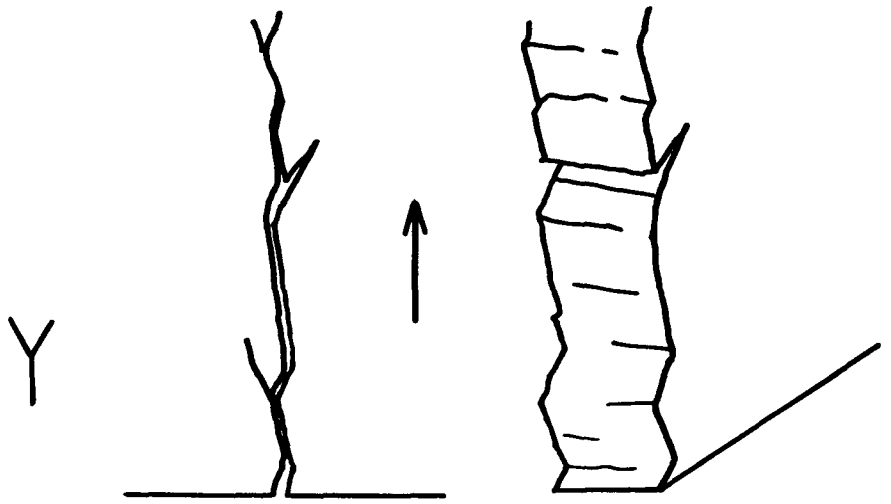

Fig. 1. Schematic representation of the Y-principle applied to crack branching. The propagation is in the direction indicated by the arrow. The crack splits resulting from branching are usually observable with the naked eye or at low magnification.

Fig. 2.

Fig. 3.

Fig. 2. Aspect of a crack split observed on the surface of a large diameter gray cast iron pipe. The crack propagation direction is indicated by an arrow.

Fig. 3. Example of crack splits observed on a ductile fracture of an H-beam weld. In this case, this feature results from small crack segments which resist the change in crack orientation dictated by the geometry of the component. The crack propagation direction is in the direction indicated by the arrow.

dence. To determine which of the three possible struts failed first on the side at which the failure had initiated, the effect of the failure of one or two struts on producing a second tensile or compressive stress parallel to the width of the plate and parallel to the fracture surface on the remaining strut(s) was considered, since it was noted that some of the chevron patterns were very different from the others.

Each strut failure produced a fracture surface perpendicular to the length of the plate under the effect of the weight of the bridge, which produced the primary bending moment. The fracture surface was always perpendicular to the tensile stress from this bending. The previous failure of other struts on the same side added a secondary bending moment. The principal stress from this secondary bending moment acted parallel to the fracture plane and in the direction of the plate width.

Two types of chevron patterns were observed on the different fracture surfaces situated on or near the end plates. In most cases, the point of the chevron pattern was situated near the quarter thickness of the plate, as schematized in Figure 4a, and their aspect indicated that the crack did not experience any difficulty in propagating. On two different fracture surfaces which came from the same strut, the point of the chevrons was situated very close to the external surface and the river lines were very pronounced and tended to propagate preferentially across the plate thickness, as shown in Figure 5 and schematized in Figure 4b. This was an indication that crack propagation parallel to the plate width was very difficult near the lateral surface at which cracking had initiated. On one of these fracture surfaces, in fact, propagation in this lateral direction was sufficiently difficult, that at two sites there was crack reinitiation before the plate had completely fractured. This aspect permitted to identify the chevrons of the type shown in Figures 4b and 5 as having propagated under a biaxial tension-compression stress state. A few of the macroscopic river lines propagating across the plate thickness actually changed direction very near the plate surface opposite to that at which initiation had occurred (Figure 5), indicating that propagation became easier as the secondary compressive stress was reduced. The compression stress arose from the other two struts having already fractured and from the bridge already leaning to one side. This biaxial stress state resulted in a low hydrostatic component of stress for propagation in the direction of the width. This was clearly reflected in the aspect of the chevron patterns, in the very marked macroscopic river lines propagating preferentially in the plate thickness direction and in the need to reinitiate the propagating crack twice before obtaining final fracture. The more classic chevron pattern indicated in Figure 4a resulted from cleavage cracks which had propagated under a biaxial tension-tension stress state, which is more favourable to lateral cleavage propagation because of the higher hydrostatic stress component which results.

This macrofractographic study of the fracture surfaces of the different components which had fractured was performed not having visited the failure site and not having being shown photographs of the failed bridge (so as not to risk biasing the study which was to be based completely on the fractography of the fractured components) until the study was completed and the preliminary report had been written. Subsequent study of the detailed photographs of the collapsed bridge quickly indi-

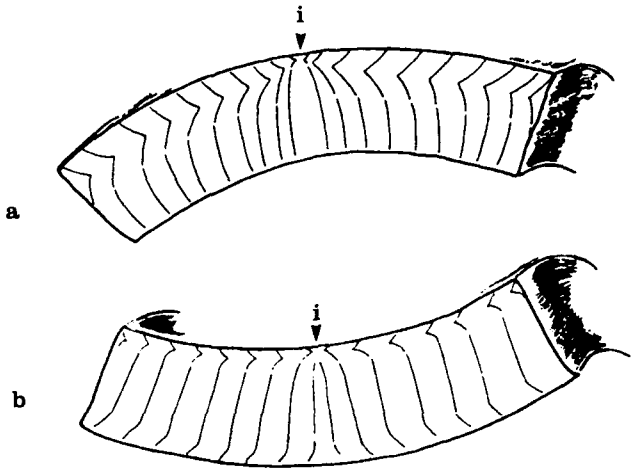

Fig. 4. Schematic representation of the aspect of chevrons produced under a biaxial stress state due to the effect of two perpendicular bending moments. In a) the biaxial stress state is tension-tension; in b) it is tension-compression.

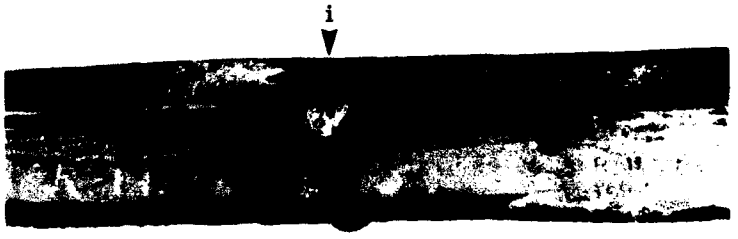

Fig. 5. Aspect of chevrons produced under tension-compression biaxial stresses.

cated, from the manner in which the bridge had deformed, from its final position and from the relation of this position to the land topography that the only possible fracture sequence was that which had been established by the fractographic study. It was not possible to identify completely from the photographs of the collapsed bridge whether the middle strut or a side strut had failed first, while the fractographic study permitted to identify which of these two struts had probably failed first, by the presence of three crack arrest marks on the fracture surfaces of the more likely candidate, with crack reinitiation then occurring by ductile fracture before retransforming to cleavage propagation.

Microfractographic features permitting to identify fracture mechanisms:

Microfractographic features of a hydrogen embrittlement failure: The first type of microfractographic feature which will be described were found on a part brought in by a student for a laboratory failure analysis case study course. The part which failed corresponds to a mild steel galvanized bar used as a man-hole type rung ladder. The fracture produced three almost semi-circular portions of the fracture surfaces corresponding to slow crack-propagation covered with corrosion product which was difficult to remove. The presence of these cracks resulted in a brittle (cleavage) fracture when a worker accidentally dropped his tool chest on the rung. Cleaning of the fracture surface in a dilute, inhibited HCl solution resulted in the removal of the corrosion product from the freshest portion of the slow crack growth regions. Study of the cleaned regions by scanning electron microscopy showed that the slow crack growth had occurred partly by a cleavage-type fracture and partly by an intergranular fracture, with a very large number of crack reinitiations ahead of the previous crack tip (Figures 6-8). These reinitiations generally were situated at grain boundaries (Figures 6-8) and at times in the vicinity of inclusions at grain boundaries (Figure 6). As well, localized deformation markings were present on the fracture surface in the region of many of the crack reinitiation sites (Figures 6a, 7 and 8). Some of these localized deformation markings appeared to indicate logical intermediate positions of the crack front of these newly initiated crack segments (Figures 7 and 8).

These different observations clearly demonstrated that the slow fracture portion of the fracture surface had been caused by hydrogen-assisted cracking. The galvanized coating resulted in a cathodic potential favouring the entry of hydrogen at sites where the coating was damaged near the curved portion of the bar. The stresses causing this cracking were probably residual stresses which resulted from metal forming. The microfractographic aspects of the fracture surface showed several interesting features with respect to the cracking mechanism, including frequent initiation of cracking at grain boundaries and inclusions (both types of interfaces are traps for hydrogen) and the presence of line features indicating considerable localized plasticity about the newly reinitiated crack portions. These indications of localized plasticity at the crack reinitiation site are particularly interesting in light of the suggested role of such plasticity in hydrogen-assisted and other environmentally-assisted cracking mechanisms [1].

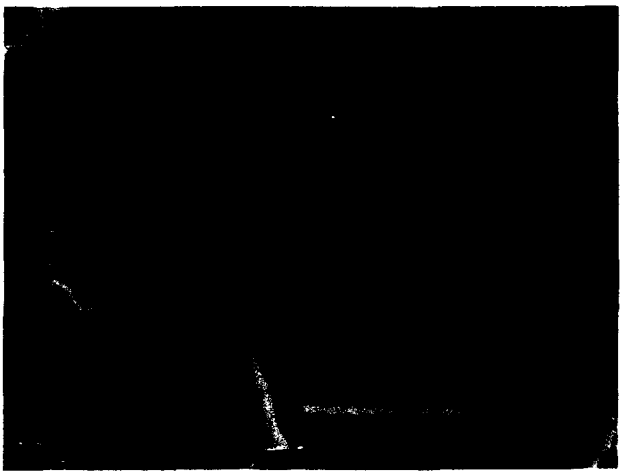

a)

b)

Fig. 6. Typical crack reinitiation sites observed on the fracture surface of a galvanized structural steel bar. Crack reinitiation is situated at the grain boundaries and at times at or near inclusions at these boundaries. Fig. 6a shows an inclusion at the initiation site and a few line-markings near this site.

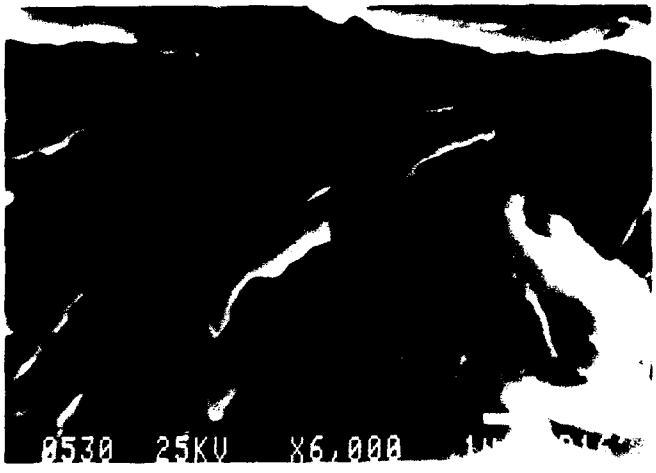

Fig. 7. Localized deformation markings observed in the vicinity of a crack reinitiation site observed on the galvanized steel bar. Their aspect suggests that they correspond to intermediate crack front positions.

Fig. 8. Localized deformation markings present mainly on a small intergranular portion of the fracture surface in the vicinity of a crack reinitiation site. The aspect of some of these lines, particularly those on the transgranular cleavage facets ahead of the arrow, indicate that they correspond to intermediate crack front positions.

Microfractographic similarities between stress corrosion cracking and near-threshold fatigue: The last microfractographic aspect which will be briefly considered concerns the similarity between the microfractographic features of transgranular stress corrosion cracking in face-centre cubic metals and of near-threshold fatigue cracking. In both cases, the microfractographic primary facets (Figures 10-12) are very crystallographic and can be very flat with a cleavage-like aspect [2-8]. In both cases, the primary facets are found to present microfacets (Figures 9-12) under certain conditions, with these microfacets corresponding in f.c.c. metals to {111} planes and therefore to slip planes [2-8]. It has also been shown [4,5] in metals of other crystalline structures that the microfacets associated with near-threshold fatigue cracking also correspond to slip planes (Figure 12). In the case of stress corrosion cracking, the microfacets tend to become larger and clearer with increasing stress intensity factor K [7,8], indicating that these facets indeed follow slip planes. In both types of fractures, the primary facets correspond to a plane bisecting one of the angles between the planes of the microfacets. For austenitic stainless steels during stress corrosion cracking, the primary facets generally correspond [6-9] to {100}; for α-brass (Figure 11) and copper-based alloys, these [8,10] generally correspond to {110}. In contrast, for near-threshold fatigue of f.c.c. metals, large {111} facets are favoured by very low da/dN and ΔK values [3,4], since this favours slip which is highly localized on individual slip planes, while higher values of da/dN and of ΔK result in primary facets (generally {100} in f.c.c. metals) which bisect the angle between the microfacets, indicating that, for these conditions, slip is favoured on two slip planes symmetrically oriented with respect to the average crystallographic fracture plane. Other primary facet orientations can be obtained such as {110} and {111} (Figure 10a).

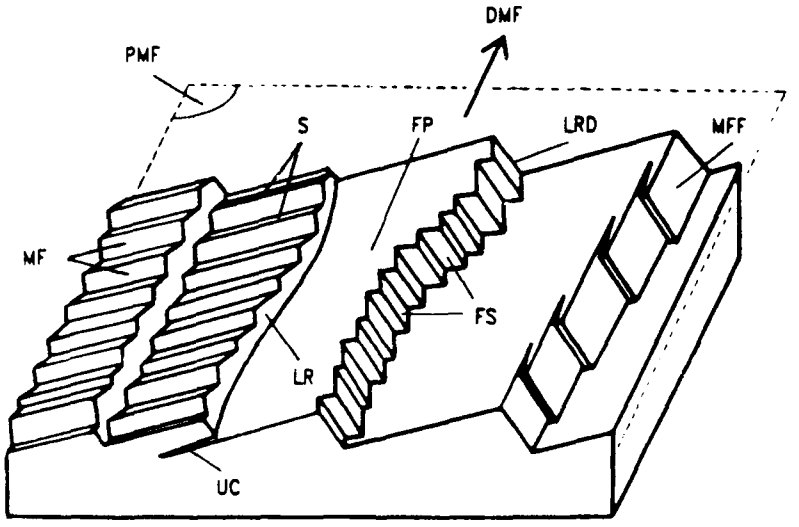

Fig. 9. Schematic representation of the crystallography of transgranular stress corrosion cracking and near-threshold fatigue. The primary facets FP often can be shown to consist of two sets of microfacets (MF). Sheet-like microfacets MFF are at times found for stress corrosion cracking at high K [7].

a)

b)

Fig. 10. Comparison of more complex microfractographic features of a) near-threshold fatigue cracking [2] and b) stress corrosion cracking [7] of 316 stainless steel. The cracking crystallography is identical except for the feathery aspect in b), which results from the presence of numerous sheet-like {111} microfacets during stress corrosion cracking at high K. The etch-pits produced in a) permit to identify the presence of primary {100}, {111} and near-{110} primary facets, with the last type consisting clearly of two sets of {111} microfacets.

Fig. 11. Microfractography of stress-corrosion cracking of 70Cu-30 Zn in an ammoniacal solution. The primary facets are {110} and two sets of fine {111} microfacets are also present [8].

Fig. 12. Microfractography of near-threshold fatigue of Fe-3% Si [5]. The primary {100} facets consist of two sets of microfacets consistent with {112} orientations.

While the cracking crystallography can be explained as being produced solely by shear (reversed slip) in the case of fatigue cracking since reversed plasticity results from the fatigue cycling, this is not the case for stress corrosion cracking produced under a monotonic load or displacement. This then suggests that this transgranular stress corrosion cracking should involve both localized slip as well as cleavage cracking which on a very microscopic scale follows {111} slip planes [7,8]. These aspects then indicate that the stress corrosion cracking mechanism may incorporate aspects of the theories based on the environment enhancing localized plasticity [1,11] and those on the environment embrittling a small zone of material in the vicinity of the crack tip [9,12]. The observations indicate that the influence of the environment or of the "corrosion" is to favour local conditions which favour slow crack propagation, which, however, involve fracture mechanisms which, from the fractographic evidence, appear to be basically mechanical in nature.

The fatigue near-threshold fractographic features in b.c.c. metals as well as in h.c.p. titanium also indicate [4,5] that the cracking involves decohesion on microfacets which are along pairs of slip planes, with the average orientation of the primary facets then generally being a bisector of the angle between these slip planes. Such observations indicate clearly that such near-threshold factigue involves decohesion on the slip planes which have been active at the crack tip. It is less clear but certainly possible that such cracking may also involve a cleavage or cleavage-like component to produce the decohesion on the microfacets. In f.c.c. metals, especially when the orientation of the near-threshold primary facets are perpendicular to the tensile axis, the microfacets are often not discernible. This is also often the case for stress corrosion cracking in f.c.c. metals at low K values, although the stress intensity factor at which these microfacets become visible also depends on the material [6,7]. When they are not visible, it is either that the microfacets are too fine to be detected or that they are not present. That these become visible at higher K values in stress corrosion cracking or on primary facets less perpendicular to the tensile stress in near-threshold fatigue suggests that they are not observed because they are too fine to be resolved. If they are in fact not present a cleavage-like mechanism or a localized plasticity mechanism of the type proposed by Lynch [11] appears required to explain these microfractographic features.

The presence of the microfacets parallel to slip planes on the transgranular stress corrosion cracking fracture surfaces, while not permitting to identify completely the fracture mechanism indicates that this mechanism must be able to account for these features. Most mechanisms which have been previously proposed must at least be modified to be able to account for these features, the existence of which has often not been noticed.

Conclusions: Macrofractography is very useful in failure analysis, especially for helping identify the sites of crack initiation. Some less well-known macrofractographic principles can be useful in such studies, for example, by employing the Y-principle to identify the local crack propagation direction on fracture surfaces of lamellar gra-

phite, gray cast irons. A biaxial state of stress can have a strong influence on the chevron patterns produced during brittle fracture of steel plates. Knowledge of this influence can be very useful in identifying the fracture sequence in the failure of large multi-component structures.

Detailed microfractography is one of the most important tools in identifying fracture mechanisms. If the fracture surface has not been damaged after fracture, any proposed fracture mechanism must be fully compatible with the detailed aspects of the fracture surface.

Acknowledgments: The authors are grateful for financial support from the NSERC (Canada) and FCAR (Quebec) research support programs.

References:

1. S.P. Lynch, Metallography, Vol. 23 (1989), pp. 147-171.
2. J.I. Dickson, Li Shiqiong and J.-P. Baïlon, in " Fatigue 87", R.O. Ritchie and E.A. Starke (eds.), EMAS Ltd., Warley, England, 1987, Vol. 2, pp. 759-768.
3. J.-P. Baïlon, J.I. Dickson and Li Shiqiong, in "Basic Mechanisms in Fatigue of Metals", P. Lukas and J. Polak, Academia Press, Prague, 1988, pp. 361-371.
4. J.-P. Baïlon, J.I. Dickson, Li Shiqiong and D. Larouche, in "Fatigue 90, H. Kitagawa and T. Tanaka (eds.) MCEP Ltd, 1990, Vol. 3, pp. 1333-1343.
5. Li Shiqiong, J.I. Dickson and J.-P. Baïlon, in "Fatigue 90", H. Kitagawa and T. Tanaka (eds.) MCEP Ltd, 1990, Vol. 3, pp. 1375-1380.
6. J.I. Dickson, D. Groulx, Li Shiqiong and D. Tromans, Mater. Sci. Eng., vol. 94 (1987) pp. 155-73.
7. Li Shiqiong, J.I. Dickson, J.-P. Baïlon and D. Tromans, Mater. Sci. Eng. A, vol. 119 (1989) pp. 59-72.
8. J.I. Dickson, Li Shiqiong and J.-P. Baïlon, to appear in "Corrosion sous contrainte: phénoménologie et mécanismes" Proceedings of a conference at Bombannes, France, September 1990.
9. T.Magnin, R. Chieragatti and R. Oltra, Acta Metall., vol. 13 (1990) pp. 131-1319.
10. J.A. Beavers and E.N. Pugh, Met. Trans. A, vol. 11A (1980) pp. 809-820.
11. K. Sieradzki and R.C. Newman, Phil. Mag. A, vol. 51 (1985) pp. 95-132.
12. S.P. Lynch, Metal Science, vol. 15 (1981) pp. 453-466.

CATASTROPHIC TEMPERATURE INCREASE DURING THE SEPARATION OF HIGH STRENGTH ALLOYS IN TENSILE LOADING

D. D. Makel and H. G. F. Wilsdorf
Dept. of Materials Science
University of Virginia
Charlottesville, VA 22903

ABSTRACT: During the separation at fracture of tensile samples local plastic strain rates are typically orders of magnitude higher than the rates calculated using the gage length and the applied strain rate. This is due to two factors, strain localization and stored elastic energy. Necking, geometrical and textural softening, shear localization, i.e. sometimes including adiabatic shear, and ligament separation at void coalescence contribute to strain localization. Elastic energy stored in the test system dominates the driving force for deformation after the point of instability, when the rate of decrease in load-bearing capacity of the sample with elongation is greater than the rate of elastic load decrease in the test system as a whole due to elongation. During the separation process the high plastic strain energy density caused by localization and high plastic deformation rates combine to create favorable conditions for adiabatic heating. Our research has concentrated on the characteristics of this post-instability adiabatic heating, primarily to explain the presence of locally melted areas on the fracture surfaces of certain high strength alloys. Although the regions of local melting typically represent only a small portion of the total fracture surface area, melting at failure, which has been shown to be accompanied by visible light emission and the ejection of melted particles, is an important phenomenon, both for what it indicates about instability leading to separation and also for its technological implications regarding systems which may be unstable in the presence of high temperatures. It is suggested that knowledge of the requirements for the initiation of these important instabilities can help to guide a designer away from potentially dangerous combinations of materials and loading conditions.

Key Words: Adiabatic shear; catastrophic failure; ductile fracture; instability; localized melting; microroughening; open surface shear zones; strain localization; temperature increase; transition dimples

Introduction: During the past two decades the exploration of microstructural events at crack initiation and propagation as well as void coalescence has been spectacular [1]. However, applications of this new knowledge are still limited. In this paper an attempt is being made to show that the awareness of microstructural detail during fracture could be of assistance in possibly predicting the event of an unexpected and sudden failure.

In the course of post fracture scanning electron microscope (SEM) investigations of the fracture surfaces of Ti-8Mn [2] and Ti-10Al-2Fe-3V [3] tensile samples unexpected features were found at the outer edges of

large shear areas, typically shear lips [4,5]. These features include dimple-free bands (hereafter referred to as "Open Surface Shear Zones"), flat topped dimples ("Transition Dimples"), spheroidized dimple walls and surfaced debris, and a general fine surface roughening ("microroughening") [2,6,7]. These highly localized features, which are briefly described in Table I and examples of which will be given in the next section, were unexplainable in terms of a typical void initiation, growth and coalescence model prompting further research.

Microstructural Feature	Description
Open Surface Shear Zones	Dimple-free bands found at the perimeters of some shear areas (frequently shear lips). These are found on one but not both of the matching fracture surfaces.
Transition Dimples	Flat-topped dimples connected by a common shear plane, rather than the more typical sharp dimple walls.
Localized Melted Dimples and Surface Debris	Areas of shallow dimples which are separated by locally melted dimple walls and scattered with spheroidized melted debris.
Microroughening	Fine roughening of surfaces which form by separation through concentrated shear bands.

Table I. *Brief description of the unusual features found on the fracture surfaces of certain tensile loaded alloys.*

The presence of spheroidized and apparently melted bits of material on the fracture surfaces were particularly puzzling. A search of fractographs from different sources turned up structures called "knobbles" which are found above adiabatic shear bands on the fracture surfaces of ballistic impact samples [8]. Striking similarities between the observed spheroidized structures and the "knobbles" pointed to a possible role of adiabatic shear although adiabatic shear had never been reported and was generally considered to not occur in tensile samples [9,10].

As a next step selected samples were sectioned parallel to the tensile axis and these sections, such as the one shown in Figure 1, proved highly instructive [2,4-7]. Directly below the unusual spheroidized surface regions the microstructures showed indications of highly localized shear and this strengthened our suspicion that adiabatic shear might have played an important role in raising local temperatures to the melting point.

To check the possibility that the spheroidization was primarily an oxidation artifact tensile tests were performed in an argon atmosphere. Resulting fracture surfaces contained features identical to those found on the samples fractured in air [2,6,7], ruling out an oxidation mechanism for their formation.

At this point it was reasoned that if localized melting was actually occurring during separation visible light emission should also occur. Photos of the final separation process taken using an open shutter and fast film in a darkened room, such as the one shown in Figure 2, clearly

show not only visible light emission but also the ejection of bright bits of material away from certain areas of the fracture surfaces. When these photos were compared with SEM micrographs it was found that the areas of light emission correspond with localized surface areas containing spheroidized structures [2,6,7].

Figure 1: *Subsurface section below locally melted surface features of Ti-8Mn tensile sample.*

Figure 2: *Light flash caused by localized melting during the separation of Ti-6Al-4V quasi-static tensile sample.*

Further testing showed that localized melting can also be found on the surfaces of Ti-6Al-4V [2,11] and AISI 4340 steel tensile samples [12]. Heat treatment of the Ti-6Al-4V showed that localized melting is suppressed when the samples have a colony α microstructure [11]. Likewise, the localized melting in the AISI 4340 samples can be suppressed either by heat treatment or temperature, as long as the material in the region of separation is above the ductile/brittle transformation temperature range [12]. In the AISI 4340 samples localized melting was always accompanied by radial cracking, a sign of rapid crack propagation at failure [13,14,15] and, in an interesting twist, it was found that both radial cracking and localized melting could be suppressed by testing at high applied strain rates. Plastic energy analyses of the overall gage and neck deformation showed that this reduction in crack propagation rate with increasing applied strain rate was due to adiabatic heating of the incipient volume of separation above the ductile/brittle transformation temperature range [12].

Separation Model: Formation of the unusual surface features can be explained by a separation model which incorporates commonly excepted elements of ductile fracture and a highly localized shear event resulting from material instability. The following proposed model shows how this shear instability can provide conditions conducive to catastrophic temperature increase during final separation.

When a tensile sample or a structural member is strained beyond its ultimate strength the load bearing capacity of the piece decreases with further straining. As long as the decrease in elastic stress of the whole stressed system with strain is greater than the accompanying decrease in load bearing capacity straining can continue in a stable manner. When the decrease in load bearing capacity decreases faster than the decrease in elastic stress, however, the system becomes unstable and further deformation to fracture occurs rapidly, even when the applied strain rate

is low. In this manner extremely high plastic deformation rates typically occur during tensile separation regardless of the applied strain rate.

Except in the unusual case of a continuous reduction of area to rupture, separation during ductile fracture occurs by void initiation, growth and coalescence. Although specific sites for void initiation depend on both the material and the loading conditions in most cases of tensile loading voids begin to grow in areas of approximately plane strain (typically inside of a deforming member.) During this initial stage of separation the resulting surfaces usually grow approximately perpendicular to the tensile stress and as these voids grow and coalesce the cross sectional area remaining intact bears an increasingly larger stress. In tensile samples this initial separation results in the easily recognizable central crack portion of the fracture surface.

With sufficiently ductile material central crack growth ends when the deformation is localized by geometrical and/or textural softening into shear directions connecting the central crack to an outer surface. As deformation continues voids initiate and grow inside of the incipient shear lip region, further increasing the load on the remaining material.

Subsurface sections performed in our studies, such as the one shown in Figure 1, indicate that in certain regions the deformation in shear directions becomes localized into extremely thin planes. The microstructural features which result from this highly localized shear deformation are identical to deformational adiabatic shear bands and it is therefore quite reasonable to assume that softening of the rapidly shearing material actually causes the initiation of adiabatic shear bands. In this manner the initial shear localization may act as a precursor to the adiabatic shear bands in much the same way as localized shear deformation has been observed to initiate adiabatic shear in high strain rate shear studies [16,17].

Where bands of highly localized shear intersect with previously existing open surfaces they shear the surface onto the plane of deformation. Since

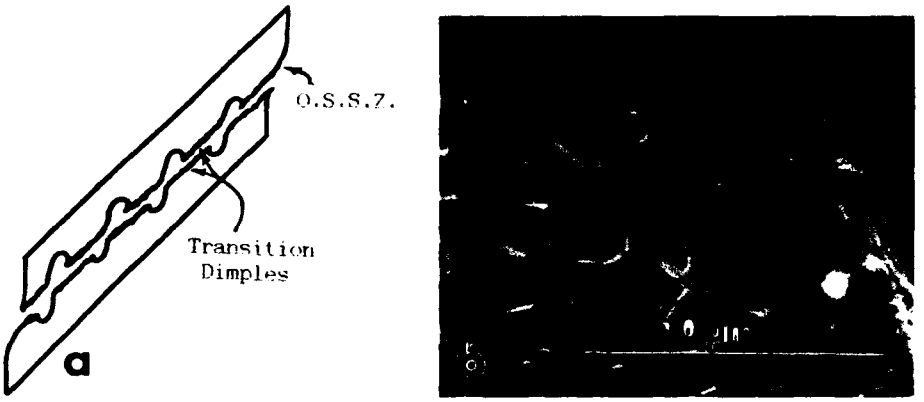

Figure 3: *a.) Schematic post-fracture section of both sides of a separated volume including an "Open Surface Shear Zone" (right) and "transition dimples". Note that the OSSZ only forms on one of the two matching surfaces. b.) Example of an Open Surface Shear Zone (right) and transition dimples (left) on a Ti-8Mn tensile sample fracture surface.*

fracture often occurs through the localized shear bands the portions of the fracture surfaces formed from sheared, pre-existing open surfaces do not result from material separation and, therefore, do not contain dimples. These dimple-free "open surface shear zones" are very distinctive especially since, as depicted in Figure 3a, they are found on only one of the two surfaces formed during separation.

As the concentrated and possibly adiabatic shear bands cut through the remaining material they encounter both void free regions and regions in which voids have already initiated and begun to grow. When a shear band cuts through a pre-existing void sheet this results in flat topped "transition dimples", so named because they are form during the transition from void growth to concentrated shear linkage. A schematic of a separated volume which includes transition dimples is shown in Figure 3a and examples of transition dimples are shown to the left of Figure 3b.

In the void free areas the shear bands form narrow planes and additional void initiation and growth is restricted to these narrow bands, resulting in the shallow dimples which display melted dimple walls, examples of which are shown in Figure 4. An unusual characteristic of these locally melted fracture surface features is that they do not show signs of forming during shear, rather they appear to have formed during tensile separation.

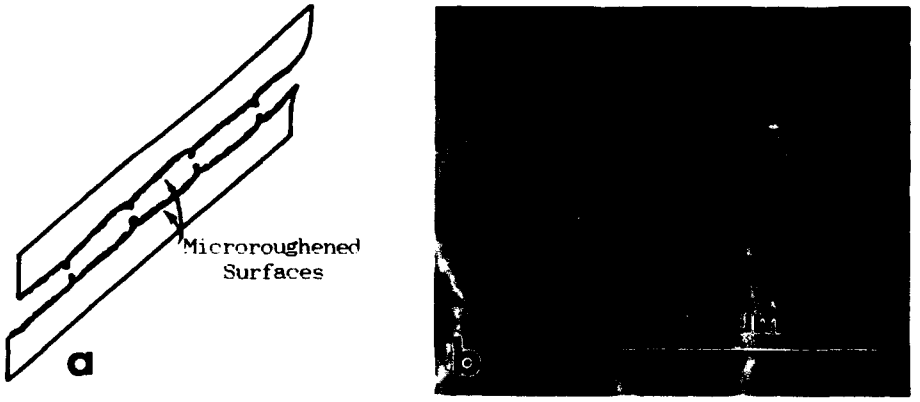

Figure 4: *a.) Schematic post-fracture section of both sides of a separated volume including locally melted dimple walls and surface debris.*
b.) Example of localized melting on the fracture surface of a Ti-6Al-4V quasi-static tensile sample.

In the titanium alloys investigated the surfaces which result from separation through highly concentrated shear bands, as depicted in Figures 3 and 4, are uniformly covered with a fine texturing, called "microroughening". Because "microroughening" occurs from separation through highly sheared and possibly very hot bands and also because it has been reproduced by flash heating of non-microroughened surfaces [2,6,7] it is highly likely that this type of texturing, a higher magnification micrograph of which is shown in Figure 5, is high temperature artifact.

Although the formation of adiabatic shear bands may cause very high temperatures it is important to realize that the surface areas which contain spheroidized structures are covered with dimples. This means that the final separation through these highly localized bands occurs by void

Figure 5: *Higher magnification micrograph of the fine texturing called "microroughening", on the surface of a Ti-8Mn tensile sample.*

coalescence. Local plastic strain energy values in the thinning and ultimately separating ligaments are extremely high. Since this deformation occurs very quickly and the deforming ligaments are surrounded on both sides by already heated shear band material the conditions are very nearly adiabatic. This high rate adiabatic deformation during the separation of the last ligaments has been shown in earlier investigations to be caused by localized adiabatic shear [4] and it is this deformation which provides the ultimate temperature increase to the melting point.

A further indication that it is the process of adiabatic shear during ligament rupture and not the earlier, larger scale adiabatic shear process which actually causes the melting is that there are no indications of phase transformations in the subsurface sections which show localized shear bands. The adiabatic shear which is responsible for melting during final ligament separation is on a micro-scale [4] and the energy released is too small to affect a general phase transformation detectable by the sectioning methods used in this study.

The heating which occurs at the tip of a running crack has been the subject of a number of different studies [3,19-22] which use relatively simple deformational models for the estimation of the plastic energy generated during separation and crack propagation. In the most fundamental terms deformational heating occurs in metals as a result of the dissipative forces present during dislocation motion. Unfortunately, because of the tremendous numbers of dislocations involved in the separation process and the complexity of their interactions, even the best understood concepts of dislocation theory have typically been forsaken in mathematical and computer analyses of fracture.

The previously reported experimental results have been the incentive for a recent dislocation-based model which has been used to analyze the mechanisms responsible for the temperature rise in the plastic zone at the tip of a fast crack [23]. This analysis also differs from previous models in that it uses experimentally measured values of the critical parameters needed for the computation of the energy dissipated during crack propagation. An example of the computed temperatures ahead of the moving cracks is given in Figure 6, which shows temperature profiles at increasing times of crack propagation. Two other important results which have been derived from this analysis are; i.) the temperature ahead of the crack goes through a maximum with increasing crack propagation rate, decreasing at extremely high rates and ii.) at high crack tip velocities the dislocation generation rate is more important for the development of high temperatures than the dislocation velocity.

Although this model uses a number of necessary approximations, both numerical and conceptual, its use of dislocation theory and

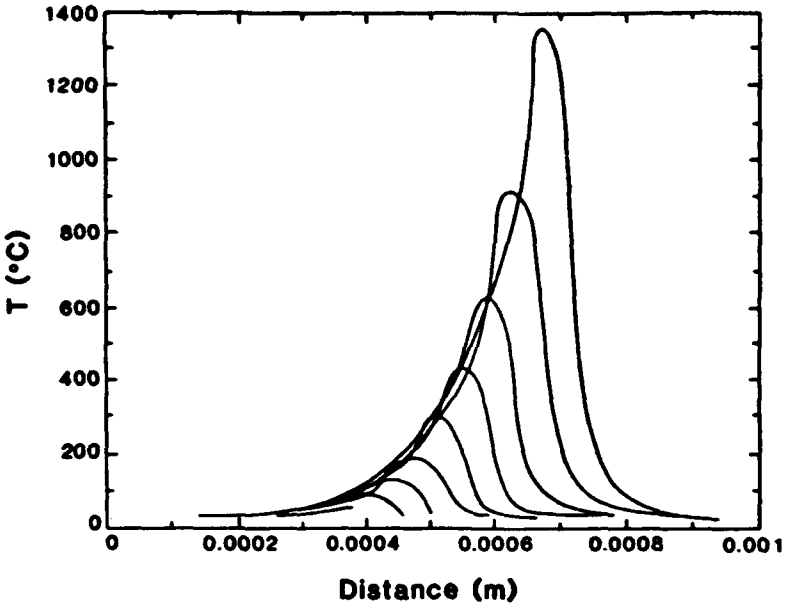

Figure 6: *Calculated temperatures in the plastic zone of a moving crack tip. The crack is assumed to start moving at the left hand side of the graph with a velocity of 0.4 m/s and the curves represent the temperatures in the plastic zone with increasing time as the crack moves from left to right. The progressive positions of the crack tip are approximately located the temperature maxima (reprinted from [23]).*

experimentally-based parameters is an important step forward in the computer modelling of the processes involved in material separation and the resulting generation of high temperatures.

Importance of the Observed Phenomena: Although the total amount of surface area covered by the unusual surface features and in particular the areas of localized melting represent only a small portion of the total fracture surface area there are important consequences of the presence of these structures in regards to shear localization, fractographic analysis, and safe component design.

Adiabatic shear or near-adiabatic shear is a deformation mechanism of great importance because it dramatically changes the local temperature, and therefore the properties of localized sheets of material. In most cases the tendency to deform by adiabatic shear is a highly undesirable material characteristic because, compared to most ductile plastic deformation mechanisms, it uses considerably less energy to produce a given amount of strain. The localized, highly deformed bands which result from adiabatic shear also frequently become preferred separation sites, resulting in an overall reduction in the energy absorbed during separation [8-10].

When separation energy is a design consideration for components made of materials prone to adiabatic shear the present study has shown that it cannot be assumed that adiabatic shear can necessarily be avoided by loading in tension. Shear localization and instabilities occur during the later stages of failures caused by tensile as well as shear and

compressive loads and there is now strong evidence that adiabatic shear may result from these tensile-driven shear instabilities.

Fractography is a commonly used post-failure analytical tool. Using characteristic structures and general fracture surface morphologies as clues one can often reconstruct many of the specific events which occur during the failure of a component. Open surface shear zones, transition dimples, microroughening and locally melted regions are all important features to be aware of, since, as discussed in the aforementioned separation model, they are indications of shear localization and rapid, unstable separation.

Finally, potentially dangerous secondary damage could occur if high temperatures caused by rapid, ductile, tensile fracture provides sufficient energy to "ignite" or otherwise destabilize material in close proximity to the separating surfaces. For this reason the failsafe design of highly stressed components for use in or around unstable material includes knowledge of the possibility of very high temperatures caused by strain localization during failure. It should also be recognized that fracture is often driven primarily by stored elastic stresses making rapid and catastrophic failure and adiabatic shear insensitive to the applied strain rate, even when the applied strain rate is quasi-static.

When it is necessary to use materials which are prone to adiabatic shear under tensile loading conditions localized melting at separation can generally be avoided by reducing the crack propagation rate. With some materials such as the AISI 4340 steel samples, the crack propagation rate can be decreased by insuring that separation occurs through material whose temperature is above the ductile/brittle transformation range [12]. In other materials the crack propagation rate can be decreased by prior heat treatments which increase the crack path tortuosity, as in the case of the Ti-6Al-4V samples [11].

Conclusions:

1. Highly concentrated shear and localized melting occur during the separation of certain tensile loaded materials.
2. Localized melting occurs even at quasi-static applied strain rates because unstable separation is driven primarily by stored elastic energy.
3. The possible occurrence of unstable shear and presence of very high temperatures during tensile separation are factors which should be considered during the design of certain highly stressed members.
4. Localized melting in adiabatic shear prone materials can be avoided by using the materials in conditions which reduce the crack propagation rate.
5. "Open surface shear zones", "transition dimples", "microroughening" and locally melted regions are easily observable microstructural fracture surface features which contain valuable information regarding the final separation events, and thus are a warning of likely catastrophic failure.

Acknowledgement: This research was supported by the U. S. Office of Naval Research (Grant N00014-88-K-0111), Dr. George Yoder program director. We would like to thank Dr. Yoder for his encouragement and insight. Thanks also to Professor Dr. Hans-D. Kunze, Dr. L. W. Meyer, and B. O. Reinders at the Fraunhofer-Institut fur angewandte Materialforshung for conducting high rate tensile tests. The authors also acknowledge the award of a travel grant from the NATO Scientific Affairs Division, Brussels, Belgium.

Bibliography:

1. H. G. F. Wilsdorf, Materials Sci. and Engr., 59, 1983. p.1.
2. D. D. Makel, "Strain Rate Dependent Processes in the Fracture of Ti 8w% Mn", PhD. Dissertation, University of Virginia (1987).
3. J. D. Bryant, "Deformation Heating at the Crack Tip and its Role in Fracture of Ti-10V-2Fe-3Al, PhD. Dissertation, University of Virginia (1987).
4. J. D. Bryant, D. D. Makel and H. G. F. Wilsdorf, "Metallurgical Applications of Shock-Wave and High-Strain-Rate Phenomena", eds. L. E. Murr, K. P. Staudhammer and M. A. Meyers, Marcel Dekker (1986) pp. 723-739.
5. J. D. Bryant, D. D. Makel and H. G. F. Wilsdorf, Mater. Sci. and Engr., 77, 1987, pp. 85-93.
6. D. D. Makel and H. G. F. Wilsdorf, "Impact Loading and Dynamic Behaviour of Materials", eds. C. Y. Chiem, H. -D. Kunze and L. W. Meyer, DGM Informationsgesellschaft, Verlag, vol. 2 (1988) pp. 587-594.
7. D. D. Makel and H. G. F. Wilsdorf, Scripta Metallurgica, 21, 1987, pp. 1229-1234.
8. A. J. Bedford, A. L. Wingrove and K. R. L. Thompson, J. Aust. Inst. of Metals, 19, 1, 1974, p.61.
9. H. C. Rogers, "Adiabatic Shearing; a Review", Drexel University Report Prepared for the U. S. Army Research Office (1974).
10. M. Stelly and R. Dormeval, "Metallurgical Applications of Shock-Wave and High-Strain-Rate Phenomena", eds. L. E. Murr, K. P. Staudhammer and M. A. Meyers, Marcel Dekker (1986).
11. D. D. Makel and D. Eylon, Metallurgical Transactions A, 21A, 1990, pp. 3127-3136.
12. D. D. Makel and H. G. F. Wilsdorf, accepted for publication in Materials Sci. and Engr., 1990.
13. F. R. Larson and F. L. Carr, Metal Progress, February 1964 pp. 26-30.
14. F. R. Larson and F. L. Carr, Metal Progress, March 1964, pp. 75-79.
15. F. L. Carr and F. L. Larson, Journal of Materials, JMLSA, 4, 4, (1969), pp. 865-875.
16. J. H. Giovanola, Mech. of Mater., 1988, 7, pp. 59-72.
17. J. H. Giovanola, Mech. of Mater., 1988, 7, pp. 73-87.
18. H. G. F. Wilsdorf, Acta Metall., 30 (1982) p. 1247.
19. J. M. Krafft and G. R. Irwin, Symposium on Fracture Toughness Testing, STP 381, ASTM (1965) pp. 114-129.
20. R. P. Kambour and R. E. Barker, Jr., J. Poly. Sci., A2, 4 (1966) p. 359.
21. J. R. Rice and N. Levy, "Physics of Strength and Plasticity", ed. S. Argon, MIT Press, Cambridge, MA (1969) pp. 277-293.
22. A. H. Priest, "Proc. Int. Conf. on Dynamic Fracture Toughness", Welding Inst., ASM, Metals Park, OH (1977) pp. 95-111.
23. K. Jagannadham and H. G. F. Wilsdorf, Z. Metalkde., 80 (1989) p.698.

DISLOCATION MECHANISMS AHEAD OF A CRACK

M. Nabil Bassim
Department of Mechanical Engineering
University of Manitoba
Winnipeg, Manitoba
R3T 2N2
Canada

Abstract: Failure of ductile materials is usually preceeded by significant plastic deformation, causing the initiation and propagation of a stable crack through heavily deformed material. The characterization of fracture in these materials is now performed using J-integral evaluations. However, the relationships between this fracture criterion and material properties, particularly ahead of the crack, have not been explored. In this study, a review of the evolution of dislocation configurations ahead of the crack and within the grains in the material, and its relationship with fracture toughness expressed by the J-criterion, namely J_{Ic}, are presented from a theoretical development. Results are also presented which substantiate the conclusions derived. It is demonstrated that there is an intimate relationship betweem macroscopic fracture toughness and dislocation mechanisms ahead of the crack, relating plastic deformation at the crack tip to incipient failure.

Key Words: Fracture toughness; plastic deformation; J-integral; crack tip; dislocations; dislocation structures; grains and subgrains; Hall Petch Relationships.

Introduction: The fracture toughness of ductile materials is commonly described in terms of an energetic criterion for failure, namely the J-integral. This had been introduced as early as 1968 [1,2] and is presently determined by a standardized procedure described by the ASTM [3]. The use of the J-integral and the corresponding fracture toughness criterion J_{Ic}, reflects the acceptance that the behaviour of the material ahead of the crack follows an elastic-plastic state where significant plasticity occurs at the crack tip. Such plasticity has resulted in a different procedure for evaluation of J_{Ic} from measurement of the extent of stretching (plasticity) which takes place ahead of the crack until the onset of crack growth occurs and a meaningful J_{Ic} is measured. This procedure, thus, involves stretch zone width measurement using a scanning electron microscope. The extent of the stretch zone is related to the opening displacement ahead of the crack, which in turn, is related at

the point of crack instability, to the parameter J_{Ic} [4,5]. Recognizing that considerable deformation occurs ahead of the crack leading to the building up of stresses sufficient to cause the crack to propagate, the major current mechanism of describing such deformation is in terms of the theory of dislocations and dislocation mechanisms. Until recently, no direct link has existed between plastic deformation expressed by dislocation behaviour, and fracture of ductile materials and dislocation arrangements ahead of the crack.

Early work [6-9] has dealt with dislocation mechanisms contributing to crack blunting. Friedel [9] describes blunting as due to crack dislocations climbing perpendicular to their Burgers vector, and to crystal dislocations uniformly distributed on slip planes adjacent to the crack tip. The emitted dislocations of opposite signs to the crack dislocations are attracted to the crack tip. As they move towards the crack tip they produce the stress field of the leading dislocations and are neutralized by dislocations of opposite sign producing a stress relaxation in a region surrounding the crack. This allows dislocations from the centre of the crack to move to the vicinity of the crack tip producing a blunted crack.

Another mechanism of crack blunting involves punching out a dislocation from the crack, producing a step at the crack tip [10]. The density of crystal mobile dislocations sources is the most important parameter which determines the ductility and toughness of the material.

Other authors have developed models to describe the ductility at the crack tip and the evolution of a plastic and process zone. These models, however, do not provide a direct relationship between dislocations and fracture toughness.

Theoretical Considerations: Amouzouvi and Bassim [11-13] have conducted a series of investigations on the effect of prior deformation on the fracture toughness of AISI 4340 steel. The fracture toughness was measured as J_{Ic}. They found that when prior straining increased from 0% to 2%, a significant increase in J_{Ic} took place. Also observed was a significant blunting of the crack tip at 2% prestrain caused by availability of large amounts of mobile dislocations. Based on these experimental observations, the model shown in Fig. 1 of interaction of mobile dislocations at an inclined plane to the crack tip with the crack was proposed. The extent of blunting must then depend on the number of slip lines intercepting the crack tip.

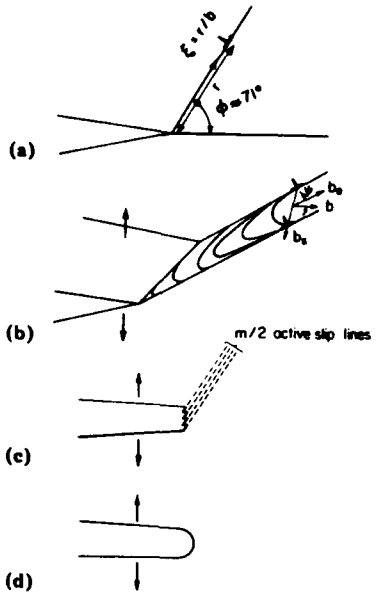

Fig. 1: Steps of interaction of a mobile dislocation in an inclined plane with the crack tip causing blunting.

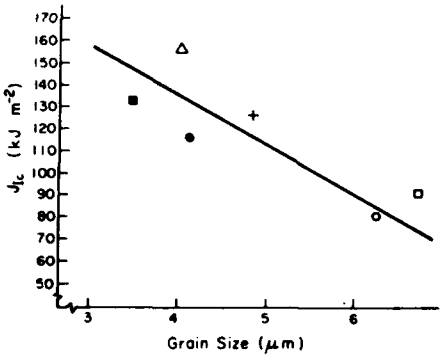

Fig. 2: Variation of J_{Ic} with grain size for HSLA steels.

This analysis [14] leads to an equation relating J_{Ic} to dislocations of the form

$$J_{Ic} = 2\sigma_f \frac{\alpha}{K} \sigma_{\phi\tau} Nm\ nb \qquad (1)$$

where σ_f is the flow stress (the average of the 0.2% yield stress and the ultimate tensile stress). $\sigma_{\phi\tau}$ is the resolved shear stress developed on the inclined slip planes. K is a parameter describing the work hardening rate of the material. α is a proportional factor less than unity which takes into account dislocations which, because of their unfavourable position with respect to the crystallographic slip system or because of the interference with each other in their motion, do not have a possibility of becoming activated, Nm is the number of mobile dislocations. n is the number of each dislocation entering the crack at a given slip line, and b is the Burgers vector.

This equation shows that the fracture toughness is directly proportional to the number of mobile dislocation sources, to the number of dislocations in each slip line, and to the resolved shear stress. The critical value J_{Ic} of the J-integral corresponds to the resolved applied shear stress $(\sigma_{\phi\tau})i$ corresponding to crack initiation.

The effect of microstructure, contributing directly to improvement in toughness, has been investigated. Experimentally for a number of steels, J_{Ic} varies with grain size as shown in Fig. 2, showing an increasing fracture toughness with decreasing grain size. Emperical equations relating the yield stress and grain diameter had been suggested by Hall and Petch [15,16]. A similar equation has been found to describe the results in Fig. 2, namely [17]

$$J_{Ic} = J_o + Dd^{-1/2} \qquad (2)$$

where J_o and D are material constants determined from the plot in Fig. 3.

The significance of the parameters J_o and D is further understood by considering that J_o is a fracture toughness parameter independent of grain size. Thus, J_o would correspond to the situation where grain boundaries are not a factor in restraining dislocations. The term $Dd^{-1/2}$, on the other hand, suggests the strong dependence of J on the grain size d, which occurs when dislocations are interacting with the crack tip within the grains, with no significant role played by the grain boundaries.

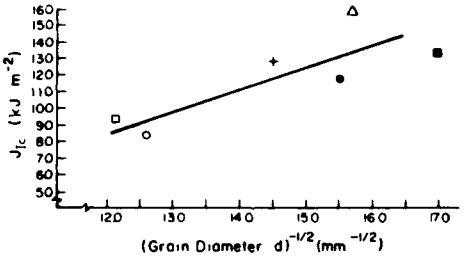

Fig. 3: Plot of J_{Ic} versus $d^{-1/2}$.

While Eq. 1 relates J_{Ic} to individual dislocations interacting with the crack tip, further work has been published relating fracture toughness of the formation and evolution of dislocation structures ahead of the crack [18,19]. The model of interaction of a crack tip by dislocation structures was derived by Bassim [20] and is illustrated in Figs. 4 and 5 for different amounts of deformations (extent of prestraining for instance) leading to the prior formation of dislocation cells.

In case A (annealed), very few inherent dislocations are present and these dislocations have not formed structures. The number of dislocations initially present is smaller than that required to blunt the crack by dislocation interaction with the crack tip.

In case B, with a relatively high density of individual dislocations, these dislocations will interact with the crack tip causing blunting, according to Equation 1. Those dislocations which do not interact with the crack arrange themselves into dislocation structures. This plastic work also contributes to the relatively high level of toughness. Eventually, the crack propagates in a region where dislocation structures are present. This has been verified experimentally by determining that the dimple size in fractured 4340 steel is of the same magnitude as the dislocation cells observed by TEM in this material.

In case C, where the material is initially predeformed, plastic work is expended in shrinking the dislocation structures and in driving the crack through these regions. The scarcity of mobile dislocations reduces the blunting mechanism and hence, the fracture toughness is low.

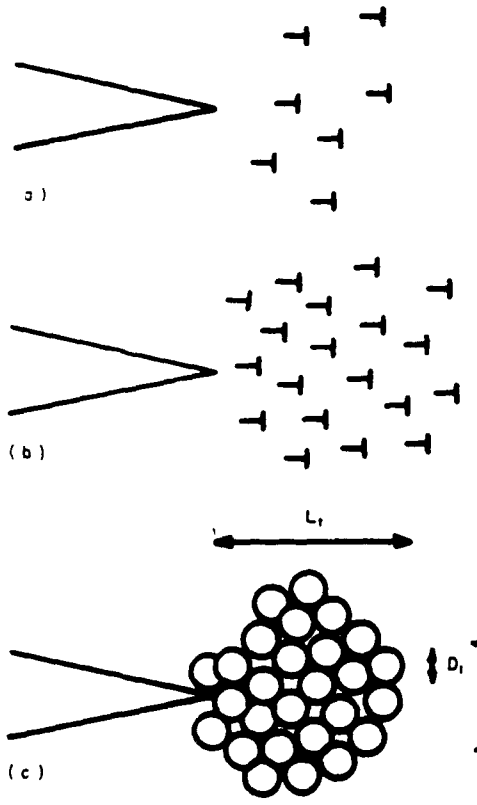

Fig. 4: Interaction of a crack with dislocation structures.

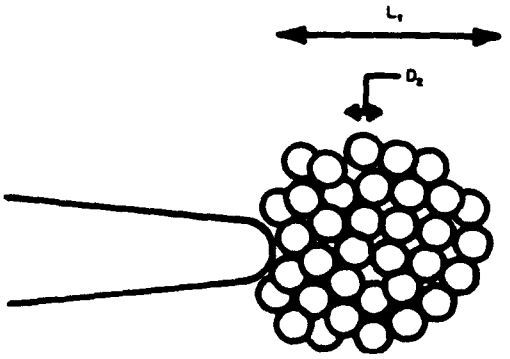

Fig. 5: Blunting of the crack due to plasticity (dislocation structures) at the crack tip.

Fig. 5 describes the final stage of a material containing

dislocation structures at the crack tip. The cells have reached a minimum size D_2 and extend over a distance L from the crack tip. The stress associated with these cells is sufficient to induce crack growth.

Discussion: Experimental validations of the previously outlined concepts have been carried out in a number of materials, among which is prestrained AISI 4340 steel. Specimens were loaded to three different values of J. A comparison of slip patterns is given in Fig. 6. The material containing large numbers of mobile dislocations shows, at the point of onset of crack growth (Fig. 6b) a diffuse slip pattern relative to that of an annealed material. A very well-rounded crack tip resulting from an extensive blunting was obtained.

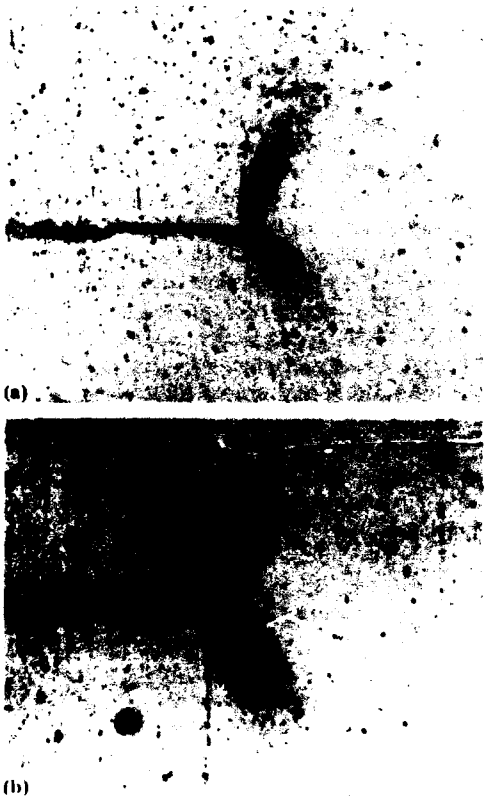

Fig. 6: Slip band pattern developed ahead of the crack.

On a general scale, most analysis of the microscopic aspects of fracture dealt with the intersection of individual dislocations with the crack tip. These models may be suitable to explain the fracture toughness of materials with a relatively low dislocation density and in cases where unstable crack growth takes place.

The present model, depicted in Equation 1 and Figs. 4 and 5

define the dislocation mechanisms at the crack tip accurately and their role in fracture toughness. The plastic work is absorbed mostly by formation of dislocation structures ahead of the crack, with insignificant interactions of mobile dislocations with the crack tip. As the density of mobile dislocations increases, however, more dislocation-crack interactions take place resulting in higher toughness. The crack propagates in a heavily deformed region populated heavily with rather small size dislocation cell structures.

While the model is qualitative, it visualizes the relationship between toughness and ductility quite readily and explains the role of dislocation structures in the fracture process.

Acknowledgements: The Natural Sciences and Engineering Research Council of Canada is acknowledged for support of this investigation.

References:

[1] J.R. Rice, J. Appl. Mech., 35 (1968) 379.
[2] J.R. Rice, J. Mech. Phys. Solids (1974) 17.
[3] Standard Test Method for J_{Ic}, ASTM Stand E813-81 in ASTM, Philadelphia, PA, 1983.
[4] M.R. Bayoumi and M.N. Bassim, in Int. Conf. on Materials, ICM, Stockholm 1983, Pergamon, New York, Vol. 2, 803.
[5] K.F. Amouzouvi and M.N. Bassim, Mater. Sci. Eng., 55 (1982) 257.
[6] J. Weertman, Philos. Mag. A,43 (1981) 1103.
[7] H.G.F. Wilsdorf, Mater. Sci. Eng., 59 (1983) 1.
[8] E. Smith, Acta Metall., 16 (1968) 313.
[9] J. Friedel in B.L. Averbach, D.K. Felbeck, G.T. Hahn and D.A. Thomas (eds), Fracture, Wiley, New York, 1959, p. 498.
[10] A.S. Tetelman and A.J. McEvily, Fracture of Structural Materials, Wiley, New York, 1967, p. 200.
[11] K.F. Amouzouvi and M.N. Bassim, in L. Simpson (ed), Fracture Problems, Pergamon, Oxford 1982, p. 179.
[12] K.F. Amouzouvi and M.N. Bassim, Mater. Sci. Eng., 60 (1983) 1
[13] K.F. Amouzouvi, Ph.D. thesis, University of Manitoba, 1983.
[14] K.f. Amouzouvi and M.N. Bassim, Mater. Sci. Eng., 62 (1984) 137.
[15] E.O. Hall, Proc. Phys. Soc. London, 1364 (1951) 747.
[16] N.J. Petch, J. Iron Steel Inst., London, 173 (1953) 25.
[17] R.J. Klassen, M.N. Bassim, M.R. Bayoumi and H.G.F. Wilsdorf, Mater. Sci. Eng., 83 (1968) 39.
[18] S.M. Ohr, Mater. Sci. Eng., 72 (1985) 1.
[19] M. Kaczorowski, C.S. Lee and W.W. Gerberich, Mater. Sci. Eng., 81 (1986) 305.
[20] M.N. Bassim, Mater. Sci. Eng., 95 (1987) 199.

METALLURGICAL EVALUATION OF HIGH STRENGTH STEEL PLATE CRACKS ASSOCIATED WITH WELD REPAIRS

E.M. Hackett, M.E. Natishan, A.V. Brandemarte, M.T. Kirk and T.W. Montemarano

David Taylor Research Center
Annapolis, Maryland 21402

Abstract: Two cracks were discovered during final visual inspection of a high strength steel plate used in ship construction. These cracks were associated with weld repairs which were performed at the time of original production of the plate. The weld repairs were performed prior to final heat treatment of the plate. The David Taylor Research Center (DTRC) was tasked to determine the metallurgical cause of the cracking found in the plate.

The metallurgical investigation included non-destructive inspection, metallographic profiles, fractographic characterization and characterization of oxides found on the fracture surfaces. The investigation focused on using features of the oxides formed on the crack surfaces to determine whether the cracks were formed prior to, or subsequent to, the final plate heat treatment.

The majority of the metallurgical evidence pointed to the hypothesis of a two-stage formation process for the cracks. This two stage cracking hypothesis involved transverse cold cracking of the weld repair to approximately the weld repair depth before final heat treatment, followed by initiation of a brittle base-plate crack after water quenching from austenitization.

Key Words: Austenitization; cold cracking; heat treatment; oxides; quenched and tempered steel; quench cracks; fracture mechanics

Introduction: During final visual inspection of a high strength steel plate to be used in ship construction, shipyard personnel discovered two cracks in the exterior surface of the plate. Crack 1 was reported to be 1-7/8 inches in length while crack 2 was reported to be 1-1/16 inches long. Cracks 1 and 2 were estimated to be 0.90 inches deep and 0.87 inches deep, respectively, using ultrasonic testing (UT). The two inch thick plate had been cold-formed to the final shape required for ship insertion, resulting in convex curvature on the plate exterior. As a result, both cracks were open on the exterior surface of the plate by approximately 1/16 inch and were "dimpled" at the ends, most likely due to the cold forming. General details of the segments of the plate cracks that were provided to DTRC are shown in Figure 1.

Further examination at the shipyard revealed that both cracks were associated with a large plate weld repair that had been performed by the original plate producer at the time of plate production. The weld repair was approximately 30 inches in length by 1-1/2 inches wide by approximately 0.113 inches deep. This weld repair was the

largest of a total of eight (8) documented weld repairs performed on the plate by the producer. Two (2) of the weld repairs (including the 30 inch long repair with the cracks) were on the exterior surface of the plate and six (6) were on the interior surface of the plate. Non-destructive inspections by the shipyard of the other weld repairs did not reveal any crack like indications.

A second plate from the same heat, containing un-documented weld repairs, was also examined. This as-received plate had not received the cold forming operation for ship insertion. Visual inspection revealed the presence of two additional cracks (cracks 3 and 4) which were associated with the plate weld repair (see Figure 2). Crack 3, the larger of the two, was observed to extend across the entire width of the weld repair. No dimpled regions were observed at the ends of the crack as was the case for the cold formed plate cracks. Crack 3 was open at the surface to approximately 1/32 inches. Crack 4 was not measurably open at the surface and was more difficult to discern visually. The entirety of crack 4 was contained within the weld repair. The length of crack 3 that was open to the surface was approximately 1.0 inches, while that for crack 4 was approximately 0.5 inches.

Records from the plate producer indicated that the weld repairs on these plates had been performed prior to final heat treatment of the plates. At the time that the plates were produced, the military specification for the plate required the use of heat-treatable welding electrodes in order that defects could be repaired before final heat treatment. The specification was later revised to allow use of non heat-treatable shielded metal arc (SMA) electrodes for post-heat treatment weld repairs. This method is now preferred since the high carbon content of the heat treatable electrodes increased the sensitivity to weld metal cold cracking [1].

Objective and Approach: The goal of this investigation was to determine the metallurgical cause of the plate cracking. The approach included (1) Examination of the plate cracks; (2) Development of a crack formation hypothesis; and (3) Testing of the crack formation hypothesis. The examination of the plate cracks included non-destructive inspection, weld/heat-affected-zone (HAZ) identification and location, fractographic characterization, metallographic profiles and characterization of crack oxides. Tests of the crack formation hypothesis included laboratory heat treatments to simulate oxide formation and a fracture mechanics evaluation of the stresses required to initiate the cracking.

Material: The plates examined in this investigation were a high strength, 3% Ni steel with a yield strength exceeding 80 ksi. Heat treatment, chemical composition, and mechanical properties of the plates are provided in Table 1. This information was obtained from the mill test reports supplied by the plate producer. The plate met the military specification requirements for mechanical properties and chemical composition. Results of a chemical analysis performed on the weld metal used for the repair on the cold formed plate are presented in Table 2.

Table 1 - Chemical Composition, Heat Treatment and Mechanical Properties for High Strength Steel Plates

Chemical Composition (Wt %):

C	Mn	P	S	Si	Cr	Ni	Mo	Cu
0.15	0.30	0.010	0.012	0.31	1.65	2.86	0.47	0.20

Heat Treatment: Austenitized at 1650°F for 30 minutes followed by water quench. Tempered at 1280°F for 30 minutes and air cooled.

Mechanical Properties:

0.2% Yield Strength (ksi)	Ultimate Tensile Strength (ksi)	Elongation (%) in 2 inches	Reduction in Area (%)
82.3	107.7	24	66

Table 2 - Chemical Composition of Cold Formed Plate Weld Metal Repair

C	Mn	P	S	Si	Cr	Ni	Mo	Cu
0.16	0.29	0.010	0.012	0.32	1.65	2.81	0.45	0.19

Non-destructive Examination: The pieces of the cold formed plate and the as-received plate were examined non-destructively using a liquid penetrant (PT) inspection procedure in accordance with MIL-STD-271. MAGNAFLUX Spotcheck dye penetrant (SKL-HF/S) and Developer (SKD-NF/ZP-9B) were employed for these examinations. The PT inspections of the cold formed plate pieces revealed no linear indications, other than the already noted locations of cracks 1 and 2. The PT examination of the section from the as-received plate revealed a linear indication at the edge of the plate weld repair, approximately 1/16 inches below the plate surface and 3/16 inches in length. This indication was denoted as crack 5 and is shown in Figure 3.

Destructive Analysis: The plate segments containing cracks 1 through 4 were sectioned to open the crack surfaces for fractographic examination. The general procedure involved: (1) removing (saw cutting) as much of the material surrounding the crack as possible, without damaging the crack itself; (2) chilling the specimen to liquid nitrogen temperatures; (3) supporting the specimen such that the crack section could be subjected to bending resulting in mode I (opening) loading of the crack surfaces; and (4) subjecting the specimen to impact loading from either a hammer blow or a drop tower.

Using this procedure, the mating surfaces of cracks 1 through 4 were opened and are shown in Figures 4 through 7. Low magnification (up to 40X) optical examination of the fracture surfaces of these cracks revealed generally elliptical shapes, with corrosion products

and other oxides covering the majority of the surfaces. Distinct "river patterns" were also evident on all of the fracture surfaces. These river patterns pointed to the weld/Heat-Affected Zone (HAZ) region as a possible region for crack initiation. The measured depths for cracks 1 through 4 are provided in Table 3.

Table 3. Measured Crack Depths in High Strength Steel Plates

Crack	Maximum Depth (Inches)
1	1.23
2	0.82
3	0.65
4	0.25

The dimpled region at the ends of cracks 1 and 2 was observed to be un-oxidized upon opening, indicating that the dimpling was most likely the result of the cold forming operation performed on the plate.

Fractography: Approximately one half of one fracture surface from each of cracks 1 and 2, were preserved for characterization of the fracture features using low magnification optical and scanning electron microscopy (SEM), while one entire fracture surface from cracks 3 and 4 were preserved for fractographic analysis. These samples were cleaned in soap and water and rinsed in methanol for characterization of the as-received fracture surfaces. As mentioned previously, the fracture surfaces were heavily oxidized. Attempts at oxide removal involved cleaning in a solution of 70% citric acid and water for approximately 2 to 4 hours (time varied with sample) to remove as much of the oxide as possible to characterize any fracture features remaining under the oxide.

Characterization of the as-received fracture surfaces showed several features that were common to all fracture surfaces. The oxide film was very adherent on all surfaces, making high magnification examination impracticable. At low magnifications, all fracture surfaces showed a distinct "river pattern" (Figure 6) indicating a brittle fracture mode [2], and a dual region appearance to the oxide layer. The fracture surface oxide near the plate exterior surfaces appeared heavier with the underlying features more obscured than that on the fracture surfaces deeper in the cracks, possibly indicating a thicker layer oxide towards the outer surface of the plate. On cracks 3 and 4, where the "river patterns" were apparent in their entirety, the river patterns pointed to initiation regions just below, or just into the region of heavier oxide. Due to the obscuring nature of the oxide film, details of the fracture modes were not discernible.

Metallography: Several transverse sections were made through each crack such that the entire crack profile was intact. One section of each crack was mounted using a thermosetting epoxy powder in a 2" diameter mold and another crack section was broken open to reveal the two fracture surfaces. Of these surfaces, one was preserved in the as received condition and the other was cleaned in methanol to

prepare it for fractographic examination. The mounted specimens were examined as polished and photographed to record the oxide layer thickness and morphology. Next the specimens were etched in 2% Nital to reveal their microstructure. Location of the weld region and it's relationship to oxide morphology and crack depth was of particular interest. Crack 5 was mounted intact and polished to reveal both a blow-hole defect and nonmetallic inclusions associated with the crack. This specimen was then analyzed, using wavelength dispersive spectroscopy, in a microprobe to identify the inclusions.

The five cracks analyzed fell into two categories. Cracks 1 through 4 were transverse cracks which extended beyond the the depth of the weld repair and, in the worst case (crack 1), extended 1.1 inches into the parent plate material. Crack 5, in contrast, ran parallel to the plate surface at a depth of 0.050 inches below the plate surface. The following discussion shall treat each category separately.

Cracks 1-4: Upon initial visual examination it was evident that these cracks were heavily oxidized. The oxide layer extended from the top or weld repair surface, down to the bottom of the crack indicating that the entire crack had been open during some stage of heat treatment. Marked differences were apparent in the oxide morphology and thickness from top to bottom for cracks 1 through 3 as shown for crack 3 in Figure 8. The top region of all of the cracks had a very thick oxide layer and the morphology of the oxide in this region suggested intergranular or interdendritic attack with long fingers extending into the metal adjacent to the fracture surfaces. This is in contrast to the oxide further down the crack where an abrupt decrease in thickness occurs. Here the oxide is not only much thinner but also smoother with no indication of intergranular attack.

The oxide thickness was measured as a function of crack depth and is reported for cracks 1, 3 and 4 in Figure 9. The sudden decrease in oxide thickness observed for each specimen coincides with the change from an intergranular/interdendritic attack to a smooth oxidation. The abrupt, simultaneous change in both thickness and morphology of the oxide, as opposed to a more linear change, suggested that two different oxidation rates/mechanisms were at work. It was postulated that this difference could be attributed to oxidation occurring as a result of austenitizing at the top of the cracks, versus oxidation due to tempering in the bottom of the cracks. Such oxide formation could result from a crack formation hypothesis consisting of cold cracking of the weld metal, followed by propagation of the cracks into the base metal due to stresses from subsequent quenching and tempering of the plates. In such a case, the weld cracks would have been open to austenitizing temperatures (1650°F) with specific oxide characteristics, while the cracks that propagated into the base metal would only have seen tempering temperatures (1280°F) with different oxide characteristics. A simple laboratory heat treatment simulation study was conducted in an attempt to duplicate the oxide types.

Oxide Simulation Study: Fatigue precracked specimens, removed from high strength steel plate procured to the same specification as the

plates being investigated, were prepared for heat treatment. One was austenitized at 1600°F for 30 minutes, water quenched and tempered at 1200°F for 30 minutes, the other was simply tempered at 1200°F for 30 minutes. The samples were then sectioned and metallographically prepared to examine the oxide layers. Figure 10 shows the difference in the oxide layers which were formed. Note the intergranular attack of the high temperature oxide as opposed to the smooth oxide layer formed at 1200°F. This evidence further supports the theory that the crack formed in two stages. The top of the crack (weld metal region) opened prior to austenitization, saw the high temperature and experienced the heavy intergranular type oxidation, while the lower portion of the crack formed during quenching from the austenitization temperature and prior to tempering.

Crack 5 (Sub-surface Crack): Crack 5 was located approximately 0.050 inches below and ran parallel to the plate surface. The heavy oxidation associated with cracks 1-4 was not present. This being the case, it was felt that this crack formed under different conditions and may in fact be the type of plate surface defect that was weld repaired. Metallographic grinding and polishing of crack 5 revealed a blow-hole defect in the weld metal associated with the crack (Figure 11). Also, inclusions were discovered at the crack interface. The inclusions were analyzed on an electron microprobe and proved to be Mn-Al silicates. Both microprobe and SEM also confirmed the presence of sulfur in the crack. These types of nonmetallic inclusions are commonly associated with plate surface defects such as seams and laps [3]. The blow-hole defect in the weld is a common occurrence when attempting to weld over an existing crack or defect [1]. The included material and gases in the crack may out-gas and cause this type of defect. It was considered that crack 5 was a pre-existing plate defect that was possibly of the type being weld repaired. Out-gassing of the defect most probably caused the blow-hole in the weld metal.

Fracture Toughness Testing: To investigate the possibility that the cracks found in the plates were caused by stresses established during quenching, it was necessary to determine the fracture toughness typical of the plate material in the as-quenched condition. This toughness was determined using a fatigue cracked compact tension (C(T)) specimen removed from the plate material. After fatigue cracking at a cyclic applied stress intensity range (ΔK) of 25 ksi$\sqrt{in}$ to a total crack length of 1.1 inches, the specimen was austenitized at 1650°F for 30 minutes and then water quenched. Austenitization was performed after fatigue cracking to simulate the condition of a plate containing a cracked weld repair being austenitized and quenched.

After quenching, five Rockwell C-scale (HRC) hardness measurements were made according to the procedures of ASTM Standard Test Method E-18; five measurements were made with an average value of 39 HRC. Data relating Rockwell hardness to strength level for the plate material were then used to estimate both yield and tensile strengths of the as-quenched plate. For the average hardness of 39 HRC, these data indicate a yield strength of approximately 147 ksi with an ultimate tensile strength of approximately 165 ksi.

Prior to testing, it was uncertain whether the C(T) specimen would fail under predominantly elastic loading, and thus give a K_{Ic} value, or fail under elastic-plastic loading, and thus give a J_{Ic} value. To insure that the test results were useful in either event, the procedures of ASTM E813, "Standard Test Method for J_{Ic}", were used. The results of this test indicated that the specimen failed catastrophically shortly after achieving maximum load. The test record was analyzed using the procedures detailed in the ASTM E399 "Standard Test Method for K_{Ic}". This analysis indicated that the specimen had a plane strain fracture toughness, or K_{Ic} of 83 ksi$\sqrt{in}$. While this procedure, testing a specimen per the requirements of one standard and analyzing the results per the requirements of another, is not currently sanctioned by ASTM, such techniques are currently being considered for standardization by ASTM task group E24-08-01.

The oxide data discussed above suggests that the weld region cracks existed prior to austenitization, however the larger cracks in the plate material existed after austenitization, but before tempering. This evidence suggests that the weld region cracks may have served as initiation sites for the larger cracks in the base material, and that these cracks propagated into the plate during or after the austenitization and quench cycle. To investigate this possibility, the far field bending stresses needed to initiate brittle fracture from the weld regions of cracks 1-4 were calculated assuming that K_{Ic} = 83 ksi$\sqrt{in}$ as measured using the C(T) specimen. These result of these calculations are summarized in Table 4. These calculations indicate that stresses below the yield stress of the material could have initiated the growth of the larger cracks from the weld region cracks for cracks 1-3. However, for crack 4 this analysis indicates that stresses exceeding the material yield strength would be necessary to initiate a larger crack into the plate.

Table 4: Stresses needed to initiate cracks from weld regions in cracks 1 - 4 into as-quenched plate. As quenched plate yield strength: 147 ksi

Crack No.	Weld Region Crack Size Length [in]	Depth [in]	Total Crack Size Length [in]	Depth [in]	Stress to Generate K_{Ic} (83 ksi$\sqrt{in}$) from Weld Region Crack [ksi]
1	1.83	0.11	3.67	1.23	138
2	1.06	0.17	2.10	0.82	130
3	1.13	0.14	1.38	0.65	134
4	0.38	0.20	0.47	0.25	154

Summary: The majority of the metallurgical evidence pointed to the hypothesis of a two-stage formation process for the cracks. This two stage cracking hypothesis involved transverse cold cracking of the weld repair to approximately the weld repair depth before final heat treatment, followed by initiation of a brittle base-plate crack after water quenching from austenitization.

Acknowledgments: The authors gratefully acknowledge the following personnel at DTRC who assisted in the testing and analysis performed for this report: F.T. Connell, T.M. Scoonover and R.J. Stockhausen, DTRC 2812; J.P. Waskey, DTRC 2814; P.W. Holsberg and R.H. Juers, DTRC 2815. The authors are also grateful to D. Jordan and W. Mayott of the General Dynamics Company for helpful discussions and suggestions during the course of this effort. The authors are especially appreciative of technical discussions with E. Hamburg, G. Martini, C. Roper and A. Wilson of the Lukens Steel Company; S. Manganello of the United States Steel Company, and R. Jesseman of the Armco Steel Company.

References:

[1] Welding Metallurgy, G.E. Linnert, 3rd. Edition, Volume 2, American Welding Society, pp. 243-245, 1966
[2] The Metals Handbook, Vol. 10, Failure Analysisi and Prevention, Eight Edition, The American Society for Metals, pp. 92-93, 1975
[3] The Making, Shaping and Treating of Steel, United States Steel, Seventh Edition, 1957, pp. 493-495

Figure 1 - Low Magnification Surface View of Cracks 1 and 2

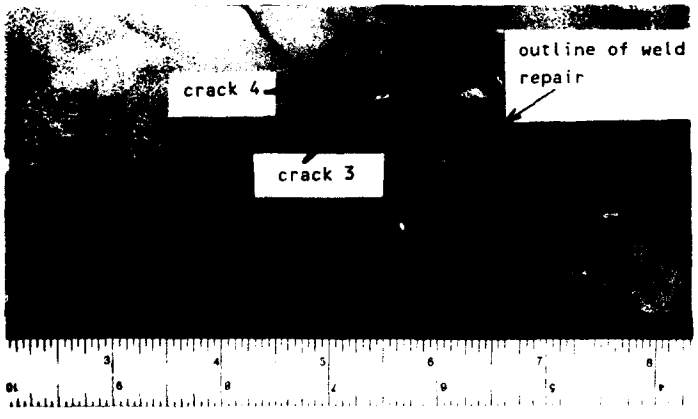

Figure 2 - Low Magnification Surface View of Cracks 3 and 4

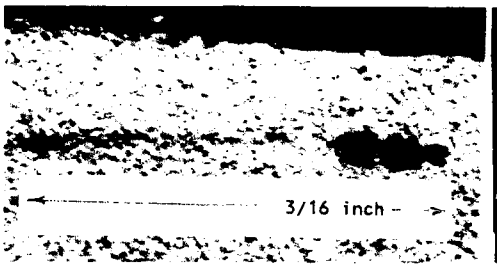

Figure 3 - Penetrant Examination Indication of Crack 5

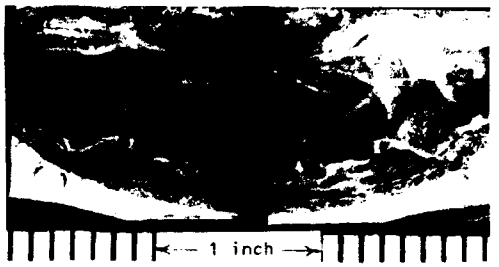

Figure 4 - Low magnification View of Crack 1

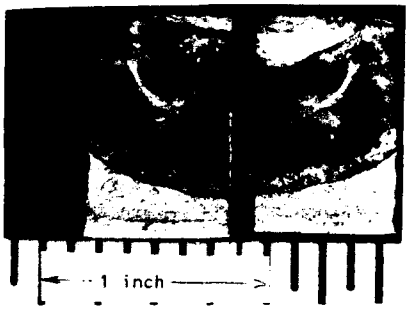

Figure 5 - Low Magnification View of Crack 2

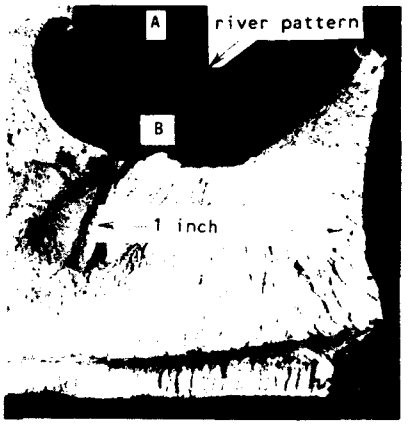

Figure 6 - Low magnification View of Crack 3

A - weld repair region B - base metal region

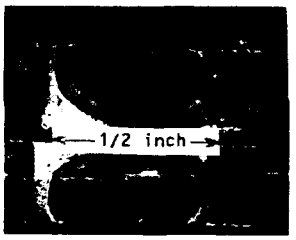

Figure 7 - Low magnification View of Crack 4

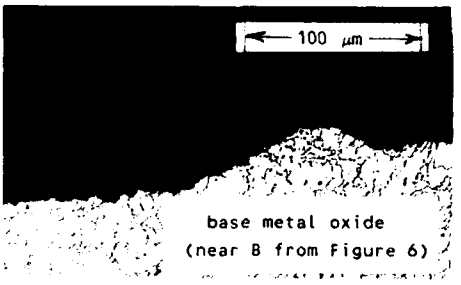

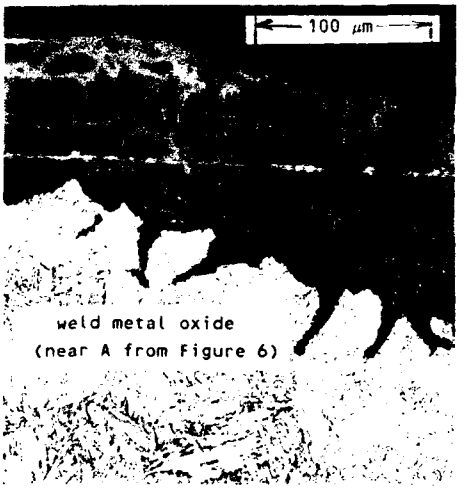

Figure 8 - Fracture Profiles of Crack 3 Showing Oxide Morphology

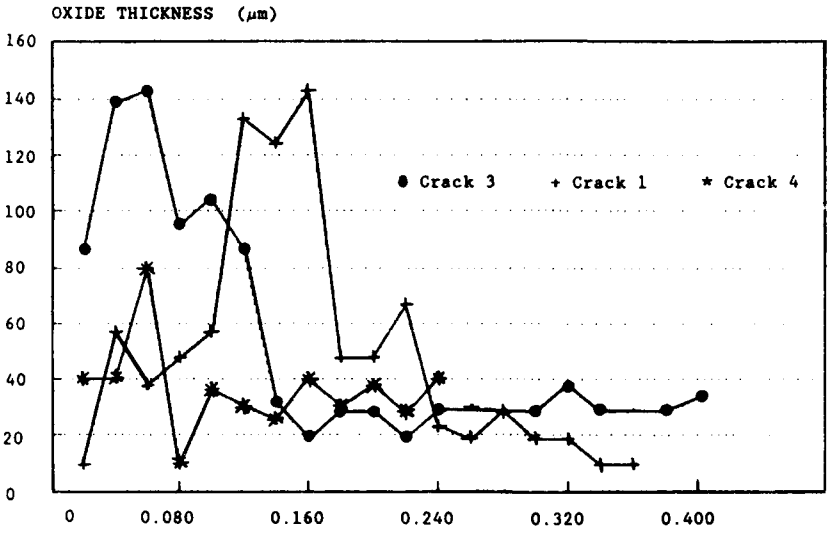

FIGURE 9 - OXIDE THICKNESS vs. CRACK DEPTH, CRACKS 1, 3 AND 4

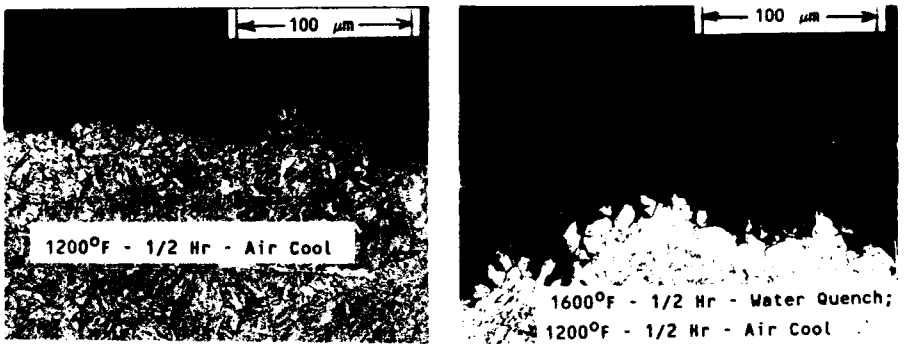

Figure 10 - Fracture Profiles of Dynamic Tear Specimens Showing Oxide Morphology

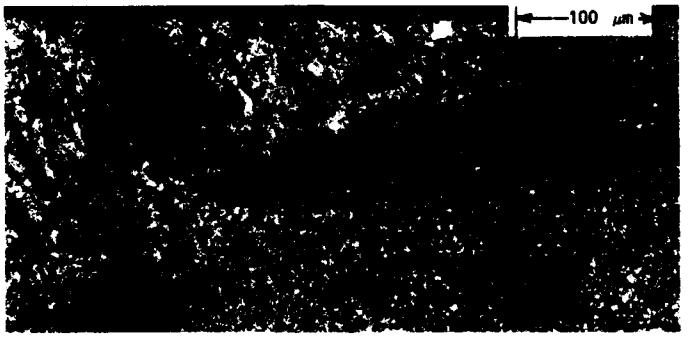

Figure 11 - Metallographic Profile of Crack 5, Showing Blowhole

EXPERT SYSTEMS (I and II)

Chairmen: James Taylor
Naval Station Norfolk
and
Dick Fairman
Engineering Consultant

AN INTELLIGENT STANDARDS FILTER FOR A PC-BASED EXPERT SYSTEM

Eric C. Pawtowski
Graduate Project Assistant

Marcello Typrin
Graduate Research Assistant

R. G. Kirk
Associate Professor

Mechanical Engineering Department
Virginia Polytechnic Institute and State University
Blacksburg, VA 24060

Abstract: Using a data acquisition system controlled by a personal computer to monitor a turbomachine's response can have many benefits. Such a system has been created by the VPI&SU Rotordynamics Lab as part of an ongoing expert system project. This data acquisition system is capable of reading data from an operating turbomachine, comparing it to a series of user-defined standards, and determining the machine's operational status. It has been successfully used to read vibration data from a small test rig.

Key Words: Expert system; data acquisition system; standards; PROLOG; personal computer; rotating machinery; turbomachinery; vibration

Introduction: Industrial turbomachines are extremely complex pieces of equipment, and are thus subject to a wide range of possible mechanical problems that can manifest themselves in a number of ways. To minimize maintenance and downtime costs, it is essential to detect and diagnose developing problems while the machine is operating, hopefully before significant damage is done.

In order to catch potential trouble, turbomachines are commonly monitored by electronic data acquisition systems. Simple systems determine overall vibration from a single probe, often handheld. More complex ones use multiple probes to monitor quantities such as flow rates, temperatures, and complex forms of vibration data. Many systems are controlled manually, with a human operator to take and record data. The efficiencies of these systems can often be improved by computer control.

Computer-controlled data acquisition systems are capable of automatically taking and recording data from many sources over a long period of time. If properly programmed, they can also analyze data and call attention to possible trouble. There are many advantages to computer control: their constant monitoring is less likely to miss a rapidly developing problem, such as a cracked blade. They are capable of monitoring and judging many probes simultaneously, and will always draw consistent conclusions from the data. Over the long term, they can be less expensive to operate than a human operator.

The latest generations of personal computers are ideal for this task. They are portable and rugged enough to be used on a factory floor. They can be reprogramed and repaired easily if the need arises. Many different types of data acquisition and analysis boards are currently available that plug directly into the expansion slots of a standard PC.

For the past two years, the Virginia Polytechnic Institute & State University Rotordynamics Laboratory has been developing an on-line expert system for turbomachinery, as a part of the WOT ("Wizard of Tech") project [1,2,3]. This system will ultimately be capable of acquiring data from turbomachines, analyzing it, performing a diagnosis of potential problems by consulting a database, and providing possible corrective procedures from that same database. As an intermediate step, the project has created a computer-controlled data acquisition system, known as the WOT intelligent data filter. This system is capable of analyzing data and determining if a problem is developing, although it cannot provide guesses as to what the problem may be at this stage in its development.

Data Acquisition Systems: Setting up a PC-based data acquisition system is a relatively straightforward task, thanks to the multitude of expansion boards and PC-compatable monitoring sensors and equipment that are currently available. A single PC can easily monitor a large number of channels, and perform many sophisticated analyses functions such as an FFT analysis. A schematic of the data acquisition system at the Virginia Tech rotor lab is shown in Fig 1. It includes a series of Metrabyte boards, a Bently-Nevada DVF-3, a Rapid Systems FFT analyzer, and a personal computer, connected to a tabletop test rig called a "rotor kit". This system is quite capable of acquiring all vital data from a full-size machine.

A problem with such data acquisition systems is that the magnitude of data collected is often more than anyone can interpret, even with a machine as simple as the rotor kit. The potential of such a system can be wasted if the person checking the output is incapable of analyzing it properly, either due to a lack of skill or lack of time.

The easiest way around this problem is to teach the computer to mimic a humans's ability to judge data and determine the operational status of the machine. A human turbomachine expert will compare data coming off of a machine to some kind of standard, be it a published standard accepted by industry or a personal one developed from experience. A computer is capable of the same task. The WOT data acquisition system was taught to read data and compare it against three different types of standards: scalar, vector, and graphical. These standards must be pre-defined by a human expert before the computer can use them.

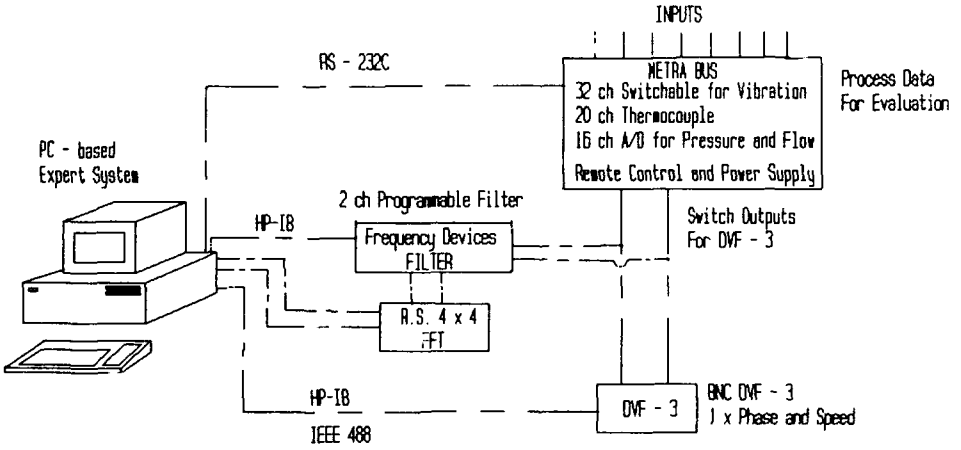

Figure 1.
Schematic of Experimental Data Acquisition System at
VPI&SU Rotor Lab

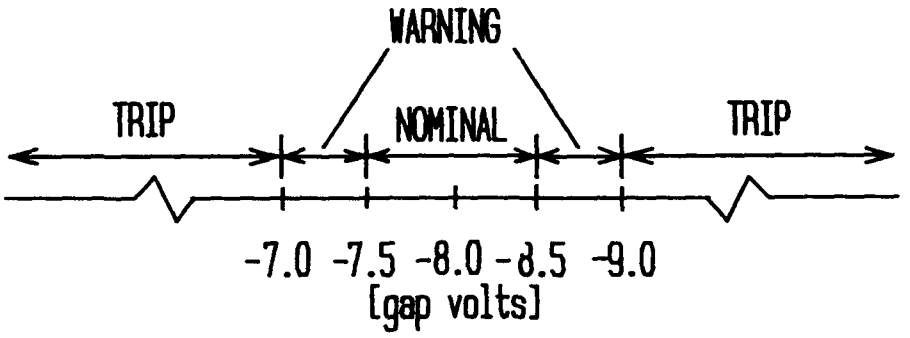

Figure 2.
Illustration of Scalar Standard for Filter Program

Standards: Scalar standards are the simplest. They involve only a single piece of data, such as rotor speed or gap voltage at a probe. The standard is set by defining an acceptable median value for the data, and a series of one or more deviations by which the data's value may vary around the median. A scalar standard for gap volts for the rotor kit is illustrated in Fig 2. Here, the median value is 8.0 volts, and any value within 0.5 volts of the median (7.5 volts to 8.5 volts) is considered "nominal". Any value greater than 0.5 but less than 1.0 volts from the median (7.0 to 9.0 volts) is considered to be in a "warning" condition. Deviations greater than 1.0 volts are considered an "alarm" condition.

The median value and the magnitudes of the deviations are pre-defined by an operator before the system is run for the first time. The median can be reset by an operator while data is being acquired, presumably after the machine has reached a steady-state condition. There are two ways of reseting the median: either by manually entering in a value, or by instructing the program to take the next piece of data acquired as the new median.

Vector standards are slightly more complex: they involve two variables that can be used to define a two dimensional vector, such as vibrational amplitude and phase angle. The standard is set by defining the nominal magnitude and phase angle of the vector formed by the two variables, and another series of one or more allowable deviations by which the magnitude of the actual vector is allowed to vary from the nominal one. An illustration of this type of standard for 1x vibration and phase of the rotor kit is shown in Fig 3. It is basically a two-dimensional version of a scalar standard. The nominal vector is 2 mils at a phase angle of 40 degrees. Actual vectors whose tips fall to within a one mil circle of this vector are considered nominal. Those greater than one and less than two are considered marginal, greater than two and less than three are taken as a warning, and greater than three are in an alarm condition. Please note that these standards are only applicable to the Tech rotor kit, which uses oil-impregnated brass bearing with no seals. These standards cannot be applied as-is to full size machines.

A vector standard could be approximated by a pair of linked scalar standards on magnitude and phase, as shown in Fig 4. As the figure shows, this type of approximation creates condition regions shaped like sections of a ring, rather than the circular condition areas defined by true vector standards. The computer could interpret this as a vector standard with a deviation magnitude somewhere between the maximum and minimum magnitudes, illustrated by the circles in the figure. Thus, this approximation allows greater deviations of magnitude and phase in some directions than others, which could result in inaccurate estimates of the machine's condition.

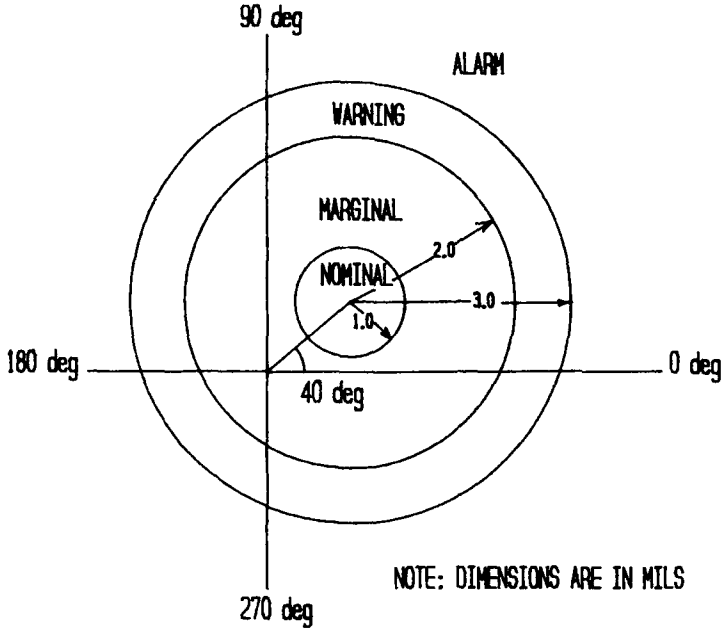

Figure 3.
Illustration of Vector Standard

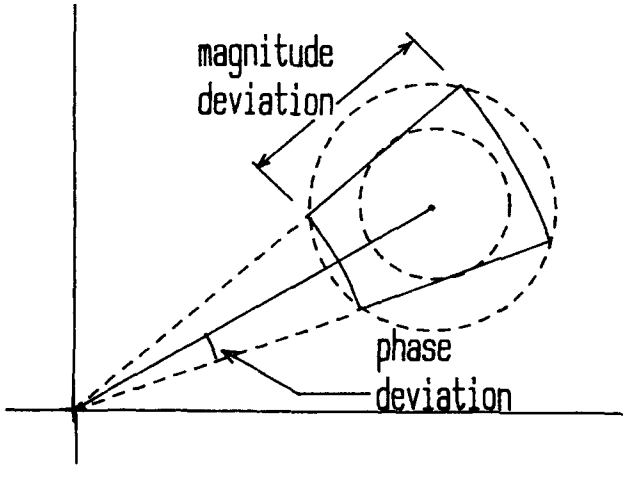

Figure 4.
Approximation of Vector Standard with Scalar Standards

Like scalar standards, the nominal magnitude, phase, and deviations for all vector standards are set before the system is used for the first time. The nominal vector can be reset once data acquisition has begun, after a steady operational condition has been reached. This can be done by either manually entering the new median magnitude and phase or instructing the program to take the next pair of magnitude and phase acquired as the new median values.

The final form of standard used in this project employs a graphical format. An example is shown in Fig 5. Like many published standards, these standards are defined by selecting two variables, such as amplitude and speed, and creating a graph of one variable vs. the other. The graph is divided into regions, each of which represents a different operational status of the machine. The computer then creates an electronic equivalent of the graph which it can compare data against. These standards must be created and set before the system is run.

Intelligent Filter System: The WOT intelligent filter system consists of three parts, all written in PDC Prolog. The first is the filter program itself, which reads acquired data in an ASCII file, compares it to a series of pre-defined standards, and outputs the results to another file. The second part is a setup program, which configures the filtration program so that it knows the format of the data files, and sets up the initial standards to be used. The setup program is used to define all scalar and vector standards, and to select which graphical standards, if any, are to be used from a file of pre-defined graphs. The final part is the standards program, which is used to create the graphical standards.

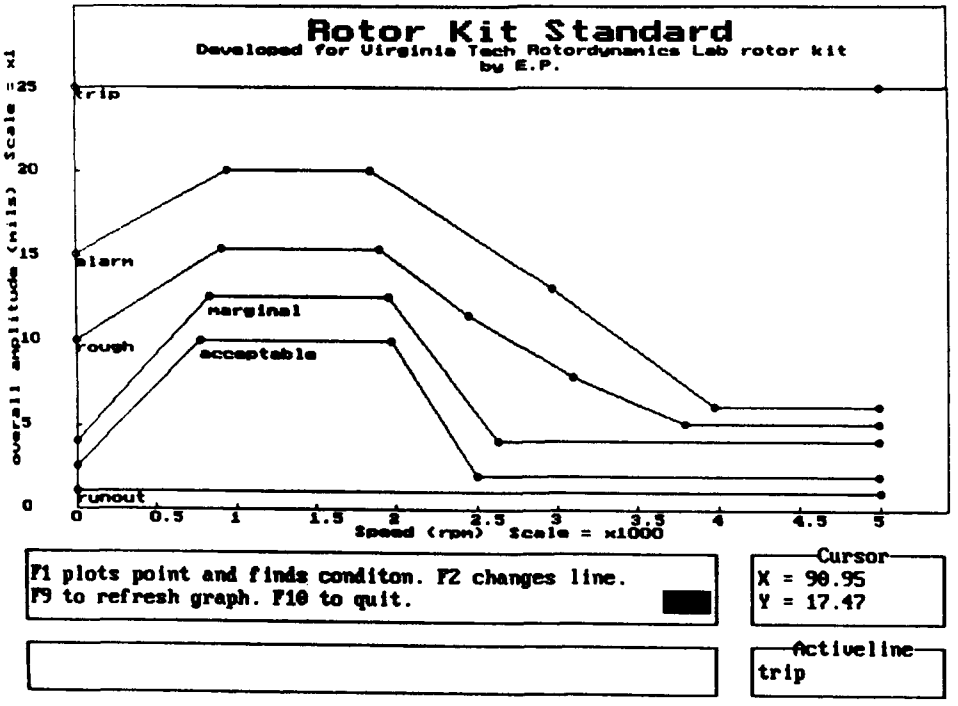

Figure 5.
Graphical standard for WOT intelligent filter system

A separate program must be used to acquire data, store it in a file for the WOT filter to read, call up the filter program, and display the results of the analysis. A program, called the DAC program, has been written in BASIC to accomplish this.

The DAC program can accept inputs from up to sixteen transducers mounted on a machine, although only two (one vertical and one horizontal) are installed on the rotor kit. Currently, the VPI rotor lab data acquisition system is capable of reading nine pieces of data from the rotor kit: overall vibration amplitude, 1x amplitude, 1x vibration phase angle, and gap volts at each probe, as well as shaft speed. The settling time of the DVF-3 makes the system unsuitable for reacting to sudden, extreme changes, such as unexpected blade loss. Transducers are read two at a time. Once the data from a pair of transducers has been read, it is stored in program variables. The next pair is then read, until data has been taken from all available transducers. The DAC program then saves the data in a file and calls the WOT filter program. For developmental purposes, the filter program was configured to analyze the data from each probe with several different standards: scalar standards for gap volts, overall amplitude, and 1x amplitude, a vector standard for 1x amplitude and phase (See Fig 3), as well as a graphical standard for overall amplitude vs. shaft speed (See Fig 5).

The DAC program produces an output file similar to that shown in Fig 6a. The data is expressed as a series of numbers. The first is shaft speed, the next are overall amplitude, 1x amplitude, 1x phase, and gap volts for each of the two probes. After these numbers is a series of reset variables, each of which is associated with one or more of the resetable standards. If a standard's reset variable is zero, the filter program will simply compare the data to the standard and not reset anything. If the variable is one, the program will reset the standard's nominal data equal to the current data. A variable of two will cause the filter program to interrupt data acquisition and ask for the new nominal values, which must be entered manually.

The filter program can be configured so that each resetable standard has its own reset variable in the data file, or several can share a variable. All standards that share variables will be reset together. If a standard does not have a reset variable, its nominal values cannot be changed from the values established by the setup program.

Once the data file has been read by the filter program, data analysis takes only a fraction of a second on a reasonably fast computer. Unless manual resets are called for, it will not write to the screen. The program then creates an output file, similar to that shown in Fig 6b. The results of the analysis are expressed in a form that can be interpreted by looking the file directly, although a program such as DAC would normally be used to read it and present it in a more easily understandable format. Each line in Fig. 6b represents the results of comparing the data to a single standard. A line begins with the variable name or names of the data, (which were defined by the setup program), the value of the data, the type of standard (also defined by the setup program), the nominal value of the standard (if applicable), and finally the status of the machine according to that standard.

Once the output file is written, the filter program calls the DAC program and terminates. The DAC program reads the output file and displays the results. Output can be either to a monitor, disk, or printer. Fig 7 shows a typical output for the monitor. The first numerical column shows the latest acquired value of data. The second displays the status of the data relative to broad standards (scalar, vector, or graphical) that are intended to cover the entire possible range of data. These standards are not intended to be reset often, if at all. A different series of fairly narrow standards (scalar or vector only), referred to as "deviation" standards, were defined to alert the operator to changes in the data, even if it remains within acceptable boundaries. The reference levels of these standards are intended to be reset whenever the operator determines the machine has reached a stable operating point. The third column shows the value of the latest acquired data minus the current nominal reference levels, for that data which is compared to a deviation standard (overall, 1x, phase, and gap volts). The last column shows the status of the data compared to the deviation standards. Due to space limitations, only two channels can be shown on the monitor at a time. If more than two channels are available, the F1 key may be used to select which ones appear.

```
BEGIN
3601 1.7 1.2 40 8 9.8 7.3 154 7.3 0 0 0 0 0 0 0 0 0 0 0 0 0 0 0 0
END
```

Figure 6a
Sample Output File for DAC Program

```
Data:Overall_H Value: 1.7 Data:Speed Value: 3601 Type:Graph Status:Acceptable
Data:Overall_H Value: 1.7 Type:S_Deviation Nominal: 1.6 Status: Acceptable
Data:1x_H Value: 1.2 Type:S_Fixed Nominal: 1.0 Status:Acceptable
Data:1x_H Value: 1.2 Type:S_Deviation Nominal: 1.4 Status: Acceptable
Data:Phase_H Value: 40.0 Type:S_Deviation Nominal: 43.0 Status: Acceptable
Data:1x_H Value:1.2 Data:Phase Value: 40 Type: V_Deviation Nominal: (2.0,40) Status: Nominal
Data:Gap_H Value: 8.0 Type:S_Fixed Nominal: 8.0 Status: Nominal
Data:Gap_H Value: 8.0 Type:S_Deviation Nominal: 7.9 Status: Nominal
Data:Overall_V Value: 9.8 Data:Speed Value: 3601 Type: Graph Status:Trip
Data:Overall_V Value: 9.8 Type:S_Deviation Nominal: 3.6 Status: Trip
Data: 1x_V Value: 7.3 Type:S_Fixed Nominal: 1.0 Status:Trip
Data:1x_V Value: 7.3 Type:V_Deviation Nominal: 2.0 Status: Trip
Data:Phase_V Value: 154.0 Type:S_Deviation Nominal: 180 Status: Alarm
Data:1x_V Value:7.3 Data:Phase Value: 154.0 Type: V_Deviation Nominal: (2.0,40) Status: Alarm
Data:Gap_V Value: 7.3 Type:S_Fixed Nominal: 8.0 Region: Warning
Data:Gap_V Value: 7.3 Type:S_Deviation Nominal: 6.1 Region: Alarm
```

Figure 6b.
Sample Output File for WOT Filter program

```
Rotor Kit Status Screen                              Date: 1/15/91  Time: 16:35:10
CH 1  2  3  4  5  6  7  8  9  10  11  12  13  14  15  16
   -  -  -  -  -  -  -  -  X   -   -   -   -   X   -   -
CHANNEL 1; COMPRESSOR OUTBOARD BEARING - X PROBE                    SPEED=3601 RPM
PARAMETER       CURRENT VALUE     STATUS      CURRENT - REF.    DEVIATION STATUS
---------       -------------   ----------    --------------    ----------------
OVERALL [MILS]        1.7       ACCEPTABLE          0.1           ACCEPTABLE
1 x     [MILS]        1.2       ACCEPTABLE         -0.2           ACCEPTABLE
PHASE   [DEG]          40       *                    -3           ACCEPTABLE
1 x and PHASE          *        *                    *            NOMINAL
GAP VOLTS [-V]         8        NOMINAL             0.1           NOMINAL
-------------------------------------------------------------------------------
CHANNEL 9, TURBINE INBOARD BEARING - Y PROBE                        SPEED=3601 RPM
PARAMETER       CURRENT VALUE     STATUS      CURRENT - REF.    DEVIATION STATUS
---------       -------------   ----------    --------------    ----------------
OVERALL [MILS]        9.8       TRIP                6.2           TRIP
1 x     [MILS]        7.3       TRIP                5.3           TRIP
PHASE   [DEG]         154       *                   -26           ALARM
1 x and PHASE          *        *                    *            TRIP
GAP VOLTS [-V]        7.3       WARNING             1.2           ALARM
_______________________________________________________________________________
SELECT CHANNEL DISPLAY.....F1          CHANNEL RESET.............F3
GLOBAL RESET..............F2          PAUSE ACQUISITION.........F4
```

Figure 7.
Simulated Monitor Output for DAC Program

One of the most useful features of the WOT data filters is its flexibility. The filter program can be configured to read almost any possible ASCII data file. Text may be interspersed with the data. It will ignore any irrelevant lines in a data file, and read only those lines that fit the format defined by the setup program.

The DAC program was written to acquire data from the experimental system located at the VPI rotor lab. It can be modified to accommodate different data acquisition systems, or an entirely new program in a different language can be created to take its place. The filtration program can work with any data acquisition program that reads and writes standard ASCII files, and follows a few broad rules of syntax. Thus, if an existing system is already controlled by an "unintelligent" data acquisition program, modifying it to work with the WOT filter should be a straightforward task.

Conclusions: It has been shown that the present system can monitor overall and changing vibration characteristics. The intelligent filter can compare these characteristics to a series of graphical and non-graphical standards. The results are expressed by classifying the data into a series of status zones. This gives the system certain capacities of a human operator to judge the current status of the machine. Its application to other sensors in a data acquisition system can be accomplished by reconfiguring the setup files and the optional monitor output. With the current hardware, the system can adequately respond to slowly changing machine conditions.

Acknowledgement: This work has been sponsored by a joint industry/Virginia Center for Innovative Technology Grant No. CAE-88-011-01, with additional support from Amoco Research, Bently Nevada, Dresser-Rand, DuPont, Ingersoll-Rand, and Virginia Power. The authors are especially grateful for the support given by Dr. Ira Jacobson, Director of the Institute of Computer Aided Engineering, Charlottesville, Virginia, and for the technical assistance given by Mr. Roy E. Mondy, Rotating Equipment Specialist, Virginia Power, Richmond, VA.

References

1. Kirk, R. G., J. Hoglund, and R. E. Mondy, "Development of a PC-based Off-line Expert System for Evaluation of Turbomachinery Response," Proceedings of the 1st International Machinery Monitoring & Diagnostics Conference, Las Vegas, Nevada, Sept. 11-14, 1989, pp. 439-444.

2. Kirk, R. G., J. Hoglund, and J. Keesee, "Application of Artificial Intelligence for Rapid evaluation of Turbomachinery Dynamic Response and Stability," Proceedings of the JSME International Symposium on Advanced Computers for Dynamics and Design, Tsuchiura, Japan, Sept. 6-8, 1989, pp. 149-154.

3. Kirk, R. G., J. Hoglund, and R. E. Mondy, "Development of a Unique Off-Line PC-based Turbomachinery Expert System," Proceedings of IASTED Conference, Zurich, Switzerland, June 24-26, 1989.

NAVSSES HPAC/HPAD EXPERT SYSTEM

Marc Monaco
Agnes Gardiner
Naval Ship Systems Engineering Station
Philadelphia, PA 19112

Abstract: The Naval Ship Systems Engineering Station (NAVSSES) has developed an online Expert System capable of predicting and diagnosing CG-47 Class air compressor and dehydrator failures. The Expert System is heuristic in nature and PC-based operating under DOS. The knowledgebase contains rules developed in conjunction with NAVSSES machinery experts. These rules describe the interrelation of physical parameters within the machine and relate symptoms to failures. The Inference Engine employs the backward chaining algorithm in an attempt to solve for the goal variable.

The Expert System receives near real-time thermodynamic and vibration data from the Data Acquisition System. Once per minute diagnoses are provided with minimal operator interaction. The result is a system capable of improving shipboard troubleshooting abilities and reducing unnecessary routine maintenance.

A prototype Expert System, including all sensors and signal conditioning, was packaged and installed aboard the USS NORMANDY (CG-60) for shipboard evaluation. The original remains at the NAVSSES Air Compressor and Dehydrator Test Facility for continued improvement and refinement.

Key Words: Artificial intelligence, backward chaining; condition based maintenance; expert system; heuristics; inference engine; knowledgebase; shell

With the rising cost of machinery maintenance and the simultaneous decline in maintenance dollars, the Navy is actively pursuing new and creative methods of predicting and diagnosing machinery failures. This pursuit has led to an area of Artificial Intelligence known as Expert Systems. A heuristic-based Expert System is a computer recreation of the human reasoning process. It contains rules that relate symptoms to failures.

Ideally, the Navy would like to clone its human machinery experts and put one on every ship providing expert analyses of the machine while it is operating. In essence, an online Expert System does just that. It is an attempt to capture

the human expertise gathered over the course of a career and store it in a manner conducive to distribution. The entire fleet may then continually benefit from this expertise instead of a limited number of ships visited by an individual. An initial system to prove this concept was developed at NAVSSES.

NAVSSES serves as the Navy's principle In Service Engineering (ISE) agent for all Hull, Mechanical and Electrical (HM&E) equipment. In addition, in-house testing is performed on full scale prototype units. The majority of in-house testing is supported by a Data Acquisition System (DAS) network spanning the main facility and other remote sites situated within a one mile radius of NAVSSES headquarters.

The NAVSSES Expert System targeted the high pressure air compressor and dehydrator (HPAC/HPAD) aboard CG-47 class surface ships. HPAC's have been a nagging problem throughout the Navy. Low mean time between failures and the expense of re-occurring overhauls makes it a prime target for Conditioned Based Maintenance (CBM). If a failed or failing component can be accurately identified, reduced maintenance dollars will be needed. In addition, when faults are recognized in their early stages, catastrophic failures may also be reduced.

With CBM as the primary objective, the first action taken in the development of the Expert System focused on the design of the system. Several design parameters guided the development. They include the following:

* There are to be minimal user inputs.
* Ease of use is of high priority.
* It should enhance, not replace the tech manual.
* Information must be reported in a clear and concise manner.

Several steps were taken in order to reach the final product. With the project deadline in mind, attention was first focused on promptly selecting a shell. An Expert System Shell is a software package that performs the tasks of loading the knowledgebase and solving for a desired variable using a pre-determined regime. After reviewing several popular commercially available shells, PC Expert Professional was selected based on ease of implementation, ability to import data from the DAS, user interface, control over graphical displays, and the required learning curve. Inference Engine functions are provided by a set of library routines which append themselves to a language such as PASCAL or C. As a result, routines for importing data, controlling the user interface, generating graphics, and recording the data are written in PASCAL.

The next step was to identify the desired goals of the Expert System. SEMMSS data was analyzed to determine the most frequently occurring failures throughout the fleet. It was estimated that 85% of all high pressure air compressor failures involved air valves, rings/seals, air packing, and air coolers. A similar analysis was done for the air dehydrator. Diagnosing these failures became the goal of the Expert System. In all, 55 faults were the targets of analyses. Also included are faults diagnosed using current vibration analysis techniques.

Having defined the objective of the system, a theoretical knowledgebase was developed. Domain Experts in the fields of air compressors, dehydrators, and vibration analysis were consulted. Each was asked to determine the information required to diagnose the set of desired faults. An instrumentation list was devised based on their answers. Redundant measurements were eliminated.

The knowledgebase is comprised of rules in the form of IF... THEN... ELSE... statements. Backward chaining is employed to parse the rules to determine the value of the goal variable referred to as PROBLEM. The shell allows for variables to be declared as multi-valued. When a goal variable is multi-valued, all rules whose conclusion produces a value for the goal variable are evaluated. Using this technique, all possible faults are evaluated. In the event of multiple failures, each is detected and reported.

The complete diagnostic system is composed of two 80386-based PC's. The "front-end" serves as the Data Acquisition System and samples thermodynamic and vibration sensors. In order to maintain total control over the data acquisition and transfer process, the DAS was written at NAVSSES in C language. Thermodynamic measurements (pressure, temperature, flow) are sampled at the rate of once per second. Each of the six accelerometers are sampled at the rate of once per minute and provide a 400 line, 0-1kHz spectrum. The front-end also calculates one minute averages for each of the thermodynamic channels. At one minute intervals, all data is transferred to the Expert System for analysis.

To initiate the transfer, the DAS sends a hardware interrupt to the Expert System. The Expert immediately suspends its current operation to service the interrupt. Data is read from a high speed parallel port and is buffered in memory. Having serviced the interrupt, the CPU returns to the main procedure where the Expert analysis takes place.

With the new data set still in memory, the Inference Engine is activated and tries to determine all possible values of

the variable PROBLEM. As dictated by backward chaining, the Inference Engine searches the Knowledgebase for a rule that concludes a value for PROBLEM and tries to prove or disprove the antecedents.

```
HPAC1A: IF MaxDP > 0.05 AND
          SuspectStage = '2ND STAGE' AND
          DischTemp > NormDischTemp
        THEN PROBLEM = '1ST STAGE SUCTION VALVE' [90].
```

For example, each of the three conditions in the antecedent shown above must prove true in order for this rule to fire. If the largest pressure drop among the 5 compressor stages (MaxDP) is greater than 5% with respect to nominal, the stage with the largest pressure drop is the second stage, and the discharge temperature of the second stage is elevated then it may be concluded the 1st stage suction valve is failing. Backward chaining puts PROBLEM on the goal queue and then checks if the value of MaxDP is greater than 5%.

To make this determination, the inference engine finds a rule that concludes a value of MaxDP. If MaxDP is found to be greater than 0.05, the process is repeated for SuspectStage and finally DischTemp. If MaxDP is found to be less than 0.05, the Inference Engine discards this rule and looks for the next rule that concludes a value for PROBLEM. This is continued until no rules that conclude a value for PROBLEM remain.

Notice the conclusion of HPAC1A terminates in a number ([90]). By definition, this is the confidence factor assigned to that conclusion. In the HPAC/HPAD Expert System, this factor is used to rank the reported faults. By design, only five concurrent faults may be presented to the user at any one time. As a result, by utilizing the confidence factor as a ranking indicator, the five most imperative faults are shown. On a scale from 0 to 100, the 1st Stage Suction Valve failure rates 90 in this example.

Fault implementation was conducted using a Dresser-Rand air compressor model N20NL-10 at the NAVSSES facility. A representative sample of the faults was chosen to test the capabilities of the Expert System. For example, a baseline run was first conducted with the machine in its nominal condition. After cooldown, a 5th stage discharge valve with a minimal level of deterioration was installed and the machine was run. The operating conditions of the machine were reported by the DAS and the performance of the knowledgebase was monitored. If an incorrect conclusion was reported, the data was analyzed and the cause of the discrepancy deduced and corrected. The valve was removed and the level of deterioration was increased. This was

repeated for various components with slight, moderate and severe amounts of wear.

The information reported by the DAS is sent to the Expert System user interface for display. The screen is composed of three regions and the overall format never varies. The BLACKBOARD occupies the largest portion of the display and is used to display graphics, schematics, etc. Typically the BLACKBOARD shows a cutaway view of the compressor with color-coded parameters situated in relative proximity to their physical location.

Diagnosed faults, the time of the last update, and other miscellaneous messages are presented on the MESSAGE PAD. As many as five faults may be reported here; however, in the event more than five faults have been diagnosed, the five most severe are reported. The final region is the STATUS BLOCK where HPAC and HPAD health as well as Expert System health and status are reported in color-coded blocks. While the machine is operating within its nominal state, the parameters within the BLACKBOARD are displayed in green, HPAC and HPAD health are reported as NORMAL, and "No Problems to Report" is displayed on the MESSAGE PAD. When one or more faults occur, a brief message indicating the detected fault(s) appears on the MESSAGE PAD. Assistance for each reported fault is available to the user by pressing the respective function key. Doing so produces text on the MESSAGE PAD and a related graphic effect on the BLACKBOARD. For example, if the 3rd Stage Suction Valve is diagnosed as failed or failing, the message

3rd STAGE SUCTION VALVE (Press [F1] for Help)

is displayed on the MESSAGE PAD. If the user presses the F1 key for assistance, an isometric view of the compressor showing the location of the valve is shown on the BLACKBOARD and text is presented on the MESSAGE PAD. The text was developed to enhance the information already available to ship's force in the tech manual and was not intended to replace it. A typical text might provide the user with the paragraph number in the tech manual to be consulted before attempting a repair.

The NAVSSES HPAC/HPAD Expert System prototype is currently installed aboard the USS NORMANDY (CG-60) for shipboard evaluation. Ship's force has been directed to monitor but not act upon the diagnosed faults and repair recommendations during the evaluation period. Rather, maintenance actions are recorded and returned to NAVSSES. Data will be downloaded during the ship's next period of availability and corroborated against the recorded maintenance actions. It is anticipated proper repair actions can be endorsed and unnecessary ones identified by the analyses provided by the Expert System.

The Navy will be relying more heavily on Artificial Intelligence to improve its future capabilities of predicting and diagnosing machinery faults. For now, this system represents NAVSSES' initial contribution to the Navy's pursuit of Conditioned Based Maintenance.

SYSTEM STUDY OF CONDITION-BASED MAINTENANCE SYSTEM FOR SHIPBOARD HIGH-PRESSURE AIR COMPRESSORS

Henry R. Hegner and John P. Hudak
ECO, Inc.
1036 Cape St. Claire Center
Annapolis, MD 21401

Christopher P. Nemarich and Wayne W. Boblitt
David Taylor Research Center
Annapolis, MD 21402-5067

Abstract: This paper presents a study of a shipboard machinery condition-based maintenance (CBM) system for a high-pressure air compressor (HPAC). The paper summarizes efforts and plans, to date, on the CBM program and documents the results of program efforts during 1990. The HPAC system was selected to demonstrate detection, diagnosis and prognosis (DD&P) techniques, and a review was completed of its design. A detailed review was performed of available failure analysis data on the HPAC to select specific critical failure modes and problems for HPAC subsystems and components. These efforts were conducted so that HPAC parameters can be related to specific failure modes. This approach allows the impact of each subsystem or component degradation to be traced during the monitoring cycle until failure occurs. Several failure modes were identified for evaluation on the HPAC. The selection of preliminary DD&P parameters and sensors to monitor failures was also completed. A preliminary test plan and procedures was developed for use in the test program. This test plan and procedures will be used to establish the validity of the selected DD&P techniques and to identify new or improved sensors requiring development in order to monitor critical parameters so that the required failure modes can be monitored by the CBM system.

Key Words: Machinery performance and condition monitoring; condition-based maintenance; fault detection; diagnosis and prognosis; failure analysis; machinery parameters and sensors; high-pressure air compressor monitoring.

Introduction: The reliability of machinery systems aboard present Navy ships depends a great deal on time-directed maintenance (TDM). This often leads to under-utilized and over-maintained systems. Maintenance based on reliable on-line test and diagnostics will be needed in the future to allow maximum ship systems performance at reduced manning and cost. The development of a condition-based maintenance (CBM) approach is feasible and practical at the present time using state-of-the-art, high technology, monitoring devices, sensors, and computer-based artificial intelligence (AI) systems. Presently, the David Taylor Research Center (DTRC) on-line CBM monitoring system is limited to those parameters monitored by available sensors. The CBM approach will determine what conditions to monitor in order to provide the capability to detect, diagnose and prognose (DD&P) machinery failures and to determine required maintenance actions. This requires the identification of critical failure modes, and the corresponding parameters and sensors to measure these failure modes.

The present status of shipboard performance monitoring of installed equipment is defined as a Level O system and consists of portable, externally applied, sensing devices and data acquisition systems. The cost of present machinery performance trials is high due to the labor-intensive methods required with Level O systems. Also, standardized data acquisition methods, although under development, are not available across machinery classes. The development of advanced machinery systems with CBM philosophy designed in and an advanced CBM system with appropriate architecture and sensors will address these issues.

The DTRC has initiated a project to do research and to develop a revolutionary shipboard machinery CBM system.[1] The project was started by developing an on-line local CBM system for an existing shipboard High-Pressure Air Compressor (HPAC) in the laboratory at DTRC[2]. This system is defined as a Level I system, and it uses only sensors presently installed on the machine as well as a limited diagnostic and local display capability.

The HPAC CBM system is being expanded to include additional sensors and failure mode diagnostics but not to the point of interfacing with other equipment (Level II). Next, another auxiliary machinery item will be addressed. A similar development process will be followed for this machine making use of the experience and knowledge gained with the HPAC system. The next step will be to link the two machines via a local area network (LAN) and provide an interface to a "whole-ship" fiber optic data bus (Level IIA).

The final step will be to generalize efforts to develop CBM design guidance and sensor requirements for the entire shipboard machinery plant so that required sensors can be embedded into machinery and concurrent engineering included in machinery design. This will enable machinery developed in the future to effectively and efficiently include an integrated Level III CBM system in ship equipment designs while making optimum use of limited display and transmission resources.

The initial tasks of the three (3)-level CBM program were initiated during 1988-89 as part of the Navy's Logistics Block Exploratory Development Program. The Level II task efforts were initiated during 1990 with a review of the design of the shipboard HPAC system at DTRC.[3,4] The technical approach includes a long-life design strategy which evaluates the life content and performance characteristics of the machine when operating and aging. This approach will be used to develop techniques to DD&P impending loss of performance or failure of the machine.

A review was performed of failure analysis data available on the HPAC subsystems and components. This review allowed the selection of critical failure modes so that machinery parameters can be selected to relate to specific failure modes. This will allow the effect of an implanted component fault on system performance to be traced until component failure occurs. Specific failure modes were then selected to address on the HPAC. This required the review, prioritization and ranking of the critical failure modes identified on the HPAC. Several failures were found to be practical to implement on the test bed system.

Preliminary DD&P parameters and sensors were identified for monitoring the selected failures on the HPAC. A preliminary test plan and procedures were developed to establish the validity of the selected DD&P techniques on the HPAC at DTRC.

Design Review: High-pressure (HP) air compressor systems supply air at required pressures, flow rates, and purity to ship equipment and miscellaneous services. Typically, the system consists of a HPAC plant and a HP air main and branches. On a surface combatant ship, the HP air is normally supplied by two, motor-driven, HPACs. The compressors are reciprocating and multi-staged, vertical single-acting, saltwater cooled, and cross-connected through a single main header. The HPACs are normally operated one at a time, although they can be operated in parallel through the cross-connected main headers, if required. The compressors also have both manual and automatic controls.

The HPAC under investigation is partitioned into smaller subsystems or components as given in Figure 1. The HPAC is bounded on the inlet by the suction silencer and on the outlet by the discharge flexible hose.

Failure Analysis Data Review: The Naval Sea Systems Command (NAVSEA) recently completed a detailed system study on the same basic compressor as the HPAC system at DTRC.[2,3] The study consisted of a design review (DR), as well as review of experience (ROE). The DR was an engineering analysis of system performance with emphasis in the area of system functions and a failure modes and effects analysis (FMEA). The ROE portion of the study concentrated on past system failures, effects and maintenance practices.

The DR included a FMEA to determine possible HPAC system failure modes and their effects. This FMEA provided the failure modes and effects for each HPAC function at the system, subsystem and component level.

The ROE used a variety of sources for the HPAC system. An analysis of the historical data was conducted to identify failure modes and problems. The following were established as high failure items as reported from all sources: running gear; cylinders, heads and pistons; air valves; air subsystem; separator drain subsystem; cooling water subsystem; cylinder lubricators; motor subsystem; and discharge flexible hose and fittings.

During the ROE, maintenance actions were reviewed. The major contributors to the HPAC maintenance burden were identified. Two (2) of these components and their related failure modes and problems are summarized in Table 1.

The following account for over 81 percent of the failures in the HPAC as a result of the ROE: the sump, piston/piston rings, suction/discharge valves, air-stage relief valves, air-suction flexible hose, separator subsystem automatic drain valve, cooling water automatic shutoff valve, zinc anodes, cooling water flexible lines, cylinder lubricators, air-pressure switch, temperature monitoring unit, compressor discharge flexible hose, and resilient mounts. The addition of the motor subsystem would account for over 95 percent of the HPAC failures now experienced.

Test Bed Facility Description: An on-line CBM demonstration model system was developed and installed on the HPAC test bed system at DTRC.[1] The CBM model is a distributed, microprocessor-based, system incorporating graphical man/machine interface (MMI), a diagnostic rule-based expert system and LAN software. The CBM model integrates commercially available hardware and software packages with DTRC developed software, sensors and monitoring techniques. The demonstration model makes use of new sensor types, programmable logic control, and industrial process control hardware and software.

The HPAC test bed system provides a means of demonstrating CBM on an actual shipboard auxiliary machine. The HPAC is a motor-driven, oil-lubricated, water-cooled, four-cylinder air compressor. Because it is complex and has a variety of subsystems and components, the HPAC is ideally suited for demonstrating CBM.

The existing CBM demonstration model is shown in Figure 2 and consists of a pair of 386 PC/AT computers and a Gould 984 programmable logic controller (PLC) with 32 analog input channels. A commercially available process control software package is used for system control, data management and display. The software package supports the communication with the PLC, the DD&P software, and the LAN software. Reference 1 provides additional information on the demonstration model system.

Test Bed Failure Mode Selection: To select specific failure modes to be addressed on the HPAC test bed system, the major failure modes and problems had to be reviewed and prioritized. All of the major failure modes related to the HPAC were evaluated and given a

rating. Each of the candidate failures were rated by means of eight criterion. All of the criterion were considered of equal importance with no weighting of the individual factors.

The criteria were used to rank failure modes. All of the candidate failure modes were then reviewed in detail to determine if it would be practical to simulate each fault on the HPAC. Table 2 summerizes the results of this review for four (4) of the candidate failure modes.

A number of the candidate failures were judged to be practical to implement on the HPAC test bed. The selected failure modes were further grouped by the previous criterion as well as the difficulty associated with the implementation of the failure. Even though a cracked piston ring is a primary failure mode, it may not be easily evaluated in the test program. This is because of the difficulty of repeatedly modifying the rings, and the difficulty of restoring the rings to their original condition to demonstrate the effectiveness of the selected DD&P techniques.

Machinery Parameter and Sensor Selection: During the DR and ROE, preliminary DD&P parameters and sensors were identified for each of the subsystem or component failure modes. The impact of each HPAC degradation can then be traced throughout the test cycle until a predetermined component failure occurs. The subsystem or component failure modes were first screened for the likelihood of occurrence or criticality, and then each item was examined for monitoring by DD&P parameters to reduce the frequency of failure or its impact on the system or component. If a DD&P technique or parameter exists, it was then evaluated for effectiveness. If a technique does not exist, one will be developed for the Level II CBM system.

To reduce the number of failure modes for monitoring by the CBM system, they were screened further to eliminate those failures which were: (1) unlikely to occur, not catastrophic, and do not result in major damage; (2) a result of improper system line-up by the operator; and, (3) malfunctions or degradation of interfacing systems.

Applying the above criteria, the following were eliminated from further consideration: unloader subsystem, running gear lubrication, and resilient mounts.

Each of the major component failures identified in the DR and ROE were investigated for possible DD&P parameters and sensors. Table 3 also provides a preliminary list of DD&P parameters and sensors for four of the major problems. In addition, system level, environmental and safety related parameters and sensors need to be selected for the test program.

To detect and diagnose a problem in a test bed subsystem or component, operational primary and secondary effect parameters need to be monitored that are effected when the problem occurs. For example, if there is a leaking, worn or broken first-stage discharge valve, then first-, second- and third-stage discharge pressure will all be lower than normal with the most pronounced effect at the first-stage. Also, the first- through fourth-stage discharge temperature will all be higher than normal with the most pronounced effect at the first-stage. The presence of these fault symptoms allow the detection, diagnosis and identification of the defective valve.

Thus, to identify a specific failure from a group of possible failures, a number of parameters will need to be monitored by the CBM system. To minimize the number of parameters and sensors, DTRC is investigating using knowledge of compressor internal processes to isolate a problem. A set of thermodynamic equations are used along with synthesized parameters for diagnosis and prognosis. This approach should allow using the minimum set of sensors

to diagnose a failure and reduce the possibility of not detecting single or simultaneously occurring failures.

To further illustrate the relationship between HPAC failures and parameters, refer to Table 4 where problems are listed down the left column for leaking suction and discharge air valves, and the corresponding DD&P parameters are listed at the top of the table. For each valve fault, the discharge pressure and temperature changes from normal are given as well as the most pronounced pressure or temperature effect. Similar discharge pressure and temperature changes from normal can also be shown for internal air leakage in the separator drain subsystem, interstage coolers, cylinder head O-rings, and piston rings.

Ideally, each HPAC fault would be identified by a unique set of a few changing parameters; but in practice, instances will exist where more than one fault produces the same symptoms. Therefore, additional parameters will need to be monitored to resolve such situations. Also, the HPAC test program should monitor a few system level, environmental and safety related parameters such as block-mounted vibration, ambient air temperature and pressure, and automatic shutdown switches.

In order to detect and diagnose the selected failure modes and problems for the HPAC test bed system, a preliminary list of 47 parameters was selected. Thirty-two (32) of these parameters are presently monitored on the HPAC test bed system. The preliminary list of parameters also include a number of parameters due to the uncertainty of some to effectively detect and diagnose certain failures. Those parameters and sensors required to conduct the test program to obtain system level, environmental and shutdown data were included. It is expected that only a few new sensors, if any, may be required by the CBM system to detect and diagnose the selected failure modes.

Table 5 provides the failure mode and test parameter matrix for four of the HPAC test bed system failure modes. This matrix provides the list of preliminary test parameters and associated sensors anticipated to detect and diagnose the four (4) selected failures. The nine (9) failures deleted from further consideration were associated with bearings and hose or line and fitting leakage. The bearing wear problem is difficult to generate and measure and requires a long test program. Although hose, line, tubing and fitting leakage is easy to generate, it was deleted from the test program due to the difficulty in measuring leakage and the fact that it is usually simple to find by visual inspection.

Test Program: As stated previously, the objective of the CBM program is to develop the technology required for the implementation of the CBM system in future ship applications. In order to achieve this objective, a general procedure is being developed to produce a Level III CBM system. This procedure will be demonstrated initially on the HPAC test bed system.

This test bed facility was selected based on program objectives, time frame, and cost. A preliminary test plan and procedures was developed to establish the validity of the DD&P techniques within a controlled laboratory environment. This will allow the implementation of the Level II CBM system in the test facility and to execute the test plan.

Conclusions: The objective of this program is to develop an automated demonstration model for: monitoring, on-line, the performance and condition of shipboard propulsion, electrical and auxiliary machinery; predicting impending failures; and improving maintenance planning and allocation of resources at all maintenance levels. This objective will be achieved by means of a three (3)-level CBM program.

This program will minimize the impact of the CBM system on the ship because the Level I system will use the existing shipboard data transmission system and engineering plant sensors. The only additional hardware and software required for the system will be that contained in the CBM system itself. In addition, the CBM software development will be limited to diagnostic and fault isolation algorithms required for the machinery under test. The CBM system will also use existing computer-based data acquisition and control hardware and software products.

The complete performance, condition and maintenance monitoring capability, including prognosis, will be achieved by the Level II system. The system will be expanded to include additional test points, advanced type sensors, and prognostic software algorithms which will require additional processing capability within the CBM system. The Level I system will make maximum use of existing hardware, software and sensor technology and can be included on a ship system with a minimum impact. The primary functions that can be provided by the Level I system are in the areas of (1) detection, diagnosis, and isolation of faults; (2) limited trending; (3) storage and analysis of performance data; and (4) machinery history maintenance data.

The Level II system will add the capability to perform: a complete trend analysis; predict impending failures and their causes; and determine maintenance requirements. Therefore, a more complete CBM capability can only be achieved by means of the Level II system development program. The advantages of this program are to (1) eliminate short falls associated with a limited Level I system, (2) minimize risks associated with the Level II development, and (3) facilitate achieving the Navy's Systems and Equipment Maintenance Monitoring for Surface Ships program objectives on future ship classes.

The Level III CBM System Development Program now underway will incorporate all aspects of integrating CBM with future ship data transmission, damage control and machinery control systems. The Level III system implementation on future ship classes will result in achieving full potential of CBM.

There is an established need in the Navy to improve methods for machinery system maintenance. Such methods have a direct impact on ship operational condition and logistics support as they strongly affect ship state-of-readiness and maintenance cost. Moreover, improved maintenance methods will reduce catastrophic failure rate, as well as decrease maintenance repair time and increase time-between-failures. The CBM program can provide the shipboard machinery monitoring capability required for future surface combatants and submarines.

Acknowledgement:
The knowledge and efforts documented in this paper were acquired and pursued in accordance with contract number N61533-88-D-0033, delivery order number 0032, Technical Support on Condition-Based Maintenance for Shipboard Machinery, for DTRC, Annapolis, Maryland. The authors express their appreciation to the Navy for the opportunity to report on the work performed by ECO on behalf of the DTRC. They wish particularly to thank Mr. G. William Nickerson for his continued support and suggestions.

References:
1. "Condition Based Maintenance for Shipboard Machinery", G. William Nickerson, DTRC, Proceedings of the 44th Meeting of the Mechanical Failures Prevention Group, April 3-5, 1990, pages 285-293.

2. "A Condition Based Maintenance Monitoring System for Naval Shipboard Machinery", Christopher P. Nemarich, Wayne W. Boblitt, and David W. Harrell, DTRC, Proceedings of the 44th Meeting of the Mechanical Failures Prevention Group, April 3-5, 1990 pages 295-306.

3. "Systems and Equipment Maintenance Monitoring for Surface Ships (SEMMSS) FF1052 High-Pressure Compressed Air System Study", Final Report, NAVSEA N00024-84-D-4312, Technical Instruction 050-501, 30 June 1986.

4. "FF1052 High-Pressure Compressed Air System, System Performance and Condition Evaluation (SPCE) Book", Final Report, NAVSEA Contract N00024-86-C-4030, Technical Instruction 8S2-702, 29 January 1988.

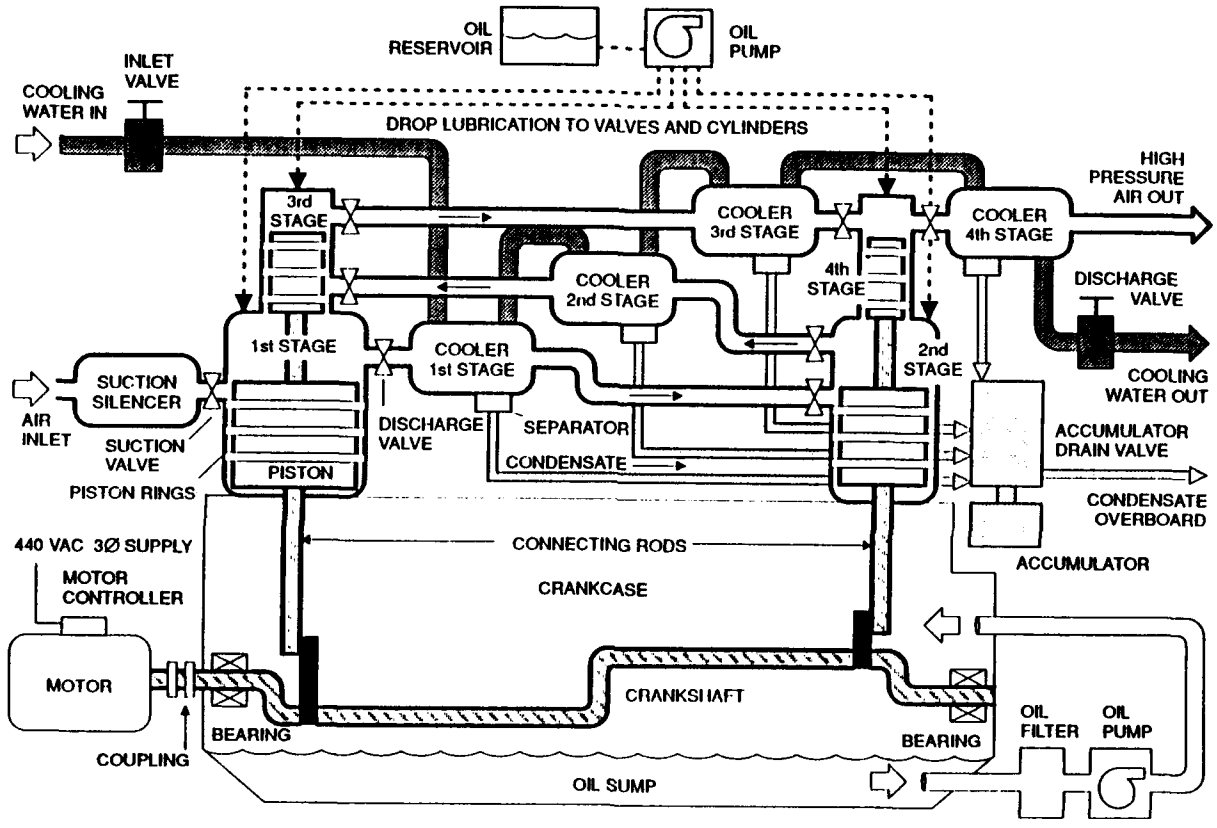

FIGURE 1. HPAC SUBSYSTEMS AND COMPONENT CONFIGURATION

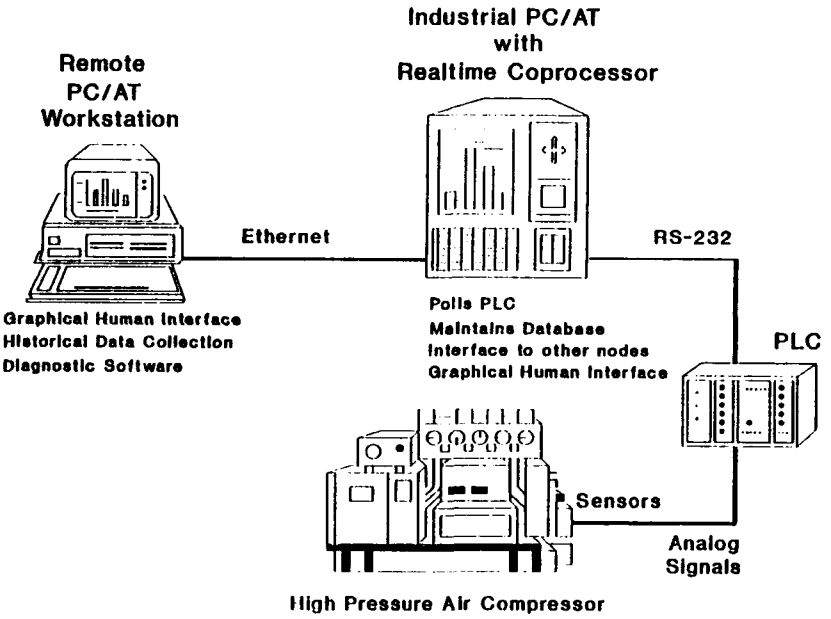

FIGURE 2. CBM DEMONSTRATION MODEL

TABLE 1. HPAC ROE SUMMARY

COMPONENT FAILURE MODE/PROBLEM	FAILURE EFFECT	CORRECTIVE MAINTENANCE
Cylinder, Heads and Pistons		
Pistons and rings worn/ scored/damaged	Noise Reduced flow/ pressure Blowby of water/ oil to sump	Compressor overhauled and pistons/rings replaced
Cylinder heads eroded/ corroded		
Air Valves		
Suction/discharge valves	Leakage Reduced/loss of flow/pressure	Repair or replace
Weak/broken springs		
Worn/corroded/burned seats		

TABLE 2. SUMMARY OF TEST BED FAULT GENERATION OR SIMULATION REQUIREMENTS

SUBSYSTEM OR COMPONENT	FAILURE MODE/ PROBLEM	FAULT GENERATION OR SIMULATION
Cylinder, Heads and Pistons	Pistons and rings worn/scored/damaged	Crack or cause ring to stick, hone liner or grind ring, increase clearance or gap
	Cylinder heads eroded/ corroded	Grind cylinder head
Air Valves	Suction/discharge valves	
	Weak /broken springs	Damage spring
	Worn/corroded/ burned seats	Damage seat

TABLE 3. PRELIMINARY LIST OF HPAC DD&P PARAMETERS AND SENSORS

SUBSYSTEM OR COMPONENT	FAILURE MODE/ PROBLEM	DD&P PARAMETER	TYPE OF SENSOR
Cylinder, Heads and Pistons	Pistons and rings worn/scored/damaged	Pressure Temperature Electrical Current	Pressure Temperature, RTD Current Transformer
	Cylinder heads eroded/ corroded	Particle quantity and size	Wear particle
Air Valves	Suction/discharge valves		
	Weak /broken springs	Pressure Temperature	Pressure Temperature, RTD
	Worn/corroded/ burned seats	Electrical Current	Current Transformer

TABLE 4. EFFECT OF INTERNAL AIR LEAKAGE
ON DISCHARGE PRESSURES AND TEMPERATURES

Leakage at:	Discharge Pressure				Discharge Temperature			
	1st Stage	2nd Stage	3rd Stage	4th Stage	1st Stage	2nd Stage	3rd Stage	4th Stage
AIR VALVES								
1st-Stage Suction	LOW	low	low	-	low	high	high	HIGH
1st-Stage Discharge	LOW	low	low	-	HIGH	high	high	high
2nd-Stage Suction	HIGH	LOW	low	-	HIGH	low	high	high
2nd-Stage Discharge	high	LOW	low	-	high	HIGH	high	high
3rd-Stage Suction	high	HIGH	LOW	-	high	HIGH	low	high
3rd-Stage Discharge	high	high	LOW	-	high	high	HIGH	high
4th-Stage Suction	high	high	HIGH	low*	high	high	HIGH	low
4th-Stage Discharge	-	high	HIGH	low*	-	high	high	HIGH

NOTES:

(1) Tabulation indicates pressures or temperatures higher or lower than normal.
(2) Capitals indicate location of most pronounced effect.
(3) *If leakage is minor, the normal final discharge pressure will not be affected.
(4) *If leakage is extensive, the normal final discharge pressure cannot be obtained.

TABLE 5. TEST BED FAILURE MODE AND TEST PARAMETER MATRIX

SUBSYSTEM OR COMPONENT	FAILURE MODE/ PROBLEM	Pressure	Ambient Air	Stage 1 Output	Stage 2 Output	Stage 3 Output	Stage 4 Output	Temperature	Ambient	Stage 1 Input	Stage 1 Output	Stage 2 Input	Stage 2 Output	Stage 3 Input	Stage 3 Output	Stage 4 Input	Stage 4 Output	Final Discharge	Oil Subsystem	Particles	Motor Subsystem	Voltage Phases A-B	Voltage Phases B-C	Voltage Phases A-C	Current Phase A	Current Phase B	Current Phase C	Power
Cylinder, Heads and Pistons Stage 3	Pistons and Rings Worn/ Scored/ Damaged			+	+	-				+		+		-		+			+			X	X	X	X	X	X	X
	Cylinder Heads Eroded/ Corroded			-	-	-	-			-		-		-		+			+			X	X	X	X	X	X	X
Air Valves Stage 3	Suction/ Discharge Valves																											
	Weak/ Broken Springs																											
	Suction			+	+	-				+		+		-		+						X	X	X	X	X	X	X
	Discharge			+	+	-				+		+		+		+						X	X	X	X	X	X	X
	Worn/ Corroded/ Burned Seats																											
	Suction			+	+	-				+		+		-		+						X	X	X	X	X	X	X
	Discharge			+	+	-				+		+		+		+						X	X	X	X	X	X	X

LEGEND
- PARAMETER VALUES LOWER THAN NORMAL
+ PARAMETER VALUES HIGHER THAN NORMAL
X PARAMETER CHARACTERISTIC MONITORED TO DETECT AND DIAGNOSE FAILURE

BEYOND FAILURE AVOIDANCE: EVOLUTION OF AN EXPERT SYSTEM OF MECHANICAL SYSTEMS INTEGRITY MANAGEMENT

Robert L. Kincaid
Spectron International, Inc.
Caparra Heights, Puerto Rico 00922-1849

ABSTRACT: The goals of the Mechanical Failures Prevention Group to "reduce the incidence of mechanical failure and to develop methods for failure avoidance" reflect a traditional approach to maintenance. One's immediate reaction is very positive; "Yes, that is the maintenance ideal!" In practice, however, does it actually fulfill the practical needs of today's maintenance and production managers and their sophisticated mechanical operations?

During the course of the past thirty years, we have, in close cooperation with our clients, engaged in identifying precisely those needs and developing means to fulfill them. The result has been the development of a stand-alone expert system of advanced maintenance through applied tribology, the science of friction, wear and lubrication of opposed surfaces in motion.

In tracing the development of Mechanical Systems Integrity Management from its origins in "fault detection and failure avoidance" to its present expert system status each of four evolutionary steps is discussed:

1) Identification of user needs,
2) Formulation of a maintenance philosophy to satisfy those needs,
3) Selection and development of technology to provide the needed data base, and
4) Integration of the above into a stand-alone expert system for on-site application.

KEY WORDS: Audit; expert system; Mechanical Systems Integrity Management; tribology.

I. IDENTIFICATION OF USER NEEDS: Who is the user and what are his needs?

As simple as this sounds, it is perhaps the most difficult step in the entire process of developing an appropriate expert system in the field of mechanical operations and maintenance. The over-all user, of course, is the maintenance department. Within that department, however, are various users with varying needs: mechanical personnel (field & shop), supervisory and administrative staff, and the Maintenance Manager himself. The needs of each must be determined, met and integrated into a comprehensive and cohesive system which fulfills the philosophical goals of the department as a whole.

In the early days of expert systems development, this process of needs identification would have fallen to a "knowledge engineer" who would ask appropriate questions of appropriate people and then program their responses into an "expert system". This was effective in straight-forward rule-based diagnostic reasoning. The development of an integrated program of advanced maintenance management, however, is far broader in scope, as it must apply a technical approach to a philosophical orientation and still be flexible enough to permit an evolutionary mode of development.

What then are the user needs?

Traditionally, the simplest needs have been considered those of the field and shop personnel: the mere identification of units suffering mechanical distress. This is precisely the area to which all techniques of "condition monitoring" such as oil analysis, ferrography, vibration and non-destructive testing are applied, and where we began.

The major fault our clients found with these techniques was not in their ability to detect a mechanical malfunction, but in their failure to provide information as to the *cause* of the malfunction. Maintenance based on "condition monitoring" had become a continuous cycle of detection and repair of mechanical distress rather than of detection and correction of the root *cause* of this distress. Clients felt limited by this strictly remedial approach to maintenance. While not discounting the benefits derived from "failure avoidance", they continued to seek a more efficient, cost-effective and controlled approach to maintenance and its management.

Needs of the mechanical staff were now seen to extend past the simple identification of distressed equipment to include detection and identification of causal factors of mechanical distress.

Supervisory and administrative staff needs were defined specifically as well. In addition to the information required by mechanical personnel, other information pertinent to the effective administration of maintenance was needed, such as a continuing update of equipment status, required maintenance action, equipment due for monitoring, etc.

Finally, the basic needs of the Maintenance Manager himself were determined: to maintain a management-oriented overview of his entire operation, including equipment condition, maintenance operations and control, and a means of determining trends and identifying problem areas.

As simple as these needs now appear, it took years of effort working with many types and sizes of mechanical operations to arrive at their definition. As they became more clearly defined, a maintenance philosophy began to evolve which would become the centerpoint around which Mechanical Systems Integrity Management would develop.

II. FORMULATION OF A MAINTENANCE PHILOSOPHY: It is of constant surprise to me to find so few maintenance operations that have defined their responsibilities and developed a philosophy to pursue them. Virtually none see themselves as a part of the production team, but rather as an independent damage control group. If asked where they would give priority attention, whether to units identified as suffering critical, precautionary or normal conditions, their typical response is, "To the critical." By contrast, the response from those with whom we developed this program would inevitably be, "Deadline the *critical* units, and give priority attention to the *precautionary* units to insure that production requirements for equipment are met."

Here we have the fundamental difference between the traditional maintenance approach of "fault detection and failure avoidance" and the evolved philosophy of mechanical systems *integrity management.*

III. SELECTION AND DEVELOPMENT OF TECHNOLOGY: To effectively manage mechanical systems integrity, we must understand the causal factors affecting mechanical integrity. What are these factors? Where do they reside? How do we deal with them? Answers to these questions derive from the modern technology of tribology, the study of friction, wear and lubrication.

Although we would not apply tribology as a discrete discipline until around 1980, our selection and development of analytical techniques to resolve specific problems fortuitously provided an extensive data base of tribologically significant causal factors of mechanical distress to be applied in the future development of Mechanical Systems Integrity Management and its expert system.

To cite an example, one of our first steps taken in new technology selection and development arose not from technical maintenance needs, but rather from fiscal demands imposed by the comptroller of one of our clients. He refused further funding of the existing program of "failure avoidance" as being excessively conjectural as to its cost-effectiveness, and required that future programs provide a measurable return on the cost of the program.

Extension of service intervals was a potential area for cost reduction, but new technology was required to determine the actual level of integrity of the used lubricants. In particular, additive depletion was of major concern. Fortunately, the then-emerging technology of infrared spectroscopy provided the solution to this immediate problem and, as the technology developed, opened doors to applied tribology for advanced maintenance through Mechanical Systems Integrity Management.

The development of other technologies as well enhanced Spectron's capability, but it was the major advances in electronics and computer science during the 1970s and 1980s revolutionizing analytical instrument design and desk-top computing, that made feasible the concept of on-site Mechanical Systems Integrity Management facilities utilizing expert system software.

IV. A STAND-ALONE EXPERT SYSTEM FOR ON-SITE APPLICATION: As we began the task of committing our experience and knowledge to a computerized expert system, we needed to decide how to structure this program. What type of mechanical systems and mechanical operations were to be included? What data was pertinent to each? How would the analytical data be interpreted and evaluated within the program? How would it then be reported to the end user?

The first step dealt with the mechanical systems and operations to be included. We decided to include all the diverse equipment and operations with which we were presently dealing; in short, any mechanical operation using oil-wetted components. We then decided to take a matrix approach toward classifying these components, using sub-sets to deal with "anomalies" within individual sets. For example:

INTERNAL COMBUSTION ENGINES
- Marine or "other"
  - Diesel Engine
    - Trunk Engine
      - Electro Motive Diesel
    - Cross-head Engine
      - Mirrlees
  - Gas Engine

Gasoline Engine

GEAR DRIVES
- Marine or "other"
- Transmission

GAS COMPRESSORS
- Gas Compressor
- Refrigeration Compressor

With this approach, all mechanical systems are classified within one of the three generic categories above, but may fit a more specific subset as well. The interpretive logic is common to all units falling within a given generic category, but branches specifically for individual anomalies or subsets. This enables us to deal with a myriad of mechanical systems of varying makes, models and series without the necessity of an independent program for each.

What data was pertinent to each and how would it be interpreted and evaluated within the program?

The role lubrication plays throughout the chain of causal progression from friction to wear to mechanical distress and failure derives directly from the field of tribology. As one might expect, factors of contamination, degradation and viscosity are all pertinent to lubrication, and consequently, to mechanical integrity. Just how each of these factors will effect the mechanical integrity of the individual system depends upon the friction mode of each (dry, boundary, mixed or fluid) as well as the lubrication regime (*total*, including hydrodynamic and hydrostatic; or *deficient*, including boundary or elastohydrodynamic EHD). This in turn provides the basis for ranking the level of criticality of each factor as it pertains to that unit, and setting appropriate maintenance response priorities. This interpretation and evaluation capability had to be programmed into the expert system software.

Very basically, the pertinent data is that which tells us *which* units require *what* specific maintenance attention *when*, and *why*. Interpretation and evaluation of this data would be through applied tribology.

How would all this then be reported to the various users?

As previously noted, there are three staff levels to be informed: mechanical, supervisory/administrative, and management. As the information requirements will vary with each, so must the reports they receive. An integrated system of reporting was indicated, a system consisting of a series of audits: an audit of individual unit

condition (integrity); an audit of program status with each batch of samples submitted; and an audit of comparative performance of equipment, operating divisions, maintenance staff, and even of operating and maintenance procedures.

Individual Unit Condition Reports combine analytical results and component history, specific maintenance recommendations and classification of the unit as being either *critical* (in need of immediate attention), *precautionary* (designated for closer surveillance or minor corrective action) or *normal.*

Batch Summary Reports summarize the results of each batch of samples, provide maintenance supervisors with updates of equipment status, required maintenance action, and equipment due for monitoring.

Monthly Evaluation Reports provide an audit of equipment condition throughout the operation and of program performance, indicating trends and areas requiring management attention.

Standarization of technology (both analytical and interpretive) provides this system with a stable data base from which a series of statistical programs were developed. Programs such as Confidence Factor Analysis, Index of Mechanical Integrity, and Statistical Wear Profiles were developed to provide management with information and perspectives of their equipment and operations not otherwise available. More than one of our clients has revamped maintenance policies and procedures when presented with these studies. In one case, not only did the client win a very large warranty claim supported by our data, but the manufacturer in turn discontinued as an available option the model engine involved.

CONCLUSION: Information, perspectives and options, the key ingredients in any management process, are being provided by a stand-alone expert system of advanced maintenance through applied tribology.

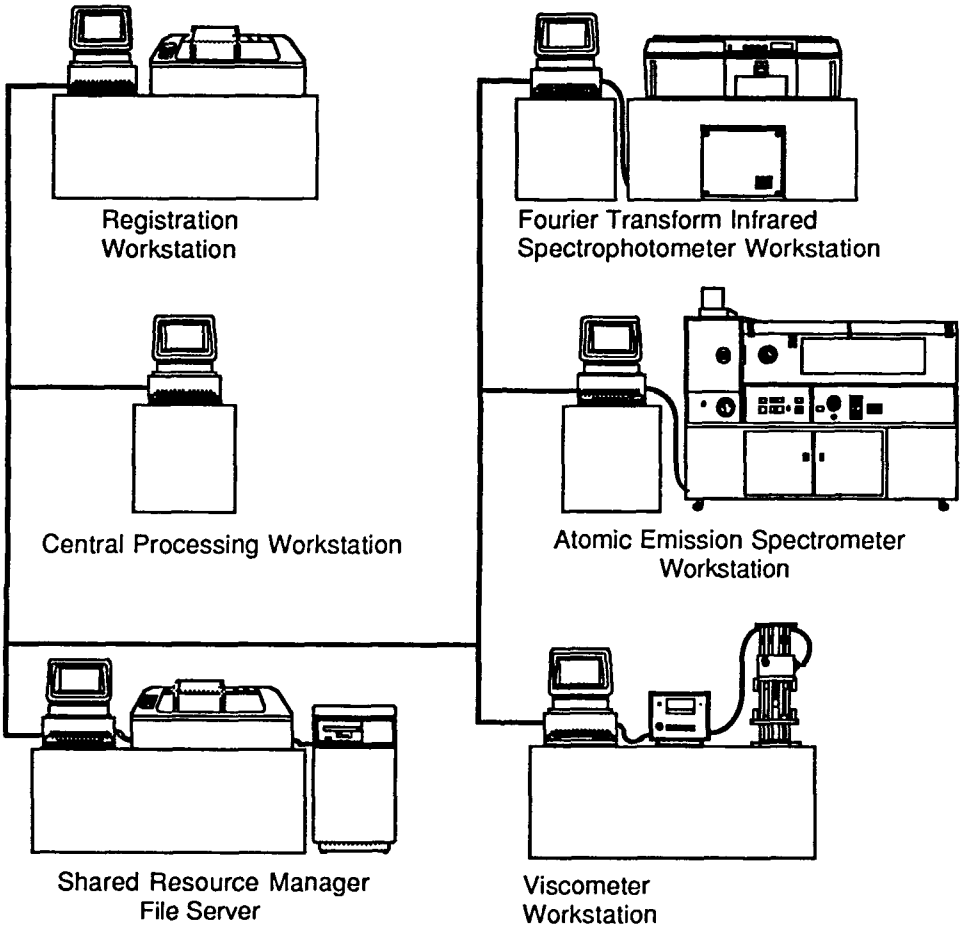

Figure 1: Tribology-based condition monitoring system

EXPERT SYSTEMS OPERATIONAL READINESS AND MAINTENANCE SELF-SUFFICIENCY THROUGH ARTIFICIAL INTELLIGENCE

E. Bruce Branham
Naval Sea Support
Portsmouth, VA 23702

Abstract: In response to changing maintenance requirements and philosophies the Naval Sea Support Center, Atlantic initiated research in January 1988, to determine the possibilities of applying the technology known as "Expert Systems" to enhance operational readiness and maintenance self-sufficiency. Based on the results of prototype development a new program has been established for the development and implementation of this technology. The program, objectives, system selection process and development requirements are presented.

Key Words: Artificial intelligence; condition based maintenance, expert systems; knowledge base engineer; knowledge engineer; software programs

Introduction: Fleet readiness and maintenance self-sufficiency has always been a major goal and objective of the U.S. Navy. In the days of the abundant defense dollar this was accomplished with comprehensive training and aggressive maintenance repair (i.e., "Class B" repairs the norm for insurance) during regular overhauls. But the national deficit and defense posture of recent years has created severe reductions in the defense budget that has mandated the need for change to accomplish these objectives.

This paper provides a review of Naval Sea Support Center, Atlantic's efforts to produce software programs that not only enhance the ability to maintain operational readiness and maintenance self-sufficiency but provide the diagnostic and prognostic ability to support the emerging "Condition Based Maintenance" philosophy.

Naval Sea Support Center, Atlantic, Naval Sea's Atlantic Fleet agency changed with Direct Fleet Support (DFS); (i.e., the promotion of Fleet readiness and maintenance self-sufficiency) and engineering analysis for the Assessment of Equipment Condition (AEC) Program (i.e., engineering analysis to support near term maintenance availabilities) was experiencing expanding demands (a 33% increase in DFS technical assist requests and the expansion of AEC to all surface ships) in the face of a projected personnel reduction of 25% by FY 95. It was apparent a need for change was required.

The answer to this need for change was through artificial intelligence, specifically "Expert System", a computer program that provides the non-expert user a highly interactive, user friendly

mechanism for obtaining expert advice and decision-making capabilities normally requiring an expert.

The objectives were to enhance the ability to accomplish the DFS and AEC mission, retain SEACEN corporate knowledge, and provide a cost effective training vehicle.

The software shell utilized for development is "Level 5" from Information Builders. The development abilities and unlimited distribution of compiled programs were the major factors for selection.

The initial effort produced two programs for 75-85 ton RI2 Air Conditioning Systems Manufactured by York, Carrier and Dunn/Bush. One is a diagnostic/prognostic program designed to support the DFS and AEC objectives of both the Fleet and NAVSEACENLANT (example, figure 1a and 1b). It also provides automated storage of program utilization for history and data-base development. This program has 3216 lines of code in determination of 43 recommendations. The other is a diagnostic troubleshooting program designed to enhance maintenance self-sufficiency through diagnostic use and interactive training. This program utilizes 4631 lines of code in determination of 153 system restoration recommendations.

These programs are solely the results of NAVSEACENLANT efforts and assets. They required approximately 1 year to develop, test, and evaluate. The test and evaluation was conducted on 33 ships for 6 months and provided CASREP/Tech assist savings of $150K/year with a 15 year lifetime return on investment of 185 to 1. As of 31 December 1990 these programs have been installed on 23 ships, most east and west coast SIMAs all AEC Performance Monitoring Teams, and are utilized exclusively for all applicable RI2 AC engineering analysis to support maintenance availabilites.

On 24 January 1991 this effort resulted in the establishment of a program to develop and implement a core base of 50 Expert Systems by FY 95. 14 systems are scheduled for development and implementation in FY 91 (figure 2).

The FY 92 development selection is in process. The criteria for development selection is DART, RIP, CASREP/Tech Assist, AEC system priority list, and sponsor requirements. Selection evaluation is in accordance with NAVSEA 51 selection assessment process (figure 3a-e). The preliminary development and implementation flow diagrams and narratives are provided in figure 4a-d.

Our observation of the major factors for the success of this effort are:

-The customer, objectives and goals were identified and established prior to development.

-Formal development, test and evaluation procedrues were estalished prior to development.

-The selection of systems for development were determined by formal criteria.

-The development expertise was matched with the customer, objectives and goals.

-The knowledge base engineers possess an engineering/technical background, as well as, computer to enhance the interface with the Knowledge Engineer.

-The final product not only has to meet the objectives it has to be cost effective.

References: Hartman, P.J., Judging where expert systems can be used in marine engineering, presented at the 1990 Chesapeake Marine Engineering Symposium, 14 March 1990.

INPUT DATA

Ships Name is USS DOYLE AC Unit Number is AC1

Ships Hull Number is FFG-39

Compressor Discharge pressure	125.00
Compressor Suction pressure	30.00
Compressor Oil pressure	82.00
Compressor Suction temperature	55.00
Compressor Discharge temperature	160.00
Liquid line temperature	95.00
Condenser Cooling Water pressure	150.00
Condenser Cooling Water Inlet temperature	64.00
Condenser Cooling Water Outlet temperature	74.00
Chiller Water Return temperature	50.00
Chiller Water Supply temperature	46.00
Chiller Water Pump Discharge pressure	66.00
Chiller Water Pump Suction pressure	9.00
Expansion Tank pressure	14.00
Motor Current	110.00
Chill Water Flow Rate	260.00
Receiver Liquid Level E 1/8 1/4 1/2 3/4 7/8 F	One quarter
Compressor Lube Oil Sump temperature (Cold, Warm, Hot or Extremely Hot)	Warm
Compressor Oil Level Sight Glass E 1/4 1/2 3/4 F	One half
Condition of Oil Sight Glass Stable or Foaming	Stable
Dehydrator Moisture Indicator Blue, Pink or White	Blue or Dry

Fig. 1a

12-06-1990 11:18:30

****

NOTE: INSURE ALL INSTRUMENTATION IDENTIFIED BELOW IS RELIABLE AND HAS BEEN COMPARED WITH AN INSTRUMENT OF KNOWN ACCURACY PRIOR TO ACCOMPLISHMENT OF REPAIRS.

FIRST OF MULTIPLE RECOMMENDATIONS HAS HIGHEST PROBABILITY OF CORRECTING DETECTED PROBLEM(S) AND SHOULD BE PERFORMED FIRST. DATA SHOULD BE GATHERED AND REEVALUATED AFTER HIGHEST PRIORITY RECOMMENDATIONS HAVE BEEN ACCOMPLISHED.

****

[redacted] A Compressor Discharge pressure of 125 and a Liquid line temperature of 95 and a Condenser Cooling Water Outlet temperature of 74 indicates Condensing cooling water is LEAKING THROUGH the condenser Inlet/Outlet header division gasket. Continued operation with this condition can cause condenser tube sheet erosion, condenser tube failure and sea water contamination of refrigerant system. [redacted]

AC-002

Inspect condenser tube sheet and inlet/outlet header for erosion and replace inlet/outlet header gasket during next availability.

[redacted] A Compressor Suction pressure of 30 and a Chiller Water Supply temperature of 46 and Motor Current of 110 indicates The Compressor Capacity Controls require adjustment. [redacted]

AC-016
(d007)

a. Adjust Capacity controls using procedures of
paragraph 2-2-4 of TM 0959-LP-022-0010 CARRIER OR
paragraph 2-2-4 of TM 0959-LP-022-0010 CARRIER

Fig. 1b

EXPERT SYSTEMS DEVELOPMENT
FY 91 POA & M

	Oct	Jan	Apr	Jul
R-12 ACs	Comp			
HPACs:				
FFG 7/DD 963 cl	X---DEV---X-ENG TEST-X---T&E---X			
CG 47 cl	X---DEV---X-ENG TEST-X---T&E---X			
CVs	X---DEV---X-ENG TEST-X---T&E---X			
R-114 ACs	X---DEV---X-ENG TEST-X---T&E---X			
Clutch: (Phil. Gear DD 963)	X---DEV---X-ENG TEST-X---T&E---X			
EVAPs	X---DEV---X-ENG TEST-X---T&E---X			
Aux Boiler Controls (Cyc. MC 800-4000)	X---DEV---X-ENG TEST-X---T&E---X			
MSD (DD 963)	X---DEV---X-ENG TEST-X---T&E---X			
400 Hz MG	X---DEV---X-ENG TEST-X---T&E---X			
Tel Sys (Dynalec)	X---DEV---X-ENG TEST-X---T&E---X			
Steering (DD 963)	X---DEV---X-ENG TEST-X---T&E---X			
CPP (DD 963)	X---DEV---X-ENG TEST-X---T&E---X			
B & A Crane (CVs)	X---DEV---X-ENG TEST-X---T&E---X			

Fig. 2

EXPERT SYSTEMS QUESTIONNAIRE
APPLICABILITY TO PROBLEM

QUESTION	RANGE OF ANSWERS	SCORE
• Is this a HIGH value application?	1 — 10 No — Yes	
• Does the program provide a large increase in capability over what is now being done?	1 — 10 No — Yes	
• Do you have people ready to use the expert system?	1 — 5 — 10 No — Not Yet — Yes	
• Is the problem easily solved by the experts in your organization?	1 — 5 — 10 No — Sometimes — Yes	
• Can the problem solving skills be readily taught to new people?	1 — 5 — 10 No — Usually — Yes	
• Is there only one right answer?	1 — 5 — 10 No — Usually — Yes	
• Can 'human' error be tolerated in the result?	1 — 5 — 10 No — Unknown — Yes	
• Does the problem use computer transferred data?	1 — 10 No — Yes	
• Can the problem solving method be written as as straight forward rules of thumb?	1 — 5 — 10 No — Mostly — Yes	
• Other: _____ _____ ?	1 — 5 — 10 Bad — Unknown — Good	
	Total Score =	
	Total Score/Maximum Score = 0._____	

SEA-QSMR PAGE 1

Fig. 3a

EXPERT SYSTEMS QUESTIONNAIRE
RISKS IN IMPLEMENTATION

QUESTION	RANGE OF ANSWERS	SCORE
• Is your upper management firmly enthusiastic about an Expert Systems solution to this problem and willing to commit needed resources?	1 — 10 Yes — No	
• Has an expert system like this been implemented by your organization before?	1 — 5 — 10 Yes — Unknown — No	
• Do you have enthusiastic experts available to work on this implementation?	1 — 10 Yes — No	
• Do your organizations' people have the artificial intelligence skills to develop and maintain this expert system?	1 — 5 — 10 Yes — Unknown — No	
• Is this problem within the State of the Art?	1 — 5 — 10 At — Near — Beyond	
• Is the problem constantly changing?	1 — 5 — 10 No — Unknown — Yes	
• Is it easy to get computer readable data for this problem?	1 — 5 — 10 Yes — Sometimes — No	
• Are 'real time' answers required?	1 — 10 No — Yes	
• Would the problem and/or data fit on small, medium, or large computers?	1 — 5 — 10 Small — Medium — Large	
• Other: _____ _____?	1 — 5 — 10 Good — Unknown — Bad	
	Total Score =	
	Total Score/Maximum Score = 0. _____	

[illegible] PAGE 2

Fig. 3b

ESTIMATED VALUE OF AN EXPERT SYSTEM

Area of Value or Benefit	Benefit Estimated ($000)
• Yearly Profit times Number of Years • Yearly Costs Avoided times Number of Years • Intangible Benefits - Relate to Organization's Goal or Products - Otherwise Unachievable Capabilities • Other	
• Total Benefit Over the Useful Program Life.	

[illegible] PAGE 3

Fig. 3c

ESTIMATED COST OF EXPERT SYSTEMS

	Default Approximations for Various Systems ($000)			Cost Estimated ($000)
	Small (Personal)	Medium (Mini)	Large (Mainframe)	
• Hardware	$5-10	$10-50	$50-100	
• Software	$0.3-5	$5-20	>$20	
• Distribution Licenses	$0-0.3/ea	$0-1.5/ea	$1.5-5/ea	
• Problem Assessment	1 s-m*	3 s-m	6 s-m	
• Feasibility Study	1/2 s-m	1 s-m	2 s-m	
• Prototype System	1-3 s-m	1 s-yr**	1-2 s-yr	
• Product Development	1/3 s-yr	1/2-2 s-yr	3-10 s-yr	
• Benchmarking	1/2 s-m	1 s-m	2 s-m	
• Training	1/2 s-m	1 s-m	2 s-m	
• Maintenance (per yr) - Software Updates Enhancements	1/3 s-yr	1-3 s-yr	3-10 s-yr	
- Hardware	$0.1-1	$1-5	$5-10	
• Other				
• Total Costs for Development and Maintenance Over the Useful Life of the Program.				

* s-m = Staff months
** s-yr = Staff years

SEA-0SMR PAGE 4

Fig. 3d

ASSESSMENT OF EXPERT SYSTEM SUCCESS OR FAILURE

SUMMARY ASSESSMENT

- Applicability Factor (A) = 0. _____
- Risk Factor (R) = 0. _____
- Applicability/Risk (A/R) = _____
- Benefits ($000) (B) = $_____
- Costs ($000) (C) = $_____
- Benefit/Cost Ratio (B/C) = _____
- Weighted Benefit/Cost Ratio (A/R) * (B/C) = _____

GRAPHICAL RESULT

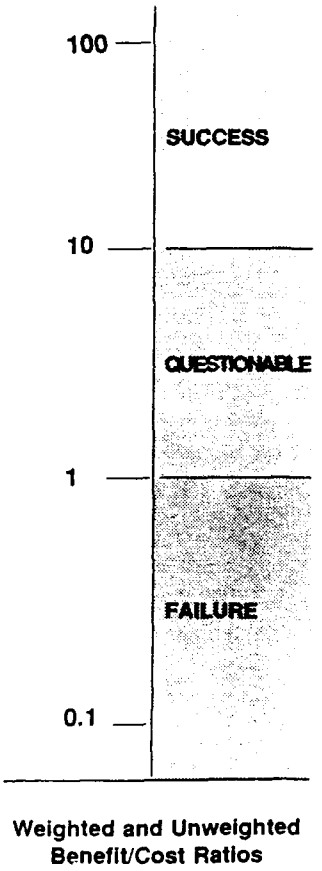

Weighted and Unweighted Benefit/Cost Ratios

Fig. 3e

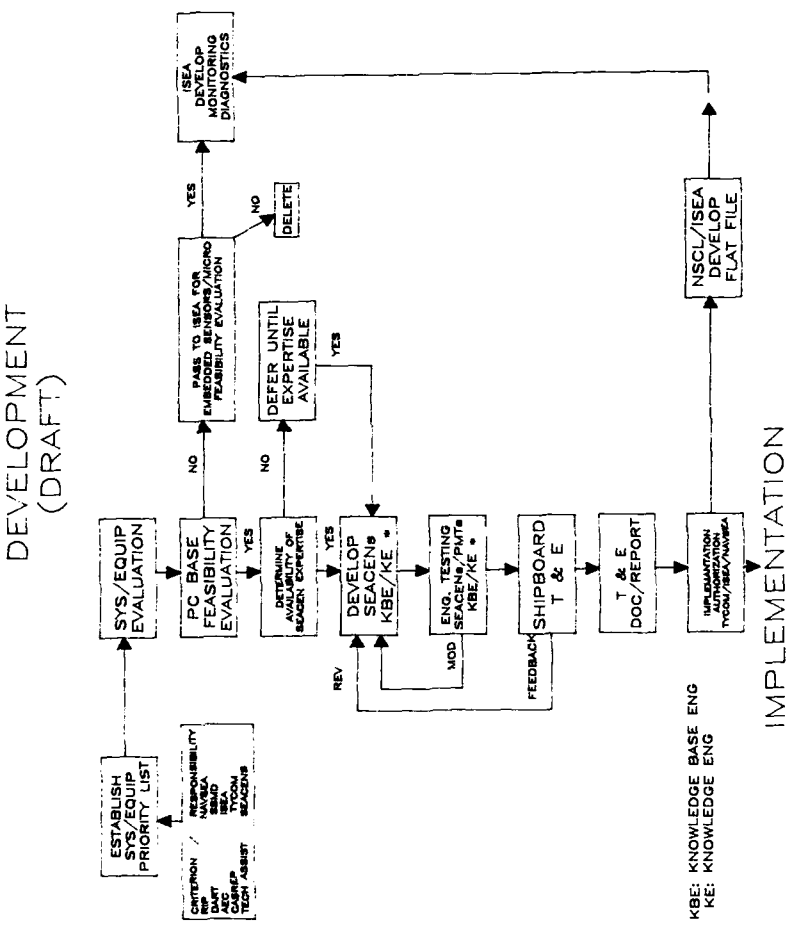
DEVELOPMENT
(DRAFT)
IMPLEMENTATION
ESTABLISH SYS/EQUIP PRIORITY LIST
CRITERION
RIP
DART
ASSET
CASREP
TECH ASSIST
RESPONSIBILITY
NAVSEA
SEMD
ISEA
TYCOM
SEACENS
SYS/EQUIP EVALUATION
PC BASE FEASIBILITY EVALUATION
NO
YES
PASS TO ISEA FOR EMBEDDED SENSORS/MICRO FEASIBILITY EVALUATION
NO
YES
DELETE
ISEA DEVELOP MONITORING DIAGNOSTICS
DETERMINE AVAILABILITY OF SEACEN EXPERTISE
NO
YES
DEFER UNTIL EXPERTISE AVAILABLE
YES
DEVELOP SEACENs KBE/KE *
REV
ENG. TESTING SEACENs/PMTs KBE/KE *
MOD
SHIPBOARD T & E
FEEDBACK
T & E DOC./REPORT
IMPLEMENTATION (LOCATION) TYCOM/ISEA/NAVSEA
NSCL/ISEA DEVELOP FLAT FILE
* KBE: KNOWLEDGE BASE ENG
KE: KNOWLEDGE ENG

Fig. 4a

Development Diagram Narrative:

-Establishment of system/equipment priority will be accomplished through the use of DART, RIP, AEC, CASREP, and Tech assist priority list in conjunction with inputs from NAVSEA (05/06), ISEAs, TYCOMs and SEACENs.

-System/equipment and PC based feasibility evaluation will be accomplished by SEACEN Knowledge Based Engineers (KBE) utilizing evaluation format developed by NAVSEA (512).

-Those systems/equipments determined feasible for PC based development (i.e., data required for analysis is available through existing instrumentation and interactive query) will be reviewed for available expertise and scheduled accordingly.

-Systems/Equipments requiring simultaneous acquisition of multiple data for analysis (i.e., FMMSS/PPCAS: Embedded sensors/micro processors) will be passed to the appropriate ISEA for automated acquisition based feasibility evaluation.

-Those systems/equipments determined feasible for automated acquisition based development will be reviewed for expertise/lab availability and will be scheduled accordingly.

-Those systems/equipments deemed unfeasible for either PC or Automated acquisition based will be deleted or documented.

-PC based experts will be developed by SEACEN Direct Fleet Support (DFS) technical experts and in-house KBEs (i.e., Artificial Intelligence computer experts).

-Developmental testing for diagnostic accuracy will be accomplished by SEACEN personnnel during routine DFS functions to minimize cost and maximize expertise.

-Shipboard testing and evaluation will consist of a formal six ship/three month plan to determine cost effectiveness and assure shipboard usability.

-The formal T & E report with supporting documentation will be reviewed by TYCOM/ISEAs and NAVSEA for implementation authorization.

-Systems authorized for implementation will be developed to utilize automated data inputs from acquisition based systems.

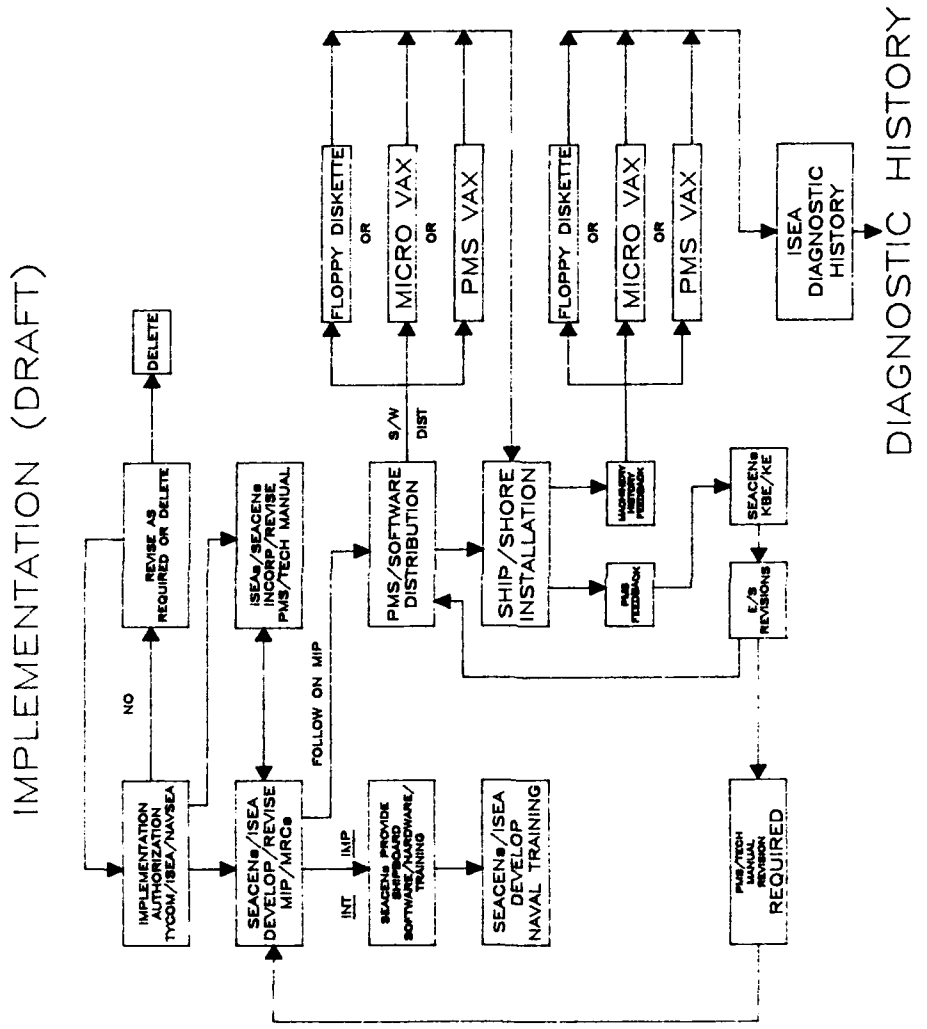
IMPLEMENTATION (DRAFT)
DIAGNOSTIC HISTORY
IMPLEMENTATION AUTHORIZATION TYCOM/ISEA/NAVSEA
NO
REVISE AS REQUIRED OR DELETE
DELETE
SEACENs/ISEA DEVELOP/REVISE MIP/MRCs
ISEAs/SEACENs INCORP/REVISE PMS/TECH MANUAL
FOLLOW ON MIP
INT
IMP
SEACENs PROVIDE SHIPBOARD SOFTWARE/HARDWARE/ TRAINING
SEACENs/ISEA DEVELOP NAVAL TRAINING
PMS/SOFTWARE DISTRIBUTION
S/W
DIST
FLOPPY DISKETTE
OR
MICRO VAX
OR
PMS VAX
SHIP/SHORE INSTALLATION
MACHINERY HISTORY FEEDBACK
PMS FEEDBACK
SEACENs KBE/KE
E/S REVISIONS
PMS/TECH MANUAL REVISION REQUIRED
ISEA DIAGNOSTIC HISTORY

Fig. 4b

Implementation Diagram Narrative:

-Systems authorized for implementation will utilize the PMS system to assure configuration control, distribution, scheduling, utilization and feedback.

-ISEAs will review and revise Tech Manual (TM) troubleshooting sections to utilize authorized systems replacing standard fault logic matrix charts.

-Initial shipboard implementation will be accomplished by SEACENs and will include formal training, software, hardware and a training video. Systems will also be utilized in formal naval training schools.

-Follow-on implementations will be via PMS MIP/MRC and floppy disk or micro/PMS VAX for software. Feedback will be via PMS system.

-Software maintenance and revision will be accomplished by SEACENs KBE/Knowledge Engineer (KE) with distribution via PMS SFR. Feedback for PMS will be reviewed by SEACENs/ISEAs. ISEAs will review Tech Manuals for revision requirements.

-Diagnostic history will be transmitted via floppy disk, micro vax or PMS VAX (TBD).

SMART INTEGRATED MICROSENSOR SYSTEM

Paul J. Redden Jr.
Aviation Applied Technology Directorate
U.S. Army Aviation Systems Command
Fort Eustis, Virginia 23604-5577

Abstract: The concept of smart sensors is intriguing. The idea of combining a sensor with a complex integrated chip in a self-contained "smart" unit allows a host of opportunities to be considered. Currently, there is no miniature system capable of real-time fatigue analysis of strain data. Data must be recorded and later analyzed using computer processing. This paper will discuss the Aviation Applied Technology Directorate (AVSCOM) technology base program to develop a miniature sensor unit for monitoring component fatigue life usage in real time.

The challenges of designing the Smart Integrated Microsensor System breadboard unit, accommodating the rainflow algorithmic functions, displaying percentage of life remaining results, and environmental conditioning will be covered in detail. The plans for prototyping and flight testing will also be addressed.

Key Words: Fatigue; life estimation; microsensors; rainflow analysis; strain.

BACKGROUND

Fatigue, caused by alternating stress is a major concern in Army Aviation. Helicopter components are designed to be as light as possible. As such, fatigue limits the life of many of the dynamic components such as the swashplate and rotor blades. Unfortunately, these dynamic components are flight critical in nature. In other words, a failure in one of these components could cause the loss of an aircraft or the personnel onboard. Currently the Army designs these components using a safe life criteria. The designers of the aircraft are given the projected use of the aircraft. They then design each component and give operational time between replacement figures to establish a low probability of failure over the life of the aircraft. This approach has several problems. A helicopter used for training may accumulate fatigue damage faster than one that is simply used to ferry passengers. Likewise a helicopter flown during war may accumulate more fatigue than one flown during peacetime. No helicopter is actually flown with the projected average use of the fleet. This may allow some components to remain on the aircraft long after their established safe fatigue life is surpassed, while other components are removed long before they need to be. In the first case we may be endangering the lives of our service men and women; in the second case we are wasting valuable parts and manpower by replacing something that is perfectly good. Conservative estimates are used throughout the design process in an attempt to eliminate any undue danger.

Army doctrine changes over time, as does the type of battle envisioned and the type of flying required to conduct that battle. New maneuvers are added to allow such things as nap-of-the-earth flying, pop-up maneuvers, and air-to-air combat. As these maneuvers are introduced into the fleet, they introduce new stresses to the aircraft that were not envisioned in the original design and thus not considered in the component replacement criteria.

Each pilot also has his own flying style, making uniform usage difficult if not impossible to obtain. Hard landings and other damaging maneuvers may occasionally go unreported. This must be considered by the manufacturer when establishing the safe-life replacement criteria.

PROPOSED METHODS OF FATIGUE CALCULATION

Fatigue is hard to predict to a high degree of accuracy. Some method of measuring the actual fatigue damage on each aircraft or each critical component is therefore necessary to prepare adequate component replacement criteria. Several methods are being considered to accomplish this. Some methods measure flight parameters such as airspeed and aircraft attitude to determine when the aircraft is in one of several categories of flight regimes. A standard level of fatigue damage is then deducted from a calculation of the expected life of each component. Another method obtains parametric data from noncritical, nonrotating components and mathematically deduces the strains on each of the critical components. Minors rule is then used with rainflow analysis to determine the fatigue damage accumulation on the components. These methods both have the disadvantage of having to develop correlation relationships and perform on-board analyses followed by ground based data management. They lose some practicality when used parts or parts cannibalized from other aircraft are used unless extensive paperwork is used to keep track of the fatigue life of all flight critical parts in the army inventory.

CURRENT PROGRAMS

Several structural fatigue life monitoring programs are currently underway at the U.S. Army Aviation Applied Technology Directorate (AATD) located at Fort Eustis, Virginia. This paper discusses the Smart Integrated Microsensor System (SIMS), which is currently under development for AATD by the Eldec Corporation of Lynnwood, Washington. The SIMS is unique in that it is a small self-contained module which mounts directly on the component. It measures the strain directly from the component using a commercial foil strain gage. A real-time version of Rainflow Analysis is performed and Minor's rule is used to calculate accumulated fatigue damage with no recording of data, no downloading of data, and no external processing required. The SIMS unit can remain with the component when it is removed, eliminating large amounts of paperwork and parts tracking. The SIMS will give the operator and the maintainer invaluable knowledge on the safety of their flight critical parts. Replacement criteria can then be based on fatigue damage and expected life rather than an arbitrary safe life which could change unknowingly over the life of the aircraft.

The SIMS (Figure 1) is a small self-contained module which mounts directly on the part to be monitored. Strain is measured through a conventional

strain gage attached to the critical component. An analog peak detector is used to determine when a peak strain has occurred. The magnitude and sign of the peak is then sent to the rainflow algorithm. The rainflow algorithm operates on strain data in real time and can reduce a complex irregular load history into a series of constant amplitude strain cycles (1). Curve fitting logic is used to implement Minor's rule to measure and accumulate fatigue damage caused by each strain cycle. An electrical charge is then applied to the life indicator. This charge increments the life indicator a value proportional to the fatigue damage fraction. Nonvolatile memory is also included as a backup. A quick glance during the preflight inspection will tell the pilot if the aircraft is safe to fly. It will also indicate when a component is coming up for replacement.

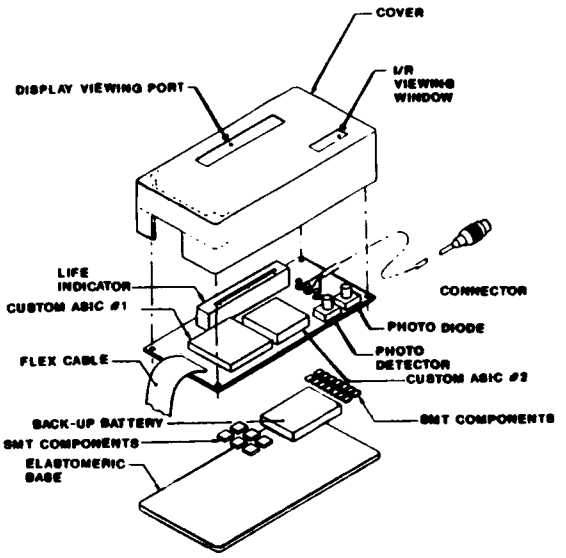

Figure 1. NOMINAL SIMS DESIGN LAYOUT

The ingenious design of the SIMS, along with dedicated high speed Application Specific Integrated Circuits (ASICs) with no processing overhead, allows the real-time rainflow calculations. This eliminates any need to analyze the actual strain data which would burden current flight-recording capabilities. Also eliminated is the requirement for post-processing of the recorded data on a mainframe computer after the aircraft has landed.

The ASICs consist of micro-chips containing thousands of digital gates and analog circuits. After the design is finalized, an interconnect layer is applied to complete the circuits. This allows a custom chip to be constructed without requiring manufacturing the chips from scratch. Fully custom designed chips would be cost prohibitive for limited applications. The use of ASICs instead of a microprocessor provides the speed required to perform the real-time analysis.

The development of the SIMS breadboard unit has not been without its difficulties. The complexity of the required circuitry provided many challenges in the areas of miniaturization and debugging. Several design iterations were required to obtain the current system. Originally the design was envisioned to be completely self-contained and battery powered. The battery was permanently installed to survive the harsh environment envisioned for the SIMS use. This, however, limited the accuracy and life of the unit. To remedy this, a requirement was added that aircraft power be provided to the SIMS unit. The battery was retained to maintain fatigue data when external power is unavailable.

Another problem encountered was with the mercury display, which will not operate below -20 degrees Celsius. Since the Army helicopter environment requires operation to -50 degrees Celsius, a small heater was added. This allows the SIMS to operate in the full range from -50 to 70 degrees Celsius.

It was originally anticipated that simple cycle counting or a limited version of rainflow analysis could be used. With testing, it was determined that the results from these methods were not acceptable. As a result, full rainflow analysis was incorporated into the design, which thus grew larger than was originally envisioned. The current prototype design utilizes two ASICs and two ACTEL programmable logic chips. Further miniaturization is possible and will be performed in a later effort.

FOLLOW-ON EFFORTS

The current program will result in the delivery of three prototype SIMS units. These units will be tested by the Army to verify their proper operation. The results will be compared with the results obtained using actual flight strain data analyzed on a mainframe computer. Environmental testing will also be performed to verify operation in the military helicopter environment.

Upon successful completion of this testing and subject to available funding, we intend to conduct a follow-on effort for miniaturization and flight testing on an Army helicopter. The possibility of incorporating an advanced silicone strain gage into the design to overcome difficulties in the durability of foil type strain gages will also be studied. The results of this program will provide a basis for future work in the area of advanced sensor technology.

CONCLUSIONS

The development of the SIMS will provide substantial benefits to the U.S. Army and should provide many commercial benefits as well. Parts tracking will be substantially reduced since the SIMS unit mounts directly on the part and will remain with the part throughout its life. Accurate predictions of fatigue life based on measurement of the actual fatigue encountered by the component will add significantly to the safety of Army aviation. The costs of maintenance will be reduced, since it will no longer be necessary to replace components well before their life has been expired simply because the extent of fatigue damage is unknown. The SIMS design concept can also be applied to many commercial applications where fatigue life considerations add to the support burden.

REFERENCES:

1. Downing, S. D. and Socie, D. F. "Simple Rainflow Counting Algorithms," International Journal of Fatigue, p 31, January 1982.

FAILURES IN COMPOSITES

Chairman: **Eugene Camponeschi**
David Taylor Research Center

EFFECTIVE INTERLAMINAR NORMAL STIFFNESS AND STRENGTH OF ORTHOTROPIC LAMINATES

Ajit K. Roy and Ran Y. Kim
University of Dayton Research Institute
300 College Park
Dayton, OH 45469-0168

Abstract: A test method for measuring the interlaminar (in the thickness direction) tensile stiffness and strength of orthotropic laminates is discussed. Due to low interlaminar properties of composite laminates compared to its in-plane properties, gripping of the specimen directly to the load frame causes unwanted end bending in the vicinity of the grips. A special gripping technique is developed to eliminate the effect of end bending of the specimens due to any misalignments of the load frame grips. The measured values of the interlaminar normal stiffness, Poisson's ratio, and strength of AS4/3501-6 composite laminates, both in tension and compression, are presented. The specimens are cut from two composite panels of about 50 mm (2", 400 ply thick) in thickness. The panels are cured using an expert curing system. The stacking sequences of the composite panels considered in this study are $[0/90]_{200S}$ and $[0/90/45/-45]_{100S}$. The effect of specimen thickness on the interlaminar properties are studied. The interlaminar tensile strength is found to decrease with increasing specimen thickness; whereas compressive strength increases with increasing specimen thickness.

Key Words: AS4/3501-6; composite laminate; Interlaminar properties; Poisson's ratio; stiffness; strength; test method.

Introduction: A significant amount of analytical work by several authors has been reported in the literature for predicting interlaminar effective moduli of laminates [1-5]. On the experimental side, in the contrary, relatively small amount of work has been done in characterizing all components of interlaminar effective moduli of fiber reinforced composite laminates. Some work has been reported in measuring interlaminar shear stiffness of laminates[6-8]. To the authors' knowledge there is no experimental data available in characterizing the interlaminar normal stiffness and strength of composite laminates. The objective of this paper is to present a test method for measuring the interlaminar normal stiffness, Poisson's ratio, and strengths of AS4/3501-6 CFRF composite in tension. Similar data is also presented for compression using the ITTRI compression test.

The experimental study is conducted by cutting test coupons from two 400 ply AS4/3501-6 composite laminated panels of lamination scheme $[0/90]_{200s}$ and $[0/90/45/-45]_{100s}$ respectively. The thickness of the test coupons are varied to observe any change in the measured values of the interlaminar normal stiffnesses and strengths. The interlaminar stiffness is much lower than the in-plane stiffness of the two laminates considered. Thus if specimens are loaded in tension by directly gripping at its end tabs, any misalignment of the load grips easily causes unwanted bending of the specimens. A special gripping technique is developed to practically eliminate the bending of the specimens when loaded in tension. Experimental data obtained for the above two laminates are compared with the three-dimensional property of unidirectional AS4/3501-6 composite, generated earlier by Kim[9].

Experimental Procedure: To measure the stiffness and strength in the thickness direction of a laminate, the test coupons are cut from a composite panel in such a way that the thickness of the panel becomes the length of the test coupon. The representative cutting scheme of the test specimens from the composite panels is shown in Figure 1. The thickness of the composite panels becomes the length of the test coupons. Incidentally, the thickness of the panels should be such that there exists an adequate gage length for the test coupons.

(a) Composite Panels: For this study two 400 ply thick (2 inches) AS4/3501-6 composite panels were consolidated with stacking sequence of $[0/90]_{100s}$ and $[0/90/45/-45]_{50s}$. Before consolidating all 400 plies of the laminate together, the prepregs of the plies for the laminates were stacked in a set of 20 ply sublaminates which were partially debulked. The partially debulked sublaminates were then stacked and cured together and cured using an autoclave qualitative process automation (QPA) curing process[10]. QPA is a rule-based autonomous curing process. Thermocouples were embedded in the panels during the final cure to control the temperature inside the panels. Several knowledge based rules were used to control the whole process, the details of which are given in [10]. The curing time for both the panels was a little over 4 hours. The curing was carried out at a constant pressure of 100 psi. The maximum temperature of the autoclave was limited to 375°F, while during exotherm, temperature inside the panel never exceeded over 425°F. The size of the cured panels was approximately 152mm x152mm x50mm (6"x6"x2"). The volume fraction of these two panels was found to be 60.5%.

(b) Test Coupons: The section of the panels containing the embedded thermocouple and its lead wires were removed and not used for the testing purpose. Moreover, about 10mm of material was cut away from all four edges of the panel for making the panels ready for cutting test coupons. The cutting scheme of the test coupons is shown in Figure 1. Thin slices of two different thicknesses (t_1 and t_2) were cut from the panels in two different directions as shown in the figure. Our composite panels were, as stated earlier, about 50mm thick. Although we had used diamond blade saw it was always difficult for us to maintain uniform thickness of the slices in cutting from the panel. Thus the cut slices afterwards were ground to get the thickness as uniform as possible. The test specimens of width, w, of 6.25mm (0.25") were cut from the slices. Our measurements indicated that there was a variation of thickness (less than 0.002") present in the slices after grounding, however the thickness variation in each specimen was almost negligible.

The length of each specimen was about 2 inches (50.8mm) which happened to be the thickness of the panels. It is always difficult to test these short specimens in tension by gripping at its end tabs. The stiffness of these specimens along its length direction (z direction) is about one order magnitude lower than that of its width or thickness direction (x or y direction). Thus any small misalignment of the load frame grips easily causes bending at the two ends of the specimen, and dissipation of such end effect along the length of the specimen is slow. Moreover, the specimens being short (all together 2 inches including 0.5 inch at each end for installing tabs) the end effect easily propagates to the gage area. Thus to avoid the end bending of the specimens a special gripping technique was employed.

The configuration of attaching the specimen ends with the load frame grips is shown in Figure 2. The end tabs of the specimens were not gripped directly to the load frame. Commercially available sheets used for circuit board materials are used for the tab materials. These sheets have a layer of brass coating on of its surfaces. At each of the two hydraulic grips of the load frame two thin (0.6 mm thick) brass shims were gripped with a grip filler in between the two brass shims for specimen end housing. The gripped brass shims were then soldered with the brass layered surface of the end tabs. The tensile load was transferred from the load frame to the specimen through the two brass shims at each end of the specimen. The brass shim connections between the load frame grips and the specimen behaved practically like hinge-joints; thus eliminated the possibility of bending the ends of the specimens.

In order to eliminate any bending induced by the differential thermal shrinkage of the soldering material, a special attention is made while soldering the specimens with the end brass shims. During soldering the specimens with the brass shims the specimens were held in place between the end shims with a compressive preload of 4.5 Kilograms (10 lbs). Incidentally, after end tabs were adhered with the specimens, the two end surfaces of specimens were ground perpendicular to the axis of specimens so that there was no bending due to the applied preload. The strain readings from two strain gages mounted on two opposite surfaces close to one of the end tabs were monitored during soldering. The time trace of the strain gage readings of two cases are shown in Figures 3(a) and 3(b). It can be seen in Figures 3(a) and 3(b) that the amplitude difference of the traces of the start and the finish of the traces was essentially same. This indicated that there was no induced bending strains in the specimen due to soldering. Figures 3(c) and 3(d) are the stress-strain curves of the strain gages in Figure 3(a) and 3(b) respectively. Figure 3 as a whole ensures the repeatability of this test procedure practically eliminating bending due to gripping of the specimen. The tensile tests were conducted under stroke control operation. The cross head movement of the load frame was first locked to a position for soldering the specimen end tabs to the gripped brass shims. After complete cool down of the soldering material, the preload was set to zero by controlling the cross head displacement. All the test specimens were instrumented with back to back strain gages mounted on two opposite surfaces at the middle of gage length. Additionally, two tensile specimens were strain gaged back to back at the center of the gage area and near the tab area to record if there existed any bending in the specimens when loading in tension. Our test measurements indicated that the bending of the specimens were practically eliminated by gripping technique employed in this test. Some of other specimens were instrumented with longitudinal and transverse strain gages. The longitudinal and transverse measurements from at least 2 specimens were used for determining the interlaminar stiffness, E_3, and Poisson's ratio, ν_{31}, of a laminate. The tensile test data is summarized in Table 1.

The width of all specimens was 6.35 mm (1/4"). Specimens with three different values of thickness (1.397, 2.54, and 5.749 mm) were tested to study the effect of thickness on the interlaminar stiffness and strength. The compression specimens were prepared as per ASTM 3840 standard. The IITRI compression test fixture was used for compression testing. Strain readings from back to back strain gages were recorded during the compression testing. The compression data is presented in Table 2. To compare the laminate data with the representative unidirectional properties, the three-dimensional properties of unidirectional AS4/3501-6 composites, reported by Kim[9], are reproduced in

Table 3. It is observed that there was no significant change in the values of the interlaminar stiffness due to change in thickness of the specimens. However, the interlaminar tensile strength decreased with increasing specimen thickness and the interlaminar compressive strength increased with increasing thickness.

Conclusions: The test data for interlaminar normal stiffness, Poisson's ratio, and strengths of AS4/3501-6 CFRP composite laminates are presented. The two laminates considered in this study are $[0/90]_{200s}$ and $[0/90/45/-45]_{100s}$. It is observed that there was no significant change in the values of the interlaminar stiffness due to change in thickness of the specimens. However, the interlaminar tensile strength decreased with increasing specimen thickness and the interlaminar compressive strength increased with increasing thickness.

Acknowledgment: This work was sponsored by the WL Materials Laboratory under contract number F33615-87-C-5239. The financial support is gratefully acknowledged.

REFERENCES

1 Pagano, N. J., 1974, "Exact Moduli of Anisotropic Laminates", Mechanics of Composite Materials, Vol 2, edited by G.P.Sendeckyj, Academic Press.

2. Chou, P. C. and J. Carleone, 1972, "Elastic Constants of Layered Media, Journal of Composite Materials", 6, pp 80-93.

3. Sun, C. T. and S. Li, 1988, "Three-Dimensional Effective Elastic Constants for Thick Laminates", Journal of Composite Materials, Vol 22, No 7, pp 629-639.

4. Christensen, R. M., "Tensor Transformations and Failure Criteria for the Analysis of Fiber Composite Materials", Journal of Composite Materials, Vol 22, No 9, 1988, pp 874-897.

5. Roy, A. K. and S. W. Tsai, "Three-dimensional Effective Moduli of Orthotropic and Symmetric Laminates", to appear in the Journal of Applied Mechanics, Trans. of ASME, 1991.

6. Adams, D.F. and D.E. Walrath, "In-plane and Interlaminar Iosipescu Shear Properties of Various Graphite Fabric/Epoxy Laminates", Journal of Composites Technology and Research, Vol. 9, No. 3, pp 88-94, Fall 1987.

7. Post, D, F. Dai, Y. Guo, and P. Ifju, "Interlaminar Shear Moduli of Cross-ply Laminates: An Experimental Study", Journal of Composite Materials, Vol. 23, No. 3, pp 264-279, 1989.

8. Roy, A. K. and R. Y. Kim, 1989, "Experimental Determination of Transverse Shear Stiffness of a Thick Laminate, 1989 SEM Spring Conference on Experimental Mechanics", May 29 - June 1, 1989, Cambridge, Massachusetts.

9. Kim, R. Y., F. Abrams, and M. Knight, "Mechanical Characterization of a Thick Composite Laminate", Proceedings of the American Society for Composites, 3rd Technical Conference, 25-29 September, 1988, Seattle, Washington.

10. LeClair, S.R., Abrams, F.L., Lagnese, T.J., Lee, C.W., Park, J.B., "Qualitative process Automation for Autoclave Cure of Composite Parts", AFWAL-TR-87-4083, AFWAL/MLTC, Wright-Patterson AFB, Ohio, July 1987.

TABLE 1. Test data for tension. Material AS4/3501-6, volume fraction: 60.5%.

Laminate	Specimen Thickness mm #	Stiffness E3 GPa	Poisson's Ratio	Strength Z MPa	Average E3 GPa	Average Poisson's Ratio	Average Z MPa
[0/90]	1.392	13.68	0.094	61	12.56 ±6.5%	0.090	58±9%
		12.26	0.086	63			
		11.70	-	61			
		-	-	50			
		-	-	53			
	2.540	11.67	0.084	56	12.5 ±8.8%	0.087	52±7%
		14.07	-	53			
		11.76	0.089	47			
	5.749	11.86	0.078	45	12.44 ±7.5%	0.085	39±15%
		13.75	-	31			
		11.70	0.093	42			
[π/4]	1.392	12.51	0.058	39*	12.57 ±2.2%	0.054	54±8%
		12.10	0.051	50			
		12.77	-	60			
		-	-	52			
		-	-	37*			
	2.540	14.29	0.060	42	13.41 ±4.7%	0.058	42±1%
		12.84	0.055	41			
		13.10	-	42			
	5.749	14.05	0.067	41	13.37 ±7.1%	0.069	42±6%
		14.05	0.071	39			
		12.00	-	45			

* these strength values are unexpectedly low, thus are not included in the average
# the average width of all specimens is 6.35 mm

TABLE 2. Test data for compression. Material AS4/3501-6, volume fraction: 60.5%.

Laminate	Specimen Thickness mm #	Stiffness E3 GPa	Poisson's Ratio	Strength Z MPa	Average E3 GPa	Average Poisson's Ratio	Average Z MPa
[0/90]	2.540	12.45 12.08	0.093 0.082	820 726	12.26 ±1.5%	0.088	773±6%
	5.749	11.86 11.92	0.089 0.080	949 807	11.89 ±0.3%	0.085	878±8%
[π/4]	2.540	12.57 12.95	0.079 0.085	834 930	12.76 ±1.5%	0.082	882±5%
	5.749	12.13 12.69	0.058 0.083	1031 1148	12.41 ±2.3%	0.070	1090±5%

the average width of all specimens is 6.35 mm

TABLE 3. Three-dimensional properties of a thick unidirectional AS4/3501-6 composite, volume fraction 67.2%. Data are reproduced from reference [9] for comparison with that presented in Tables 1 and 2.

THICK UNIDIRECTIONAL AS4/3501-6 COMPOSITES
200 plies (one inch thick), Fiber volume fraction: 67.2 percent

ENGINEERING CONSTANTS

E_x (GPa)	E_y (GPa)	E_z (GPa)	ν_x	ν_y	ν_z	E_q (GPa)	E_r (GPa)	E_s (GPa)
138	10	10	0.3	0.02	0.53	2.9	5.5	5.5

Subscripts: q for y-z plane, r for x-z plane, s for x-y plane

ULTIMATE STRENGTHS

X (MPa)	Y (MPa)	Z (MPa)	X' (MPa)	Y' (MPa)	Z' (MPa)	Q (MPa)	R (MPa)	S (MPa)
1930	52	52	1450	210	258	103	93	93

Shear: Q in y-z plane, R in x-z plane, S in x-y plane

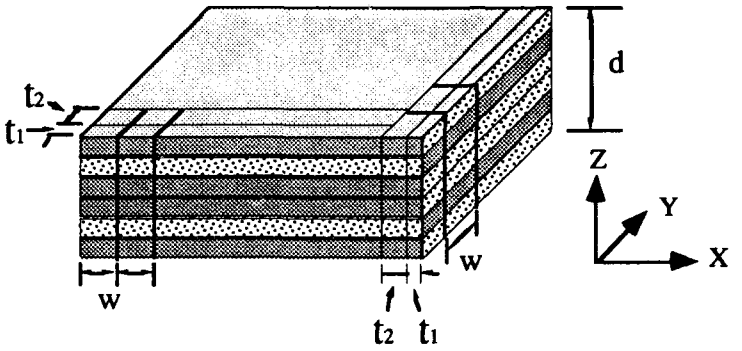

Figure 1. Representative cutting scheme of the Test Specimens out of the Composite Panel

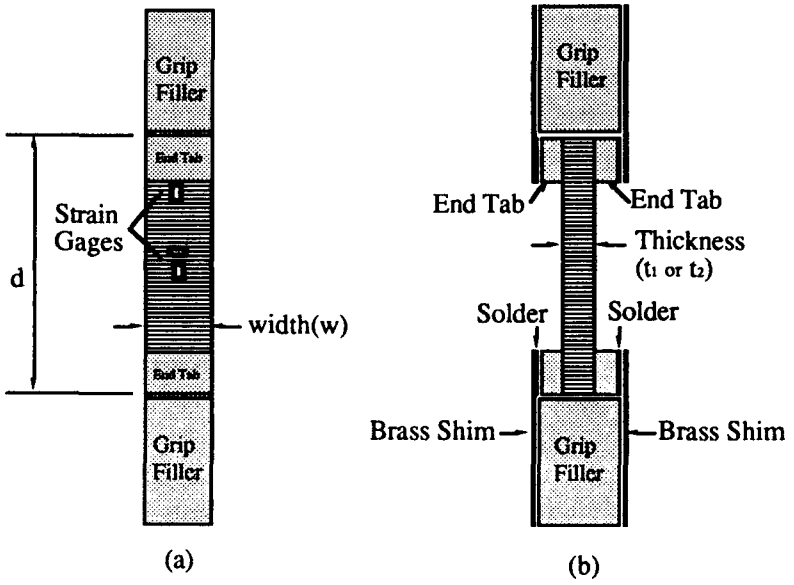

Figure 2. Test Specimen with End Tab and Grip Filler. (a) Front View, (b) Side View

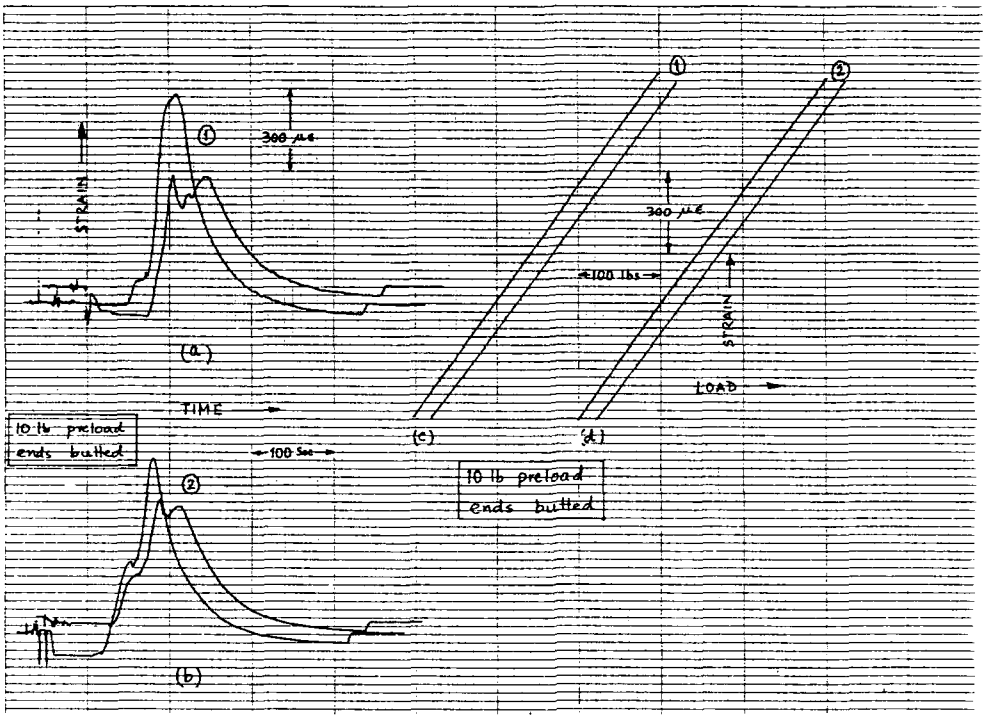

Figure 3. (a) and (b): Time trace of stress gage readings during soldering of the specimens with the end shims. (c) and (d): The stress-strain curves of the specimens used in (a) and (b).

FIBER OPTIC TEMPERATURE MEASUREMENTS IN COMPOSITES

Henry K. Whitesel and Usman A. K. Sorathia
David Taylor Research Center
Annapolis, Maryland 21402

Abstract: Temperature was measured through-the-thickness of composites with embedded fiber optic probes using a Fabry-Perot cavity mounted on the end of a multimode fiber. The Fabry-Perot probe was supported with a glass capillary tube and performed well up to 400°C (752°F). Gold coating on the lead-in fibers improved the temperature durability of the probe. Fiber optic measurements of temperatures above 400°C (752°F) were possible with reduced accuracy. Fiber optic temperature measurements were compared with thermocouple measurements and revealed that the accuracy of the fiber optic probe is nearly equal to that of the thermocouple. The fiber optic temperature probe has advantages in terms of response time and less disturbance of the heat transfer and strength properties of the composite material. Both advantages are likely due to smaller size and mass. Thermocouple technology has advantages in the of durability and low cost.

Embedded fiber optic temperature sensors are being developed for shipboard applications in the areas of measuring internal temperature and residual strength during fire tests, monitoring the curing of composites, and monitoring performance during the life of machinery. For the work described herein, temperature measurements were made during composite burn tests to aid in the selection of improved fire barrier design onboard ship. The selection will be based on heat flux calculations from fiber optic temperature measurement profiles through the thickness of the material. In addition, improved damage control monitoring is possible, using embedded sensors to provide shock and high temperature indications during extreme damage conditions.

Key Words: Sensors; temperature measurement; fiber optics; composites; embedded sensors; fire tests; thermocouples; Fabry-Perot sensors; temperature profiles

Introduction: The introduction of composite materials into the marine and aerospace industries began during the 1940's with the use of polyesters as the primary matrix material. Today, aerospace use of composites relies heavily on epoxy resins for providing optimum mechanical properties with reduced weight. Marine applications of composites have continued to depend on polyester matrices as dictated by size, cost and the ability to tailor-cure parameters, particularly gel times and exotherm rates. As requirements

for reduced weight, better fire and smoke properties, and better mechanical properties increase for a number of potential ship and submarine applications, newer or advanced resins are needed that exhibit superior properties.

Most organic matrix materials, particularly the conventional polyester and epoxy types currently used in shipboard applications, will support combustion and evolve large quantities of smoke while burning. All organic matrix materials burn when located in close proximity to a high energy heat source. During the past decade, the thermoset and thermoplastic family of polymers have seen a steady improvement in the upper temperature limits, and hence the thermal stability. The upper temperature limits have also improved fire and smoke properties of these new state-of-the-art polymers and offer the potential of improved fire resistant composite materials.

Recent shipboard fires have resulted in placing severe restrictions on using materials which support combustion and give off large quantities of smoke. The Navy has established several development programs to improve the strength, fire spread, and smoke generation properties of composite materials that might be used onboard ship for machinery, hull, and fire barriers.

This paper reports a method of measuring the internal temperature profiles of composites using fiber optic temperature sensor technology. The measurement methods are relatively well known, but the performance of the sensors as embedded devices is not. This is the major thrust of the paper. Data generated during this effort will be used to select more fire resistant composites.

Temperature Measurement Technology: A partial list of our performance requirements for a temperature sensor, embedded in composites and used during burn tests, follows:

- Accuracy within $\pm$28°C ($\pm$50°F) is sufficient; $\pm$3°C ($\pm$5°F) is desired
- Survivable to about 927°C (1700°F)
- Reliable, rugged, easy to install, and simple to operate
- Small compared to the dimensions of the composite
- Made of the same materials as the composite (no impact on the burning properties)

We considered most of the temperature sensing techniques available and very quickly settled on employing thermocouples and fiber optic sensors.

Thermocouples: Thermocouples are a standard to which most every other technique is compared. They are the most widely used temperature measurement device and have a very simple operating principle. Thermocouples utilize the fact that the electromotive force developed across the junction of two dissimilar metals, is a predictable function of temperature. Advantages of thermocouples are simplicity, low cost, ability

to measure high temperatures, and ruggedness. They have the disadvantage of utilizing metal instead of glass or resin and therefore interfere with the burning properties of the composite.

Fiber Optic Temperature Measurement: Fiber optic sensors offer the important advantages of using the same material as the composite and are smaller than thermocouples by 1 or 2 orders of magnitude. They therefore have minimum impact on the burning properties of the composite panels. Most fiber optic temperature sensors are low temperature devices compared to our desired goal of 927°C (1700°F) . However, several techniques could be modified and developed for high temperature operation. Fiber sensor types considered for the composite burn tests were the Fabry-Perot, black body radiator, Rayleigh back scatter, and polarimetric devices. The black body type offers the advantage of high temperature operation, up to 3000°C (5432°F) when sapphire probes are used. However, they are hard to embed and have low temperature limitations. The polarimetric type offers an extremely small probe, about 10 times smaller than the Fabry-Perot and black body types, but the disadvantages are errors due to strain effects, and hysteresis. The Rayleigh back scatter temperature sensor has the advantage of being a distributed measurement, detecting temperature at several points along a single fiber, but the disadvantage is that the particular fibers required for the measurement are very fragile and hard to use as embedded sensors. Fabry-Perot temperature sensors are easy to install, use more rugged fiber, have a simple design, and are readily available. Fabry-Perot sensors were selected for measuring temperature in our composites during burn tests.

Fabry-Perot Temperature Sensors: The Fabry-Perot fiber optic temperature sensor[1] utilizes two partially reflecting mirrors on the end of a fiber as shown in Figure 1. A standing wave is built up between the mirrors, giving a reflected signal similar to a sine squared function. As the optical path length between the mirrors change with temperature, the reflected signal shown in the diagram shifts to the right and left. The signal processing circuitry in

FIGURE 1 - FIBER OPTIC
FABRY-PEROT TEMPERATURE SENSOR

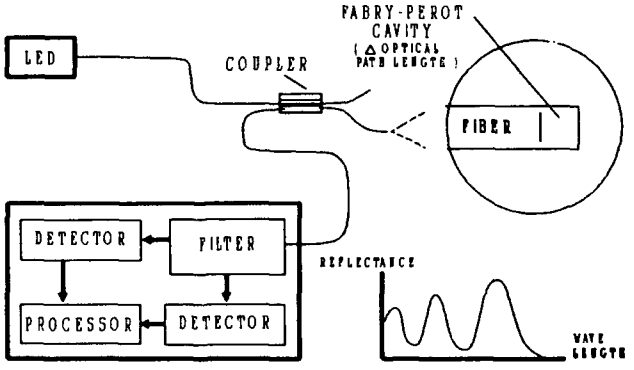

the electro-optics package then derives and displays the temperature signal.

When designing Fabry-Perot temperature sensors, material for the cavity must have a predictable optical path length relative to temperature. Also, pressure, strain, vibration, and shock must have a negligible effect on the optical properties of the cavity and the complete sensing element assembly must retain optical alignment in the presence of high temperatures and vibrations.

Fabry-Perot fiber optic temperature sensors are currently operable to a maximum temperature of 400°C (752°F) with an accuracy of ±5°C (±9°F). The sensor is composed of an electro-optics package connected to a sensor element with a single optical fiber cable. The Fabry-Perot cavity and the last 10 millimeters of fiber probe (at the sensor end) is enclosed in a glass capillary tube less than 1 millimeter in diameter. The lead-in fiber may be coated with gold to improve the durability in the presence of high temperatures. One primary advantage of Fabry-Perot temperature sensors, compared with other fiber optic techniques, is the ease of installation. They can simply be laid between the glass layers of the composites as long as the internal curing temperature do not exceed 400°C (752°F). A further improvement is needed to extend the operating temperature to the desired 927°C (1700°F). Another laboratory has disclosed a Fabry-Perot temperature sensor that operates over a range of -200°C (-328°F) to +1000°C (1832°F)[2].

Fire Tests: Glass/vinyl ester panels were fabricated with embedded fiber optic Fabry-Perot temperature sensors and Type K thermocouples. Each sensor was placed at predetermined intervals of thickness to generate a through-the-thickness thermal profile. Panels were exposed to radiant heat flux during cone calorimeter tests and temperatures were recorded directly into computers for post test analysis. Several burn tests were run, some with thermocouples alone, some with both thermocouples and fiber optic probes, and some with fiber optic probes alone. The only type of fiber optic temperature sensor used in the burn tests was the Fabry-Perot, although some preliminary experiments were done with the polarimetric type and a Rayleigh back scatter type.

The thermocouples always survived the composite burn tests. They are the more reliable temperature sensing technique.

Comparison of Fiber Optic and Thermocouple Measurements: One major burn test was completed with both embedded Fabry-Perot fiber optic temperature sensors and thermocouples with a heat source of 50 Kw/m^2. There were four thermocouples and four fiber optic probes. Each type were embedded side by side through-the-thickness of the composite sample of dimensions 4 X 4 X 0.5 inches, at distances of 0.0, 0.17, 0.33, and o.50 inches. The three fiber probes nearest the hot side were gold coated; the fiber probe on the back surface was not.

Gold coating provides structural strength for the fiber and probe, and protects it from the heat leaking around the edge of the composite sample. This maintains a coating on the fiber when the normal plastic coating would otherwise have melted or burned.

The fiber optic probes were fragile relative to thermocouples. The probe located at 0.17 inches into the specimen from the front (hot side) failed some time between the embedding process and the burn test. This was probably due to mechanical breakage from rough handling. The fiber probe installed on the back (cold side) of the composite panel also failed. This was probably due to exceeding the maximum temperature specification of 400°C (752°F). This probe was not protected with the gold coating. The two remaining fiber probes, located at 0.0 and 0.33 inches into the sample, survived the burn tests even though the maximum temperature specification of 400°C (752°F) was exceeded. A tentative conclusion is that gold coating of the fiber probes makes them more reliable.

The temperature indications of the fiber optic Fabry-Perot sensor and the thermocouple probes are shown in Figure 2. In general the indications follow each other, confirming that the fiber optic temperature sensor is a viable alternative. The fiber probes responded faster in both cases. This is thought to result from there being less mass in the fiber probe so that it more closely matches the temperature of the

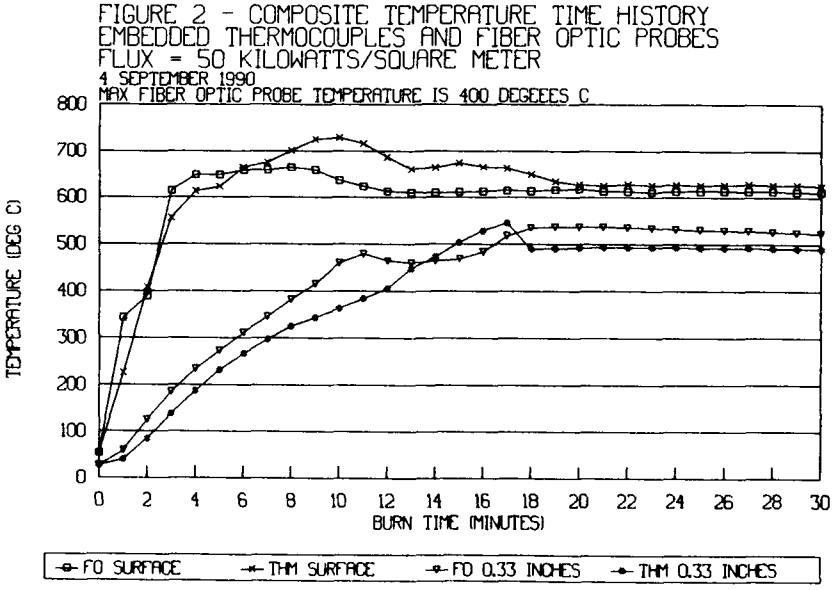

surrounding composite. There may also be some error due to calibration differences. This test should be repeated before definitive general conclusions can be made concerning the technical performance of two temperature sensing technologies when applied as embedded sensors in composites during burn tests. Note also that the maximum specified operating temperature of the fiber probes was 400°C (752°F) and was exceeded for both probes involved in the data shown in Figure 2. This provides confidence that higher operating temperature Fabry-Perot probes are possible to develop.

Embedded Thermocouple Temperature Measurements: Since fiber optic temperature sensors are still in the process of development, several composite samples were burned with only thermocouples embedded in the composite specimen. The objective was to study the heat transfer properties in the form of through-the-thickness temperature profiles. Figure 3 shows three time histories of the thermocouple temperature measurements, corresponding to heat fluxes of 25, 50, and 75 Kw/m^2 (cone calorimeter) directed on samples of thickness 0.615 inches. Thermocouples are designated 1, 2, 3, 4, 5, and 6 on the graphs and were embedded at 0, 0.120, 0.245, 0.370, 0.495, and 0.615 inches into the specimen, respectively, where the hot side is 0 inches.

There are several interesting observations concerning the time temperature diagrams. In general the thermocouples closest to the heat source register the highest temperature. The declining temperature of the surface mounted thermocouples occur when the first layer of resin has been completely burned, leaving the first glass mat uncovered. At this point there is no material to hold the heat and the thermocouple senses the air temperature which contains some colder air. There are several curves showing momentary sudden increases and decreases of temperature, notably curves 4 for heat fluxes of 50 and 75 Kw/m^2. This is thought to result from gas pockets burning in the composite, causing the local temperature to increase suddenly during combustion, and then to decrease equally suddenly when the gas has been completely consumed. The samples were not completely burned at the end of 30 minutes, as indicated by thermocouples 3, 4, 5, and 6. The temperature was continuing to rise when the test was ended. The composite was still providing heat shielding and maintained partial structural integrity. More studies are required before general conclusions can be given as to which composite materials are best suited for fire barrier design.

The analysis procedure was to convert the time temperature data of the thermocouple tests into temperature-thickness profiles as shown in figure 4. Here the temperature is plotted at 5 minute intervals into a test done with a heat source of 50 Kw/m^2. A curve fitting routine was used to smooth the data, but the actual data values are shown by the tick marks. The higher temperature indicated by thermocouple 4, at 0.370 inches, is again thought to originate by the

FIGURE 3 - TIME TEMPERATURE DIAGRAMS, EMBEDDED THERMOCOUPLES IN COMPOSITES

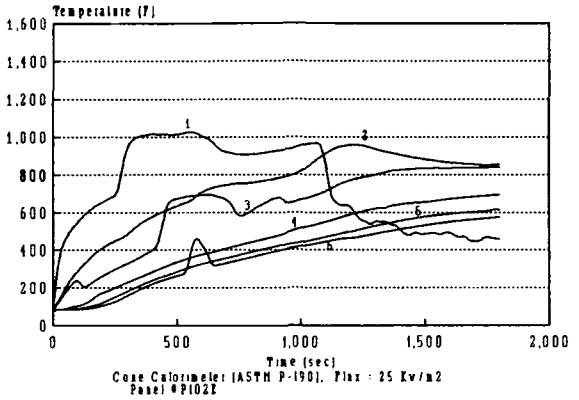

Cone Calorimeter (ASTM P-190), Flux : 25 Kw/m2
Panel #P102I

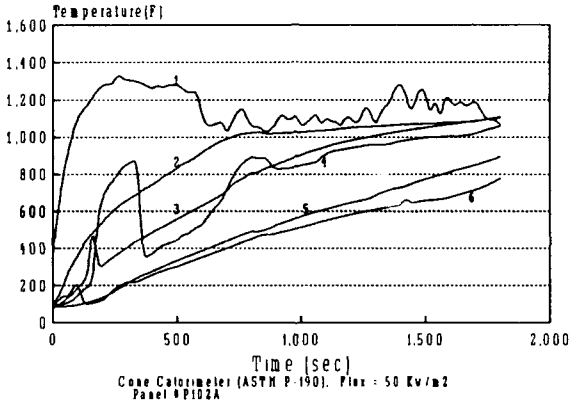

Cone Calorimeter (ASTM P-190), Flux : 50 Kw/m2
Panel #P102A

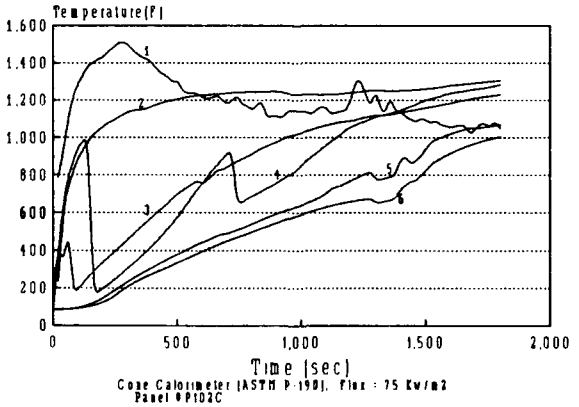

Cone Calorimeter (ASTM P-190), Flux : 75 Kw/m2
Panel #P102C

FIGURE 4 - TEMPERATURE-THICKNESS PROFILE
50 KW/M2 (P-102A)

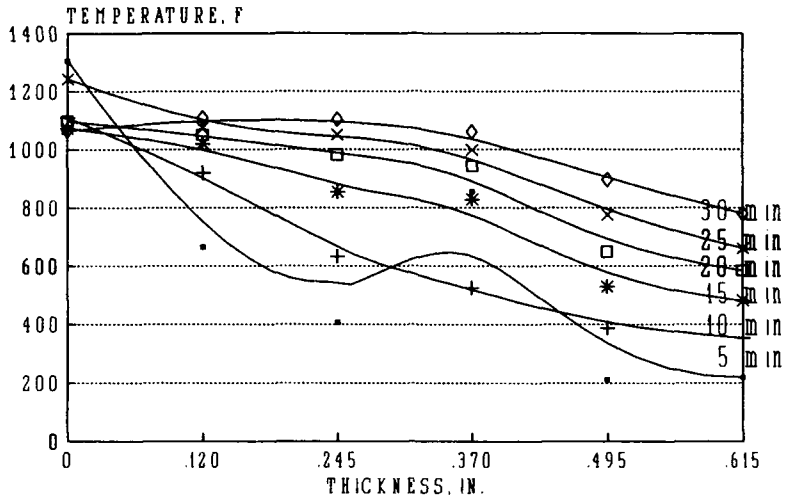

burning of gas within the composite. In general the temperature profile through-the-thickness of the composite decreases with distance from the heat source. Additional studies are required to compare the burning properties of other kinds of composites.

Conclusions: Table I summarizes composite burn test applications issues for fiber optic temperature sensors and thermocouples.

For composite burn tests, one sensor should span the entire required temperature range of 0°C (32°F) to 927°C (1700°F), to reduce complexity and to minimize disturbance of the burning properties. Thermocouples span the range, but are of dissimilar material. The fiber optic Fabry-Perot temperature sensor used in our tests, is the right material but does not span the range. An improved Fabry-Perot temperature sensor has since been reported to operate over 0°C (32°F) to 1000°C (1832°F)[2].

Fiber optic temperature sensors offer a viable alternative to thermocouples for use as embedded sensors in composite materials. They have demonstrated sufficient accuracy for the fire barrier burn tests, but additional tests are needed as results reported herein are based on one test.

The thermocouples are more reliable and durable than the fiber optic probes. However, the burn tests demonstrated that gold coating of lead-in and lead-out optical fibers improves their durability, making them very useable in this application. Additional development would likely result in more rugged fiber optic probes.

Table I - Application Issues for Embedding Fiber Optic Temperature Sensors and Thermocouples in Composite Materials.

	Fabry-Perot Fiber Optic Temperature Sensor	**Blackbody Fiber Optic Temperature Sensor**	**Polarimetric Fiber Optic Temperature Sensor**	**Thermocouple**
Temperature Span (over 2 Sensors)	0°C to 400°C (32°F to 752°F)	300°C to 1900°C (572°F to 3452°F)	0°C to 350°C (32°F to 662°F)	0°C to 2320°C (32°F to 4208°F)
Accuracy	0.2%	1.0%	About 25°C (45°F)	About 2°C (4°F)
Reliability	Unproven	Unproven	Unproven	High
Durability	Fragile	Fragile	Fragile	Rugged
Material	Glass	Sapphire	Glass	Metal
Size	About $10mm^3$	About $10mm^3$	About $1mm^3$	About $30mm^3$
State of Development	Commercially available	Commercially available	Laboratory model	Commercially available
Cost	High	High	Medium	Low
Additional Measurement Capability?	Pressure	Flame	Strain	None

The material and size of the fiber optic probes is much more desirable for burn tests because they minimize the disturbance of the burning properties of the composite. The polarimetric fiber optic probe is the smallest, but is the most undeveloped of all the fiber temperature sensors.

Cost of the fiber optic probes is about 10 times the cost of thermocouples. The importance of cost increases as the number of burn tests increase and is not yet significant in our tests.

The additional measurement capability offered by fiber optic probes is a valuable asset, particularly the strain detection capability of the polarimetric sensor. Strain measurements can be used in conjunction with temperature measurements to determine residual strength of composites during and after burn tests.

References:

1. Hartl, J. C., E. W. Saaski, and G. L. Mitchell, "Fiber Optic Temperature Sensor Using Spectral Modulation," Fiber Optic and Laser Sensors V, SPIE Vol 838, San Diego, 17-19 Aug 1987, pp 257-261.
2. Henry Taylor, Fiber Optics News, 2 July 1990, pp 4-5.

Acknowledgements: This work was supported by the Ship and Submarine Materials Technology Program, funded by the Office of Naval Technology, and managed by Ivan Caplan of the David Taylor Research Center. John Wehrle and Ed Petrisko provided encouragement and management support. Jack Overby provided technical support with the instrumentation and electro-optical technology. Tim Dapp made up the composite samples. This paper represents work of the U. S. Government and is therefore not subject to copyright.

INFLUENCE OF PLY WAVINESS AND RESIDUAL STRESS ON HYDROSTATIC COLLAPSE PRESSURE OF FILAMENT WOUND COMPOSITE CYLINDERS

John W. Gillespie, Jr.*
Travis A. Bogetti

Center for Composite Materials
Department of Mechanical Engineering
University of Delaware
Newark, DE 19716

Mark A. Lamontia

E. I. duPont de Nemours & Co., (Inc.)
Engineering Technology Laboratory
DuPont Experimental Station
Wilmington, DE 19880-0304

sponsored by
Defense Advanced Research Projects Agency
Naval Technology Program
ARPA Order No. 6661; Program Code No. 6661/22/23
Issued by DARPA/CMO under Contract #MDA972-89-C-0043
Approved for public release; distribution unlimited.

* Author to whom correspondence should be addressed.

Abstract: The influence of ply waviness and residual stress on the hydrostatic failure pressure of composite cylinders is assessed for [0/90] laminate constructions. A methodology for conducting stress and failure analyses is presented. Effective thermoelastic properties are based on a ply waviness model and represent material property input to the stress analysis. Force resultants due to pressure and thermal loads are calculated from the cylinder stress analysis and input into the ply waviness model for the calculation of ply stresses. Hydrostatic collapse pressure predictions are based on the Maximum Stress Failure theory. Parametric studies are conducted for AS4 Graphite/PEKK and S2 Glass PEKK *insitu* thermoplastic filament wound cylinders. Results show that collapse pressures are sensitive to the degree of out-of-plane rotation, material anisotropy and the interlaminar shear strength of the layer.

Key Words: Ply waviness, compression, interlaminar shear failure, filament winding, residual stress, modelling.

Introduction: A methodology to predict the influence of manufacturing on performance of filament wound thermoplastic cylinders is required. During manufacture, winding tension and consolidation may induce layer waviness. Laminate construction incorporating $[\pm\theta]$ layers have inherent waviness at cross-over locations. In both cases, ply waviness

may reduce stiffness and strength of the structure [1]. Manufacturing also induces residual stress that must be accounted for in the prediction of performance. Residual stress in cylinders subjected to hydrostatic pressure, for example, decrease the magnitude of compressive stress at the inner radius while increasing the compressive stress at the outer radius relative to the residual stress-free baseline. Residual stress may influence the magnitude of the hydrostatic failure pressure as well as the failure location. In some cases, residual stress may cause transverse cracks within the laminate. Delaminations may initiate at transverse cracks or free edges and may propagate due to thermal loads. Delaminations may also result from insufficient consolidation during processing. The effects of delamination on cylinder performance is discussed elsewhere [2].

In general, stress analysis based on effective homogeneous laminate thermoelastic properties is desirable. Complex geometries and boundary conditions necessitate numerical techniques. In most applications, ply-by-ply finite element analysis is not viable due to computer limitations and cost. In the present effort, a methodology for conducting stress analysis based on effective homogeneous laminate properties is presented. The approach is applicable to both numerical and elasticity stress analyses using effective homogeneous properties.

This work currently focuses on the influence of layer waviness on laminate thermoelastic properties and strength as well as residual stress on cylinder performance. Various submodels employed in the analysis are discussed in detail elsewhere. The submodels include the two-dimensional ply waviness model [1], three-dimensional lamination theory [3] and the generalized plain strain cylinder analysis [4].

An analytic model has been developed by Bogetti, Gillespie and Lamontia [1] to investigate the influence of ply waviness on the effective thermoelastic properties and strength of [0/90] laminate constructions commonly used in pressure hull applications. Parametric studies were conducted [1] for graphite and glass fiber reinforced laminates. Results show that thermoelastic properties and strength reduction may be significant in the direction of layer waviness. Mechanisms of stiffness reduction were attributed to out-of-plane rotation of wavy axial layers shown schematically in Figure 1. The magnitude of the property reduction increases as the amplitude, A, of the undulation increases and the half-wavelength, L, of the undulation decreases. Material anisotropy was also shown to influence property reduction in the direction of waviness with graphite fiber reinforced composites much more sensitive to layer waviness than the glass fiber reinforced composites . Typical axial modulus reduction for various [0/90] AS4 graphite/PEKK laminates is shown in Figure 2 (thickness ratio TR is defined as the ratio of hoop to axial layer thickness, h_f, in the repeating sublaminate). The out-of-plane rotation of layers within the unit cell, see Figure 1, creates interlaminar shear stress [1] that reduces axial strength. Typical axial strength predictions are shown in Figure 4. Ply waviness represents one mechanism that may partially explain why design and failure analyses of hydrostatically loaded composite cylinders based on flat, autoclave cured coupon property data (minimal waviness) do not correlate well with cylinder test results.

The ply waviness model is fully integrated with a generalized plain strain cylinder analysis [4] for the prediction of structural response and hydrostatic failure pressure as a function of ply waviness and residual stress. Effective thermoelastic properties are based on the ply waviness model and represent material property input to the cylinder stress analysis. For the cylinder analysis, the out-of-plane properties of the wavy ply configuration are also required. STIFF3D [3], an existing 3-D laminate model, is used to approximate the out-of-plane properties of the wavy ply configuration. Force resultants due to pressure and thermal loads are calculated from the cylinder stress analysis and input into the ply waviness model for the calculation of ply stresses. Two sources of residual stress are considered. Residual thermal force resultants are calculated by the cylinder analysis and are

due to the geometry of the structure and the mismatch in effective homogeneous radial and tangential thermal expansion coefficients of the laminate. This source of residual stress is self-equilibrating with respect to the structure. The second source of residual stress [1] had been previously incorporated into the ply waviness model and is due to traditional stacking sequence effects associated with the mismatch in thermal expansion between layers. This source of residual stress is self-equilibrating within the sublaminate of interest. The superposition of these two thermal stress states yields results in good agreement with the ply-to-ply elasticity solution [5].

The geometric source of residual stress represents a second mechanism that may partially explain why design and failure analyses of hydrostatically loaded composite cylinders based on flat, autoclave cured coupon property data do not correlate well with cylinder test results. The latter source of residual stress is present in flat coupons while the former is unique to cylinders.

Results: Results presented in this section are characteristic of insitu thermoplastic filament winding processes that exhibit negligible layer waviness in the hoop direction and minimal waviness in the axial layers, see Figure 1. In contrast, post consolidation filament winding processes of thick sections may exhibit significant layer waviness in both the hoop and axial directions. The methodology discussed herein is applicable to both processes.

The assessment of defect criticality and residual stress on cylinder performance is conducted by constructing biaxial failure envelops for the specific cylinder being investigated. Biaxial failure envelops based on the Maximum Stress Failure theory are generated within the ply waviness model enabling failure pressures to be predicted. Fundamental inputs to the model are the laminate stacking sequence and ply thicknesses, the amplitude of layer undulation, the half-wavelength of the undulation, and the lamina thermoelastic properties and strength allowables. Based on prior work [1], a characteristic half-wavelength of 0.1 inches is employed in all simulations. Loadings included automatically in the ply waviness model that is coupled to the cylinder analysis are the geometric residual stress force resultants in the axial and hoop directions and the stress-free temperatures which is used internally to calculate ply stresses. Failure envelops are then calculated by scaling force resultants associated with hydrostatic loading to failure while maintaining thermal residual stresses constant. Specific failure pressures correspond to the intersection of the stress vector associated with the hydrostatic loading and the failure envelop. A stress-free temperature of 200°C is used in the predictions. It should be noted that these failure predictions are restricted to strength failures at midbay. Furthermore, the influence of end effects on stress and deformation in the cylinder are not considered. The methodology could, however, be straightforwardly applied to finite element results based on smeared properties.

In Figure 4, hydrostatic failure pressures for AS4 Graphite/PEKK cylinders having [0/90] constructions is summarized as a function of undulation amplitude. Thickness ratio TR is defined as the ratio of hoop to axial layer thickness. Material properties used in the analysis are summarized in Tables 1 and 2. Collapse pressure is found to be very sensitive to layer waviness in this highly anisotropic material. In general, a plateau region at low amplitudes exists that corresponds to fiber compressive failure in the axial direction. Consequently, removing additional axial layers (increasing TR) reduces failure pressure prediction pressures slightly in this regime. At undulation amplitudes of approximately 0.005 inch, interlaminar shear failure modes are excited and a significant reduction in failure pressure is predicted (S_{13} = 16 Ksi is used).

In Figure 5, the influence of interlaminar shear strength on failure pressure is presented (TR = 2). In general, decreasing interlaminar shear strength does not reduce the initial plateau region but does shift the failure mode transition to lower undulation amplitudes.

For example, a strength reduction from 16 to 7 Ksi reduces the critical amplitude from approximately 0.005 to 0.002 inches.

Similar strength predictions are presented in Figure 6 for various S2 Glass/PEKK cylinders having [0/90] constructions using material properties summarized in Tables 3 and 4 (S_{13} = 17 Ksi). A similar response is observed where a plateau level (fiber failure in axial direction) transitions to interlaminar shear failure in the axial direction that reduces failure pressures significantly with increasing amplitudes. Note that the transition in failure modes occurs at significantly higher amplitudes (0.007 inches) since this material system is more isotropic than the AS4 Graphite/PEKK material systems.

In Figure 7, the sensitivity of hydrostatic failure pressure (TR = 2) to interlaminar shear strength is presented. An identical trend is observed where decreasing interlaminar shear strength shifts the failure mode transition to lower undulation amplitudes. For example, a strength reduction from 17 to 8 Ksi reduces the critical amplitude from 0.007 to 0.003 inches.

Discussion: The analysis for quantifying the influence of ply waviness and residual stress on hydrostatically loaded cylinder is a valuable tool enabling these manufacturing issues to be incorporated in the design and analysis of the structure. The analysis provides the designer with quantitative 'knock-down' factors for stiffness and strength for manufacturing induced ply waviness. On the other hand, the analysis quantifies what an acceptable level of waviness that does not reduce cylinder performance below design levels. The model can be used to establish quality control standards with respect to ply waviness. Furthermore, trade-off studies where the cost of increasing cylinder performance by reducing ply waviness through manufacturing can be conducted.

The influence of ply waviness on the performance of cylinders has focused on layer waviness in the axial direction because hoop waviness is believed to be less significant for insitu consolidation processes. It should be noted, however, that layer waviness in the hoop direction has been observed in numerous 7 inch monocoque graphite/epoxy cylinders tested by Garala [7]. The analysis developed by the authors [1] is also valid for this case. Trends, similar to those presented herein, would be expected. Undulation amplitudes [6] varied between 0.02 and 0.06 inches which is significantly greater than the transition amplitudes (less than 0.006 inches) identified in this study. Cylinder failures might have been initiated by interlaminar shear failure due to layer waviness in the hoop and axial directions. One notable exception was the Hitco cylinder which failed at the highest pressure (16,000 psi) and had undulation amplitudes of approximately 0.001 - 0.002 inches. These experimental observations are consistent with our model predictions.

Finally, this study indicates that ply waviness and residual stress may represent two mechanisms that may partially explain why design and failure analyses of hydrostatically loaded composite cylinders based on coupon property data do not correlate well with cylinder test results. Autoclave processed coupons may exhibit less layer waviness than observed in filament wound cylinders. Furthermore, the geometric source of residual stress discussed in this work is unique to cylinders as mentioned above.

References

[1] T. A. Bogetti, J. W. Gillespie, Jr. and M. Lamontia, "Influence of Ply Waviness on Stiffness and Strength Reduction in Filament Wound Composite Cylinders", DuPont Report, DARPA AST Program, January 1990.

[2] N. Patton and J. W. Gillespie, Jr., "The Effects of Delamination in Composite Material Cylinders: A Finite Element Approach", DuPont Report, DARPA AST Program, April 1990.

[3] B. R. Trethewey, J. W. Gillespie, Jr. and D. J. Wilkins, "Three Dimensional Elastic Properties of Laminated Composites", , CCM Technical Report, 1989.
[4] J. T. S. Tzeng and R. B. Pipes, "Development of the Generalized Plane Strain Model for Filament Wound Composite Cylinders:, DuPont Report, DARPA AST Program, January 1990.
[5] T. A. Bogetti, J. W. Gillespie, Jr. and M. Lamontia, "Influence of Ply Waviness and Residual Stress on Hydrostatic Failure Pressure of 7 Inch Monocoque Cylinders", DuPont Report, DARPA AST Program, March 1990.
[6] B. Su and K. Adams, "DARPA-AST Program - Recommended Design Data', January, 1990.
[7] H. J. Garala, "Structural Evaluation of 8-Inch Diameter Graphite-Epoxy Composite Cylinders Subjected to External Hydrostatic Compressive Loading", DTRC-89/016.

TABLE 1 LAMINA PROPERTIES: AS4 GRAPHITE/PEKK

E_1 (psi)	19.0×10^6
E_2 (psi)	1.4×10^6
E_3 (psi)	1.5×10^6
G_{12} (psi)	0.98×10^6
G_{23} (psi)	0.63×10^6
G_{13} (psi)	0.98×10^6
ν_{12}	0.36
ν_{13}	0.36
ν_{23}	0.36
α_1 (1/°F)	-5.0×10^{-7}
α_2 (1/°F)	1.55×10^{-5}
α_3 (1/°F)	1.55×10^{-5}

TABLE 2 AS4 GRAPHITE / PEKK STRENGTH PARAMETERS

XIT (psi)	2.58×10^5
X2T (psi)	5.2×10^3
X3T (psi)	5.2×10^3
X1C (psi)	2.0×10^5
X2C (psi)	2.65×10^4
X3C (psi)	2.65×10^4
S13 (psi)	7.00×10^3
	1.10×10^4
	1.60×10^4
S12 (psi)	1.90×10^4

TABLE 3 LAMINA PROPERTIES: S2 GLASS/PEKK

E_1 (psi)	8.0×10^6
E_2 (psi)	2.75×10^6
E_3 (psi)	2.75×10^6
G_{12} (psi)	1.01×10^6
G_{23} (psi)	0.59×10^6
G_{13} (psi)	1.10×10^6
ν_{12}	0.27
ν_{13}	0.27
ν_{23}	0.31
α_1 (1/°F)	2.3×10^{-6}
α_2 (1/°F)	1.85×10^{-5}
α_3 (1/°F)	1.85×10^{-5}

TABLE 4 S2 GLASS/PEKK STRENGTH PARAMETERS

XIT (psi)	2.43×10^5
X2T (psi)	7.0×10^3
X3T (psi)	8.5×10^3
X1C (psi)	1.77×10^5
X2C* (psi)	3.06×10^4
X3C (psi)	3.5×10^4
S13 (psi)	8.00×10^3
	1.25×10^4
	1.70×10^4
S12 (psi)	1.57×10^4

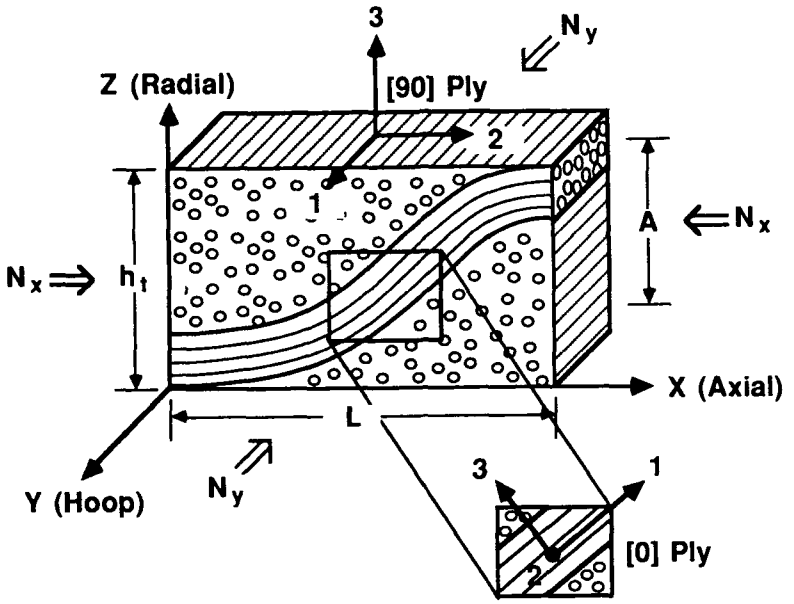

Figure 1 Unit Cell Used in the Ply Waviness Model [1].

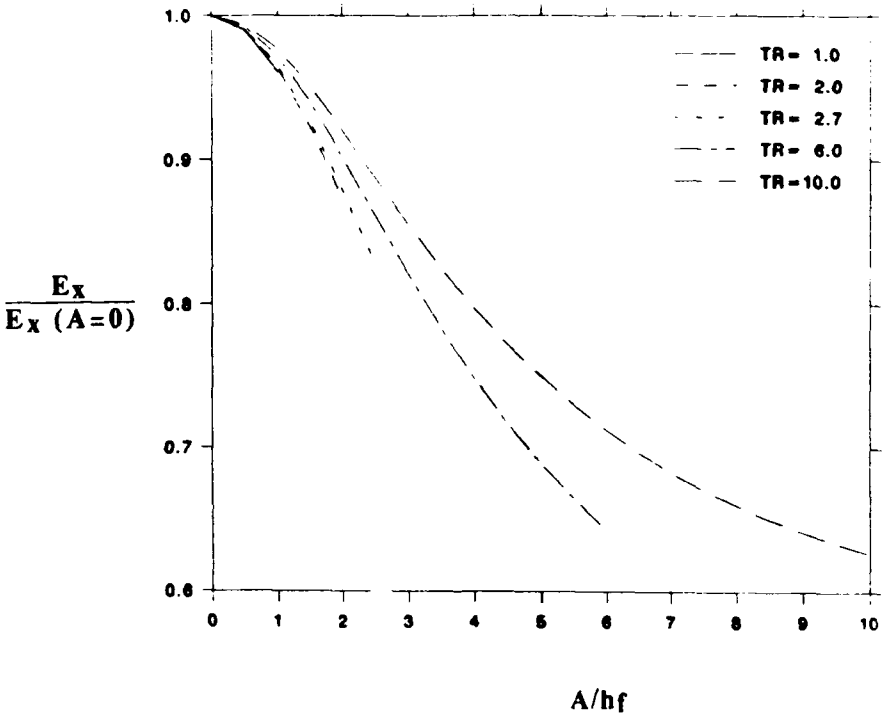

Figure 2 Influence of Undulation Amplitude (A) and Laminate Construction (TR) on Axial Modulus of AS4 Graphite/PEKK (L/h_f = 20, h_f = 0.005 inch)

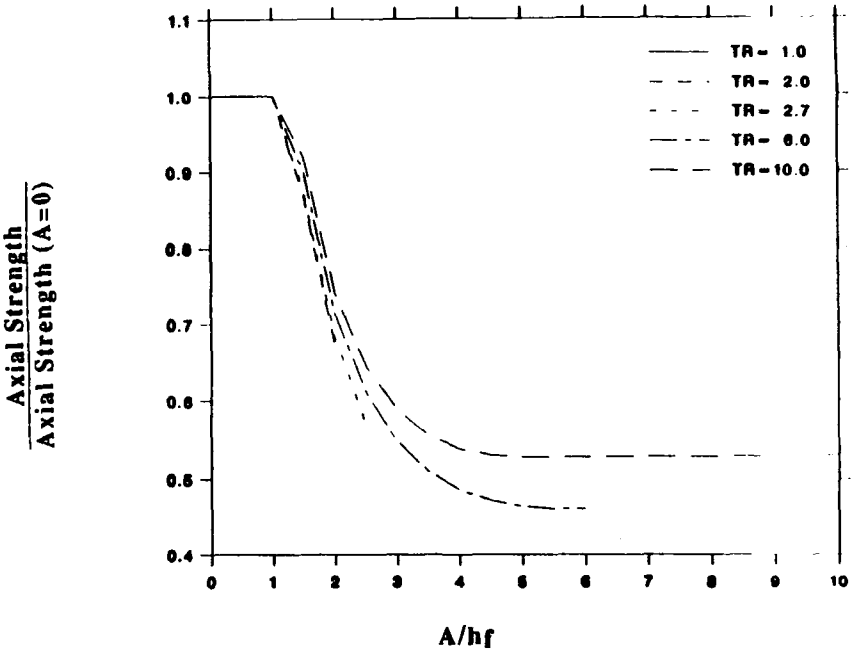

Figure 3 Influence of Undulation Amplitude (A) and Laminate Construction (TR) on Axial Compressive Strength of AS4 Graphite/PEKK ($L/h_f = 20$, $h_f = 0.005$ inch)

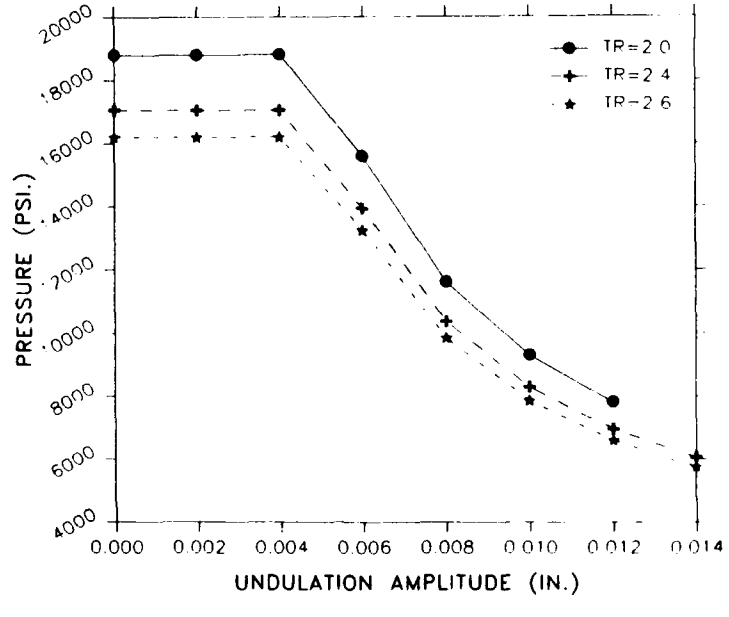

Figure 4 Influence of Undulation Amplitude and Laminate Construction (TR) on Collapse Pressure of AS 4 Graphite/PEKK Cylinders ($L/h_f = 20$)

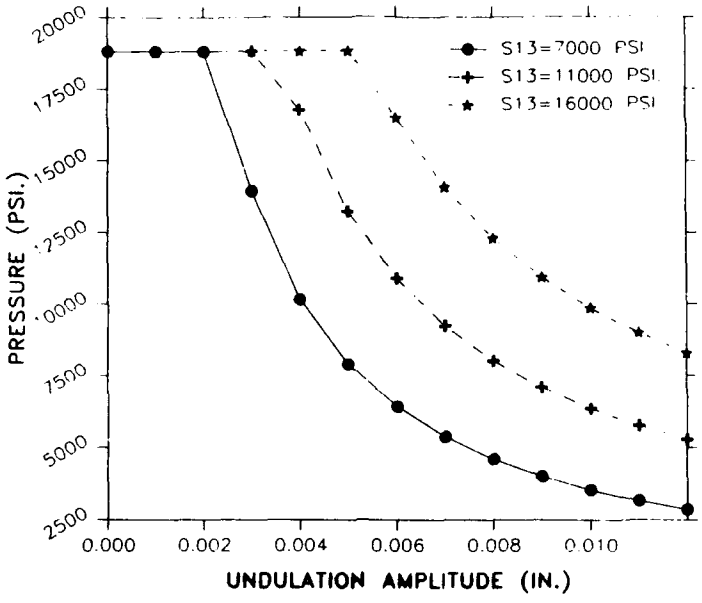

Figure 5 Influence of Interlaminar Shear Strength (S13) on Collapse Pressure of AS 4 Graphite/PEKK Cylinders (TR = 2, $L/h_f = 20$)

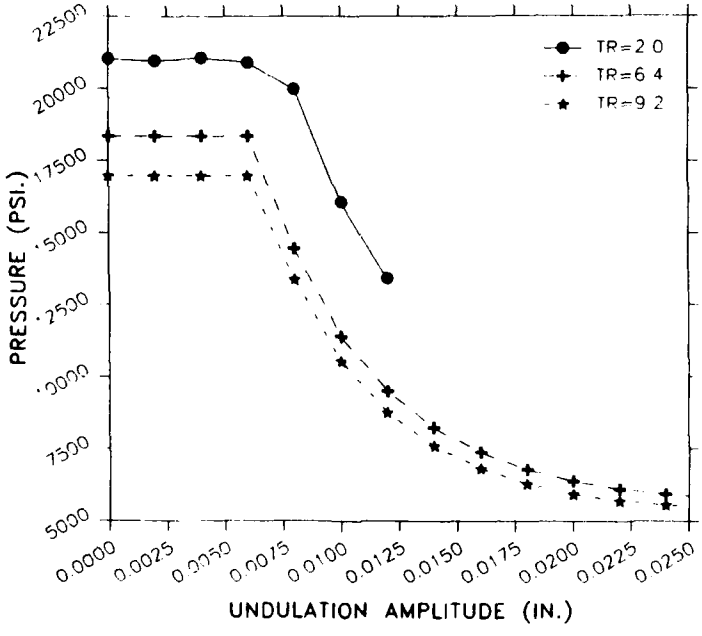

Figure 6 Influence of Undulation Amplitude and Laminate Construction (TR) on Collapse Pressure of S2 Glass/PEKK Cylinders ($L/h_f = 20$)

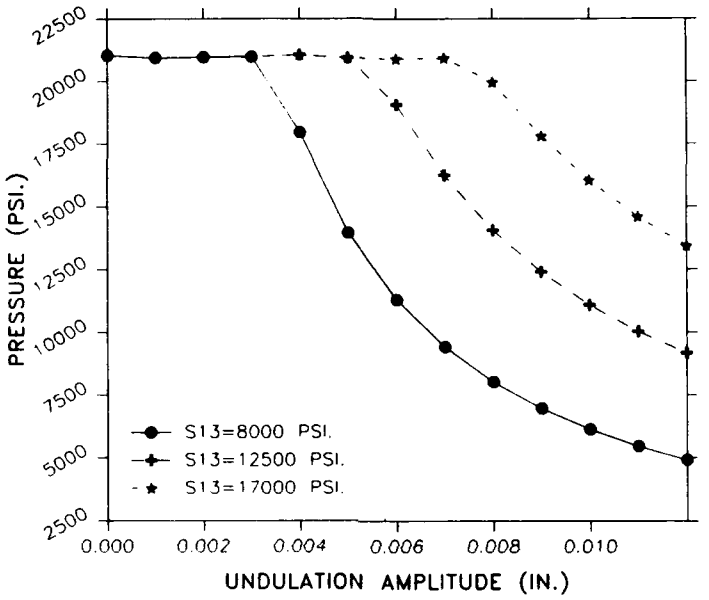

Figure 7 Influence of Interlaminar Shear Strength (S13) on Collapse Pressure of S2 Glass/PEKK Cylinders (TR = 2, $L/h_f = 20$)

PROPELLER BLADE FAILURE ANALYSIS

Patricia Stumpff
Wright Laboratory
WL/MLSA
Wright-Patterson Air Force Base, Ohio 45433-6533

William B. Pinnell
University of Dayton
Research Institute
300 College Park
Dayton, Ohio 45469-0137

Abstract: A failure analysis investigation was performed on a composite, aircraft propeller blade. The purpose of the investigation was to determine the cause of delamination located on the trailing edge of the blade. The blade consisted of a foam core overwrapped with a Kevlar/epoxy composite material.

Nondestructive evaluations (NDE), thermal analysis and fractographic techniques were implemented to help determine the cause of the delamination. The results showed that the delamination was due to a fractured ballast tube exiting the blade.

Key Words: Delamination; Failure analysis; Kevlar/epoxy; Propeller blade

Introduction: The blade being analyzed was taken from a propeller of an acrobatic aircraft which failed in service after only 20 minutes of operation. The failure consisted of a large delamination located on the trailing edge of the blade. Background information indicated that no excessive loads were placed on the blade and no extreme environmental conditions existed at the time of the failure.

The blade consisted of a foam core overwrapped with a combination of fabric and unidirectional, Kevlar/epoxy prepreg. The epoxy resin was a 250^{o}F cure system and was determined to be adequate to sustain skin temperatures on the ground up to 200^{o}F and service temperatures up to 170^{o}F. Since the propeller was part of an acrobatic type aircraft, the exact loads on the blades were unknown. However, the manufacturer indicated the blades were designed such that failure would not occur under any conditions that were expected to be encountered.

Two discrepancies were found in the manufacture of this particular blade: 1) a variation in the cure cycle, and 2) a ballast tube of incorrect size. The cure cycle for this

blade calls for a heat up to 170°F followed by a hold time of 40 minutes at this temperature. After the hold, the temperature is then raised to 250°F for the final step in the cure cycle. For this particular blade, however, the hold time was omitted and the temperature was ramped directly to 250°F. Manufacturing records also indicated that a six inch ballast tube had been installed in the blade, even though a four inch long tube was specified.

Analysis: Figure 1 shows the blade as it was received. Visual inspection revealed a delamination along the trailing edge with a maximum separation distance measured to be 5/16 of an inch. Fiber bridging of the unidirectional plies was observed within the delamination. The manufacturer stated that failures of this type had been observed after impact damage, i.e., bird strike. However, no damage was observed on the leading edge of the blade that would indicate impact.

The white line located near the trailing edge (Figure 1) outlines an area of delamination detected by the manufacturer using an impactiscope technique. However, visual observations revealed the delamination extended into the blade farther than shown by the white line. Therefore, further testing utilizing the ultrasonic pulse echo technique was performed using a non failed blade for comparison. The results are shown in Figure 2. As depicted by the white line in Figure 2, the pulse echo technique detected damage extending all the way to the hub end, further into the blade and just past the visual end of the delamination.

Thermal analysis was conducted on the material to verify the glass transition temperature (Tg) and the material's degree of cure. Thermomechanical analysis (TMA) results, shown in Figure 3, indicated the Tg of the material was 287°F (142°C). Since the cure temperature of the material was 250°F, the Tg was deemed adequate. Differential scanning calorimetry (DSC) results, shown in Figure 4, indicated the material was fully cured.

Cross sections were removed from the blade to verify material configuration and fiber, resin and void contents. A cross section taken from an undelaminated area on the trailing edge is shown in Figure 5. The fabric and unidirectional plies of the material were able to be verified. Image analysis was also performed on the cross sections to determine the fiber, resin and void contents. Result of the image analysis revealed a fairly large range of the fiber/resin content. Fiber content ranged from 33-57 percent, resin content from 41-66 percent and void content from 0-2 percent. Resin content obtained by the manufacturer at the time of fabrication was 48 percent while the nominal resin content is 45 percent indicating

that the resin content was slightly higher than normal. Figure 6, an increased magnification photomicrograph from Figure 5, depicts resin rich areas and areas of poor compaction.

The blade was sectioned transversely at approximately 11 inches from the hub end of the blade and again at 11 inches from the tip end of the blade. Figure 7 shows the cross section of the cut at the hub end. No ballast tube was evident but a three-quarter inch ragged hole was observed in the foam core in the hub end. The hole also extended into the center section of the blade. This central section was then radiographed to determine if the tube was present in this portion of the blade. The results, shown in Figure 8, revealed that the tube itself was not present, however, a path of metallic particles was evident. This path began in the center part of the blade at the hub end and moved toward the tip end of the blade, eventually exiting out the trailing edge.

The central portion of the blade was cut open such that the mating surfaces of the delamination could be examined. Refer to Figure 9. The arrows in Figure 9 indicate a hole in the foam core exhibiting the exact same path as the metallic particles seen in the radiograph. Minor damage to the composite was also noted along the path.

The fracture surfaces of the delamination were examined. The delamination was mainly interlaminar (i.e., between plies) at the trailing edge, but more intralaminar (i.e., within a ply) further inward from the edge. Scanning electron microscope (SEM) examinations of the delaminated fracture surfaces revealed mainly fiber/matrix debonding, Figures 10 and 11. Though most of the fracture surface was devoid of fracture features, some evidence of Mode I tension (river patterns, shown by short arrow in Figure 11) and Mode II shear (hackles, shown by the long arrow in Figure 11) type failures were seen. The few river patterns that were seen indicated the delamination opened up in peel from the hub end extending toward the tip of the blade.

The hub end of the blade was returned to the manufacturer for their analysis. Upon sectioning, the manufacturer discovered that only the rim of the ballast tube remained. The fracture surface of the failed tube was examined by the manufacturer and the failure mode was determined to be due to overload.

Conclusion: The results of the investigation indicate the delamination was caused by the fractured ballast tube exiting the trailing edge of the blade. Evidence supporting this conclusion includes: 1) ultrasonic analysis indicating a delamination extending from the hub end to just past the visual delamination near the tip end

of the blade; 2) large displacement of the two delaminated surfaces which indicates a high energy fracture; 3) visual indication of loss of ballast tube and resulting path through the blade; and 4) fiber bridging and river patterns indicating a peel type fracture from the hub end to the tip end (same direction as the exiting ballast tube).

The evidence suggests that lack of a hold time in the cure cycle did not permit resin flow, resulting in poor compaction and excess resin in the composite. However, although the improper cure cycle appeared to affect the consolidation, resin content and porosity, the deviation was not thought to be relevant to the cause of failure.

Acknowledgements: The authors would like to thank the following for their assistance in the investigation; Tom Dusz and Bill Price of the University of Dayton Research Institute and Dan Laufersweiler of Universal Technology Corporation.

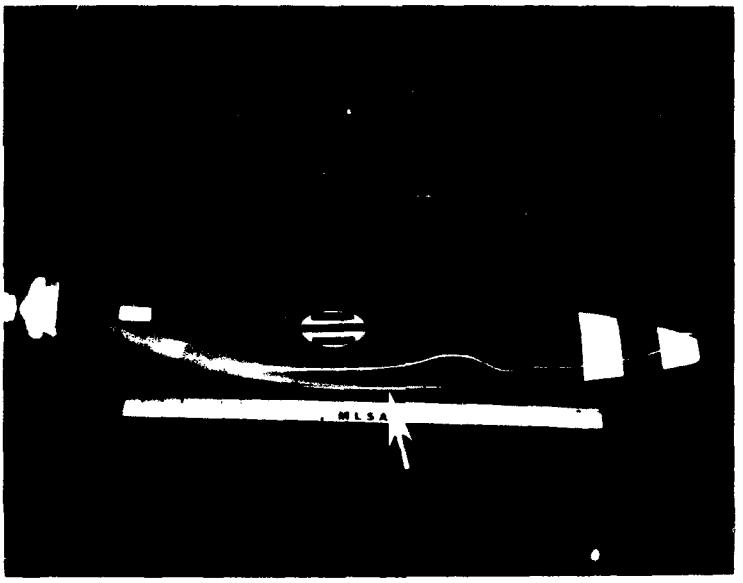

Figure 1. White line outlines the area of damage detected by an impactiscope technique. Delamination indicated by the arrow. Mag.12X

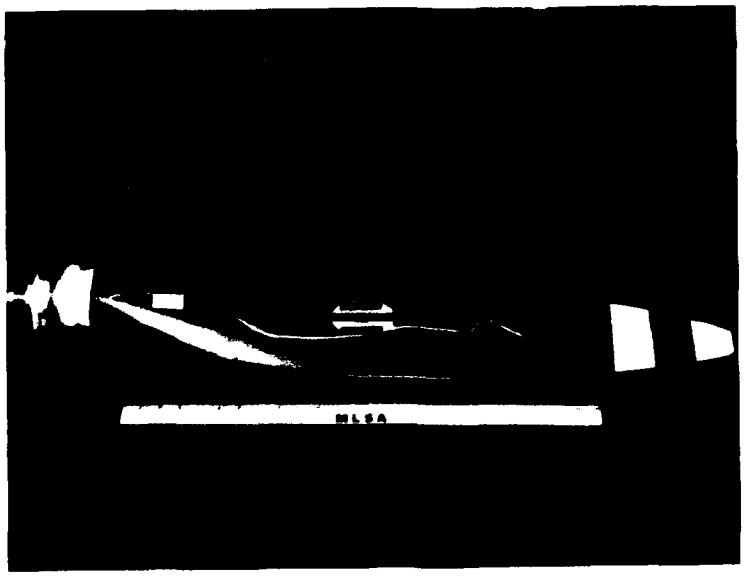

Figure 2. White line outlines the area of damage detected by pulse echo ultrasonics. Mag.12X

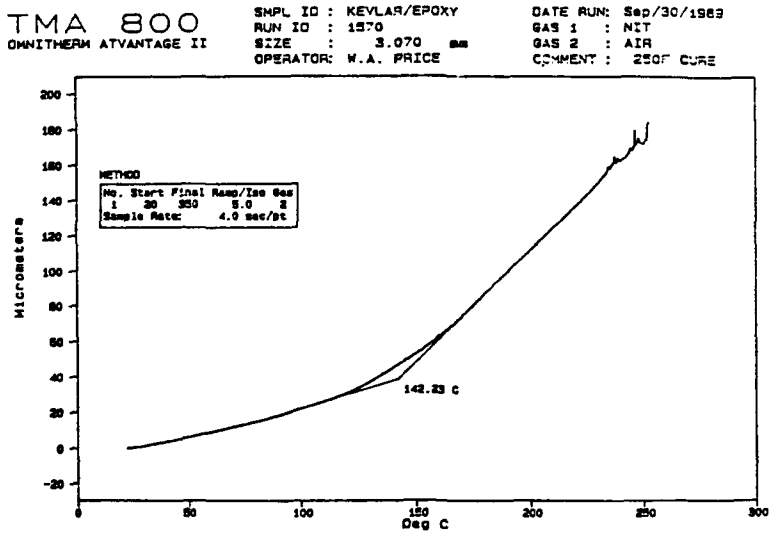

Figure 3. Thermomechanical analysis trace of Kevlar/epoxy material indicating a Tg of 142.23^{O}C (287^{O}F)

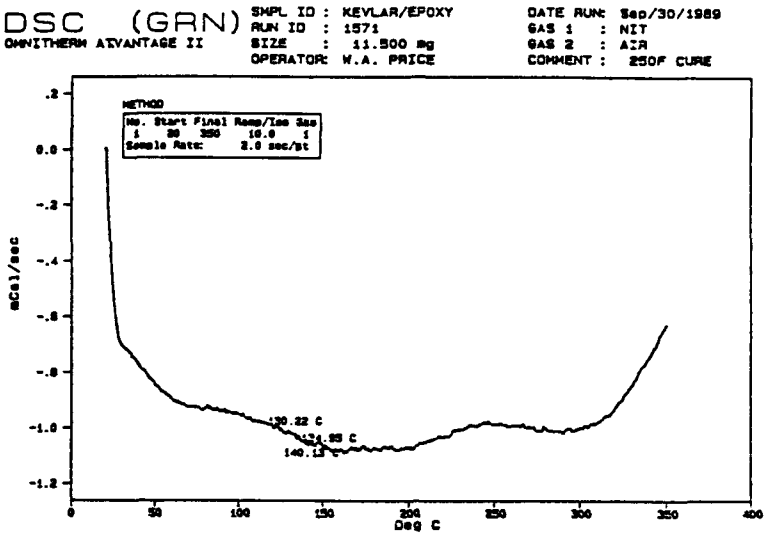

Figure 4. Results from the differential scanning calorimetry test indicating a full cure of the Kevlar/epoxy material.

Figure 5. Low magnification photograph of a cross section taken at the trailing edge in a location of no delamination. Mag 6X

Figure 6. Increased magnification of the cross section shown in Figure 5. Resin rich areas and voids can be seen. Mag 100X

Figure 7. Ragged hole in the foam approximately 11 inches from the hub end of the blade. Mag .65X

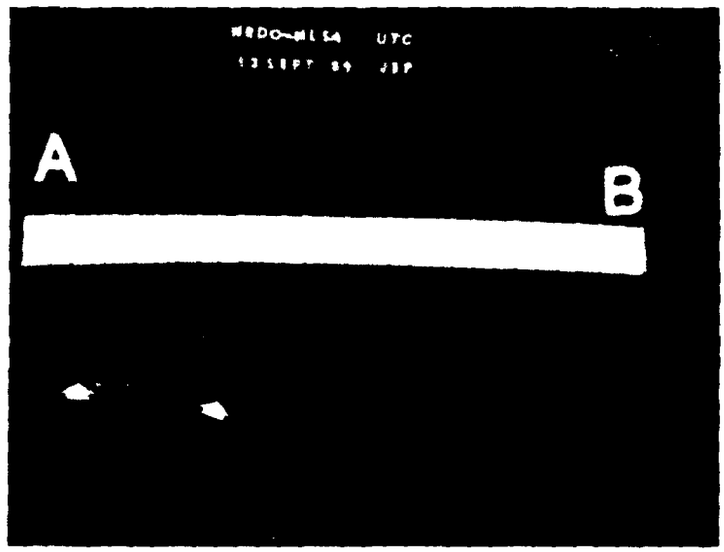

Figure 8. Radiograph taken from the central part of the blade. Arrows identify the path of the ballast tube. Mag .25X

Figure 9. Central section of the blade. Arrows identify the path of the ballast tube. Mag .25X

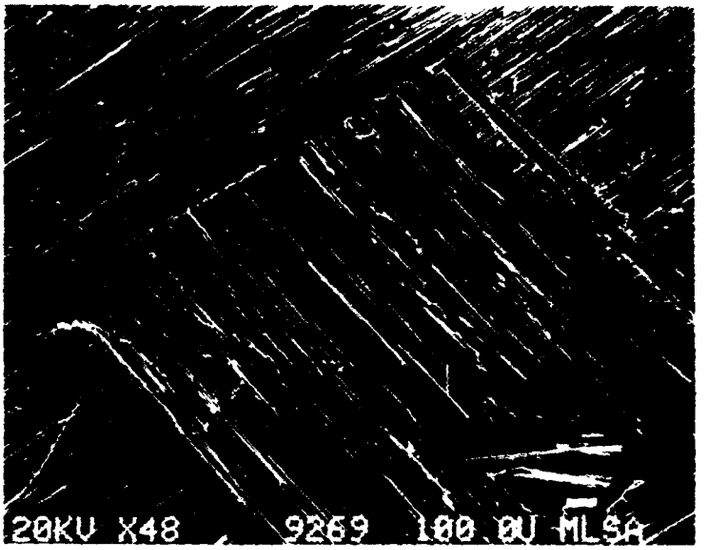

Figure 10. Low magnification SEM fractograph of the delamination depicting poor fiber/matrix adhesion. Mag 48X

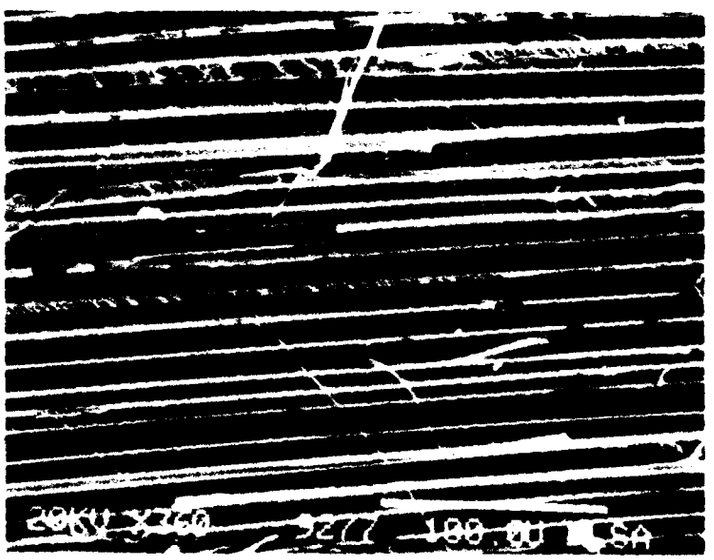

Figure 11. Increased magnification of Figure 10. River patterns shown by the short arrow and hackle formation shown by the long arrow. Mag 360X

FAILURES IN METALS

Chairman: MarjorieAnne E. Natishan
David Taylor Research Center

ANALYSIS OF A FAILURE OF A CU-NI FITTING USED IN A SHIP HYDRAULIC SYSTEM APPLICATION

D.A. Davis, E.M. Hackett and M.E. Natishan
David Taylor Research Center
Bethesda, Maryland 20084

Abstract: A failure analysis was conducted on a 70/30 copper-nickel alloy fitting in a pneumatic actuating line from a ship's hydraulic system to determine the cause of plastic deformation and cracking observed in that component. Metallurgical analyses support the hypothesis that the cracks were formed as a result of residual stresses, possible embrittlement during weld repair and microstructural alterations caused by that welding process on the fitting. Calculations suggest that the plastic, torsional deformation in the reduced section of the fitting was due to over-torquing of the component during its removal operation. Recommendations included welding procedure modification and quality and environmental control to minimize residual stresses and material damage during welding. Surface conditioning to form compressive residual stresses would suppress crack initiation. Also, more restrictive torquing specifications for installation/removal of this type of fitting were recommended to reduce the probability of torsional deformation.

Key Words: 70/30 copper-nickel; hydraulic line fitting; residual welding stresses; embrittlement; microstructural alteration; torsional plastic deformation

Introduction: The David Taylor Research Center (DTRC) was asked to determine the cause of failure of a 70/30 copper-nickel (Cu-Ni) fitting installed in a pneumatic actuating line in a hydraulic system on a naval ship. There were no records of a previous failure in this component in this type of system. It was noted by the naval maintenance group in charge of this ship that the portion of the system containing the actuating line fitting in question was worked on during the most recent repair availability on this vessel. It was also noted that the damaged fitting had since been replaced and had been subjected to "localized twisting" during each removal/installation over the life of the ship. Additionally, the maintenance group report indicated that the fitting was assumed to have "failed due to stress applied from making up the union assembly".

Macroscopic and Nondestructive Evaluation: The general features of the fitting, as received at DTRC, are shown in Figure 1. Two cracks or tears were observed in the reduced section. The cracks were oriented at approximately a 20^{o} angle from the perpendicular to the longitudinal axis of the fitting. Evidence of removal by cutting/grinding was present at the "nipple" end of the fitting, as identified in Figure 1. The entire reduced/tapered section

had a "mottled" appearance which could have resulted from weld grinding or peening. Figure 2 shows a close-up of the reduced section containing the two cracks. Plastic deformation, due to twisting of the nipple end of the fitting, relative to the union end, also shown in Figure 1, was evident in the deformation lines adjacent to the cracks. The side of the fitting opposite the cracks (Figure 3) contained no linear indications, however, plastic deformation due to twisting was evident in deformation lines.

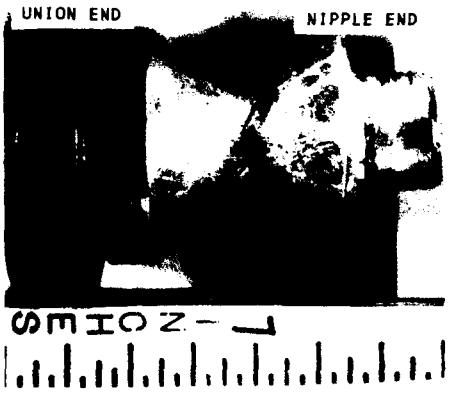

Figure 1 - Overall view of failed fitting

Figure 2 - Close-up of fitting reduced section showing cracks

A non-destructive examination of the fitting was conducted using dye penetrant to determine if cracks other than the two noted above were present. Figure 4 shows the results of the penetrant testing on the reduced section of the fitting in the region 180° away from where the cracks were located. Several linear indications were present, oriented in a similar fashion to the cracks on the opposite side. These indications were determined not to be cracks, but deemed to be a result of the torsional deformation lines.

Figure 3 - Close-up of fitting reduced section 180° from view in Fig. 2

Figure 4 - Penetrant test indications of section shown in Fig. 3

Conformance with Material Specifications: Element analysis was performed on material from the fitting to insure that it was alloy C71500 (70/30 Cu-Ni), as per specification MIL-C-15726F. The fitting constituents were all within specification requirements for C71500 alloy, as shown in Table 1.

Table 1. Chemical analysis of failed C71500 fitting

	Chemical Composition, Weight %								
	Cu	Ni	Zn	Fe	Pb	Mn	P	S	C
Fitting	67.6	31.0	0.085	0.41	0.006	0.87	0.006	0.004	0.019
MIL-C-15726F	65.0 min	29.0-33.0	0.500 max	0.40-1.0	0.020 max	1.00 max	0.020 max	0.020 max	0.050 max

Rockwell B (R_b) hardness measurements were taken across the diameter of the fitting. The average of these measurements was 37.8 R_b. Reference [1] indicates that a "soft" (annealed) C71500 alloy would typically have a hardness of approximately 40 R_b. This corresponds to the actual hardness of this fitting and further establishes the material as annealed CA71500.

Metallography: Metallographic examinations were performed on a cross-section of the fitting, with the general structure and weld metal location shown in Figure 5. Higher magnification photomicrographs were taken in both the reduced section and at a location remote from the torsionally damaged area, at points near both the inside and outside diameters for both locations. The area remote from the reduced section exhibits a uniform, equiaxed structure, shown in Figure 6, with evidence of coring that would be expected in this alloy in this condition. In the damaged, reduced section area of the fitting, distortion of the equiaxed structure can be observed in both the inside (Figure 7) and outside (Figure 8) diameter locations, with the most severe distortion occurring in the outside diameter location. This appearance would be expected in a material plastically deformed in torsion.

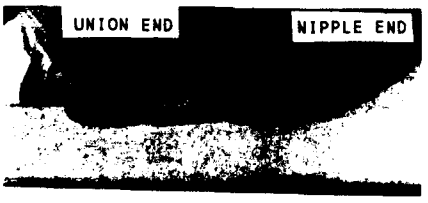

Figure 5 - General structure and weld location of failed fitting

Figure 6 - Fitting microstructure at location remote from reduced section

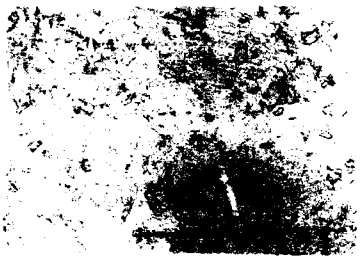

100X

Figure 7 - Microstructure of fitting in damaged area near inside diameter location

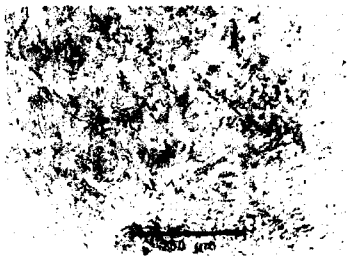

100X

Figure 8 - Microstructure of fitting in damaged area near outside diameter location

Additionally, metallography was performed on a cross-sectional profile of one of the cracks located in the reduced section of the fitting. The low magnification (10X) photomicrograph shown in Figure 9 shows both the poor quality of the overlaying bead of the weld and the close proximity of the weld to the crack

10X

Figure 9 - Overall view showing poor weld quality and close proximity of weld to crack

250X

Figure 10 - Micrograph of fitting area remote from crack location

surface. The higher magnification (250X) pictures in Figures 10, 11 and 12 begin to develop a clearer view of the cause of the cracks. Figure 10 shows an area remote from both the crack and the weld and again exhibits the homogeneous, equiaxed structure, with coring, expected in alloy CA71500. As the crack area is approached, the metallographic structure changes. Figure 11 shows an area along the crack surface but remote from the welded section and the crack initiation. In this area the crack path is obviously intergranular and the equiaxed structure is distorted but not severely. Figure 12 shows the portion of the crack adjacent to the initiation plane and in close proximity to the weld. The intergranular nature of crack in the absence of an aggressive environment, along with the close proximity to the weld suggests residual stress build-up and microstructural alteration during welding as a likely source of initiation for the cracks. Additionally, the appearance of intergranular fracture in this Cu-Ni alloy, without the obvious presence of an

aggressive environment, suggests the introduction of hydrogen, possibly by moisture at the repair site, during welding. The possibility of hydrogen-induced intergranular fracture in 70/30 Cu-Ni is not common, but has been the cause of failure in other welded shipboard components.

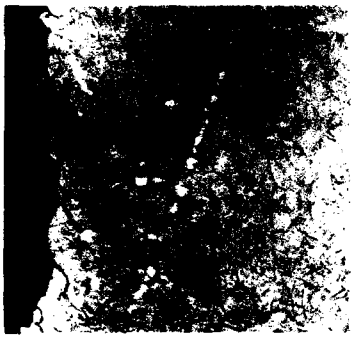

250X
AREA "A" FROM FIG. 9

Figure 11 -Microstructure of fitting adjacent to crack, remote from weld metal and initiation area

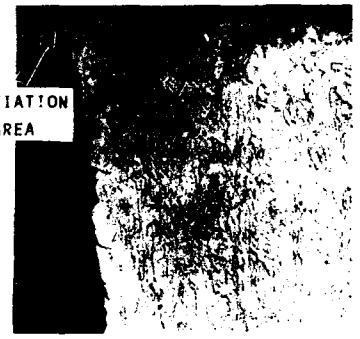

250X
AREA "B" FROM FIG. 9

Figure 12 -Microstructure of fitting at crack location adjacent to weld and initiation area

Fractographic Examination: Scanning electron microscopy (SEM) analysis was performed on the fracture surfaces of the two cracks from the reduced section of the fitting. Since similar surface appearance was observed for both cracks, the discussion here will be limited to the fractography on the larger crack shown in Figure 2. The overall appearance and shape of the crack is shown in the 20X fractograph in Figure 13. The crack is elliptical in nature, initiating at the outer surface of the fitting and growing radially towards the inside diameter of the fitting. Neither crack penetrated completely thru the wall of the fitting.

20X

Figure 13 - Overall fractographic appearance of large crack fracture surface

300X

Figure 14 - "Smeared" fractographic features apparent over entire fracture surface

A higher magnification (500X) scan along crack edge failed to reveal a definitive initiation site. Additionally, a surface scan at 300X revealed the "smeared" fracture appearance, shown in Figure 14, devoid of ductile fracture features, over the entire crack. The smearing of the surface is likely a result of the fracture surfaces of the already-present crack rubbing against each other during the torsional deformation. Also, the lack of microvoid appearance on a fracture surface in this alloy was completely unexpected due to the fact that C71500 material would typically fracture in a ductile manner in the absence of an embrittling atmosphere. Higher magnification (2000X) examination revealed both intergranular fracture (Figure 15) and areas that initially appeared to be fatigue striations (Figure 16). These fracture modes were both unexpected in view of the lack of aggressive environment that could cause intergranular fracture and the absence of a loading form that would promote fatigue crack growth. Additionally, these fatigue "striations" were growing perpendicular to an expected growth direction based on the overall crack shape and possible loading conditions. After further consideration, and correlating fractography with subsequent metallographic examination of the crack profile, it was determined that the most likely cause of the initiation and intergranular nature of the cracks was the result of high residual stresses and microstructural alteration caused by the welding process, with the possible introduction of the embrittling species coming from moisture present during the welding. The best explanation for the features originally thought to be fatigue striations is that they are slip lines appearing at the free surface of the crack due to the plastic torsional deformation occurring after the crack had formed.

2000X

Figure 15 - Fractograph showing intergranular nature of crack in fitting

2000X

Figure 16 - Fractograph showing slip lines appearing at free surfaces due to torsion

Torsion Analysis: An analysis was conducted to determine the torque necessary to plastically yield the reduced section of the actuating line fitting. The torsion formula [2] was employed for this analysis:

$$\text{Maximum Shear Stress } (s_{max}) = Tc/J \quad (1)$$

Where:

T = Torque
c = Distance from center of circular cross section to outer diameter of fitting (0.250 inches)
J = Polar moment of inertia for the circular cross section

For a thin section, J can be approximated by:

$$J = 2\pi c^3 t \quad (2)$$

Where t = the wall thickness of the tube at the reduced section (0.106 inches).

Equation (1) can be rearranged to solve for the torque, resulting in:

$$T = \tau_{max} J/c \quad (3)$$

To solve for the torque required to yield the reduced section, the yield strength in shear of the material is substituted for s_{max} in equation (3). The yield strength in shear can be estimated from the yield strength in tension by:

$$\tau_y = \sigma_y/\sqrt{3} \quad (4)$$

As stated previously, the actuating line fitting was fabricated from alloy C71500 (70/30 Copper-Nickel) in accordance with MIL-C-15726. The fitting was most probably fabricated from bar or rod product over 1 inch diameter. Table II of MIL-C-15726F requires a minimum yield strength of 20 ksi for up to 2-1/2 inch thick plate or bar stock in the M20-soft condition, and 18 ksi for over 1/2 inch thick plate or bar stock in the M20-hard condition. Table III of MIL-C-15726F requires a minimum yield strength of 18 ksi for all sizes of rod for the 060 temper, and 35 ksi for rod of 1 inch to 3 inches in diameter for the H01 temper. The ultimate strength of the fitting was also estimated from hardness testing (R_B) using data compiled by Revere Copper and Brass, Inc. [1], and was found to be approximately 54 ksi; a value which is similar to that required in Tables II and III of MIL-C-15726F.

The minimum (18 ksi) and maximum (35 ksi) yield strengths noted above were substituted in equation (4). The resulting yield strengths in shear were substituted in equation (3) providing

torques of approximately 36 ft-lbs and 70 ft-lbs respectively. These torques are within the capability of an average individual, especially if a long (greater than 1 foot) wrench, or a wrench with a "cheater" extension is used to remove the fitting. Such torques are also in the range of requirements for tightening steel bolts for certain applications [3]. This leads to the conclusion that the actuating line fitting could have been plastically deformed to the condition in which it was received at DTRC by application of torques typically used to tighten steel bolts in service.

Conclusions and Recommendations: The results of the failure analysis support the hypothesis that the cracks were the result of the welding process imparting high residual stresses in the reduced section of the fitting. Moisture present during welding led to the embrittlement and intergranular cracking. The cracks appeared to have originally been oriented parallel to the longitudinal axis of the fitting. Over-torqueing of the reduced section, probably caused by the removal operation, resulted in plastic deformation of the reduced section to the extent that the cracks were opened and subsequently twisted approximately 20^{o} to the perpendicular. A torsion analysis showed that the torques required to produce plastic deformation of the reduced section of the fitting were within the capability of an individual to produce with a long (> 1 ft.) wrench. These torques were also typical of those commonly specified for tightening of steel bolts.

The following recommendations are supported by the above conclusions:

(1) Modification of welding and weld repair procedures to insure minimizing the possibility of residual stresses and material damage that could lead to crack initiation. The modified procedures should provide guidelines to preclude introduction of an embrittling species into the repaired or welded material. Peening or other surface treatments resulting in formation of compressive surface residual stresses, would also aid in suppressing crack initiation in the reduced section.

(2) Torques used for removal/installation of the fitting should be restricted to approximately 25 ft-lbs. This would prevent possible plastic deformation of the reduced section.

(3) A re-design to provide for a thicker wall in the reduced section of the fitting would increase the torque required to plastically deform the reduced section.

References:

[1] Copper and Copper Base Alloys, Revere Copper and Brass Incorporated, Publication No. GP-200, June, 1979

[2] Popov, E.P., Mechanics of Materials, 2nd Edition, Prentice-Hall, Inc., Englewood Cliffs, New Jersey, 1976, Ch. 3

[3] Machine Design, Fasteners Reference Issue, Vol. 37, No. 6, Table 5, March, 1965

THE RESULTS OF IMPROPER MANUFACTURING TECHNIQUES ON 21-6-9 STAINLESS STEEL TUBING

Michael P Oliver
Materials Directorate
Wright Laboratory/MLSA
Wright-Patterson Air Force Base, Ohio 45433

Abstract: A failure analysis investigation was conducted on aircraft bleed air ducts to determine why they were failing (bursting, leaking, and corroding).

The analysis revealed improper manufacturing and processing procedures had been used. Discrepancies found included: substandard or nonexistent cleaning procedures prior to welding, improper fit/clearance between overlapping welded joints, lack of material passivation following surface treatment with an iron based wire brush, the absence of pickling following welding, and no post weld heat treatment. These anomalies produced general and severe, localized corrosion, including intergranular corrosion. Also, both longitudinal and circumferential cracking, in and around the weld areas, were found in a majority of the ducts examined.

Key Words: Arc strike; Bleed air ducts; Contamination; Corrosion; Crack; Dog-eared sleeve; Oxide; Passivation; Post weld heat treat; 21-6-9 stainless steel; Sensitization; Unstabilized

Introduction: The bleed air duct system, integral to one of the military's older aircraft, has long been plaqued with failures. These failures included numerous leaks, abrupt ruptures, and catastrophic failures which may have contributed to or caused several aircraft mishaps.

The ducting of the bleed air system is primarily made from 21-6-9 stainless steel. The duct system is composed of both a high and low pressure subsystem. The low pressure system operates at 120 psi and the high pressure at 190 psi. Both systems function at approximately 170^{o}F. Portions of the ducting network pass over, and are next to hydraulic lines and fuel cells.

Analysis: Figure 1 shows a photograph of Duct No. 1, one of thirteen different types of ducting submitted to the Materials Directorate for evaluation. Area A in the figure depicts a dog-eared sleeve welded onto the duct which is used to hold the duct while it is in the aircraft. The arrow in Figure 2 depicts one of the numerous cracks found in Area A of Figure 1. Note the presence of a dark colored residue, shown by Area A, which emanates from the crack in the

figure. This residue was caused from hot escaping gas and indicates the crack had propagated through the entire cross-section of the duct wall prior to removal of the duct from the aircraft. The arrows in Figure 3 show additional cracks found in Area A of Figure 1 (note that there are cracks in both the sleeve and duct). Corrosion products were found on the weldment, depicted by Point A of this figure. Extensive abrasions were found on the weld, ear, and sleeve material surfaces at this location. This suggests the area had been abused by a wire brush or abrasive wheel.

The crack in the sleeve in Figure 3 was removed and opened from the duct to reveal the area between the sleeve and the duct (see Figure 4). The initiation of the sleeve crack coincided with the heat tinted colored area shown by the arrow. Figure 5 represents the mating surface to the colored area shown in Figure 4. The colored region suggests an arc strike had occurred between foreign particles in this region and the duct and sleeve surfaces. The arrow in Figure 5 shows the origin of the crack. Figure 6 represents a scanning electron microscope (SEM) photograph of the arc strike or crack initiation site (arrow). The area to the right of the arrow represents a large oxidized pit that was formed following the arc strike. The cause of this pit could be attributed to pitting corrosion, galvanic corrosion, and/or crevice corrosion. Typically, galvanic corrosion is caused by dissimilar materials coming in contact with each other. Crevice corrosion is attributable to exposure to the environmental media, such as the sleeve's open end being exposed to the surrounding air. Finally, pitting corrosion is related to areas of dissimilar electrical potentials existing in close proximity to each other. The rate of corrosion increases as the temperatures of the duct and surrounding media increase.

Particles foreign to the sleeve and duct material were found near the origin of the crack (Figure 6). An energy dispersive spectrometer (EDS) analysis by X-ray showed the particles to be rich in sulfur, chlorine, potassium, and silicon. Note silicon is the only element found on this area to be indigenous to the base material of both the sleeve and duct.

The cracked area in Figure 2 was sectioned, mounted, and etched with Marbles reagent (see Figure 7). Evident at the right of the photograph is the through-wall crack. This was one of the areas where hot gas residue was found on the duct's outer surface. The arrows in the figure point to where intergranular corrosion was taking place. This form of corrosion is caused from material becoming "sensitized" by the precipitation of chromium carbide at the grain boundaries of the material in or near the weld heat affected zone (HAZ). As the chromium level at the grain boundaries

increases, the corrosion protection of the material decreases.

The submitted ducts were manufactured from unstabilized 21-6-9 stainless steel. "Unstabilized" refers to the lack of chemical elements present that combine or tie-up carbon, thus preventing chromium from combining with the carbon at the grain boundaries (sensitization). The degree of sensitization in unstabilized material is primarily a function of the heat input of the welding process and the level of carbon in the base material. As the temperature of the welding process increases and/or the level of carbon in the material increases, the greater the chance of sensitization.

Evidence of galvanic and/or crevice corrosion was found in the HAZ of the same metallographic cross-section examined previously (black arrows in Figure 8). Part A denotes the duct material, where sensitization had taken place through the entire cross-section, and Part B shows the sleeve material. The white arrows depict foreign material found to be lodged between the duct and sleeve. An EDS analysis identified this material to contain potassium, chlorine, and aluminum, all of which are not indigenous to the base material. Also, an oxide surrounding the particle was found to contain zinc. The specific source of zinc, chlorine, and potassium was not identified. One possibility would be from contamination occurring during pre- or post-weld cleaning processes or the lack of a cleaning process before or after welding.

Area A in Figure 9 shows an oxide layer found on the inside of the duct in the weld HAZ, where the sleeve was welded to the duct. The white arrows depict the inner surface of the duct and the black arrow denotes intergranular corrosion. An EDS analysis showed the chromium level to exist at a lower level in Area A than in Area B (base material). This type of structure and composition was found only in the HAZ of the weld. A possible cause for the oxide was from either a lack of "descaling" following the welding operations or improper shielding techniques during welding operations. When a weld is made in stainless steel, a chromium oxide scale is produced on the surface. The chromium level of this scale is of a lower concentration than present in the base material. Generally speaking, stainless steels inherently have passivated surfaces (a protective chromium oxide film) that resists corrosion. The scale produced during welding has a chromium level lower than this normal passivating film. Therefore, the material covered by the oxide scale does not rapidly passivate due to its low level of chromium, and thus is subject to pitting and intergranular corrosion.

The ducts were submitted to the Nondestructive Evaluation Group within the Materials Directorate for inspection. The inspection revealed numerous corrosion pits existing in the HAZ of the weld. A crack that existed on the duct from Figure 2 was removed from the tube and inserted into the SEM. Figure 10 shows the pits found along the crack or fracture face (fracture face is the light colored area on the right side of the photograph). Recall that a portion of the crack coincided with the boundary of the HAZ and that the chromium oxide scale, produced from welding, can lead to both intergranular and pitting corrosion.

Several other types of ducts submitted for evaluation were found to contain the same surface pits and general corrosion of the welds, HAZ, and overall surface as the ducts examined previously. These ducts were new and had not been exposed to an operational environment. The arrow in Figure 11 depicts the location of a crack found on one of the new ducts, Duct No. 2. Figure 12 is a higher magnification photograph of the crack shown in Figure 11.

The cracked area in Figure 12 was removed from the duct, mounted and polished, as shown in Figure 13. Two additional cracks were found, depicted by Areas B and C (Area A was the crack shown in Figure 12). Figure 14 shows the cracks found at Areas A, B, and C in Figure 13. The crack in photo A was probably caused from residual stresses not relieved due to a lack of post-weld heat treating. The crack in photo B resulted from the sharp fillet produced when the support bracket was welded to the duct. The toe crack in photo C was probably produced due to a lack of pre-weld heating.

CONCLUSIONS: All 13 submitted bleed air ducts suffered from corrosion and corrosion related cracks. The cause(s) for corrosion appears to be manufacturing induced rather than service related.

According to the manufacturer's procurement specification, "corrosion resistant steel shall be passivated in accordance with Specification MIL-S-5002." Passivation is a process in which iron or tool steel particles are removed from the surface of stainless steels thereby restoring the material to its natural corrosion protection surface. Passivation will not remove particles of scale or existing corroded areas. The general corrosion and pitting found on both the inside and outside duct surfaces of the HAZ of the welds, as well as the overall duct surface, leads to the conclusion that the parts were not passivated.

Most of the discrepancies prevalent on the submitted ducts are related to the lack of post-weld heat treatment. The intergranular corrosion, a result of sensitization, caused cracking in the heat affected zone of the welds where a sleeve/dog-ear assembly was welded to one of the ducts. Several cracks found on this and other ducts, including ducts which had not been exposed to an operating environment, were due to residual stresses which would have been relieved if the ducts were post weld heat treated.

All submitted ducts had voids or pits in and around the weldment. Duct No. 2 had a 0.009 inch diameter void in the weld filler material. The presence of both the void and pitting could be attributed to welding procedures, i.e., poor shielding practices and high input temperature. The ducts, which had been grit blasted on outside surface, still contained the pits and voids on the inside surfaces.

A chromium oxide scale was found on the inside surface in the heat affected zone of the sleeve/ear weld of Duct No. 1. This scale was produced as a result of welding and should have been removed by descaling prior to passivation.

Foreign material in the form of particles and oxides were found in the region between the sleeve and duct of Duct No. 1. The material was composed of sulfur, potassium, chlorine, aluminum, and zinc particulates. One end of the sleeve is open to the environment allowing the potential for post-weld cleaning solution to become trapped in this area, thus providing an excellent environment for corrosion to occur. However, some particles found in this area appeared to be too large to have entered following the welding process. Therefore, the particles must have been produced as a result of, or existed on the surface, prior to the welding process.

Numerous welds were found to not conform to established welding procedures. All of the ducts with sleeves or brackets were welded in heat affected zones of other welds without being heat-treated between each weld pass. The bracket of Duct No.1 was welded to the duct on one side, thus allowing a sharp fillet to exist. This condition produced a high stress concentrator, ultimately leading to the formation of a crack.

Several of the ducts' outside surfaces had been grit blasted. This may have been accomplished by descaling the duct following the welding procedure; however, since the inside of the tube was not descaled, total corrosion protection was not produced.

1. Photograph of Duct No. 1. Area A depicts the dog-eared sleeve which is welded onto the duct.

2. Photograph of weldment which holds the sleeve to the duct. Area A depicts the hot gas residue and the arrow depicts the crack which originated at the weld.

3. Photograph of the opposite end of the sleeve. The arrows depict cracks found on both the duct and sleeve material. Area A depicts corrosion found in the weldment of the dog-eared/sleeve interface.

4. Photograph of the crack initiation site for the crack shown on the sleeve in Figure 3.

5. Photograph of the mating face of the crack initiation site of Figure 4.

6. SEM photograph of the crack initiation site from Figure 5. Mag 200X

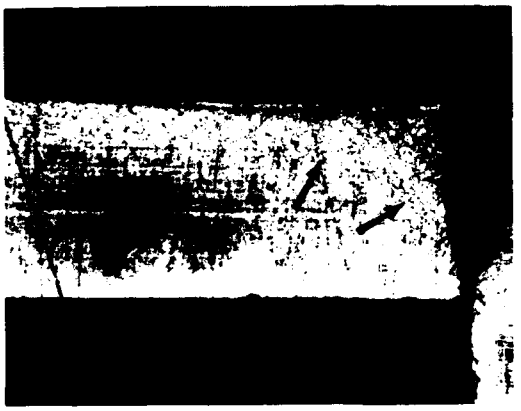

7. Photomicrograph of the crack from Figure 2. The arrows indicate the presence of intergranular corrosion. Mag 100X

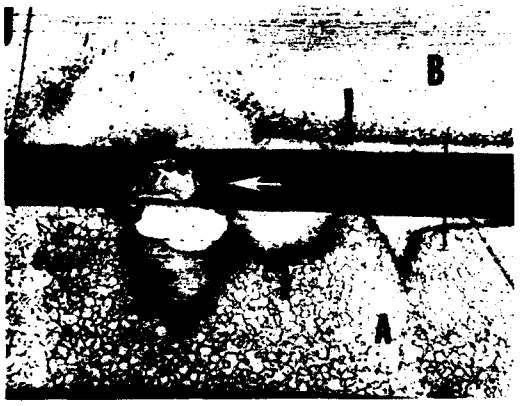

8. Photomicrograph of the area between the sleeve and duct from the area where the crack initiated from Figure 2. The white arrow depicts foreign material found between the sleeve and duct material. Area A depicts intergranular corrosion occurring in the duct's material, Area B is the sleeve, and the black arrows indicate where other forms of corrosion where occurring. Mag 100X. Marbles Etch.

9. Photomicrograph from the cracked area of Figure 2. Area A depicts a layer of chromium oxide, Area B is the duct material, the black arrow is where intergranular corrosion was taking place, and the white arrows is the outer surface. Mag 500X. Valalis Etch

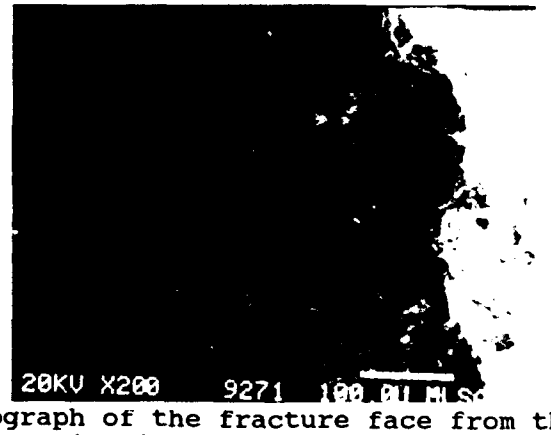

10. SEM photograph of the fracture face from the through-wall crack found in Figure 2. Mag 200X

11. Photograph of the location of a crack found on Duct No. 2.

12. Close-up photograph of the cracked area from Figure 11. Mag 15X

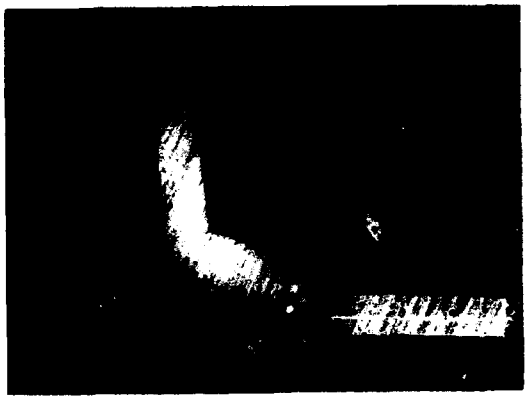

13. Photograph of a cross-section produced from the cracked area of Figure 11. Areas A, B, and C represent locations of cracks (Area A was the location of the crack shown in Figures 11 and 12). Mag 10X

14. Photomicrograph of the cracks found from Areas A, B, and C (photo A is from Area A, B is from Area B, and C is from Area C) of Figure 13.

FAILURE ANALYSIS OF A DISCHARGE PIPE SUPPORT SYSTEM IN A CHEMICAL REFINERY

Patricia L. Hackett
and
C. Mel Adams, Sc.D., P.E.
Forensic Technologies International
2021 Research Drive
Annapolis, MD 21401

ABSTRACT
During a maintenance outage, a discharge pipe at a chemical refinery fell, injuring a worker. The pipe fell due to the failure of two separate support mechanisms: a U-bolt which secured the long vertical run of the pipe and a welded channel support which supported the weight of the pipe. Both support mechanisms, when examined, were shown to have failed in an overloaded manner. Based on eyewitness statements concerning the motion of the pipe during the fall and its at-rest position, calculations were performed to model two different scenario modes: (1) the U-bolt failing first; and (2) the channel support failing first. The equations and calculations were inputted into a computer where the motion of the pipe was then modeled into an animation. The calculations and the animation clearly showed that the channel support had failed first and the U-bolt failure was a consequence of the channel support failure.

KEY WORDS
Animation; computer; piping, failure analysis; channel support; U-bolt.

INTRODUCTION
During a routine maintenance procedure at a chemical refinery plant, a member of the maintenance crew was injured when a discharge pipe fell, crushing his foot. The discharge pipe was one of four pipes which were being worked on at the time. The discharge pipes were 10 inches in diameter and 25 feet long. The length of the pipe ran vertically. At the top end, the pipes were open-ended, allowing discharge to vent to the atmosphere.

As you travel down the pipe, approximately 6 feet from the top, U-bolts were clamped on to each pipe and secured to a crossing horizontal member. Below the U-bolts, the pipes bent 45° and then continued another 15 feet, where the pipes make a 90° bend and terminate. Photograph 1, Appendix A, shows a view of the four pipes looking in an easterly direction.

The pipes are supported in three ways. The first way was the U-bolts mentioned above. The function of this U-bolt was to restrain the upper portion of the pipe from horizontal movement, while permitting vertical expansion and contraction. The second support was a channel support which was located between the pipe and an I-beam which ran horizontally, beneath the bends in the pipes. Photograph 2, Appendix A, shows these channel supports. The third support is the flange connection at the end of the 90° bend. The pipes were each connected to a relief valve at this flange. If the relief valve was removed from any discharge pipe, that pipe would then be supported primarily by the vertical channel support, 13.25 inches long, situated

at the lower 90° bend in the pipe. The top end of the channel support was welded to the 90° bend of the pipe, and the bottom end was welded to the supporting horizontal I-beam. When the relief valve was in place, the bolted flange connection to the discharge pipe constituted an ample lower support. Thus, in normal operation, the welded channel support performed no function; the only purpose for the channel support was to hold the discharge pipe when the relief valve was absent. Figure 1, Appendix B, is an elevation view of one of the discharge pipes looking in a northerly direction. Figure 2, Appendix B, shows a top view of the four pipes and their proximity to the relief valves.

The system involved in the accident and the scenario of the accident are described below:

System Description

1. An underlying steam header which was scheduled to be removed and replaced in the course of plant maintenance;
2. Four gate valves attached to and above the heater;
3. Four pressure relief valves, one above each gate valve, with a spool piece connecting each gate valve to each relief valve; and
4. Four discharge pipes, one connected to each relief valve.

The pipes and relief valves were aligned in a row, number 1, 2, 3 and 4 (in sequence from south to north), as seen in Figure 2, Appendix B.

Accident Scenario

According to witnesses, relief valve numbers 1, 2 and 3 had successfully been removed, but the crew was experiencing some difficulty with one or more stubborn bolts in their attempts to remove relief valve number 4. More specifically, a small crane (known as a "cherry picker") was in position to remove valve number 4 by means of a small wire rope (sometimes called a "choker") and, with the help of the "cherry picker", as well as some sledge hammers, the crew was engaged in some fairly vigorous actions in their endeavors to free valve number 4. It was during this struggle, and the associated vibration of the structure, that the accident took place.

At the time of the accident, the injured crewman was reportedly standing south of valve number 4, with his left foot at the top of the gate valve at location number 2. This flange had been uncovered by the earlier removal of relief valve number 2, together with its attached spool piece. When discharge pipe number 2 fell, the flange on the discharge pipe struck his foot.

The purpose of this failure analysis was to determine which support member failed first, the U-bolt or the channel support. This information was important in order to determine liability for the accident.

INVESTIGATION

In order to investigate the failure, the site of the accident was inspected and documented, the two suspect supports were examined and metallurgically analyzed and calculations concerning the motions and dynamics of the pipe were performed.

Site Investigation

At the site, the discharge pipe assemblies were all measured and fully documented. Observations and witness statements concerning the pipe and how it fell were

obtained. It was reported that the pipe fell straight down and slightly to the east. The flange impacted the foot of the crew member while it was positioned on the gate valve flange. Immediately after impact, the pipe pivoted to the west and fell, removing itself from the crew member's foot.

Evidence Examination

An initial examination of the U-bolt showed it to be in a badly corroded condition, which would tend to indicate that it was the initial failure. A thorough examination revealed that the bolt itself was still intact, with no apparent fracture. The failure was found to be due to both of the nuts stripping the threads from each end of the bolt and not due to the corroded condition.

Examination and testing of the channel support showed the welds to be of good quality and proper size. The channel support showed evidence of plastic deformation at the failure points. When examined, the fracture surfaces showed evidence of ductile overload.

DISCUSSION

Both support structures, when examined, revealed failure in an overload manner. Even though the U-bolt was corroded, this condition was not a significant factor in its failure. No evidence of any significant materials defect or problem was found with either the U-bolt or the channel support. Most probably, the actions taken by the crew in an attempt to remove safety valve number 4 caused enough vibrations and impact to cause one of the two support members on discharge pipe number 2 to overload. Once two of the three support mechanisms were no longer in place, the third would then also fail in an overload mode. In order to determine which support failed first, calculations were performed which explain the motion of the pipe when one support fails versus the other.

The static force picture is not complicated. The channel support welds carried the weight of the discharge pipe, 1390 pounds. Because of the vertical "zig-zag" in the pipe, there was a very small horizontal force exerted on the U-bolts of approximately 144 pounds.

The channel supports were quite adequate to sustain the vertical load (i.e., weight) of the pipe, but the welds were subject to bending, and shaking the structure could have induced enough bending to precipitate failure. The welds themselves were structurally sound and would have appeared sound and adequate during any visual observation or inspection prior to the accident.

Dynamic analysis[1] shows quite clearly that, if the support channel collapsed first, the action would be very rapid, completed in less than 0.26 second. Moreover, when this occurs, the vertical flange on the pipe lands squarely on the horizontal flange of the gate valve. When the channel support collapsed, as the initiating event, the pipe slid vertically downward, travelling in the direction of its own length. The friction of this abrupt sliding action of the pipe would exert a strong pull on the upper U-bolt, tearing the nuts through the I-beam, causing it to fail.

If the initiating failure had been that of the U-bolt, the pipe flange would not have

---

1 See Appendix C for supporting calculations.

impacted the horizontal flange, because the rotation of the pipe, as it fell, would change the relative positions of the two flanges. Then, when the channel support collapsed, the two flanges could not have met.

In order to demonstrate the motion of the pipe in both scenarios, the data obtained from the calculations was inputted into a computer. Using a computer program called Wavefront, the motion of the falling pipe was modeled. The modeling consisted of a three-dimensional computer animation. This animation demonstrated, in a visual manner, that the channel support had to fail first in order to cause the injury which occurred.

SUMMARY

There are four main considerations supporting the opinion that primary failure took place in the channel supports rather than the U-bolts:

1. The welded connections at the ends of the channel support were much more severely stressed than the U-bolts, because the channel support was carrying the weight of the pipe.
2. The secondary failure of the U-bolt is consistent with the friction-induced tearing action to be expected when the pipe abruptly slides vertically downward as a result of the collapse of the channel supports.
3. Because of the geometry and distribution of loads, actions producing shaking or vibration impose a much more severe stress to the channel support welds than to the U-bolts.
4. The injury to the crewman most likely occurred when the vertical flange on the lower end of the discharge pipe forcefully encountered the horizontal flange on the gate valve, catching his foot in between. Had the U-bolt given way first, the dynamics of the motion force the conclusion that the two flanges would not have met.

The channel support to discharge pipe number 2, which was available for examination, exhibited no indication of deterioration or progressive failure of the welds. The channel clearly indicated single-event, abrupt fracture of sound metal at the weld connection. No corrosion, fatigue or any other manifestation of degradation over a period of time was evident.

CONCLUSIONS

Based on the foregoing investigation and analysis, within a reasonable degree of engineering certainty, the following is concluded:

1. Failure started with collapse of the channel support, wherein the welds at the end of the channel support failed by bend-induced fracture.
2. The most probable cause of the bending action attending the collapse of the channel support on pipe number 2 was mechanical shaking or vibration.
3. Complete disconnection of the U-bolt was a consequence not a cause of the pipe falling.
4. There was no degradation of the channel support or the welded connections. They were in good condition the day of the accident, and a visual inspection prior to this incident would not have revealed that any hazardous conditions existed in the support of the discharge pipe.

APPENDIX A

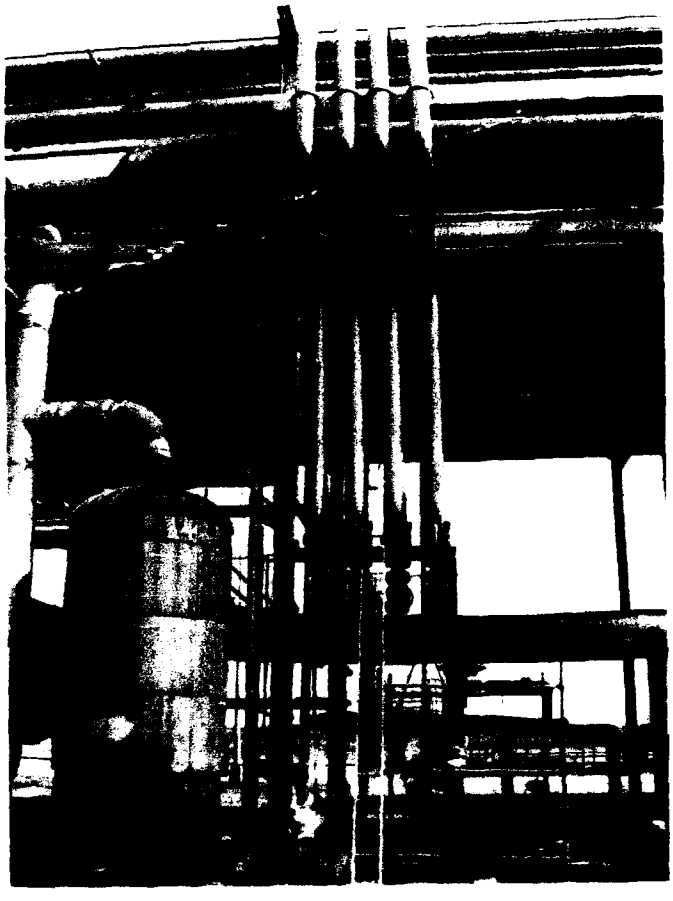

Photograph 1

View Looking East of the Four Discharge Pipes

APPENDIX A

Photograph 2

View Looking East of the Discharge Pipes and the Channel Supports

Figure 1: Elevation View of Discharge Pipe Assembly

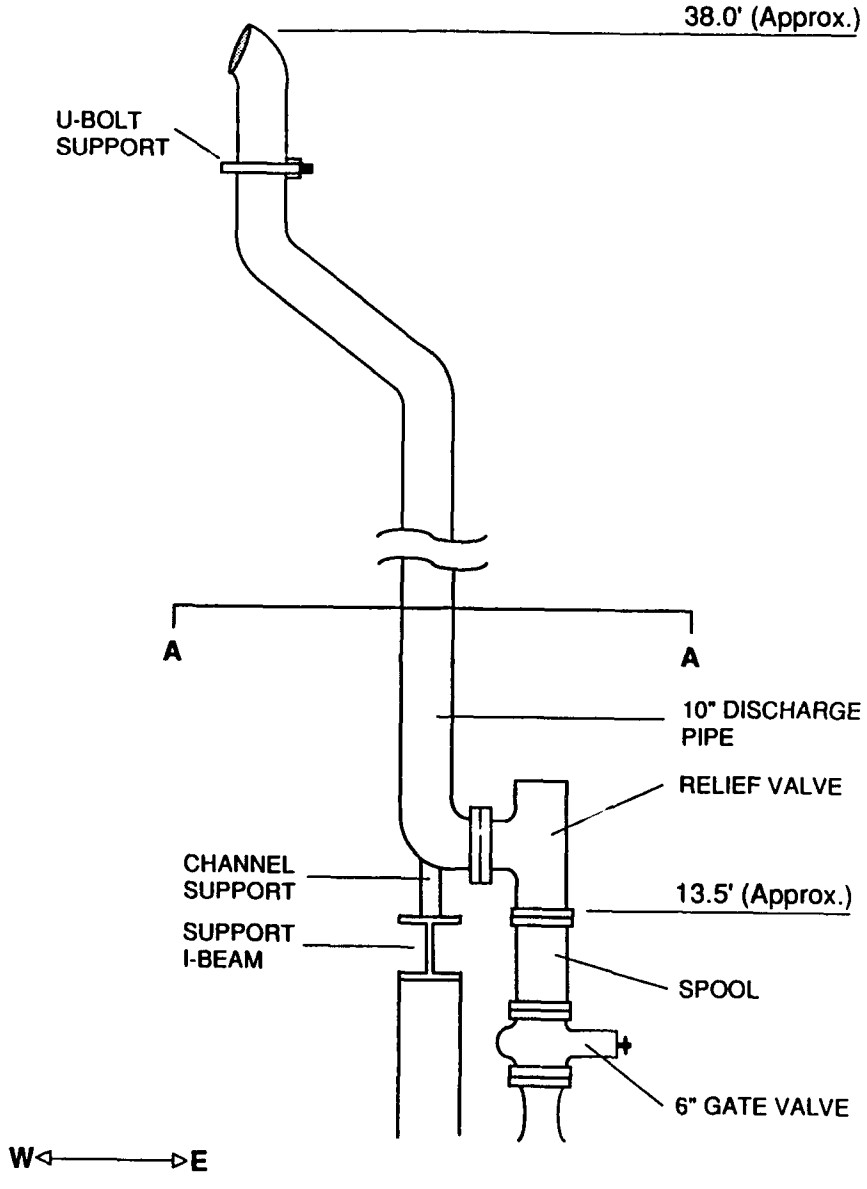

APPENDIX B

Figure 2: Top View of Discharge Pipe Assembly

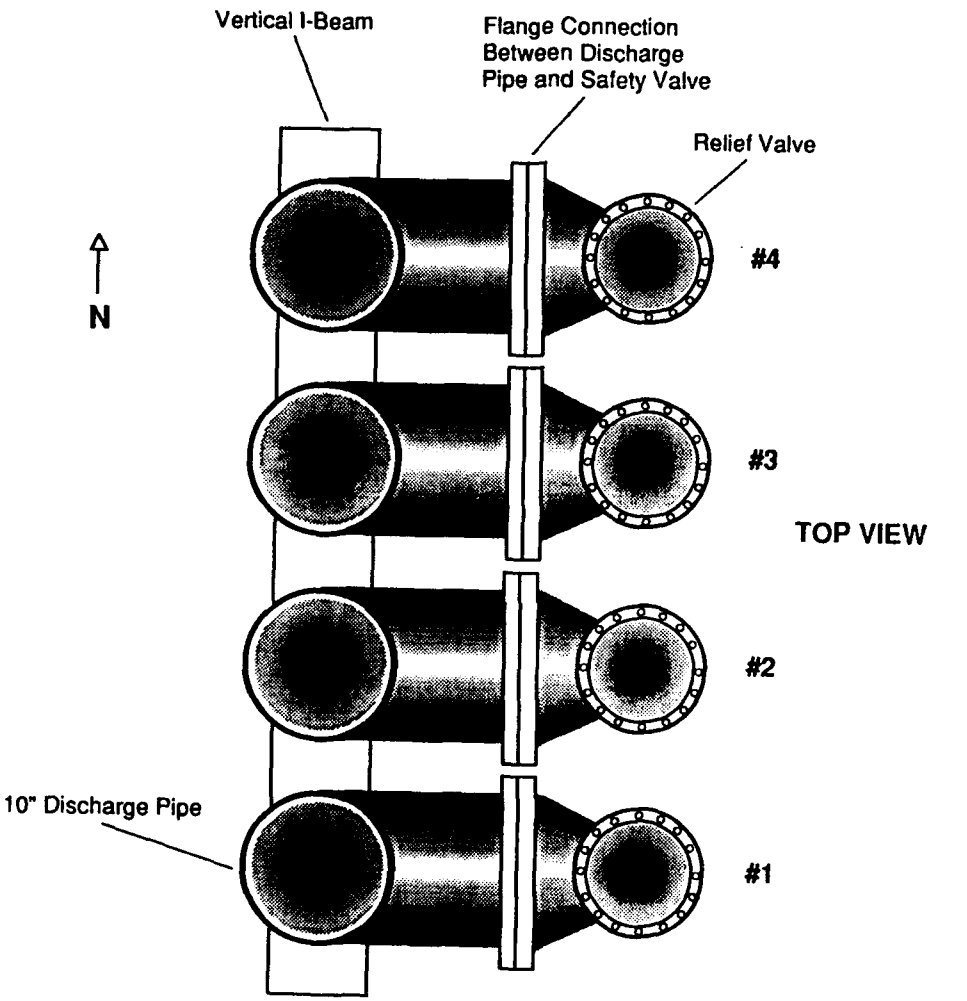

A-A

APPENDIX B

APPENDIX C: EQUATIONS OF MOTION

The collapse of the channel support is described by a relationship giving the time, "t", required for the channel support, initially vertical, to rotate to an angle, "B", from the vertical:

$$t = \sqrt{\frac{2L(1-\cos B)}{g}}$$

where L = Length of channel support
g = Gravitational constant (32.2 ft/sec^2)

If, for any reason, the U-bolt disconnects, the time, "t", required for the pipe to reach an angle, "A", from the vertical is given by:

$$t = \sqrt{\frac{2H}{3g}} \ln\left(\frac{\tan A/4}{\tan A_o/4}\right)$$

where H = Initial vertical length of the discharge pipe
A_o = Initial angle from vertical

Because of the "zig-zag" in the discharge pipe, it moves as if it had a starting tilt, "A_o", of about 10°.

DAMAGE TO ANTI-FRICTION AND SLIDE-BEARINGS WHEN SUBJECTED TO CURRENT

Karl Wolf*

David Taylor Research Center(DTRC)
Annapolis, MD, 21402

ABSTRACT

Damage attributed to electrical current was observed on roller- and slide-bearings taken from aircraft engine service. The damage associated with this effect of electrical crossing can be very critical in the proper operation of an aircraft engine. The bearings showed signs of electro-erosion and deposits of melted foreign material due to intermittent electrical contact. The characterization of this damage is unique just as the tribological damages of cohesive wear, fatigue spalling and corrosion are different. Microscopic evaluation revealed signs of fatigue fractures (spalling) associated with notches of various sizes caused by low and high heat inputs at short times. The morphology of the damage is presented and discussed using standard metallographic and electron microscope (SEM) techniques.

Keywords: **electro-erosion; roller-bearing; slide-bearing; spalling.**

INTRODUCTION

The basic idea of damage to roller-bearings due to electrical current (lightning) is that surface roughness serves to interrupt or break the metallic contact locally thereby increasing electrical current in other areas of the component. The increased electrical current serves to supply enough energy to melt highly localized areas. Solidification lines and craters are characteristic of the damage caused by electrical current over very short times. These surface defects are not easily observed optically under low magnification. The observation of this particular damage was extremely difficult early in the damage process because only very few particles from adhesive and/or abrasive wear could be detected. Only areas where damage was caused by higher electrical currents could be readily observed. Confusion occurs because morphology of the damage can be similar to that caused by other forms of wear. The aim of this investigation was metallographic and scanning electron microscopy (SEM) evaluation of bearing damage caused by electrical current to characterize the differences between similar damage morphologies.

* Exchange Materials Engineer in the Fatigue and Fracture Branch, DTRC, (Defence Scientific Institut for Material Testing-WIM, Erding/Germany).

Footnote: Submitted to the Mechanical Failures Prevention Group at the Symposium on Mechanical Failures: Mechanisms and Detection to be held in Annapolis, MD, April 9 - 11, 1991

MATERIALS

Bearings from different aircraft and construction groups were studied in this investigation. These include:

- one straight-bearing consisting of one outer-ring, two inner-rings and two of 30 cylindric rollers (designated "A").
- one straight-bearing with one outer-ring, one inner-ring, one separator and 12 cylindric rollers (designated "B").
- one straight-bearing with one outer-ring, one separator, 12 ball-rollers and two inner-rings (designated "C").
- one straight-bearing with one outer-ring, one separator and one ball-roller (designated "D").
- one straight-bearing with one outer-ring with broken off areas, one inner-ring and 16 cylindric rollers (designated "E").
- one straight-bearing (similar to "E") with one outer-ring, one inner-ring and 16 cylindric rollers (designated "F").
- one bevel-wheel-shaft with two journals for liners (designated "G").

For the described investigation it was not necessary to determine the chemical composition of the bearing units of all damaged components. From the different bearing identification markings and customer statements it was known that the single bearings were made of bearing-steel according to AISI E 52 100.

RESULTS

The straight-roller-bearing ("A"), shown in figure 1, showed the same damage at the outer-ring, inner-ring and the two cylindrical rollers. The damaged areas found on "A" were about one tenth of a millimeter, orientated in the direction of bearing rotation, and appear as striation lines. SEM-investigation show that the local and periodic damaged areas were craters formed from melting (figure 2).

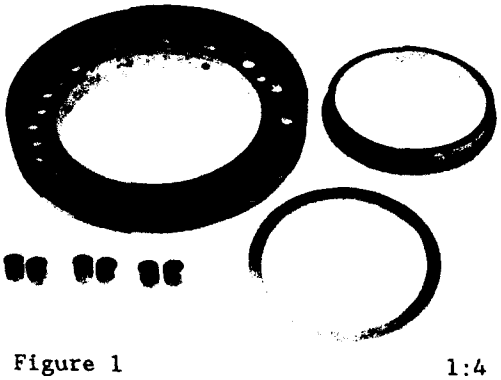

Figure 1 1:4
Photograph showing a damaged cylindrical-roller-bearing in addition to separate components;
a)outer-ring; b)inner-ring;
c)rollers.

Figure 2 140:1
SEM-image shows an area which was damaged by electrical current; crater formed from melting.

During the solidification process, the melted and/or plastic phase of the material was moved by over-rolling in the rotating direction. The rotating direction of the roller could be established locally from the orientation of the solidification lines. Additionally the rolled "tongues" observed on the bearings show the rolling direction. From these facts the time between the local melting and the solidification of the material was determined to be only a few milli-seconds. The surface structures which were the most severely damaged were a result of the combined forces of adhesive material and electro-erosion, as indicated by the craters, rolled on material, displacements, burnishes and deformations. X-ray energy dispersive (EDS) investigations showed that all the material on the affected surfaces came from the roller or ring material. The metallographic investigations of sections of rings and rollers of "A" were made along and across the running direction respectively, so that melted zones (melted craters) could be shown. Hardness measurements were conducted on a cross section of the ball-roller. The hardness measurements were performed by method HV 0.025 in order to differentiate the various parts of the structure of the damaged areas. The direction of measurement was perpendicular to the rolling direction of the roller (figure 3). About 0.025mm below the surface there was a hardness of 1180 HV 0.025 and at a depth of 0.075mm the hardness was 680 HV 0.025. The hardness of the straight-roller matrix was 63 HRC which exceeded the required 62 HRC. Figure 4 shows the structure across the damaged zone of a ball-bearing inner-ring.

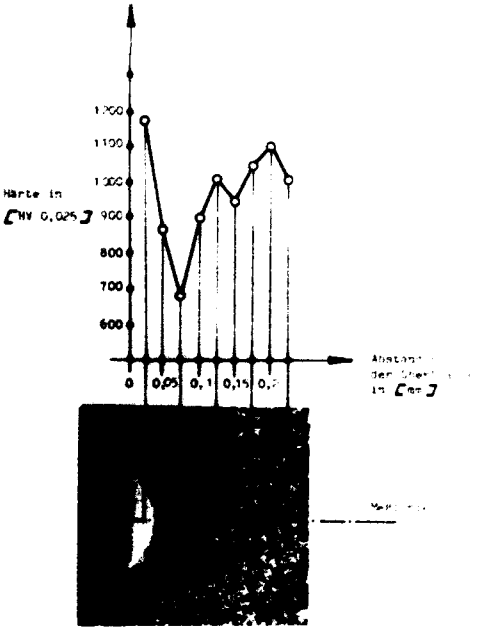

Figure 3
Transverse cross section of the microstructure from a cylindric-roller ("A") taken through a damaged area and the hardness traverse.

Figure 4 500:1
Transverse section from a ballbearing inner-ring ("C");
a)raceway
b)melted zone with retained austenite and untempered martensite
c)prior austenite and grain boundaries
d)matrix

The heat supplied into the bearing parts by electrical current caused microstructural changes which could be immediately recognized. The rapid cooling of the melted material caused a local martensitic solidification and a zone which was not possible to etch. The adjacent heat effected zone shows prior austenite grains which are clearly delineated. Both the different depths of the melted zones and the different structure development observed may have been caused by different high heat/energy-inputs combined with the surface finish. The straight-roller-bearing "B" and the ball-roller-bearing "C" (Figures 5, 6, 7 and 8) had the same appearance as described above for "A".

Figure 5 1:2.8
Damaged cylindrical-roller-bearing "B" and ball-bearing "C";
a)ball-bearing
b)cylindrical-roller-bearing

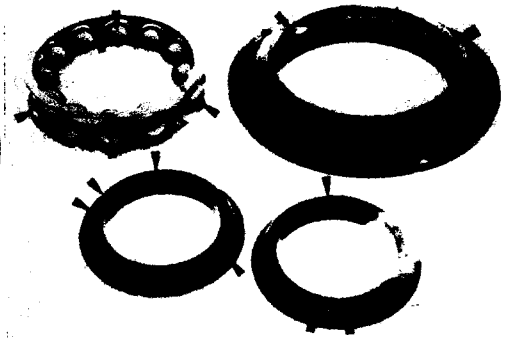

Figure 6 1:3.4
The disassembled ball-bearing "C" showing damaged zones on the outer-ring, inner-ring and balls.

Figure 7 100:1
SEM micrograph showing overrolled melted areas and craters which were found on the surface of the raceway "B".

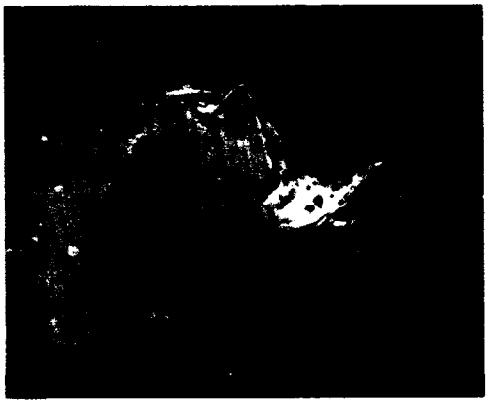

Figure 8 190:1
SEM micrograph showing a damaged area on the surface of a ball (bearing "C");
a)craters; b)solidification lines;
c)overrolled material

Bearing "D" was investigated both visually and with an optical microscope. Damages similar to those found previously were observed (Figures 9, 10, 11 and 12). With the help of a SEM it was possible to show that the damages (see Figures 13 and 14) were not caused by electrical current because the characteristics were totally different. The outer-ring, the separator and the ball were damaged at the surface by the influence of corrosion and secondary damages. Damages caused by adhesive-, cohesive- and tribo-corrosive wear and tear could be differentiated without confusion from damage caused by electro-erosion, in spite of the final condition of the surface following overrolling actions.

Figure 9 1:2.4
Photograph of straight-bearing "D"; outer-ring with damages in the marked zones.

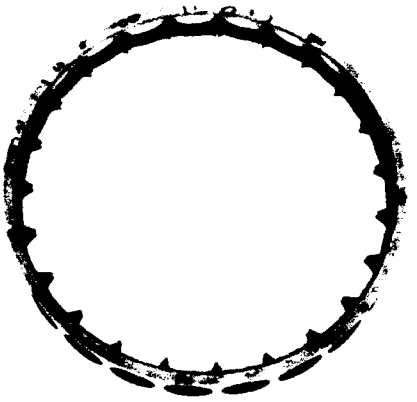

Figure 10 1:2.6
Photograph of the separator ("D") with the damaged zones marked.

Figure 11 2.5:1
Photograph of a damaged ball ("D") the damaged areas marked.

Figure 12 200:1
SE-image of the damaged outer- with ring ("D") which was typical of damages found on the bearing-seat and the race way.

Figure 13 300:1
SE-image of separator "D" showing circular damages on the face of the separator.

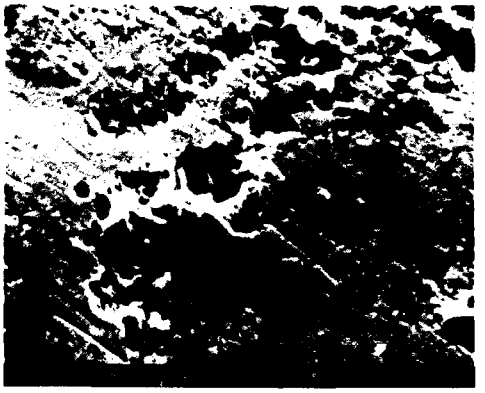

Figure 14 1 000:1
SEM micrograph showing damages on the surface of a ball ("D").

The straight-roller-bearing "E" was damaged at the outer-ring and showed areas along the face and the ball-race where material pieces had been broken off (Figures 15 and 16). The damaged ball-race areas had the same spacing as the rollers around the bearing.

Figure 15 1:2
General view of the cylindrical-roller-bearing "E" with broken pieces from the face of the outer-ring.

Figure 16 1:1
Detail from the outer-ring ("E"); race way with broken off areas within the distance between the rollers and the face.

Figure 17 5:1
Optical image of the bearing-seat (outer-ring "E") with the damaged areas showing features of melted zones.

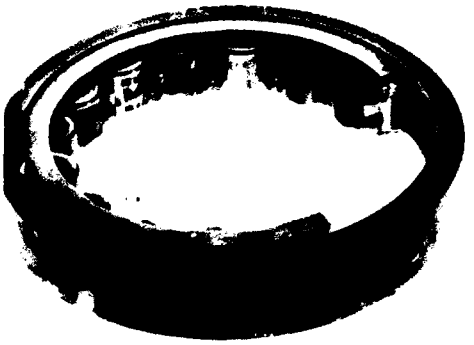

Figure 18 1:1.5
Damaged cylindrical-roller-bearing F" with melted zones on the bearing seat of the outer-ring.

On the outside of the outer-ring there were burned areas which suggested damage caused by current (Figure 17). The heavy damage at the face was caused by dynamic overloading which was due to the broken off pieces around the ballrace and shoulders. No explanation was found for the damage at the outside of the outer-ring.

The straight-roller-bearing "F" showed tracks of melted material at the outside of the outer-ring (Figure 18). The damaged area was large and clearly distinguished, similar to cases "A", "B" and "C" (Figures 19 and 20).

Figure 19 10:1
SEM-image showing melted areas(outer-ring "F") with material from the bearing and foreign material apparent-arrow.

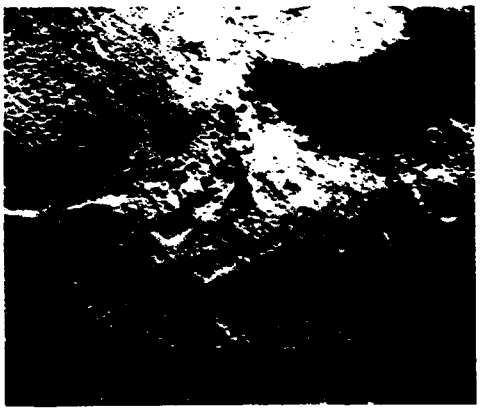

Figure 20 70:1
SE-image showing the melted material on the bearing-seat (outer-ring "F").

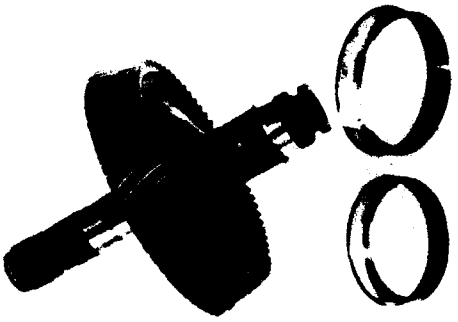

Figure 21 1:6
Bevel wheel-shaft and two liners ("G") with damaged areas on the bearing seat and the liners.

Figure 22 500:1
Transverse cross section through a liner;
a)untempered martensite

The rollers and the ball-race of the outer-ring and inner-ring were damaged by outbreaks, but not the bearing-seat. Within the melted material other bearing material and foreign material could be found. The origin of the foreign material could not be determined.

The bevel wheel-shaft and two liners, designated "G", also showed a changed surface. Visual features indicated that the damage occurred by electrical current (Figure 21). First, these machine components were etched to determine if there was untempered martensite and incident to it, electro-erosion. On the bearing-seat of the bevel wheel-shaft and on one liner there were no such indications. On the other liner there was evidence of untempered martensite (Figure 22). SEM investigations showed zones which were expected (see above) and corroborate the results given earlier.

CONCLUSION

The metallographic and microfracture investigation of electro-erosion on different anti-friction bearings and slide-bearings show the following conclusions:

The local changes in the surface of anti-friction and slide-bearings damaged by electro-erosion were not clearly visible. This damage could only be recognized with the help of an optical microscope and metallographic sections. SEM and EDS were required to fully define the characteristics of this type of damage. Electro-erosion in bearings can be recognized by the following indications: solidification lines, melted zones, material from adjoining parts and finally untempered martensite.

The different structures and depth of melted zones are indications of

variations in current and local metallic contact between the component parts. Confusion with other tribological damages (adhesive, cohesive and tribocorrosive wear and tear) seems to be possible in such cases in which the damaged areas are changed by overrolling processes.

SUMMARY

The importance of microfracture investigations to asses damage due to electro-erosion has been shown. Optical, SEM and EDS methods allow the causes of damage and its mechanism to be recognized. These methods are simple and easy to handle for such damages. Knowledge of this kind of damage is a basic necessity and ensures identification of this type of damage on components like these in future.

ACKNOWLEDGMENTS

This work has been supported by the David Taylor Research Center (DTRC), Annapolis, MD and Defence Scientific Institut for Material Testing (WIM), Erding, Germany. The author would like to thank Dr.M.E.Natishan (DTRC), M.Vassilaros (DTRC), J.Patton (DTRC) and Dr.G.Kohlhaas (WIM) for helpful discussions.

REFERENCES

1) Boyd,J., Kaufmann,H.N., The Causes and the Control of Electrical Current in Bearings, Lubrication Engineering, 1959.

2) Andre'son,S., Passage of Electrical Current Trough Rolling Bearings, The Ball Bearing Journal No.153, 1968.

3) Wallin,E., Vorbeugende Massnahmen gegen Stromschaeden in Waelzlagern, Kugellager-Zeitschrift 42(1967).

4) Allianz-Handbuch der Schadensverhuetung, VDI-Verlag 1984.

5) Unveroeffentlichte Berichte des WIM.

THE EFFECTS OF IMPROPER MANUFACTURING TECHNIQUES ON A TI 6-2-4-6 COMPRESSOR BLISK

Michael P Oliver
Materials Directorate
Wright Laboratory/MLSA
Wright-Patterson Air Force Base, Ohio 45433

Abstract: A failure analysis investigation was conducted on an axial compressor blisk for a gas turbine engine, made from Ti 6-2-4-6. The investigation was conducted to determine why eight blades, from a wheel which originally had thirty blades, catastrophically failed.

The investigation showed manufacturing induced anomalies either contributed to or caused cracks to form in all eight blades. The anomalies resulted from excessive dry grinding which created both a brittle oxide layer and work hardened the surface, deep abrasive marks which created stress risers, and dull cutting tool bits which tore the material instead of removing it.

Key Words: Abrasive marks; Air foil; Alpha case; Burning; cracks; Fatigue; Oxide; Surface roughness; Work hardened

Introduction: Prior to failure, the submitted blisk had compiled approximately 100 hours of operating time in rig testing. Following a warm-up period at 50 per cent operational speed for about 35 minutes, the rig vibrated excessively, after which a loud bang was produced.

Following removal of the blisk from the rig, it was discovered that the fracture surfaces of all eight separated blades contained evidence of fatigue. The crack initiation site for all eight separated blades was in the same location, on the suction side of the airfoil, located approximately at the midspan of the chord, and immediately above the root/airfoil transition point.

Analysis: Figure 1 is a photograph of the suction side of Blade No. 1 from the blisk. Point A in the photograph is where the crack originated. Subsequently, all fatigue striations emanate from this point. Evidence of material overload, covered by a thin oxide scale, was found at the crack initiation site on the fracture face. Note the presence of numerous scratches and abrasive marks on the surface of the blade and hub. Figure 2 is a scanning electron microscope (SEM) photograph of the crack initiation site on Blade No. 1. Region 1 is the side of the airfoil and Region 2 is the fracture surface. Point A is the crack initiation site. Point B in the figure depicts one of several abrasive marks on the side of the airfoil. This

particular scratch intersects the initiation point of the crack. Also note the sporadic presence of small particles on the side of the airfoil. An energy dispersive spectrometer (EDS) analysis by X-ray determined these particles to be composed of iron, copper, sulfur, potassium, and silicon. These elements, with the exception of iron, are foreign to the blade material. However, an EDS check of the fracture surface (which should be free from surface contamination) indicated no detectable amount of iron was present. The maximum level at which iron can exist in the Ti 6Al-2Sn-4Zr-6Mo material is 0.015 per cent. The source of the foreign particles on the surface of the blisk was not readily apparent. However, introduction during the manufacturing and/or processing procedures is a strong possibility. Contamination, due to handling of the submitted sample following failure, was ruled out due to the nature of cleaning of the sample prior to placement into the SEM (ultrasonically cleaned for half an hour in acetone).

Figure 3 shows a photograph of the blisk's hub, depicted by Area A, and root area, shown by Area B, of the blade. Note the abrasive markings and small nodules on the hub area. An EDS analysis indicated the nodules were composed of sodium, sulfur, chlorine, and calcium. These elements, once again, are foreign to the blisk's titanium material.

Figure 4 shows the fracture surface on Blade No. 2 from the failed blisk. Points 1 and 2 in the photograph depict areas were an oxide layer was present. The oxide layer was thicker at Point 2 than at Point 1. Point 1 is on the suction side of the airfoil and Point 2 is on the pressure side. Note that the oxide layer was almost non-existent in the middle of the blade, the area between Points 1 and 2. The location of Point 1 is almost identical to that of the crack initiation point of Blade No. 1. There were indications of abrasive marks at and near Point 1, much like that near Point A of Figure 2. However, no evidence of cyclic loading was found (evidence of cyclic loading might be present but the oxide layer was too thick for the SEM to penetrate in order to obtain an image). Figure 5 is a rotated representation of Point 2 from Figure 4 (photograph of the side of the airfoil). Note the coloration, shown by the arrows, on the airfoil in the middle of the photograph. This coloration was probably caused by excessive dry grinding which burned the surface of the airfoil, confirmed by the presence of the grinding marks in this area. Also, small foreign particles were found to exist in the cracks surrounding the burned area (arrows in Figure 6). An EDS analysis indicated these particles were composed of iron, calcium, sulfur, chromium, potassium, copper, phosphorus, silicon, and chlorine.

Blade No. 2 was subsequently cross-sectioned (near the location of the colored area, parallel to the longitudinal

direction of the airfoil), polished, and etched (etched with a 1 per cent HF solution). Figure 7 is a photomicrograph of an area on the pressure side of the airfoil, on the surface, located approximately halfway between the fracture face and the root transition zone of the airfoil. The dark area is the mounting material. Note the crack starting at the surface of the airfoil and propagating into the airfoil. Also note the coloration of the both the surface and subsurface material in the photo micrograph (shown by the arrows). This coloration is the same type as that seen Figure 5. Figure 8 shows a higher magnified photomicrograph of the surface of the airfoil, from Figure 7, where the initiation of the crack occurred. Note the blue coloration (darkening) and change in appearance of the matrix which surrounds the alpha and beta material near the surface of the airfoil. Point 1 in the figure depicts the depth at which the coloration occurred in the crack. The topography on the inner portion of the crack, shown by the arrows, only exits to the left of Point 1. As previously stated, the coloration of the material was induced by excessive grinding during manufacturing. This finding indicates the crack existed prior to the catastrophic failure of the blade which subsequently caused secondary cracking to occur (crack propagation to the right of Point 1). Also, Point 2 in the figure depicts a second crack. Figure 9 is a photomicrograph of an area closer to the fracture face of the airfoil (on the pressure side of the airfoil) than shown in Figures 7 and 8. Note the same type of coloration and cracking, evident in the previous figures, are present in this photomicrograph. The suction side of the airfoil was also examined. Coloration was also detected with the same type of cracking as shown previously; however, the coloration was not as severe as found on the pressure side of the airfoil.

A microhardness traverse, from the colored areas of the cross-sectioned blade, found hardness values that ranged from approximately 51 to 56 HRC. The base material was found to have a hardness of approximately 33 to 40 HRC. Microhardness measurements were also taken on several of the remaining submitted blades and were found to range from 33 to 37 HRC. The material specification, AMS 4981B, requires the hardness of the material to be between 33 HRC and 45 HRC.

The rationale for the increased hardness of the colored areas of the blade is two fold. First, the coloration of the matrix, as previously stated, was probably caused from excessive dry grinding. The grinding operation caused local heating to occur, which subsequently caused an oxide layer to be created. The oxide layer, or "alpha case", is an oxygen-enriched, alpha-stabilized surface which results from elevated temperature exposure in air. The alpha case is a hard, brittle layer, which is harder than the material

immediately beneath it. When the case is stressed, a crack will form, subsequently, the substrait will crack. Secondly, the surface of the material was probably work hardened, also due to the excessive grinding operation. The grinding operation would induce local high stress areas and would either remove material and redeposit it elsewhere (which would cause pitting) and/or change the local mechanical properties of the material. Removal of material is shown by the arrow in Figure 10. Figure 11 depicts an area were work hardening has probably taken place (no evidence of burning was found). The arrow depicts a crack in the middle of the micrograph, on the surface of the material.

Four other failed blades were examined and were found to contain the same type of surface anomalies, near the crack initiation sites, as the two blades previously discussed. The location of these initiation sites matched those found on the previously examined blades, i.e., on the suction side of the airfoil. Also, EDS analysis showed the same type surface contamination found on the other blades examined.

Surface roughness measurements of the airfoil, root, and hub of several of the blades were taken. The average surface roughness for the hub, root, and airfoil were 48 x 10^{-6} inches, 34 x 10^{-6} inches, and 64 x 10^{-6} inches, respectively. Manufacturing specifications state the surface shall have a surface roughness no greater than 32 X 10^{-6} inches. The surface finish on all three areas of the blade examined surpassed this maximum. Also, the blade, which was cross-sectioned, was found to contain several scratches approximately 390 X 10^{-6} inches deep.

Conclusions: The crack initiation site for all eight of the failed blades was located on the suction side of the airfoil, immediately above the root transition zone. The cracks in each of the eight blades initiated by some type of overload mechanism (tensile, shearing, and a combination of the two) and propagated via fatigue.

There were deep scratches and abrasive marks on the hub, root, and airfoil of all submitted samples. On all failed blades examined, the abrasive marks and scratches existed at the point were the cracks had initiated. These surface anomalies acted as stress risers, existing in an area which is inherently highly stressed, which will promote crack initiation when loaded. The mechanism causing crack initiation could possibly be linked to manufacturing and/or loading during operation (i.e., vibration).

One of the failed blades contained a burned area which was caused from excessive grinding. The location of this burned area was on the pressure side of the blade, and immediately

area showed the existence of an oxide layer, "alpha case", and work hardened areas located on and around the surface of the burned area. Also, both the suction and pressure sides of the airfoil of this blade displayed evidence of material removal and smearing. All of which could be caused from excessive grinding operations or a dull tool bit.

Foreign particles consisting of sulfur, iron, silicon, potassium, calcium, chlorine, and sodium where found to be deposited on the surface of all blades examined. Particles rich in iron and silicon were also found imbedded in many of the scratches on the blades. The blade, which had burned areas contained particles consisting of iron and silicon which leads to the conclusion they were introduced during the manufacturing/processing operation. These foreign particles did not cause or contribute to the failure of the blisk; however, their presence may or may not pose a problem as more hours are placed on the blisk, providing the same manufacturing process is used on subsequent parts.

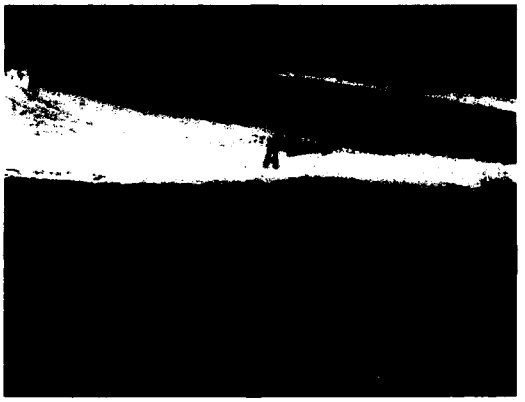

1. Photograph of the suction side of Blade No. 1. Point A depicts the crack initiation site.

2. SEM photograph of the crack initiation site of Blade No. 1. Region 1 is the surface of the airfoil and Region 2 is the fracture face. Area B depicts a scratch which intersects with the fracture surface at Area A.

3. Photograph of the hub, shown by Area A, and the root, shown by Area B of the suction side of Blade No. 1. Mag 60X

4. Photograph of the fracture face from Blade No. 2. Points 1 (suction side) and 2 (pressure side) depict crack initiation sites. Mag 20X

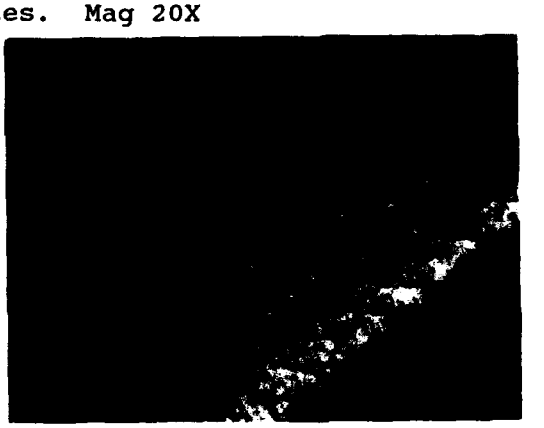

5. Photograph of Point 2 from Figure 4. Note the coloration in the center of the photograph.

6. SEM photograph of the colored region from Figure 5. Mag 300X

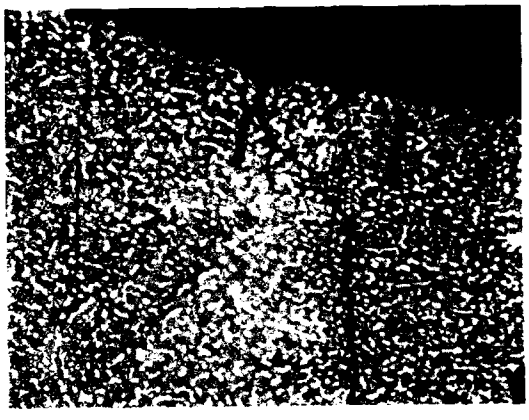

7. Photomicrograph of the cross-section of the colored area of Figure 5. Note the existence of the crack which originated at the surface of the airfoil. The arrows depict the colorization found. One per cent HF etch. Mag 250X

8. Close-up photomicrograph of the region where the crack and the surface coincide. Point 1 depicts the depth of the burning or coloration, Point 2 depicts a second crack found, the arrows show the burning inside the crack. One per cent HF etch. Mag 1000X

9. Photomicrograph of an area closer to the fracture face than those depicted by Figures 7 and 8. Note the presence of the crack and coloration (shown by the arrows). One per cent HF etch. Mag 1000X

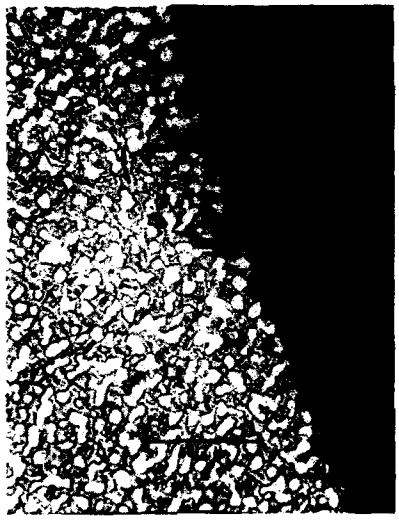

10. Photomicrograph of an area on the suction side of the airfoil of Blade No. 1. Note the presence of a crack and a separated particle, shown by the arrow, in the figure. One per cent HF etch. Mag 500X

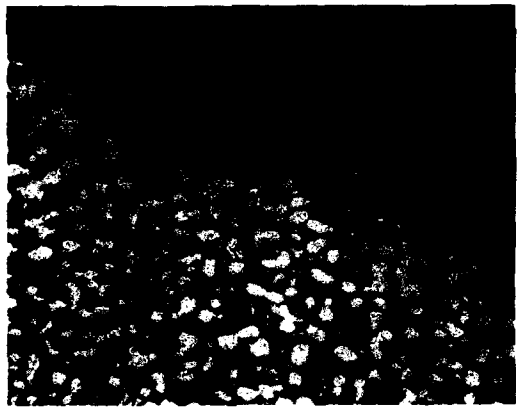

11. Photomicrograph of the root area from Blade No. 2, on the pressure side of the blade, where apparent work hardening had taken place. Note the crack on the surface shown by the arrow. Mag 615X

DIAGNOSING FUNCTIONAL PROBLEMS IN RECIPROCATING MACHINERY

Chairman: Reginald G. Mitchiner
Virginia Polytechnic Institute and State University

Cylinder Stretch as a Source of Vibration in Reciprocating Compressors

Brian C. Howes, M.Sc., P.Eng.
Kelly N. Eberle, B.Sc.
Val Zacharias, M.A.

Beta Machinery Analysis Ltd., Beta Monitors & Controls Ltd.
300, 1615-10th Avenue S.W.
Calgary, Alberta, Canada
T3C 0J7

Abstract

Vibration problems on reciprocating compressor pulsation dampeners and piping systems have several causes, such as pressure pulsation induced unbalanced forces, and forces and moments from the reciprocating and rotating components in the machine. However, an additional cause of vibration problems on the vessels and piping in close proximity to a compressor cylinder is cylinder stretch, that is, the elongation of the cylinder assembly, due to the gas forces generated by the internal pressures in the compressor cylinder. Case histories are presented which illustrate observed vibration problems due to cylinder stretch excitation and the solutions implemented to reduce vibrations.

Keywords

Compressor vibration; cylinder motion; cylinder stretch; design guidelines; modelling of compressors; vibration; reciprocating compressors.

Introduction

Twenty-five years of vibration trouble-shooting of reciprocating compressors, together with the analysis of almost 500 compressor installations at the design stage, has shown that conventional analyses of reciprocating compressors in the design stage are not always sufficient. While many potential problems are prevented, others may appear. For example, a phenomenon called cylinder stretch often causes excessive vibration. This paper analyzes cylinder stretch and provides case histories which illustrate it. Field measurements and modelling predictions are compared, and solutions are provided.

Vibration of vessels and piping attached to reciprocating compressor cylinders often results in high stress levels in the vessels and piping. If high enough, these stress levels will lead to failure. The cost of such failures can be significant, not only in terms of repair costs but also in safety and lost production time. Therefore, it is important to understand the sources of vibration in the design of the piping systems.

Description of Problem

General Definitions

The terms and examples given here refer to reciprocating compressors used in natural gas production but can generally be applied to any reciprocating machinery application. Shown in Figure 1 is a schematic drawing of a typical reciprocating compressor in a section view. The typical elements include the compressor frame, crosshead and crosshead guide, distance piece, piston, and cylinder. The cylinder, crosshead guide and distance piece will be referred to collectively as the cylinder assembly. The compressor cylinder is designed to be double acting, that is, it can compress gas on both the head or outer end and crank or frame end of the cylinder. Changing the loading of the cylinder is usually accomplished by increasing the clearance volume at the head end of the cylinder, or by removing valves from the cylinder. Attached to the top and bottom of cylinder are the suction and discharge pressure pulsation dampeners.

The direction of vibration is described as either horizontal, axial, or vertical, with respect to the compressor. A horizontal vibration refers to vibration in the direction of piston motion. The axial direction is parallel to the centre line of the compressor crankshaft.

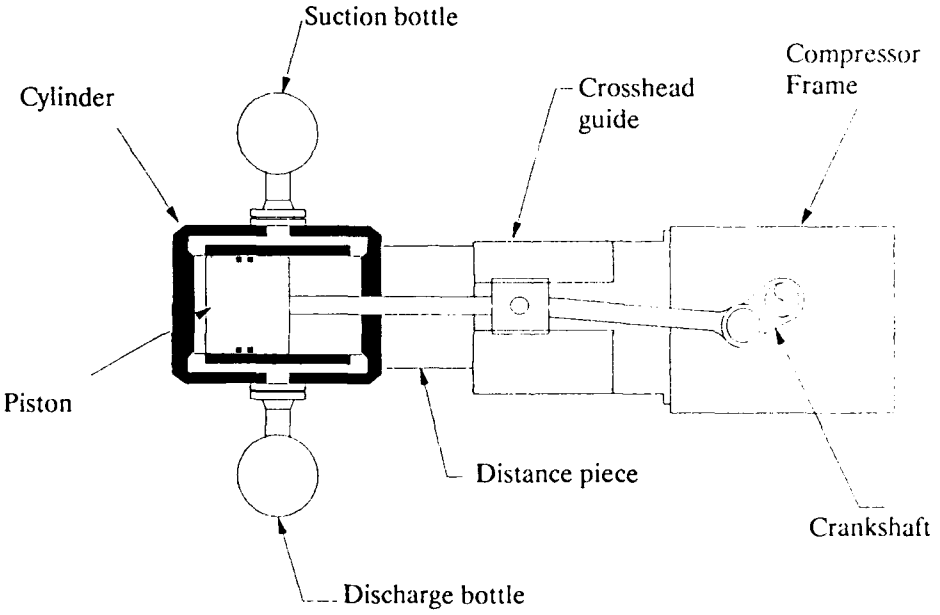

Figure 1. Section view, typical reciprocating compressor.

Definition of Cylinder Stretch

Cylinder stretch refers to cylinder motion in the horizontal direction. This motion is generated by the pressures inside the compressor cylinder. During each stroke of the piston, gas is compressed on first the head end and then the crank end of the piston. A corresponding pressure also acts on the cylinder during each stroke. This

pressure results in an alternating force acting on the compressor cylinder. These forces cause the cylinder assembly to lengthen and shorten during each stroke. This lengthening and shortening is referred to as cylinder stretch. Refer to Figures 2 and 3 for typical plots of cylinder pressure and rod load versus crank angle.

Cylinder stretch results in vibration of the piping system, which is analogous to vibration of a building due to an earthquake. A single vibration source, in this case at the connection of the pulsation dampener to the cylinder, results in vibration of the attached vessels and piping. When the magnitude of the source vibration is high enough, or the frequency of the source vibration is equal to the resonant frequency of the attached piping, excessive vibration results and failures can occur. Reducing the vibration levels involves reducing the strength of the vibration source, which is often difficult, or changing the piping system or its support to reduce the response.

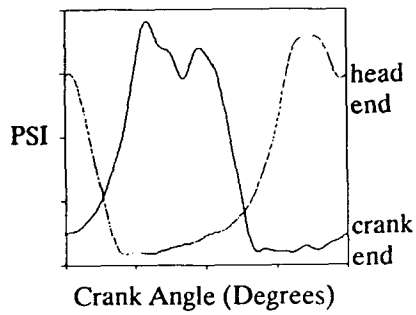

Figure 2. Cylinder pressure versus crank angle.

Axial and vertical vibrations of the cylinder can also result in failures of the attached vessels and piping. These are different problems and will not be considered in this discussion.

Note that cylinder stretch is inherent in the compressor. Steps can be taken to minimize the cylinder stretch in the compressor design or the loading of the cylinders. However, cylinder stretch and its resultant vibration will always be present to some extent. Therefore, it is prudent to analyze the response of the attached vessels and piping to this source of vibration when designing the installation.

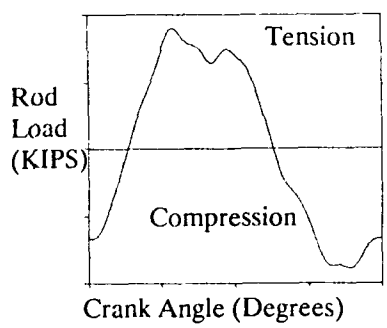

Figure 3. Rod load versus crank angle.

Associated Spectra

Force Spectrum of Gas Rod Load

A typical spectrum of the gas rod load forces, as taken from the rod load versus crank angle plot given in Figure 3, is shown in Figure 4. Note that the highest forces are typically below 7 or 8 times compressor run speed. The force level after the 8th order of run speed is generally very low. However, the magnitude of the gas forces

at high frequencies can be affected by valve plate resonances, which can cause pressure oscillations which can result in higher than normal gas forces.

Cylinder Stretch Spectrum
A typical spectrum of the cylinder stretch or cylinder vibration in the horizontal direction is given in Figure 4. The magnitude of the cylinder stretch generally follows the force spectrum. The highest cylinder stretch occurs at frequencies up to 7 or 8 times compressor run speed in this example.

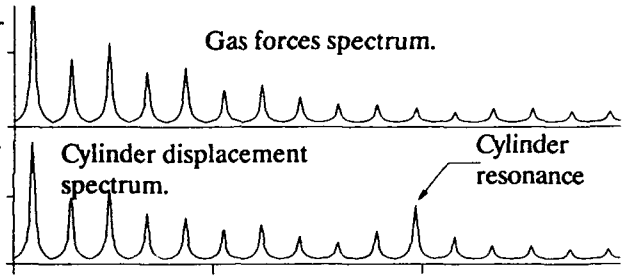

Figure 4. Gas forces and cylinder stretch vs frequency.

Note that at 11 X run speed, cylinder displacement is much higher than at adjacent harmonics, even though the corresponding cylinder gas force is no different. This higher response indicates the mechanical natural frequency of the cylinder assembly in the horizontal direction.

Mechanical Design Guidelines

Conventional Guidelines

A conventional guideline states that mechanical natural frequencies of piping and vessels near the compressor must be above twice maximum compressor run speed. The purpose of this guideline is to avoid resonance of these mechanical natural frequencies with the shaking forces at one and two times run speed. This is a necessary *but insufficient* guideline.

Expanded Guidelines

Analyze Higher Harmonics
Since considerable vibration can be generated above the second harmonic, both from cylinder stretch (as shown in Figure 4) and from pulsation induced unbalanced forces, analysis at the design stage must include frequencies above twice compressor speed.

Analyze Phasing Effects on Multi-Cylinder Dampeners
When a pulsation dampener is attached to two or more cylinders, the phasing between the throws of the crankshaft will cause the two cylinder stretches to vectorially add, depending upon the order of compressor speed.

Consider the example of a compressor which has two cylinders and a common pulsation dampener. If the phasing between the throws is 90 degrees, the cylinder stretch forces will also be 90 degrees apart at one times compressor run speed. However, the phasing between the cylinder vibration will be 180 degrees at two times run speed, 270 at 3 times, 360 or 0 at 4 times and so on. High vibrations can result at a

mechanical natural frequency above twice run speed, if the piping vibration mode is susceptible to a cylinder stretch phasing of 0, 90, or 180 degrees.

Analyze Response at All Operating Conditions

Cylinder loading affects cylinder stretch. Changing from double acting to single acting will tend to increase cylinder stretch at odd integers of run speed and decrease cylinder stretch at even integers. In the single-acting case, having a mechanical natural frequency at 3 times compressor run speed may result in excessive vibration, whereas a mechanical natural frequency at 4 times would be acceptable. In general, the double-acting case is easier to solve than the single-acting one.

Typical Solutions To Cylinder Stretch Problems

Altering Cylinder Loading

One solution to cylinder stretch vibration problems is to load the cylinder so as to minimize the cylinder gas forces, or for multiple cylinder cases, the vector sum of the gas forces. This approach is not always practical since specific operating conditions are often required.

Changing The System Mechanical Natural Frequencies

Piping vibrations are typically found to be highest at mechanical natural frequencies of the piping system. Vibration can be reduced by shifting the mechanical natural frequency to a frequency where the cylinder stretch is less. In the case of multiple cylinder pulsation dampeners, shifting the mechanical natural frequency to an order of run speed with different phasing can reduce vibrations.

The mechanical natural frequency of the system can be altered by changing the mass, mass distribution, or stiffness of the system. The mass of the system is increased by adding a weight to the piping or vessels. Distribution of the mass can be changed by moving a flange set located at the top of a pipe riser down to the level of a support. Stiffness can be changed by adding or removing braces or supports, or by changing pipe diameters. The mechanical natural frequency can also be changed by altering the pipe or vessel layout. These changes are least expensive in the design stage.

Increasing The System Damping

Vibration at resonance can be reduced by increasing the system damping. Methods of increasing damping include installing shock absorbers or using a constrained layer damping treatment [1,2]. Designing and installing these damping devices is often difficult and costly. Maintenance is required because of degradation due to normal wear and operation in harsh environments.

Modify The System Mode Shape

The mode shape of a structure is defined as the displaced shape of the structure as it vibrates. Each natural frequency has a distinct mode shape. Each mode shape consists of at least one point with no movement, referred to as a node point, and at least one point with maximum movement, referred to as an antinode.

Consider the example of a cantilever beam vibrating at its second mechanical

natural frequency (or second mode) as shown in Figure 5. Points A and C represent antinodes on the mode shape and point B represents the node of the mode shape. (Refer to Thomson[2] or Henderson[1] for a further definition of these terms.)

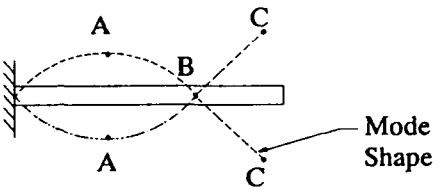

Fiure 5. Vibration on a cantilever beam.

Moving the node point of the mode shape closer to the source of the vibration results in reduced vibrations, since force on the node point does not excite vibration in that mode.
Changing the mass and/or stiffness of the system is required to change the mode shape.

Additional Considerations In Cylinder Stretch Problem Solutions

Any solutions must be considered not only for their effect on cylinder stretch vibration, but also for their effect on the system response to other vibration sources. For example, lowering a mechanical natural frequency out of the range of 3 times run speed to avoid a cylinder stretch vibration may create a new vibration problem due to high residual unbalanced moments from the compressor at two times run speed.

Case Histories

Method

In the first case history, two models were analyzed. These included:

- a digital computer model of the acoustical pulsations and the resultant unbalanced forces, and
- a finite element model of each system.

Each model included the suction piping, suction bottle and compressor cylinder. In the second case, an acoustical model was not required because the direction of vibration precluded pulsation induced unbalanced forces.

The cylinder gas forces were calculated for the compressor operating conditions and used in the model to predict the response due to cylinder stretch. The modal damping used in the finite element model was determined from field measurements.

Case 1: Cylinder Stretch Vibration in a One Cylinder Bottle

Background

The system consists of a motor driven 4 throw, 3 stage separable reciprocating compressor. The compressor operates in natural gas service with typical suction and final discharge pressures of 110 and 1140 psig. The operating speed range was 650 to 900 RPM. Both the second and third stage suction bottle were attached to one cylinder on the same side of the compressor. Phasing between the two cylinders was

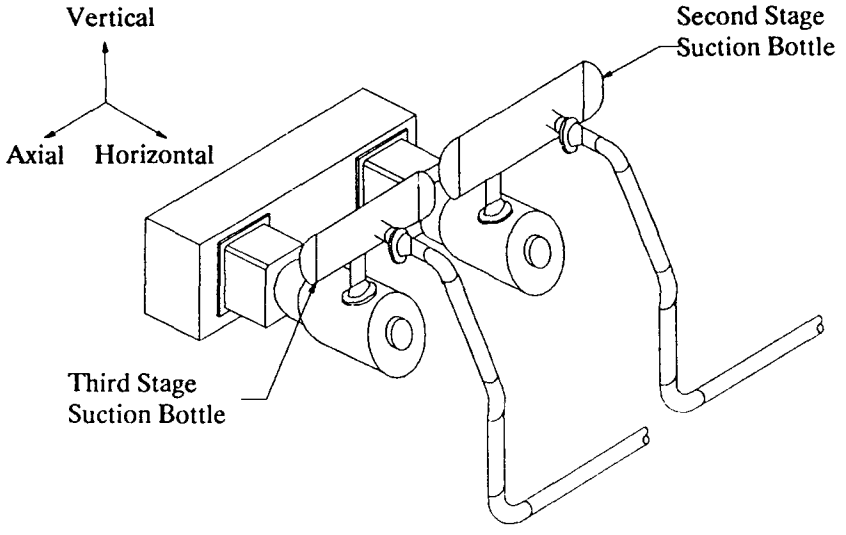

Figure 6. Compressor layout, Case 1.

90 degrees at one times compressor run speed. The operator noted high vibration on the second and third stage suction bottles and on the suction piping into the bottle. See Figure 6 for sketch of system.

Field Measurement

Maximum vibrations measured on the second stage suction bottle were 7 mil p-p at 41.6 Hz and 12 mil p-p at 52.0 Hz. The third stage suction bottle and piping had maximum vibration of 12 mil p-p at 38.4 Hz and 6.5 mil p-p at 55.2 Hz. Pressure pulsations recorded at several locations were within guidelines.

Analysis

The pipe and bottle vibration was attributed to cylinder stretch, based on the vibration mode shape and magnitude of the cylinder gas forces. Low system damping was a contributing factor.

Mechanical natural frequencies of 42.7 Hz and 50.0 Hz were predicted for the second stage system and 35.0 Hz and 53.4 Hz for the third stage system. Vibration levels of 7.3 mil p-p at 42.7 Hz and 11.2 mil p-p at 50 Hz were predicted for the second stage system and 10.8 mil p-p at 35.0 Hz and 6.2 mil p-p at 53.4 Hz for the third stage system.

These predictions agreed closely with the measured vibrations.

Several modifications were analyzed to determine a method of reducing the vibration. These modifications included

- increasing the stiffness of the cylinder nozzles
- changing the pipe layout

- adding bracing to the piping
- clamping the ends of the two suction bottles together, and
- redesigning the bottle and pipe layout.

After consulting the compressor operator, recommendations were agreed upon which predicted the reduction of vibrations to guidelines. The final modifications included:

- stiffening the cylinder nozzle on the second stage suction bottle
- bracing the second and third stage suction risers, and
- clamping the ends of the suction bottles together.

Clamping the suction bottles together was done by installing a flat bar clamp around each bottle and bolting braces between tabs on each of the clamps. Damping material was installed between the clamp and shell of each bottle to prevent wear on the shell as well as to add damping to the system.

Results

After the modifications had been installed, vibration on the second and third stage suction bottle and piping was acceptable.

Conducting a cylinder stretch analysis in the design stage would have predicted these vibration problems. Changes in the bottle design and system layout could have been implemented at that time. The repair cost, and the use of braces which limit access, would thus have been avoided.

Case 2: Cylinder Stretch Vibration in a Three Cylinder Bottle

Background

The system consists of a motor driven 6 throw, 2 stage separable reciprocating compressor. The compressor operates in natural gas service with typical suction and final discharge pressures of 200 and 850 psig. The operating speed range is 600 to 900 RPM. The second stage suction bottle is common to three cylinders on one side of the compressor. Phasing between cylinders 2, 4, and 6 is 0, 120, and 240 degrees at one times compressor run speed. See Figure 7.

The operator was concerned with high vibration on the second stage suction bottle and the suction piping into the bottle.

Field Measurement

Maximum vibration of 5.0 in/s pk at 42.5 Hz was recorded on the inlet nozzle into the suction bottle in the horizontal direction. Mechanical natural frequencies of the bottle and the riser into the bottle in the horizontal direction were found to be 42.5 Hz and 69.3 Hz . The 42.5 Hz mode shape was a translation mode of the bottle and suction piping in the horizontal direction. Pressure pulsations recorded at several location were within guidelines.

Analysis

Cylinder stretch was suspected to be the cause of the pipe and bottle vibration, based on the vibration mode shape and the phasing of the cylinders. The horizontal translation mode of the bottle and piping was particularly susceptible to cylinder stretch since all 3 cylinders are in-phase at 3 times compressor run speed.

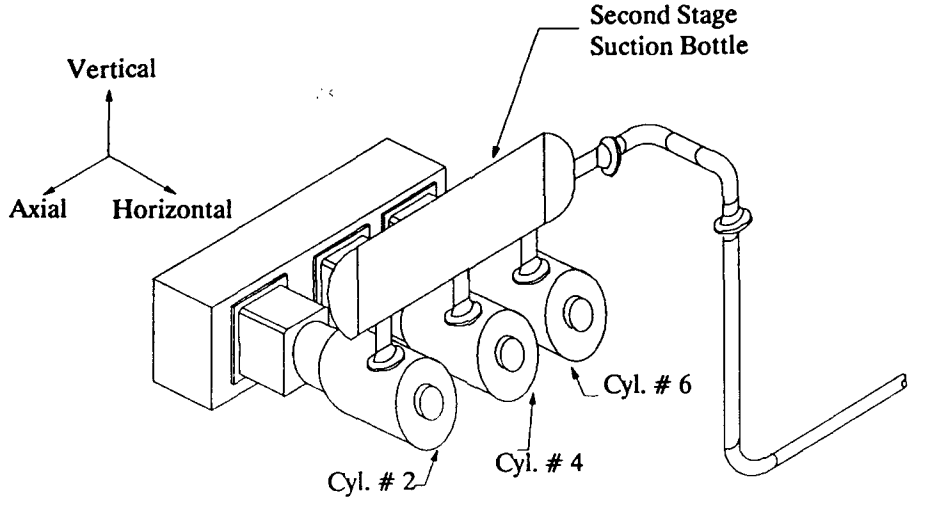

Figure 7. Compressor layout, Case 2.

Mechanical natural frequencies of 42.1 Hz and 71.8 Hz were predicted by the model. Maximum vibration of 4.3 in/s pk at 42.1 Hz was predicted on the suction bottle inlet nozzle due to cylinder stretch. These predictions agreed closely with the as-found vibrations and mechanical natural frequencies.

Several modifications were analyzed to determine a method of reducing the vibration. These modifications included:

- adding bracing to the piping and
- changing the pipe layout between the suction bottle and scrubber.

The one change which both reduced the vibration to acceptable levels and met the requirements of the compressor operator was changing the pipe layout between the suction bottle and scrubber. Maximum vibration of 0.8 in/s pk at 64.3 Hz was predicted for this new layout.

Results

After the new pipe spool piece was installed, maximum vibration of 0.7 in/s pk at 63.0 Hz was recorded. The measured vibration compares closely to predicted levels.

Analysis of the cylinder stretch response in the design stage would have indicated this vibration problem.

Conclusions

Cylinder stretch may generate vibration problems in the piping and vessels attached to reciprocating compressor cylinders. These problems can be avoided in the design stage by modelling the forced response of the piping due to cylinder stretch. This analysis must include frequencies above two times run speed.

This analysis may also benefit other reciprocating machines, such as Diesel engines and pumps.

References

1. Henderson, J.P., Jones, D.I., Nashif, A.D. Vibration Damping. New York, John Wiley and Sons, 1985.

2. Thomson, W.T. Theory of Vibration with Applications, 2nd Edition. Englewood Cliffs, New Jersey, Prentice-Hall Inc., 1971.

RECOVERY OF COMBUSTION PRESSURE FROM DIESEL ENGINE VIBRATION

David L. Bowen
RH Lyon Corp
691 Concord Ave.
Cambridge, MA 02138

Abstract: Transient events in machines can often be associated with source signatures that can be used for machinery diagnostics and control. Unfortunately, the direct monitoring of such signals, occurring deep within a machine, is often impractical. For example, in an engine such transients could include cylinder combustion and fuel injector pump pressures, and forces due to valve impacts and piston slap. The vibration signals that these transients produce are more easily measured, since they are usually accessible on the exterior of the machine. However, they are usually more complicated than the source signatures, due to complex transmission paths and the broad frequency content characteristic of transients. Because transmission characteristics can vary from one copy of a machine to another, signal processing procedures for recovering a source signature (or facsimile thereof) must take into account this variability, as well as the complexity of the vibration transfer function. In this paper we describe a robust procedure for recovering a diagnostic signal related to combustion, based on cepstral windowing and inverse filtering. The application of the procedure to large and small diesel engines, where we wish to recover cylinder pressure from block vibration, is discussed in some detail.

Key Words: Cepstrum; combustion; diagnostics; diesel; faults; inverse filtering; smoothing; transfer function; transients; vibration; windowing

Introduction: The condition or operational monitoring of machinery requires that we detect a signal related to the event of interest and identify features that reveal information about that event. Many commercial monitoring systems for rotating machinery are based on analysis of the signal power spectrum, and events are identified by the frequencies of line components in the spectrum. Conditions of imbalance or misalignment will produce identifiable frequencies that allow quick evidence of a developing problem.

Impact or transient events that occur in machines may also be periodic. Piston slap in a diesel engine for example occurs cyclically, as do gear-tooth contacts and bearing race or ball defect impacts. Because these forces are abrupt, their frequency spectra occur over a wide range and spectral methods may fail because the desired data are masked by other sources. To assist in recovering such signals, one may use a resonant transducer tuned to some high frequency, or a resonance of the structure itself.

There are many situations, however, in which we want more information about the transient event. First, it may not be periodic, and methods based on many averages over a pre-set period may not be suitable.

Second, we may want a time waveform of the force, pressure, or motion that is intimately associated with the event in question. If a disturbance occurs deep within a machine and generates energy over a broad frequency range, then structural wave dispersion and reverberation change the source waveform as it propagates to a conveniently located sensor. Recovering such a waveform from the signal obtained at this sensor requires that we separate the vibration pulses by a combination of temporal windowing and dereverberation. Spatial separation is achieved somewhat in larger engines by the natural isolation provided by the segmented structure of such engines. The more monolithic construction of smaller engines (e.g., automotive diesels) means a more uniform amplitude of vibration throughout the structure, and more emphasis must be placed on temporal separation of the vibration pulses.

In the following sections, a procedure for recovering the important parameters of event amplitude and timing will be described. We will illustrate its use with examples drawn from our application of the method to combustion pressure recovery in diesel engines.

Waveform Reconstruction: Most of the transient events in an engine have potential diagnostic value. Examples include impacts such as piston slap, valve and valve seat collisions, cam-follower interaction, and the sudden change in the rate of force onset caused by combustion. Some of these sources may be broadband enough to excite the machine structure over a wide range of frequencies, with the response consequently involving a large number of structural modes. The resonant response of these modes will extend the vibration signal in time, and the resonances will cause fluctuations in the frequency response (see, for example, the cylinder pressure and vibration data displayed in Fig. 6). It is the objective of waveform reconstruction to "undo" these propagation path effects, leaving us with a signal more closely tied to the source of vibration. A vibration transfer function, determined during a "calibration phase," can be employed for this purpose.

In this work, we are interested in recovering the combustion pressure waveform from part of the vibration signal measured on the engine exterior. Since an engine is a complex machine with many mechanisms, there exist vibration contributions from many sources other than combustion. Some of these may occur near the times of combustion (although in a diesel, vibration due to combustion is usually the strongest), some may occur sporadically, and some occur well away from the times of combustion. In order to "screen" the raw vibration data from a particular sensor, we have found it useful to display several complete engine cycles in waterfall fashion, after first performing a short-term RMS moving average on the data. For example, Fig. 1 shows such a display obtained from acceleration measured on a large diesel under light and heavy loading. From this display, we see that events seem to "stand out" better under the lighter loading condition.

With the aid of a timing or other suitable signal that indicates TDC ("top-dead-center") of a known cylinder, an ensemble of cylinder pressure and casing vibration signals can be collected. From this ensemble, a vibration transfer function from pressure to vibration can be calculated after windowing out that portion of the response not related to combustion.

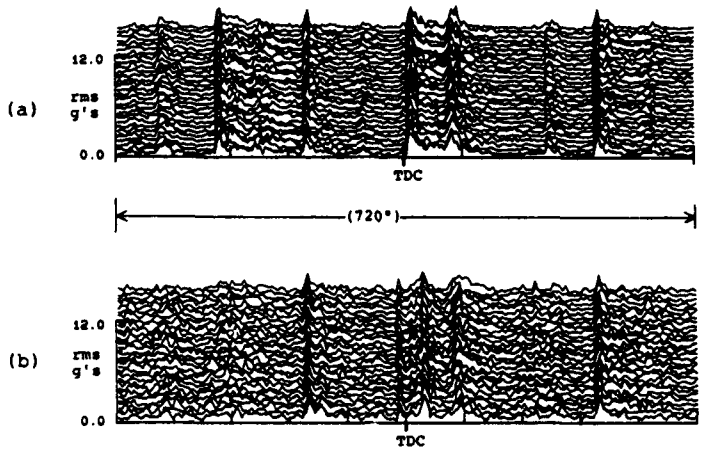

Fig. 1: Short-term rms plots from 30 cycles of vibration measured on 12-cylinder engine (TDC of cylinder nearest to sensor denoted); (a) idle, (b) turbocharged.

In our work we have found that a short, tapered window such as a Hanning centered near the time of combustion works well for this. It is also wise to explore various response locations on the machine exterior, in an effort to further enhance the "signal-to-noise" ratio in the response ("noise" here referring to signal energy due to other sources in the machine). The coherence function between pressure and vibration can be a useful indicator of "good" and "bad" response locations. In general, we have found that locations away from the head, and oriented so that the sensor measures vibration in the same direction as piston travel are best suited for pressure recovery.

Fig. 2 shows the magnitude and phase of a transfer function from cylinder pressure to casing acceleration, obtained from measurements made on an

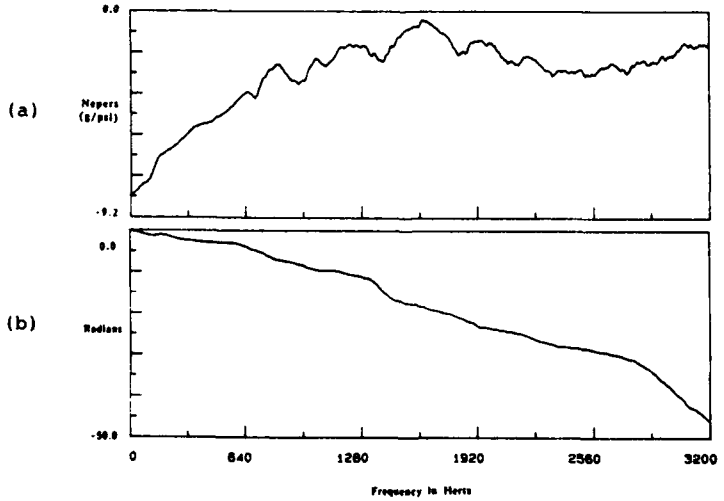

Fig. 2: Transfer function from cylinder pressure to casing accelerometer, measured on small diesel engine (average of 30 cycles at idle); (a) log magnitude, (b) phase.

idling four-cylinder automotive diesel. Here the phase is displayed as acontinuous function of frequency, rather than being "wrapped" between $\pm\pi$. The magnitude units are nepers (the range shown in Fig. 2 is equal to 80 dB), which are consistent with the phase units of radians.

The number of peaks and notches in a transfer function is related to the complexity of the transmission path. The peaks and notches are caused by poles and zeros of the transfer function, and the bandwidth of each peak is determined by the damping (due to both structural and time windowing effects). Each pole and zero is represented by a complex number pair. If there are N resonant structural modes, then there are approximately 4N parameters needed to describe the transfer function. For the sake of discussion, suppose that the structure has 20 resonant modes in the frequency bandwidth of the source, and the source waveform is simple enough to be described by 10 parameters. Then the response waveform is governed by 90 parameters. If we want to recover a fault in the source, the 80 "path" parameters are a "noise field" that we need to somehow repress to determine the source parameters. A common procedure for eliminating the effects of a path is inverse filtering - using a filter that has magnitude and phase properties that are inverse to the path effects. Some care is needed in its application, however, because frequency regions for which the transmission is weak (near a transfer function zero) are most likely to be noise contaminated, while it is those same frequency regions that are most amplified by the inverse filter. Therefore, unless some limit is placed on this amplification, spurious outputs of amplified noise will contaminate the recovered signal.

Transfer Function Variability: In most instances, a diagnostic system will be tailored to a single class of machines, perhaps of the same model and type. If the machines all transmitted vibration in exactly the same way, then an exact inverse filter could be applied to all of these machines. Unfortunately, there appears to be a large amount of variability in the transfer functions on typical machine structures. In Fig. 3 we show the mean and standard deviation of transfer functions measured between the same two points on 46 diesel engines, tested after assembly on the production line [1]. For these measurements, the engines were not operating - a mechanical shaker was used as the source of excitation. Although all the engines were made according to the same specifications, the standard deviation in the magnitude of the transfer function is about 8 dB at the higher frequencies. For a log normal distribution, this means that 5 out of every 100 machines have transfer functions that differ by more than 30 dB at any particular frequency! Even more significant from the viewpoint of waveform recovery, standard deviations of phase are of the order of 10 radians in the mid-frequency range (some studies [2,3] have indicated that details in phase are more important for waveform reconstruction than details in spectral magnitude). Although we expect that this deviation would decrease after the engines are "broken in," there would probably still remain a large enough uncertainty in magnitude and phase such that an inverse filter designed for one copy of a machine model would probably not be successful when used on a second copy of that same model machine.

These variations in transfer functions between machines are caused by differences in material and assembly parameters, which lead to variations

in resonance frequencies, damping and mode shape. In addition to these structural differences, transfer functions within a single machine may also change with time and operating condition, due to factors such as wear, temperature, and transmission path changes caused by differing loads or slight changes in geometry. From the viewpoint of source recovery, transfer function variability is a problem, and the signal processing procedures must deal with it. In the next section we describe a procedure used to create more "robust" inverse filters. These filters are applicable to a wider class of problems than are the "exact" inverse filters from which they are derived, but at the cost of reduced information in the recovered signatures.

Cepstral Windowing: A recovery procedure based on inverse filtering can be made more robust if we reduce the number of parameters needed to describe the source, path, and response. As a first step towards this, we multiply the measured response signal by a time-window. The primary purpose of this step, of course, is to separate the vibration pulse of interest from the "background" vibration. In a diesel engine, combustion is usually strong enough to produce an easily detected vibration pulse at some convenient location on the exterior of the engine. The next step involves windowing the complex cepstrum of this vibration. This provides us with a consistent way to implement a frequency-domain smoothing of the data, and has the advantage that it tends to dereverberate signals. From the smoothed source and response signals, we can then obtain a smoothed transfer function.

The effect of cepstral windowing on a response signal is illustrated in Fig. 4. An input force (due to cylinder pressure for example) excites a reverberant structure which has a complicated impulse response, producing a reverberant response. If we examine this process in the frequency domain, and express these quantities in terms of log magnitude and con-

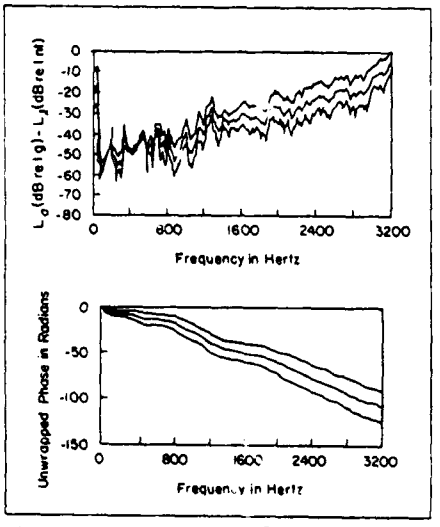

Fig. 3: Average value of a transfer function measured on 46 new engines of the same model, ± one standard deviation.

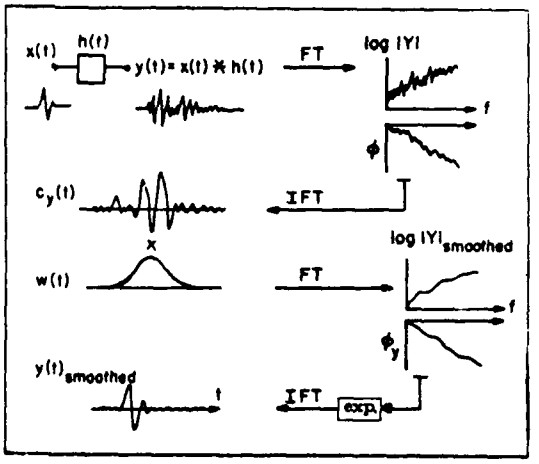

Fig. 4: Illustration of cepstral windowing procedure applied to a reverberant response signal.

tinuous (or "unwrapped") phase, then the source and path spectra add to make up the output spectrum. If we take the inverse Fourier transform of this log spectrum to return to the time domain, we generate the complex cepstrum - a real function. The even part of the cepstrum is determined by the log magnitude spectrum, and its odd part by the phase spectrum. It is also additive - the output cepstrum is a sum of the input and system response cepstra.

When the cepstrum is windowed by a function W(t), the functions in the log frequency domain are convolved. This convolution amounts to a smoothing in the frequency domain. In Fig. 4 we have shown a Gaussian window, which tends to have continuous derivatives, rather than the better known rectangular or Hanning windows. A Gaussian window applied to the cepstrum causes a Gaussian weighted smoothing of the log magnitude and phase functions. Any low-time window can be used, but sometimes the discontinuities in derivatives or value can be a problem. The smoothed log magnitude spectrum and the phase can then be reconstructed into a modified signal by complex exponentiating and inverse Fourier transforming.

The cepstrally windowed response will usually have a shorter time extent than the original response because the frequency domain smoothing tends to remove the effect of resonances in the path. This dereverberated signal will have many of the extra parameters removed that were introduced by the reverberant path.

The cepstral windowing procedure tends to be energy conserving, i.e., the stretched out energy of the received signal is concentrated into a shorter time period and not lost, as it would be if the signal were time-windowed only. Cepstral windowing can also be regarded as a "robust" process because the reduced parameter set needed to describe the signal is less variable over a population of structures, as is demonstrated in Fig. 5. There is some evidence [4] that the Gaussian window is better suited than other windows for decreasing this variability.

In the context of recovering cylinder pressure, cepstral windowing of the source has another implication. The measured pressure is composed of components due to both compression and combustion. The former is much less variable than the latter, being essentially a function of engine speed only. For diagnostic purposes, the combustion component provides us with more information about the "health" of the engine. Proper cepstral windowing of the pressure signal will give us an estimate of the combustion component since, compared to the total pressure, combustion is an impulsive event and will thus be mainly represented in the low-time portion of the cepstrum. We have observed a

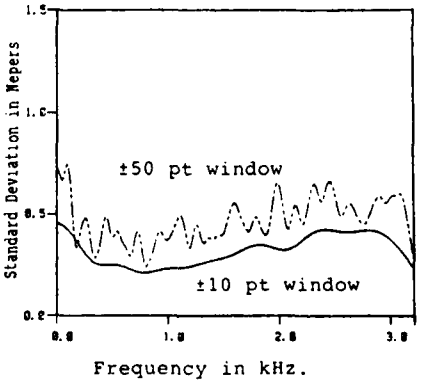

Fig. 5: Effect of cepstral window width on standard deviation of T.F. log magnitude [4].

high degree of correlation between the strength and timing of such "diagnostic signals" obtained by cepstrally windowing the directly measured pressures, and the actual combustion pressures, under a variety of conditions.

Fig. 6 shows the effect of cepstral windowing on a typical cycle of measured cylinder pressure and engine vibration, in both the time and frequency domains. To reduce the effect of extraneous sources, the acceleration signal was first time-windowed with a 10 msec wide Hanning window. The cepstral window was a Gaussian, the value of which fell to .0067 in ± 3 msec. This length was chosen since it yielded a cepstrally windowed pressure signal that was close in amplitude to a combustion pressure estimate obtained by subtracting cylinder pressure measured when combustion did not take place from a cycle of normal cylinder pressure. After obtaining the smoothed log magnitudes and phases of pressure and acceleration from several engine cycles, a robust (smoothed) transfer function between the two can be assembled from the averaged log magnitudes and phases of both signals.

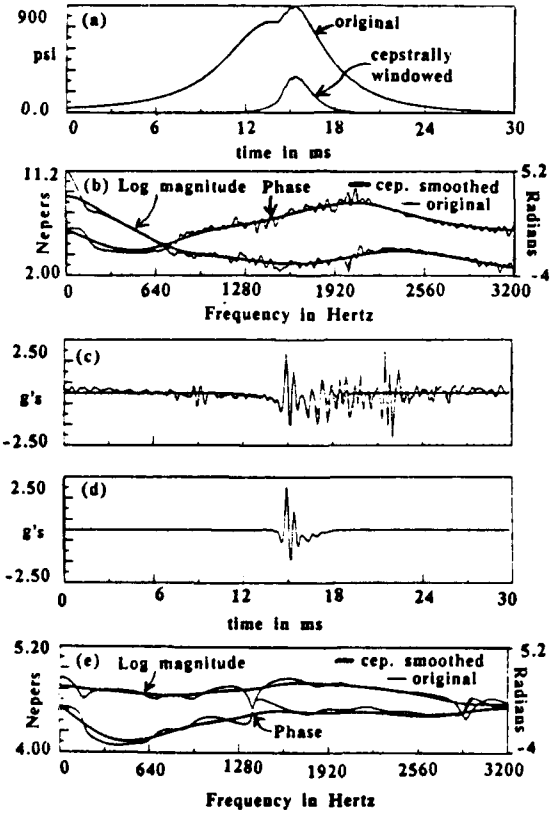

Fig. 6: Effect of cepstral windowing on source and response. (a) measured cylinder pressure waveform, (b) pressure spectrum, (c) original and Hanning windowed casing acceleration, (d) cepstrally windowed acceleration, (e) acceleration spectrum. Phase is displayed with linear component removed.

By using a curve fitting algorithm it is possible to further simplify this transfer function (as well as the associated recovered source waveform), such that it can be represented by 10 or so parameters. Such simplification might be desirable if an "adaptive" approach to recovery were taken, in which the transfer function was continuously updated.

Results: After first generating an estimate of the smoothed transfer function (perhaps from pressure and acceleration measured on a similar engine, or at an earlier time on the same engine), we now measure the response with the engine operating in its present condition. We window the cepstrum of this new signal, producing a new response signal which has the general appearance of Fig. 6(d), but will differ in detail. It is important that the time and cepstral window parameters be kept the same as when the transfer function was determined. This new signal, combined with our old smoothed transfer function, allows us to estimate an input signal. The deconvolution is accomplished in the frequency domain by subtracting the log magnitude and phase of the smoothed transfer function from those of the smoothed response, followed by the steps necessary to convert back to the time domain. Using the resulting "diagnostic signals" it is straightforward to pick out the strength and timing of combustion.

In many cases, the resulting estimates of the input waveform will be accurate enough for diagnostic purposes. For example Fig. 7 compares the

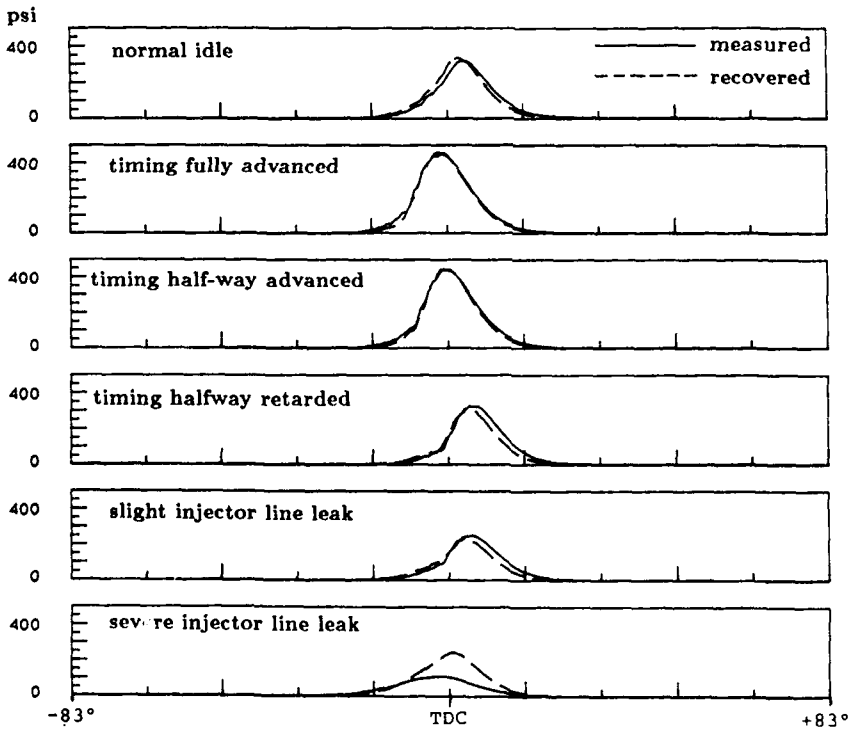

Fig. 7: Comparison of recovered and measured combustion pressures in one cylinder of a small diesel engine, for six different conditions at idle (average of 30 cycles each).

average recovered and measured combustion pressures obtained on a small diesel engine for a variety of operating conditions ("measured combustion pressure" here means the measured cylinder pressure after application of cepstral windowing). The transfer function used was obtained on the same engine, but on a different day. The time window on acceleration was chosen out of a range of window lengths and center points as the one which resulted in the most accurate recoveries over 30 consecutive cycles.

In Fig. 8 we show results obtained by applying the same procedure to vibration measured on the exterior of a much larger diesel engine. Shown are the average recovered and measured combustion pressures for three different conditions, in two of the cylinders. Since the two cylinders were on opposite sides of the engine, separate accelerometers (and transfer functions) were used for each. The magnitudes of these combustion pressures are less than those obtained for the smaller engine because a shorter cepstral window was used. For the most part, the recovered pressures are accurate enough to enable us to distinguish between the different conditions. However, as the last plot shows, accuracy suffers when combustion becomes so weak that it is no longer the "dominant" source of vibration within the time window.

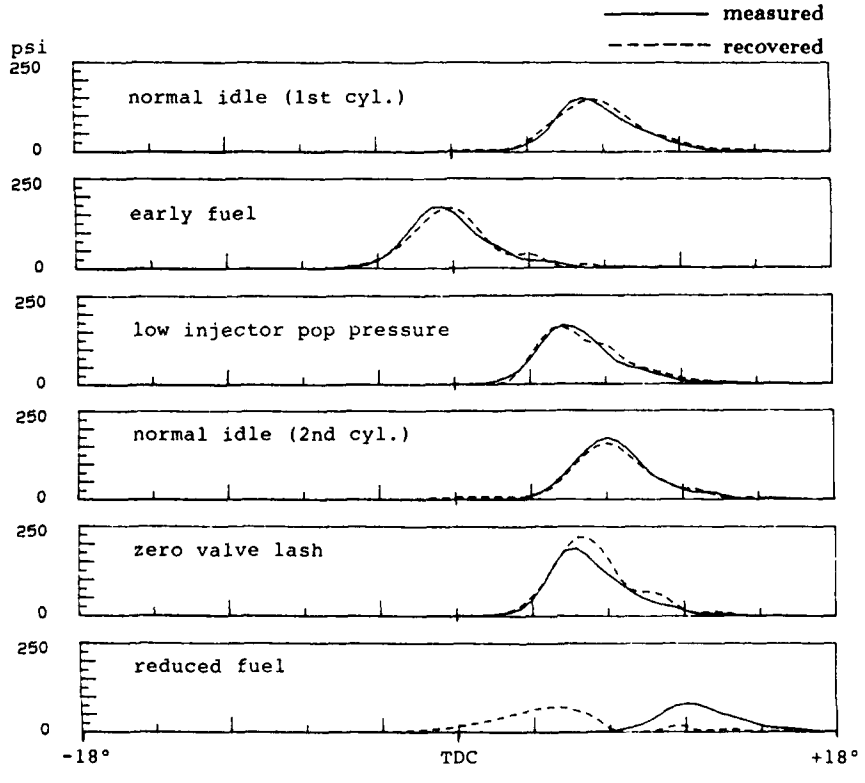

Fig. 8: Comparison of recovered and measured combustion pressures for two cylinders of a large diesel engine at idle. Top three plots correspond to one cylinder, bottom three to another (average of 15 cycles each).

Conclusions: Transient events in machines and structures produce vibration signals that can be used for machine diagnostics and control, but because of the complexity and variability of structural transmission, the procedure for using these vibration signals is not straightforward. This paper has discussed the use of a combination of cepstral windowing and inverse filtering to deal with the complexity and variability of the transmission path. Experience with diesel engine vibration signals indicates that careful application of this robust deconvolution procedure can result in signals which provide us with critical information about cylinder pressure - an important component of a system for determining the overall health of a diesel engine. Successful application depends on selecting response locations where vibration is well-correlated to combustion, the availability of a stable timing or tachometer signal, knowledge of the times of different events in the engine, and the availability of directly measured pressure for computing a transfer function during the calibration phase. With slight modification, the same procedure can also be applied to other transient signals in an engine, as well to other reciprocating machines.

References

1. R. G. Gibson, "Phase Variability of Structural Transfer Functions," MSc Thesis, Department of Mechanical Engineering, M.I.T., 1986.

2. R. H. Lyon, ***Machinery Noise and Diagnostics***, Butterworths, Boston, 1987, p. 195.

3. M. V. Hayes and A. V. Oppenheim, "Signal Reconstruction from Phase and Magnitude," ***IEEE Transactions on Acous., Speech and Signal Proc.***, V. 28, No. 6, December 1980.

4. J. T. Kim and R. H. Lyon, "Reducing Transfer Function Variability and Complexity by Cepstrum Windowing," ***Proceedings of Noise-Con '88***, Purdue University, 1988, p. 493.

Parameter Identification and Fault Diagnosis in Reciprocating Machinery

Reginald G. Mitchiner

Department of Mechanical Engineering
Virginia Polytechnic Institute and State University
Blacksburg, Virginia 24061-0238

Abstract: This paper presents a new method of identifying operational parameters in electric motor-driven reciprocating machinery. This method relys upon the computer-aided non-obtrusive observation of shaft (rotor) dynamics and power (current and voltage) consumption of the driving electric motor.

In a reciprocating machine, an air compressor for example, the rotor is acted upon by torque pulses from the motor and by torque pulses from the load machine. These torques, when summed together, act upon the rotor of the machine and directly influence the angular acceleration of that rotor. The acceleration of the rotor may be sensed; thus, the acceleration of the rotor may be known in both the time and the frequency domains. The currents and voltages driving the motor may also be sensed. From this data, the output torque of the motor may be ascertained. Then, subtracting the motor torque from the sum of torques, the apparent torque imposed on the rotor by the load machine is quantified in both domains.

There will exist a unique set of parameters, i.e. reciprocating mass, friction, gas pressures, and others, that will directly influence the torque exerted by the load machine. Either directly, or in a least-squares sense, these parameters may be determined such that the observed torque function is generated consistent with the observed dynamics of the rotor.

In a reciprocating compressor, the goal is the identification of the machine by quantifying the output pressure, expansion constant, clearance volume, and friction coefficient between the piston and the cylinder wall of the compressor. These compressor parameters are determined using the dynamics and kinematics equations of the compressor.

This procedure demonstrates that measurements of two operating parameters of a motor driven reciprocating machine, the instantaneous speed and the instantaneous electric power consumption, can provide data rich in the mechanical parameters affecting machine dynamic behavior.

Keywords: Parameter identification; fault diagnosis; reciprocating machinery; rotor dynamics; induction motor; torque; angular shaft acceleration; air compressors; gas pressures; coefficient of friction; power consumption; power losses

Introduction: In this paper and discussion, the term reciprocating machine shall refer to a reciprocating air compressor with pistons moving along paths that are transverse to the axis of the crankshaft of the compressor.

As shown in Figure 1, in the typical high-performance air compressor system, the electric motor, most often a three phase induction motor, drives the compressor directly. Thus the motor rotor, coupling, and the compressor crankshaft comprise a single rotor whose eigenvalues are sufficiently high and removed from the operating range of the motor, that the rotor may be considered to be a rigid body in rotation.

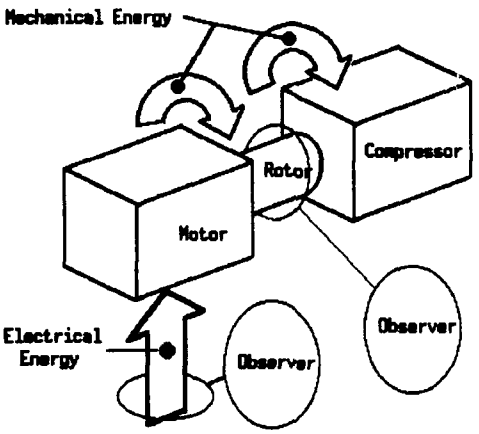

Figure 1. Motor/Rotor/Compressor with Observers

From an energy point-of-view, electrical energy is continuously transferred into the motor. Associated with the motor are losses such as stator and rotor heating losses, hysteresis losses, stray losses, and windage losses. From a gross electrical energy transfer into the motor, a net energy transfer is accomplished by the motor into the rotor. The rotor energy is manifested as kinetic energy. The compressor serves to extract the energy available from the dynamics of the rotor to perform work upon the working fluid by raising the pressure of that fluid as it is moved through the compressor.

To ascertain the state of the compressor and to quantify the processes within the compressor, it is necessary to know the state of the dynamics of the rotor and the instantaneous energy available at the rotor from the driving motor.

Expressing this relationship, as is seen in Figure 2, the sum of the torques acting upon the rotor may be written as:

$$T_M - T_L = J\ddot{\theta} \qquad (1)$$

where T_M = Torque developed by the driving motor

T_L = Torque imposed by compressor on rotor

J = Rotary inertia of rotor

$\ddot{\theta}$ = Angular acceleration of the rotor

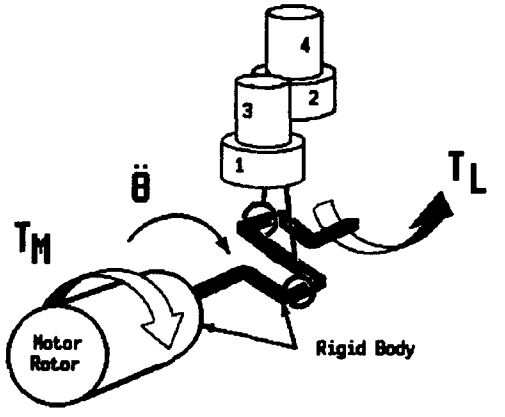

Figure 2. Torques Acting on the Machine Rotor

Equation 1 may be rewritten as:

$$T_L = T_M - J\ddot{\theta} \qquad (2)$$

Thus, if through observations of the rotor and of the electric motor, T_M and the angular acceleration of the rotor are known, Equation 2 shows that the torque imposed upon the rotor by the driven machine, the compressor, T_L, may be inferred. It should be noted that it is not inferred that the experimental determination of those two parameters is without difficulty. The reader is referred to Mitchiner, Williams, and Kanth [1] for a detailed discussion of velocity and acceleration measurements in reciprocating machinery.

The multi-stage research compressor used at Virginia Tech is an Ingersoll-Rand 242 compressor. The details for this two stage, two cylinder, 5 horsepower machine are given in Table 1. On the test stand, using the methods discussed above, phase voltages, phase currents, and the instantaneous angular velocity are acquired using a modern high speed data acquisition system.

The Identification Process:

Step 1: *Using the voltages, currents, and motor characteristics, the gross or input power waveform is constructed. Losses are calculated or simulated and the input power function is corrected to an output or net power function, accounting for heating, hysteresis, and stray losses.*

Crank Radius	1.381 In
Rod Length	6.750 In
Angle between Cylinders	90 Degrees
Low Pressure Cylinder	
Reciprocating Weight	2.070 Lbf
Diameter	4.000 In
Clearance Volume	3.471 In^3
High Pressure Cylinder	
Reciprocating Weight	1.425 Lbf
Diameter	2.500 In
Clearance Volume	1.627 In^3

Table 1. Ingersoll-Rand 242 Compressor Specifications

Step 2: *Using the net motor power and the instantaneous angular velocity, the instantaneous output torque of the motor is computed. Note that this torque is not measured, but is inferred from motor measurements and characteristics.*

Figure 3 shows a plot in time of the net torque function generated by the induction motor.

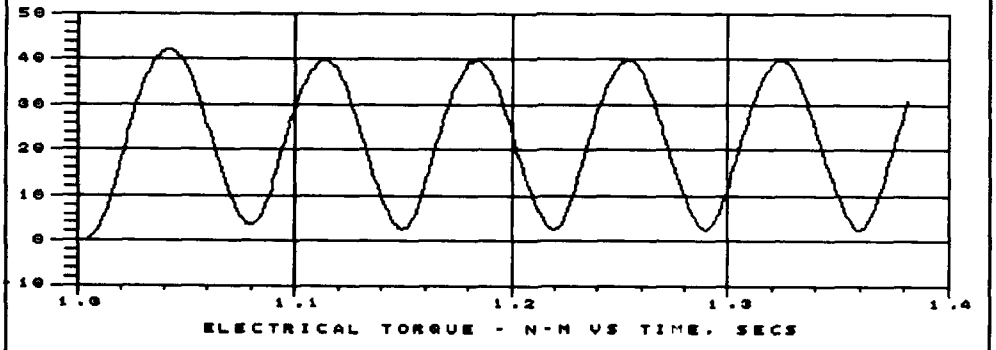

Figure 3. Net Torque Generated By the Motor

Step 3: *Differentiate the measured angular velocity function to obtain the angular acceleration of the rotor.*

Step 4: *Now, Equation 2 may be employed to yield at every point in a cycle, the apparent torque imposed upon the rotor by the load machine, the compressor. Throughout the cycle both the torque developed by the motor and the angular acceleration of the rotor are known. Thus the differential*

equation of motion, Equation 2, of the rotor may be solved algebraically at every point with a cycle.

Figure 4 shows the shaft acceleration for the I-R compressor, while Figure 5 shows the derived torque imposed on the rotor by the compressor.

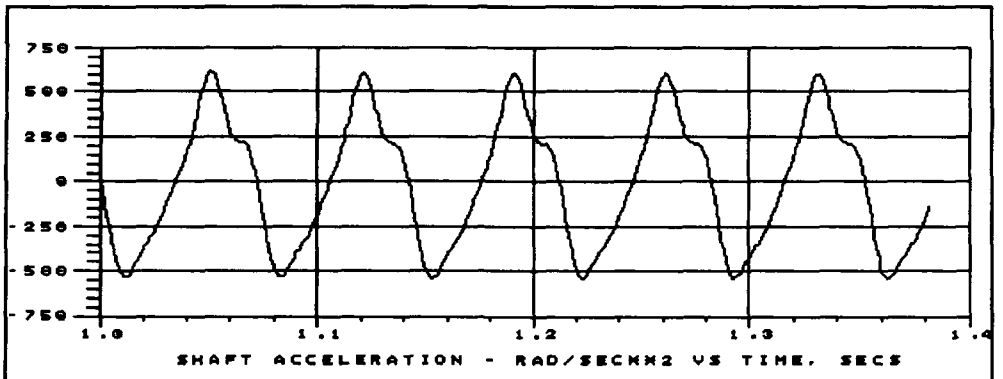

Figure 4. Rotor Acceleration

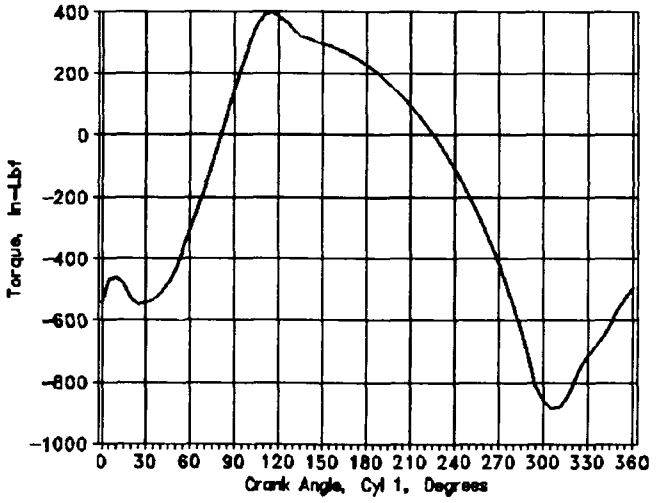

Figure 5. T_L, Compressor Torque, Total

Because the angular velocity and the acceleration of the rotor are known, and because for the purposes of this analysis, the compressor is kinematic chain of rigid components, the state of dynamics of each and every component of the compressor is known. Thus, with the knowledge of the mass (and inertia) of all moving components, the torque required to drive these components at the known dynamic state may be computed. This torque, the mass effects torque, may then be subtracted from the load torque of Step 4. Figure 6 illustrates this "mass" torque.

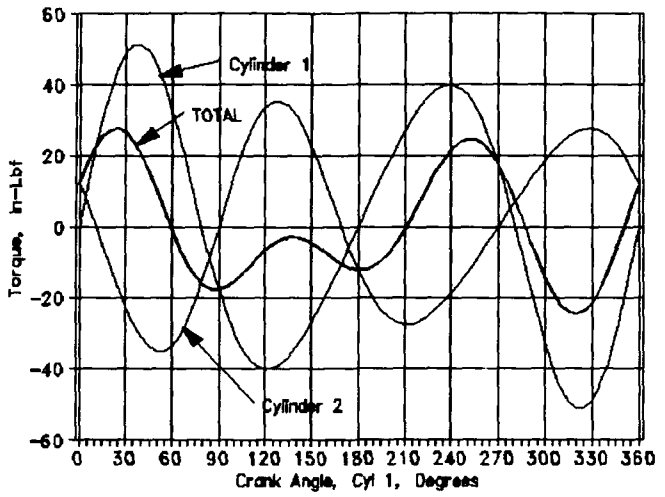

Figure 6. Reciprocating Mass Torque

Step 5: *Reformulate the load torque into a net torque, thus removing the effects of reciprocating masses.*

Having dealt with acceleration effects in Step 5, now attention is given to viscous (or velocity) effects. Presuming that there is a rotary viscous damper on the rotor and a translational damper at each piston, calculate the values of these damping constants consistent with the velocities that are known.

Step 6: Calculate a new net torque, removing the viscous effects.

Note that at this stage the net torque has been modified to remove all effects traceable to the dynamics of the load machine. All of the remaining torque effects are due to statics (position) only. These effects are pressure and coulomb friction effects.

Step 7: *Assuming an ideal compression cycle, solve for the defining parameters for that cycle for each cylinder/piston. Also, at the same time, solve for the average coefficient of friction between the piston and cylinder. Note that the pressure forces and Coulomb friction forces are coupled.*

Figure 7 shows, for the low and high pressure cylinders of the I-R compressor, assumed idealized profiles.

Step 8: *Generate a new net torque by removing from the "old" net torque the constant suction/exhaust effects. This new net torque now includes only the effects of suction and exhaust pressure fluctuations.*

Step 9: *Solve for suction and exhaust fluctuations at each piston.*

Step 10: *Perform an energy balance using the electrical energy input,*

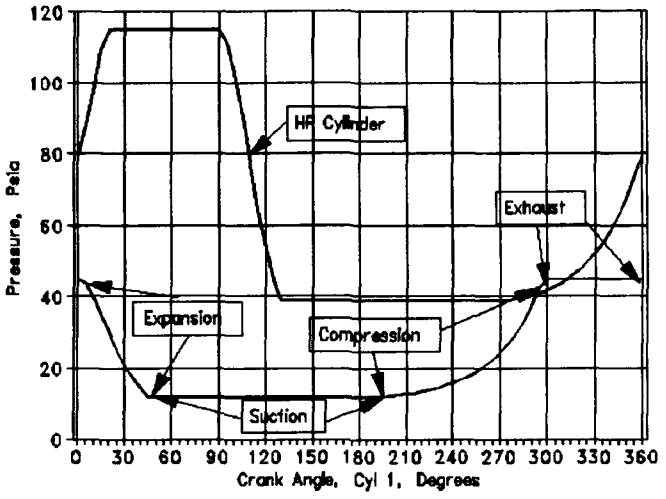

Figure 7. Pressure Diagrams for I-R 242 Compressor

electrical losses, mechanical losses, leakages, and energy delivered to the working fluid.

The ten steps detailed herein will lead to the determination of the following parameters for each cylinder of the compressor:

1. Mean suction pressure
2. Mean exhaust pressure
3. Compression and expansion constants
4. Leakage during compression and expansion
5. Coefficient of Coulomb friction at cylinder wall
6. Coulomb forces at cylinder wall and nature of these forces
7. Viscous forces at cylinder wall
8. Pressure variations during suction and exhaust

Further, utilization of the above parameters, along with geometrical and other characteristics, can lead to the estimation of such operational characteristics as intercooler performance and others.

Current research at Virginia Tech is directed toward developing the capability to acquire rotor dynamics and electrical input data for the motor in a continuous and real-time fashion. A separate computer from the data acquisition machine, but still a cooperative machine, will perform the manipulations described herein, successively distilling parameters from the acquired data.

Conclusion: If one can, in either a continuous or a periodic fashion, accurately ascertain the operating parameters for the compressor as described above, these parameters may be trended to predict when the parameter will become critical.

It should be noted that this identification process does not define those operating characteristics which but indirectly affect performance. For example, low lubricant levels are in and of themselves no sin. The consequence of low lubricant levels most often is increased frictional losses and the attendant elevated temperatures. This identification process directly defines the friction coefficients, friction forces, and temperatures.

Fault diagnosis in this class of machinery is the identification of those operating parameters which because of their nature and magnitude, the current or continued operation of the machine is imperiled. Simulations performed using both observed and simulation derived data indicate that the techniques described herein can estimate machinery operating parameters to within 1% in a non-obtrusive manner. Thus, using a minimum of robust observers coupled with modern high-speed dedicated computers, operating parameters may be identified and faults diagnosed or predicted.

References:

[1] Mitchiner, R. G., Jeremy Williams, and R. Kanth, "Measurement of the Instantaneous Angular Velocity of a Reciprocating Machine Crankshaft," *Proceeding of the 1990 ASME Mechanisms Conference, Chicago,* September, 1990.

VALVE DIAGNOSTICS

Chairman: Henry R Hegner
ECO, INC.

USE OF ULTRASONICS AS A CHECK VALVE DIAGNOSTIC TOOL

Gary Hill
Charles Burton
ITI MOVATS
200 Chastain Center Blvd.
Suite 250
Kennesaw, GA 30144

ABSTRACT: Non-intrusive examination of check valves is rapidly becoming a priority in the nuclear industry. Methods of examining check valve internals are available, and prevent unnecessary disassembly and inspection. This paper discusses the use of ultrasonics for testing check valves as part of a preventative maintenance and In-Service-Testing (IST) Program. Ultrasonics is used to gather information on valve internal performance. A computer controls acquisition and features automated analysis including Fast Fourier Transforms (FFT) and disc angular velocity calculations. A technical description of the technology is discussed as well as system capabilities and recommended uses.

KEYWORDS: Non-intrusive; Check valve internals; Disassembly; Inspection; Preventative maintenance; Ultrasonics; Computer; Automated analysis; FFT, Angular velocity

INTRODUCTION: Check valves are one of the most common components found in a power plant. They are located in almost every safety and non-safety-related fluid system. Failure of one of these valves during plant operation or in some cases, under cold shutdown conditions, could significantly affect plant safety. Failure can also result in costly and time consuming maintenance. A major cause of check valve failure has been excessive wear. Operation under conditions that cause the valve disc and hinge arm to oscillate or flutter can lead to degradations which, if uncorrected, may result in failure. Examples of such degradations include wear of the hinge pin, hinge pin bushings, and disc stud. In addition, disc tapping at the backstop may lead to fracturing of the disc stud.

In the past, two primary methods have been used in an attempt to prevent failure or excessive wear. The first method is employed during the design phase. System fluid velocity is determined and a check valve with a calculated minimum flow velocity for stable operation less than the anticipated system flow is selected. The goal of this action is to match the theoretical operating characteristics of the valve with the system flow dynamics to prevent or minimize excessive flutter thereby reducing wear.

However, experience has shown that the analytical or theoretical operating characteristics of check valves frequently do not match their actual operating characteristics. The second method centers around a periodic disassembly and inspection program. Once operation has commenced, selected valves are disassembled and their internals inspected for signs of wear. This method is costly and time consuming. Frequently, the disassembled valves show little or no signs of wear, which highlights the inherent inefficiency of an inspection program. Neither of these methods verify actual valve performance during plant operation. A system is available to observe valve performance under all operating flow velocities and to measure and quantify instability. With proper use of the equipment, potential problem valves can be identified based on the valve's actual operating characteristics, making it possible to implement design changes or maintenance prior to failure or significant degradation.

DESCRIPTION: The ultrasonic check valve analysis system uses ultrasonic technology to test various types of check valves typically found in nuclear power plants (refer to Figure 1).

Figure 1. Ultrasonic System Configuration

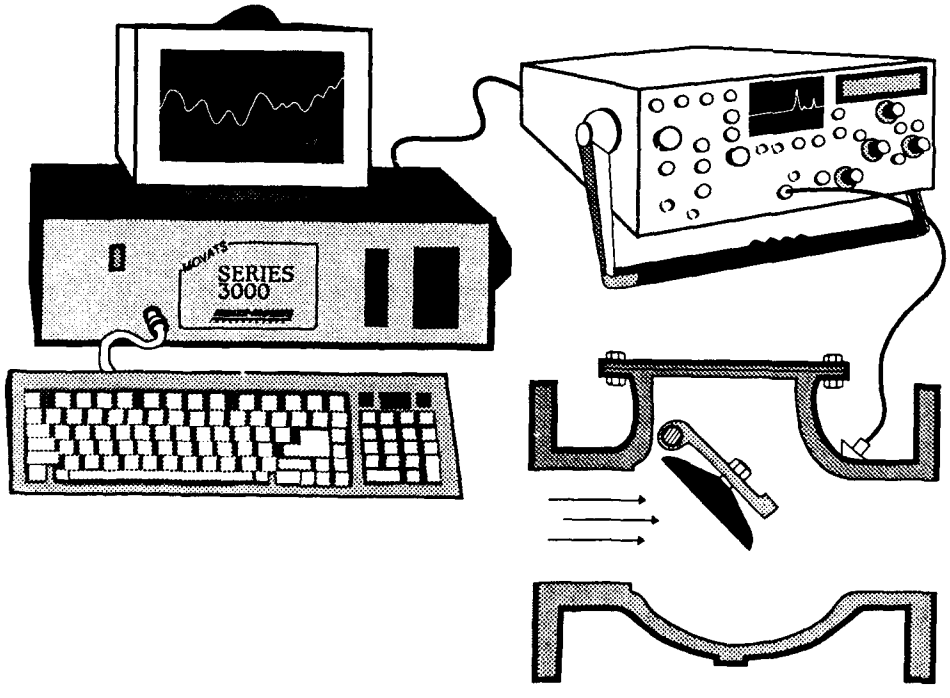

Testing of most plant valves can be performed while the power plant or system is in service provided flow can be passed through the valve. Signal transmission and reception is accomplished by use of a modified ultrasonic flaw detection oscilloscope and associated transducers. The unit has been modified to improve its signal-to-noise ratio and method of calibration for greater ease of use on check valves. The ultrasonic transducer is attached to a small wedge that is used to position the transducer so that it is nearly normal to the target. Typically the transducer and attached wedge are hand held; however, if desired, the wedge or entire assembly may be permanently mounted. The ultrasonic beam generated in the transducer passes through the valve wall and fluid and is reflected off the internal valve part. The returning signal is captured and displayed on the oscilloscope and passed to the data storage and analysis computer.

The returning signal can be analyzed using the automated software to determine disc position and stability while at the valve.

SIGNAL PROCESSING: A 0 to 10-volt time varying signal is passed from the oscilloscope to the analysis computer. The signal represents target position as a function of time. The analog data signal is digitized and digitally filtered. A Fast Fourier Transform is performed on the filtered data, and a frequency spectrum developed. Additional information such as key valve dimensions and transducer location in reference to the hinge pin are entered into the program via a keyboard. The information is requested via a data sheet screen.

The computer monitor is capable of displaying a three-trace plot of input data (displacement versus time, unfiltered), filtered data, and the frequency spectrum. In addition, multitrace plots (up to three) of the same parameters from the same or different valves may be displayed on the same screen. This feature is very useful in comparing the relative motion of components within a valve and in comparing similar degradations in different valves. All the traces viewed on the monitor may be sent to a plotter for hard copy generation. The computer software generates a test report summary that includes calculated values for stability number, disc position expressed as degrees off seat, and average target displacement.

DIAGNOSTIC CAPABILITIES: Computer assisted analysis can validate and quantify the following concerns:

Free Flutter: This condition occurs in a check valve when the flow in the system (refer to Figure 2) is less than that required to push the disc up to the backstop. Free flutter would not be expected at a base-loaded plant in systems that normally operate at design flow provided the check valve application and sizing was correct.

Figure 2. Physical and Signature Representation of Free Flutter

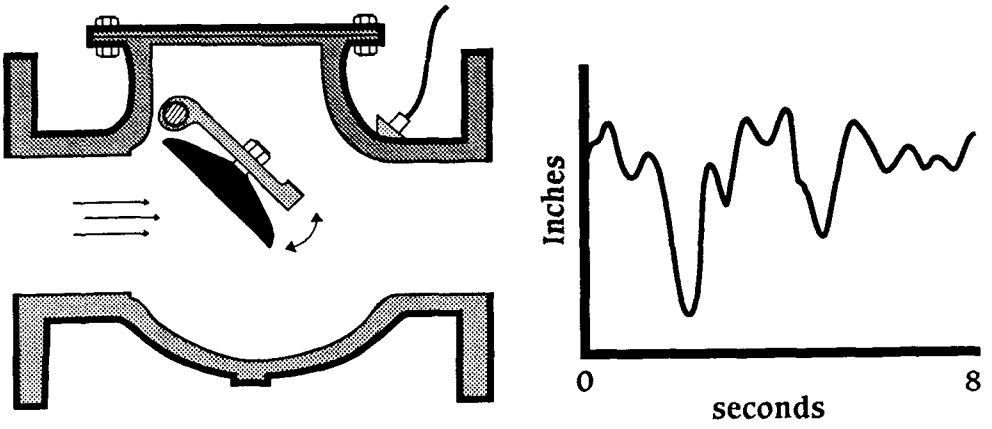

However, it can occur in safety-related systems in which a check valve designed for accident flow conditions is part of a normal operating flow path where flow is less than design accident flow. It can also occur if the plant is operated at reduced power resulting in a reduced system flow. The disc movement is believed to be caused primarily by vortex shedding that results from the disc partially blocking the flow stream. This type of movement causes hinge pin wear, which over a period of time could result in improper seating or, in extreme cases, loss of the disc. A typical ultrasonic signature from a valve experiencing free flutter would appear as a sine wave on the computer. By analyzing the signature, the total hinge pin travel over a period of time can be determined. The travel can be used to calculate hinge pin wear rates.

To characterize the stability of a valve, the software assigns a stability number to the signature. The stability number represents the amount of flutter that a valve's disc is exhibiting. A valve with a stability number of 10, for example, is said to be fluttering or oscillating at 10 degrees per second. While a specific correlation between stability number and wear rate cannot be given because of variations in material, weight, design, etc., it can be generalized that valves with high oscillations wear much more quickly than more stable valves. Specific wear rates based on stability number, component material and weight, disc orientation and other design information can be calculated on an individual valve basis. Wear calculations typically would be done for valves that exhibit a moderate or high degree of flutter. Typically valves with a stability number of 0-3 are considered stable, 4-11 exhibit flutter, and 12 and up are considered unstable and may be unsuitable for use in their current application.

Backstop Tapping: As flow through a check valve in free flutter increases, the disc eventually begins to tap against the backstop. This tapping can cause fatigue damage to the disc stud, stud nut, and hinge arm. A more severe form of tapping occurs at very high flow rates (much greater than the flow required to hold the valve open). This condition results in the disc periodically leaving the backstop and then returning with significant force.

A ultrasonic signature of a valve experiencing backstop tapping would also appear as a sine wave; however, the upper peaks may be flattened. Additionally, backstop tapping may be identified through analysis of the disc position versus time signature to determine actual disc position relative to the location of the backstop. Figure 3 shows the signature of a disc impacting the backstop at a distance of 14.35" from the location of the transducer. By analyzing the signature prior to the disc hitting the backstop, the energy level of the impact can be determined. This, combined with the frequency of impact, can be used to predict fatigue damage of the valve internals.

Figure 3. Physical and Signature Representation of Backstop Tapping

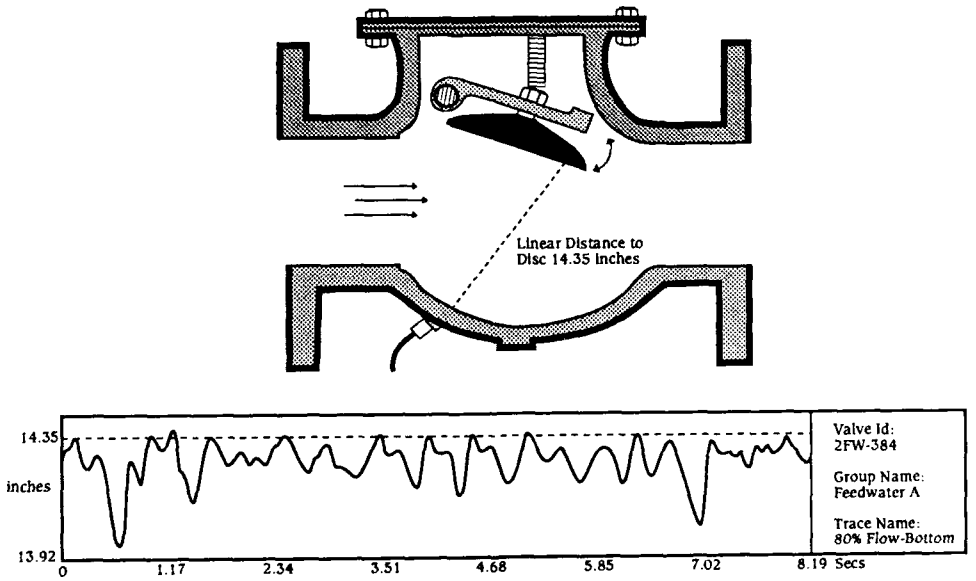

Seat Tapping: This condition occurs at low flow rates that cause the valve disc to move off the seat and then swing back into it. Leakage past a normally closed stop valve can result in check valve seat tapping. Seat tapping can also occur in the downstream safety injection tank (accumulator) check valve when it is used for residual heat removal flow. Extended operation with seat tapping can lead to seat damage and back leakage when the check valve is shut. The signature obtained from a valve tapping against the seat would be similar to that of a valve backstop tapping, except the peaks on the target point position versus time signature would indicate the disc is in contact with the seat.

Missing or Stuck Disc: These conditions can occur as a result of excessive wear, improper assembly, broken or defective parts. The degradation may allow flow in reverse of the intended direction. This can result in overpressurization of the upstream system or a diversion of flow from its intended flow path. If the system contains radioactive or other potentially hazardous fluids, contamination may be spread to previously clean systems. The signature received from a stuck disc will not change as flow is varied. Additionally, the indicated position of the disc may not be consistent with that expected for the measured flow rate, i.e., the disc may be fully open with limited flow through the valve.

If the disc is missing, no signal will be returned from the disc; however, a signal may be returned from the hinge arm if it remains intact. Under similar flow conditions, the signature of a hinge arm without a disc will exhibit a higher frequency flutter than that of a hinge arm with the disc attached (refer to Figure 4). This higher frequency flutter is also evident in the frequency spectrum analysis shown in Figure 5. In this figure, the frequency distribution is shifted to the higher frequency range when the disc is removed.

Figure 4. Comparison of Hinge Arm Signature with and without Disc

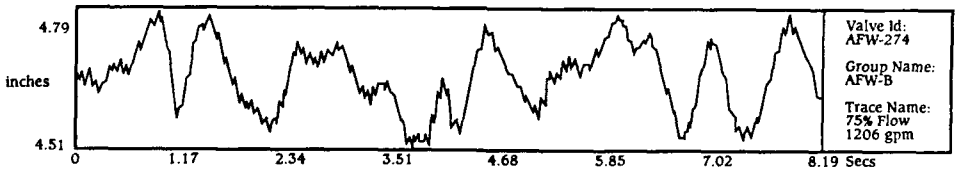

4a. Hinge Arm with Disc Attached

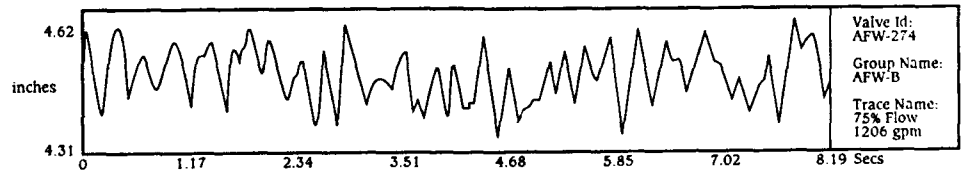

4b. Hinge Arm with Disc Removed

Figure 5. Frequency Spectrum Comparison of Hinge Arm Movement with and without Disc

5a. Hinge Arm with Disc Attached

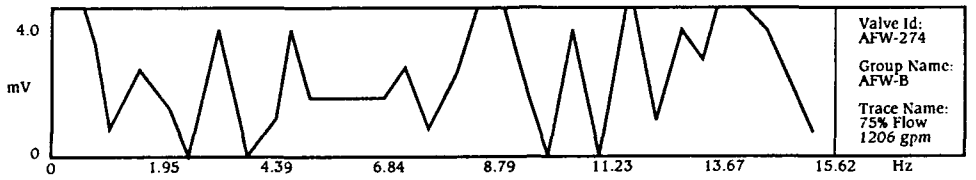

5b. Hinge Arm with Disc Removed

Hinge Pin and Disc/Stud Wear: These conditions may occur as a result of the flutter or tapping concerns identified above. Excessive wear will degrade valve performance and may lead to leakage or failure of internal valve parts. Analysis of ultrasonic signatures can be used to identify reduced hinge pin diameter, which is indicative of wear. Additionally, an analysis of the relative motion of a disc and hinge arm can be performed to identify wear in the area of the disc and stud on may types of valves. A loose or worn disc stud will typically result in a relative or wobble between the disc and hinge arm. A comparison of signatures taken of hinge arm and disc position is used to identify relative motion between the two parts. Figure 6a is a signature taken of the hinge arm of a stable valve against the backstop. Figure 6b is a signature of the disc taken under identical flow conditions. This trace clearly shows disc motion relative to the hinge arm.

Figure 6. Signature Representation
of Disc/Stud Wear

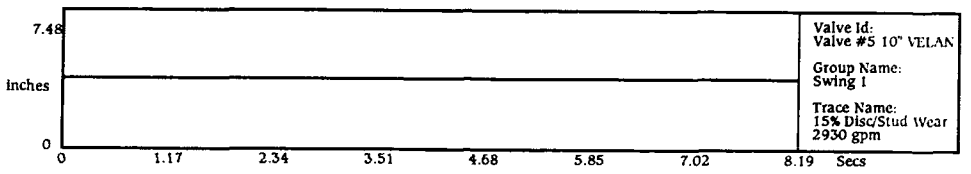

Figure 6a. Motion of Hinge Arm

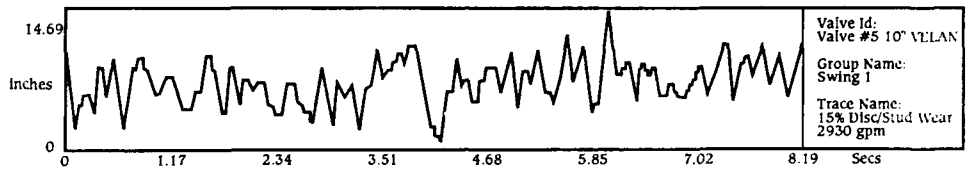

Figure 6b. Motion of Disc

APPLICATIONS: The ability to monitor check valve performance under actual operating conditions provides the maintenance planner with a clear picture of the current condition of the check valve. Additionally, based on the valve's observed stability, the maintenance planner has a good indication of the likelihood of degradations. This information may be used to schedule visual inspections, delay or expedite valve refurbishment or to adjust the noninstrusive test schedule consistent with observed performance.

A plot similar to Figure 7 may be developed for check valves that can be subjected to varying flow rates such as feedwater or some residual heat removal valves. The figure shows valve stability for different flow rates through the valve. The example chosen shows a relatively high degree of flutter or instability in the 60% to 80% flow range. Accelerated wear can be expected if the valve continues to operate in this flow range. If prolonged operation in an unstable area is required due to a power restriction, equipment limitations, etc., the maintenance planner should consider an increased inspection/refurbishment frequency. It should be noted that valve stability is dependent on many factors including valve and system design, flow rate, turbulence, etc. As a result, similar valves may exhibit different stability for the same flow rate. This precludes the ability to develop a "generic" stability plot for a class of check valves.

Figure 7. Valve Stability at Varying Flow Rates

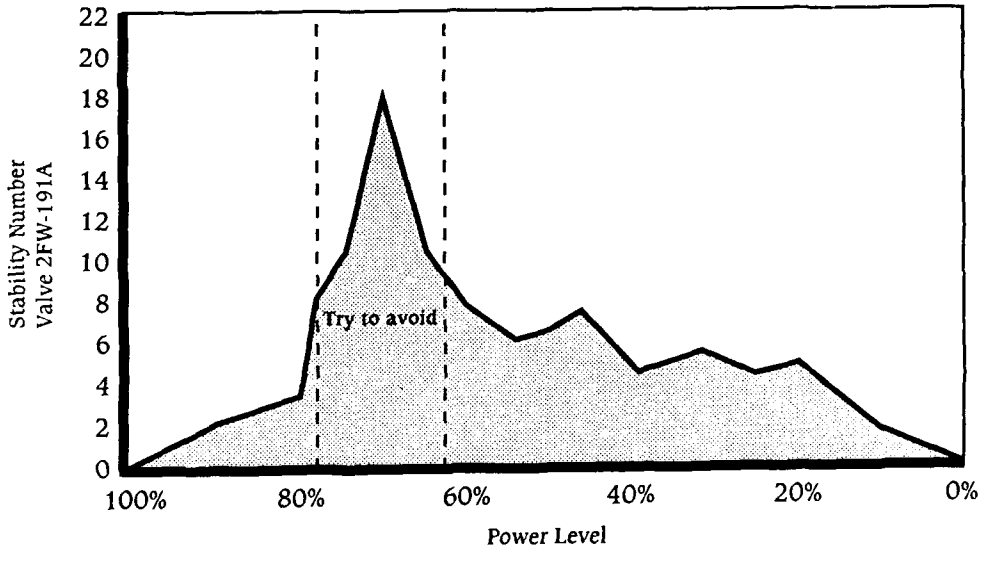

Verification of check valve operation using ultrasonics may be used as a basis for satisfying other in-service test/inspection requirements that require the valve to be disassembled. Frequently, ultrasonics can monitor the full stroke of the check valve from either open to close or close to open. This capability verified operability, without disassembly, to physically cycle the disc. This nonintrusive method removes any possibility of misassembly after disc cycling since nothing on the valve is disturbed.

In addition to the acquisition and analysis software, a check valve degradation and prediction model has been developed to predict wear rates and times to failure for the following modes:

Swing Check/Tilting Disc:

* Wear of hinge pin and hinge arm
* Wear of hinge pin at hinge pin bushing
* Wear of backstop/disc stud from impact
* Fatigue of disc nut/stud threads leading to thread cracking

Split Disc (Duo):

* Wear of hinge pin at the hinge pin bushing

Knowledge of the wear rates and time to failure will enable the maintenance planner to truly optimize preventive and corrective maintenance activities.

SUMMARY: A number of check valves have been tested at various plant sites, several flow loops, and during an industry-sponsored test program utilizing the Checkmate™ ultrasonic Check Valve Analysis System. The results of these tests clearly demonstrate that the ultrasonic system can easily identify many common check valve problems and degradations. In many cases, simple nonintrusive testing may be used instead of costly and time consuming disassembly and inspection programs to satisfy regulatory or INPO operability verification requirements. Additionally, many check valves can be monitored during plant operation when normal flow exists thereby reducing outage work.

NEW DIAGNOSTIC TEST SYSTEMS ASSIST IN FAILURE PREVENTION OF PNEUMATIC OPERATED VALVES

Rodney M. Eslinger
ITI MOVATS
200 Chastain Center Blvd.
Suite 250
Kennesaw, GA 30144

ABSTRACT: Diagnostic technology has taken a quantum leap in the area of valve testing over the last 5 years. Air operated valves are vulnerable to many kinds of mechanical and electrical degradations. Diagnostic testing of these valves can detect problems before mechanical failures occur. These test systems can aid in implementing efficient preventative maintenance programs as well as determining cause and solution for existing problems. Precise set-up of new or refurbished actuators improve system efficiency and reduce chances of future malfunction. Data is permanently stored on computer disk for easy reference. Automated analysis of test data saves time and is cost effective. Maintenance scheduling and decision making is easier for management personnel when using this "tool."

KEY WORDS: Air-operated Valves; Automated Analysis Program; Diagnosis; Electropneumatic Converter; Signature Trace; Transducers

INTRODUCTION: Air-operated valves (AOVs) are used extensively in many industries including power, petrochemical, and pulp and paper. All of these industries have varying degrees of problems with AOVs. Unfortunately AOV failures seldom occur at a time when it is convenient to repair them. Plant or system operation is frequently adversely impacted by the failure. The result of an AOV problem may be a reduction in unit output or a loss of operational flexibility. If the apparent cause of failure is not obvious, such as a broken or damaged part, crimped air line, etc., diagnosis of the cause may be tedious and time consuming. Replacing components in an attempt to cure an AOV problem without also determining the root cause of failure can be costly in both component and manpower costs and can result in additional plant downtime.

The search for better ways to identify developing degradations before they result in AOV failures and to determine the root cause of failures has led to the development of a state-of-the-art diagnostic system.

At a nuclear power station, many AOVs are located in radiologically controlled areas. Usually these valves will require a longer time to repair due to the special controls required to be exercised on work performed in radiation areas. Additionally, radiation levels may be high in the vicinity of the valve, further limiting access to the valve.

This paper reviews some of the common problems that occur with AOVs and discusses methodologies for diagnosing these problems and benefits that can be gained from using diagnostics. The information presented this paper is based on the joint development of an AOV diagnostic system by ITI-MOVATS Incorporated and Valtek.

TYPICAL AOV DEGRADATIONS: Air leakage is one of the most common AOV problems. Air leaks can occur both internal and external to the actuator. Internally, diaphragms and piston o-rings can begin leaking due to wear and hardening of the rubber parts or improper installation. Hardening is caused by heat, age, and in some cases radiation exposure.

External leaks can occur in a variety of locations about the actuator, positioner, and controller. Fittings, hoses, and metal tubing connections are occasionally at fault. More common sources of leaks are components with rubber seals, especially the diaphragm or flapper valve in some positioners. Sometimes solenoid seals fail causing air leaks. Any leakage of signal or piston/diaphragm air can cause an actuator to malfunction or even fail if the leak is severe enough. Other pneumatic problems such as loss of air or restriction of supply air are also common. Broken, pinched, or otherwise damaged supply lines can leave an air valve incapacitated.

In addition to pneumatic leakage problems, positioners can also exhibit mechanical degradations. Many positioners have flapper valves, which can become dirty or even deteriorate slowly and will cause shifting of calibration, erratic action, or other problems. Positioner spool valves can also become dirty or damaged and cause erratic behavior. Electro-pneumatic converters are subject to the same dirt buildup on the flapper valves, causing inconsistent action and/or calibration problems.

Mechanical degradations in the valve and actuator might include bent stems, pilot valve misalignment, cage-to-plug galling, incorrect packing configurations and adjustments, loose connecting/mounting bolts, and a weakened or broken diaphragm or cylinder spring.

DIAGNOSTIC TEST EQUIPMENT: An effective method to address AOV problems is through the use of an automated diagnostic system. Diagnostic systems have been widely used for several years to set up and troubleshoot motor-operated valves in the nuclear industry. These systems are considered a "must have tool" at most nuclear stations because of the information on valve and actuator operability that can be obtained through their use. Research performed by ITI-MOVATS Incorporated on AOVs at our flow loop, at Valtek facilities, and in field testing, has demonstrated that by monitoring selected key actuator parameters a significant amount of information concerning valve operability can be determined. Packing load, pneumatic leaks, spring characteristics, stem thrust, and valve and pneumatic actuator degradations can be identified and quantified in a simple and straightforward manner.

This type of testing can be used for verifying operability during static or dynamic system conditions. Design specifications can also be verified. The early detection of potential mechanical failures is also possible with a properly designed diagnostic testing program. Many mechanical, electrical and pneumatic degradations can be detected and diagnosed prior to component failure, thereby preventing an unscheduled system shutdown. Periodic testing can determine specifically when and if maintenance is required.

Diagnostic systems typically have a built-in data base that stores all applicable valve and actuator data including actuator specifications, serial numbers, size, type, and model. Process system information should also be included. This information can be very useful when ordering replacement parts. A maintenance history can also be included, which is useful in developing and scheduling future maintenance. Test data (line graphs) provide records of past operability and may also serve as a baseline for comparison to future tests.

TEST PARAMETERS AND HOW THEY ARE MONITORED: Typically an air-operated valve has up to four (4) pneumatic pressures to monitor. These include upper and lower cylinder or diaphragm pressures, signal pressure, and supply pressure. Diaphragm-type actuators normally have air pressure on one side of the diaphragm only; whereas, the cylinder types can have air on one or both sides of the piston. The signal pressure is either the output of an electro-pneumatic converter or a pneumatic process controller. In some cases an isolation-type valve might be controlled by a solenoid valve, which, when energized, would open allowing supply air to stroke the valve (normally closed solenoid valve) or would close, causing the valve to stroke (normally open solenoid valve). These pressures are monitored by solid-state pressure transducers which tap into the appropriate lines using tees and quick-connect fittings. If the valve is to be tested periodically, as with certain problem valves, the tees and quick connects can be left in place. In some plants, this may require a design change.

Stem position can be monitored using a variety of methods. A cable potentiometer is one method used. This device requires mounting hardware for the transducer and some type of stem connection in the form of a bar that clamps onto the stem, providing a point to attach the cable. This connection should allow the cable to move parallel with the stem. Stem movement can also be monitored using an LVDT (linear variable differential transformer) or optical measurement devices.

Limit switch and solenoid valve actuation times can be monitored using voltage sensing circuitry. These test signatures can be used for verification of proper switch settings and to check the response time of an actuator after energizing the solenoid. Upstream and downstream system pressures can be monitored with external pressure transducers using the input jacks designed for this purpose. An external thermocouple can also be used with its appropriate input jack.

SYSTEM DESCRIPTION: The following two sections discuss a specific diagnostic test system and the analysis of the data from this system. The system (See Figure 1.) is a 16 channel microprocessor-based diagnostic acquisition module. This module interfaces with a portable industrial computer. The industrial computer has both a hardrive and a 3.5-inch disc drive. A full size, full function keyboard is used to operate the menu-driven software. The data aquisition module has the capability to monitor eleven different parameters and is composed of electronic circuitry, pressure transducers, a current and volt meter, pneumatic tubing and solenoid valves. The module has two different electro-pneumatic converters that can be selected to control AOVs that are pneumatic only. These signal converters are designed to be interchangeable due to the number of different pneumatic and electrical signals used in various industries. The unit also has a built-in pneumatic pressure calibrator. Prior to data acquisition, the diagnostic system is calibrated to the valve actuator assembly.

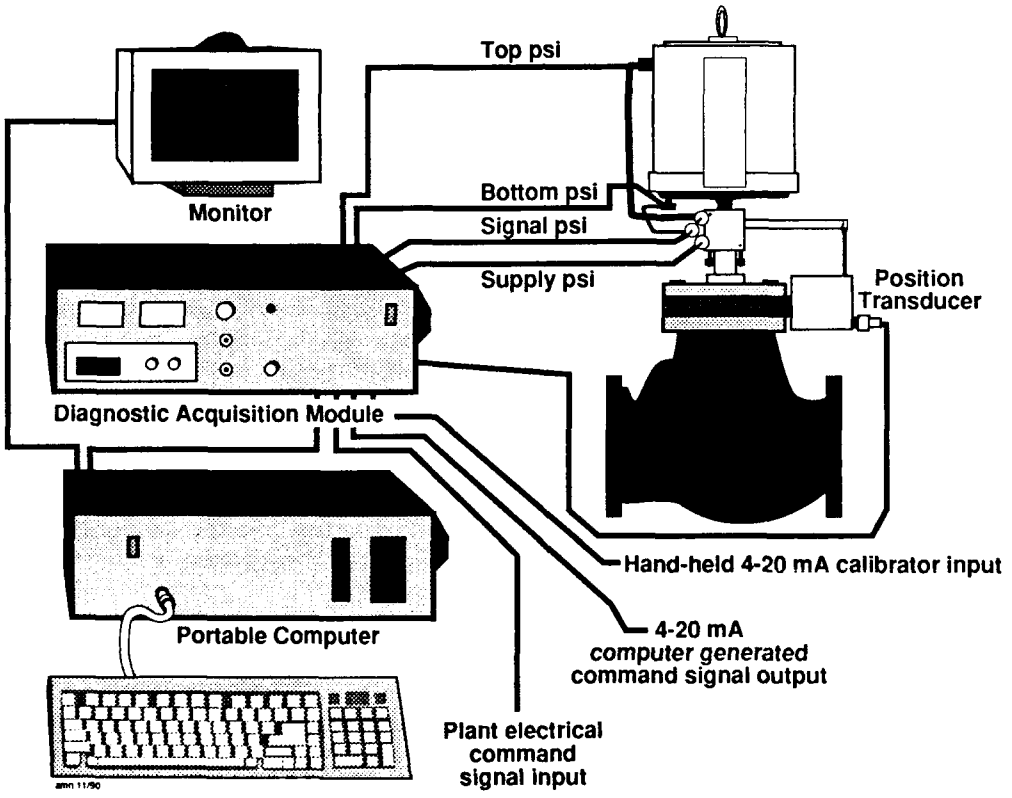

Figure 1. AOV Diagnostic System

SIGNATURE ACQUISITION AND CHARACTERIZATION: This system can display up to sixteen signatures traces at one time. The acquisition display is in real time on an EGA color monitor and the traces are color coded for easy identification. The acquisition screen has a percent scale (for position and pressure) on the left "Y" axis and a pressure scale in psi on the right "Y" axis. Time in seconds is on the "X" axis. In characterizing the signature traces (See Figure 2 for typical signatures.), the positioner supply pressure will be considered first. This is the source of the pneumatic force. The supply pressure trace normally will be a stable horizontal line that may dip down somewhere near the beginning of the stroke. The dip (point A) is an indication of the demand on the supply volume. If this minimum pressure decreases over time, it is an indication of a clogging air filter.

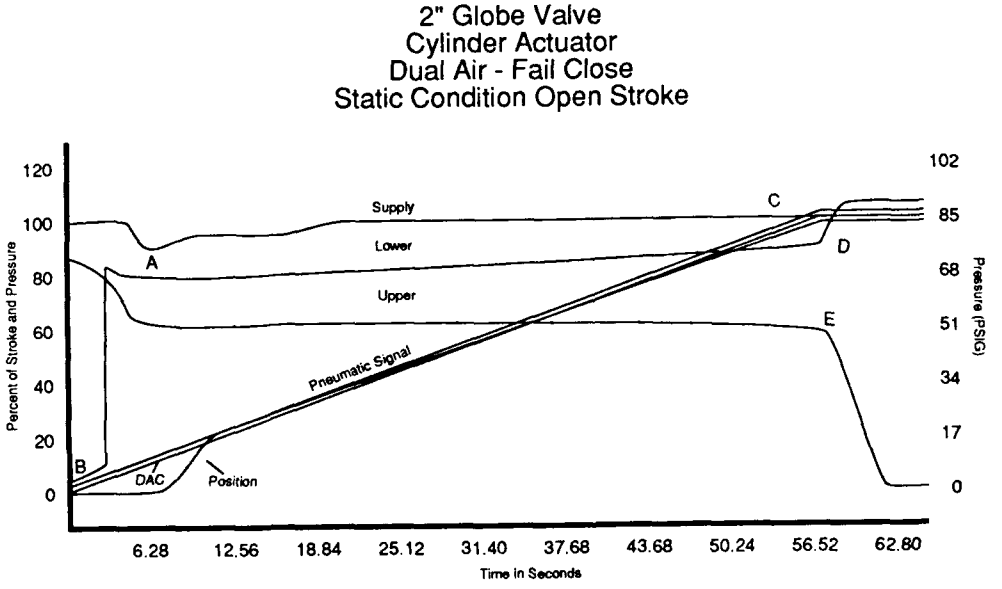

Figure 2. Normal Signature Set

Figure 3 shows the effects of a seriously restricted air supply line. The drop in supply pressure is greater than normal. The applied pressure trace is very rounded during the first 20 percent instead of being a sharp peak that levels off. The applied pressure gradually increases, moving the valve stem slower than normal. Also the difference in magnitude of the upper and lower cylinder pressures is much less than normal.

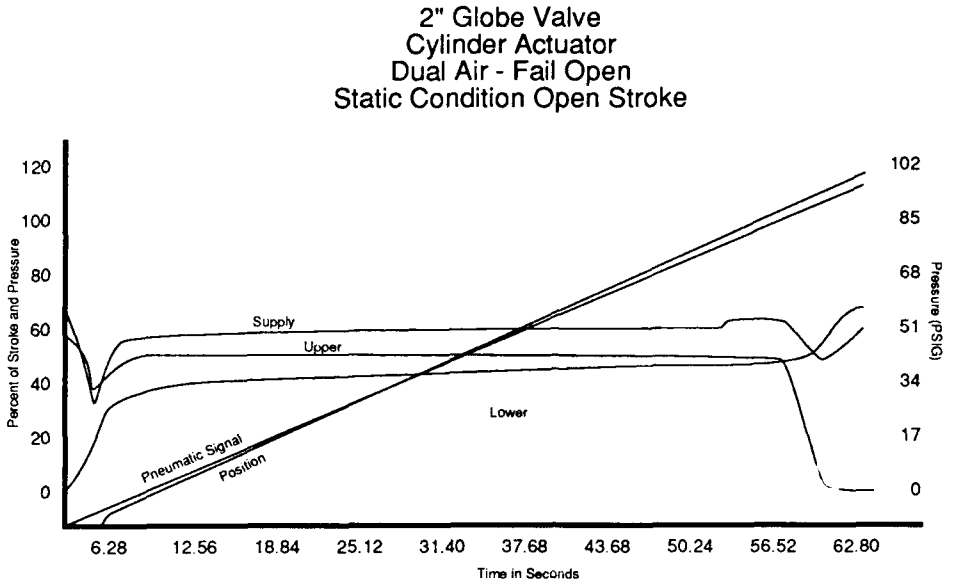

Figure 3. Restriction in Supply Line

Top or bottom output pressure (to the diaphragm or piston) signatures vary with regard to the type of actuator and its application. On diaphragm air-to-close actuators, the applied pressure trace starts at zero psi (open position) and increases quickly for a step change signal or gradually increases on a ramped signal until the valve hits the seat, and at that time, the pressure would begin to increase at a greater slope. An air-to-open diaphragm has signatures that are the inverse of the ones described above. As the valve goes open and contacts the backseat, (point C), the output pressure increases and the exhaust pressure decreases, each at a greater rate (point D and E respectively). Actuators that have upper and lower air pressures like most cylinder types will have two opposing pressure signatures. Figure 2 is a set of signatures from a cylinder type actuator. Using these pressure signatures, (from both the open and close strokes), packing loads, spring characteristics, and stem thrust can be determined.

Figure 4 shows 3 different parameters from 2 different tests on the same valve. These parameters are upper and lower cylinder pressures and stem-position. The changes between tests reveal the increased stem loads caused by tightening the packing. The solid line signatures represent the baseline test data and the dotted signatures represent the data acquired after the packing adjustment. The output pressure level increased, and the exhaust pressure level decreased. The stem position signature shows that it took longer for the stem to overcome static friction forces after the packing load was increased.

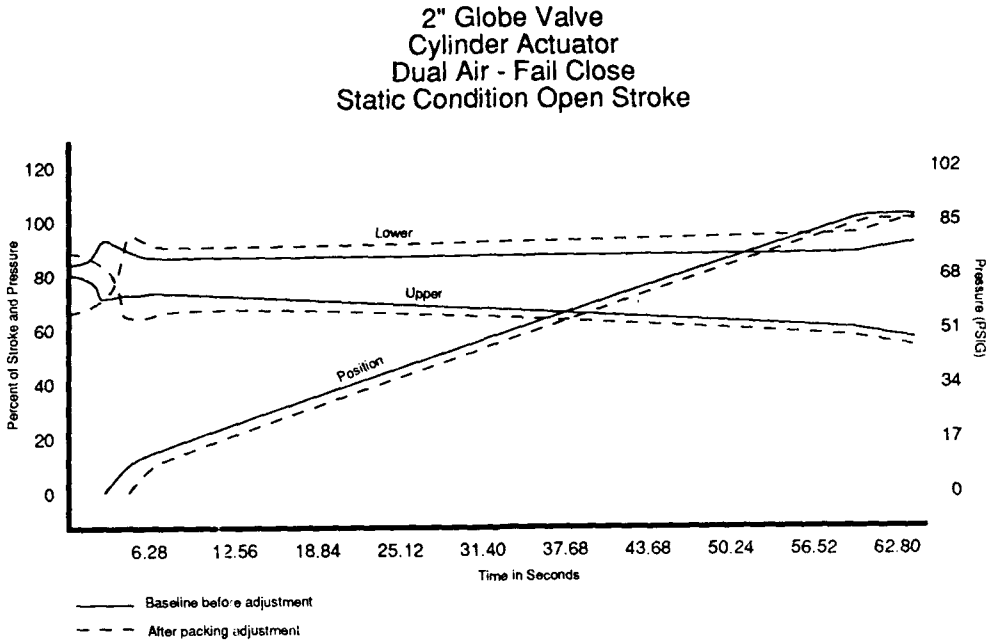

Figure 4. Packing Load Increase

The pneumatic command signal is a diagonal trace that should be linear and should parallel the computer generated digital to analog conversion (DAC) signal. Nonlinear deviations in the pneumatic signal could indicate that the electro-pneumatic signal converter is dirty or out of calibration. This could also indicate significant fluctuations in the supply pressure.

There is usually a small portion, maybe 5 - 10 percent of the stroke, that is nonlinear. This normally occurs at the minimum signal area. The data acquisition module produces a 4- to 20-milliamp signal and sends it to the valve positioner through the AOV's electro-pneumatic convertor. If the valve is pneumatic only, then the electrical signal is sent to an internal signal convertor, which produces a pneumatic output signal. This pneumatic signal is then sent to the test valve's positioner. The system has two built-in electro-pneumatic convertors, and another device that has the capability to convert the system's 4- to 20-milliamp signal to any other electrical signal used by a plant (i.e., 0 to 10 volt, etc.). This makes the system very universal.

The 2 diagonal command signal traces can be compared to the stem position trace that is also diagonal. The position signature should parallel the command signal traces if calibration of the positioner is correct. The solenoid and switch signatures are straight line traces with step changes that identify the actuation times.

ANALYSIS TECHNIQUES: Many methods are available for analysis of these signatures. The test data can be displayed as one complete test, or any combination of like signatures can be displayed for comparison. Eight signatures of the same parameters can be compared at one time. This feature is beneficial in trending of problem or potentially degrading air-operated valves. All signatures can be expanded for a detailed analysis.

The use of a mouse or trackball device is designed into the system for convenience and ease. The mouse can be used to select a region that is to be expanded. The mouse can be used to control cursor movement. When the cursor is moved to any point, there is an automatic display of three parameters: stem movement (position) in percent (0 - 100%), pressure in percent (0 - 100%), and pressure in psi (0 - 120 psi).

Manual analysis can be performed in several ways. The signatures can be compared to a baseline signature and parameters can be measured manually. Using guidelines that have been developed through testing and research, the numeric values of each parameter can be examined and determined acceptable or unacceptable. Each signature should have a certain relationship with the others. When trending signature sets of the same valve, any significant change in relationship between these signatures would indicate a degrading component. A mathematical comparison can be performed on the data, comparing it to standard engineering force equations to determine deviations. Signatures can be visually inspected for certain obvious degradations based on analysis guidelines.

An automated analysis program has also been developed. This software will generates reports describing the standard performance characteristics of the AOV. The software is capable of determining the following information from the AOV system output data:

- Calculate and display stroke time following each stroke.
- Calculate and display stem travel in inches.
- Calculate and plot stem thrust for the entire stroke time.
- Calculate and display packing load at several points during the stroke. This will require that the software overlay opening and closing signatures using stem position as a reference.
- Calculate and display spring rate.
- Calculate and display spring force.
- Calculate and display spring force margin.
- Calculate and display spring preload.
- Calculate and display solenoid actuation time.
- Calculate and display limit switch actuation time.
- Determine if leaks are present in diaphragm or cylinder, tubing, seals, and gaskets.
- Determine if supply air is insufficient or filter is clogged.
- Determine linearity and hysteresis of the positioner.
- Determine if calibration of positioner is incorrect.

The analysis software will provide the capability to overlay signatures from test to test and identify changes between tests. The data acquisition and automated analysis programs are user friendly and are designed to be used by maintenance personnel and engineers alike.

CONCLUSION

Plant or system operations can be adversely affected by AOV failures. Determining the exact root cause of the failure can be difficult and time consuming. An automated diagnostic test system can quickly identify the root causes of problems allowing for a timely and cost effective response to the situation. Further, diagnostics can help in predicting future problems and aid in the scheduling of maintenance. Valve/actuator specifications, maintenance and performance history can be stored and easily recalled when needed. Diagnostic testing has become a vital part of effective plant maintenance programs.

SYSTEMS FAILURE ANALYSES - CASE HISTORIES

Chairman: Cedric A. Beachem
Naval Research Laboratory

ANALYSIS OF THE FRACTURE OF AN AIRCRAFT WING

D.A. Meyn & R.A. Bayles
Code 6327
Naval Research Laboratory
Washington, DC 20375-5000

Abstract: Separation of an aircraft wing in flight resulted in a concentrated effort to ascertain the cause of failure and whether the cause involved an inspectable flaw. The fracture origin was located near the trailing edge of the lower wing skin, which is the major tensile structural element of the wing, at a point just outboard of the fuselage attachment. Failure was first thought to have initiated by fatigue at a fastener hole near the aft edge in the full-thickness part of the plate. Re-examination proved that larger fatigue cracks initiating at a hole closer to the aft edge of the skin, in a thin extension tab not part of the main load carrying section, had propagated into the thicker section leading to complete wing fracture. The process of discovery and fracture analysis, the characteristics of the actual origin of fracture which initially masked its importance, and the presence of an unusual overload-induced fatigue-like thumbnail crack found in another fastener hole are described.

Key Words: Aircraft; Aluminum alloy 7075; Failure analysis; Fatigue; Fractography

Introduction: The catastrophic loss of a wing from an aircraft in flight is a rare event, and is cause for considerable re-evaluation of the aircraft type's fitness for continued use. Separation of the port (left) wing in this case caused the aircraft to explode in a fireball before impact; fortunately for purposes of failure analysis the aircraft came to rest with the port side down so that the portion of the wing stub still attached to the fuselage was buried in the earth and therefore was protected from further effects of fire. The wing itself landed some distance from the aircraft, suffering mechanical and abrasion damage from its impact with the ground. The wing structure can be pictured as a box beam of smoothly varying aerodynamic cross-section, with longitudinal beams machined integrally in the internal surfaces of the lower skin, and both longitudinal and lateral stiffeners attached between the upper and lower skins by threaded fasteners or rivets. During flight, the upper skin is in compression, the lower skin in tension. The lower skin is 7075-T651 aluminum plate of substantial thickness varying from 9 to 16 mm, and comprises the main tensile element of the wing supporting the weight of the fuselage in flight. An accident investigation team examined the area of impact, removed all parts of the aircraft which could be identified and recovered to a repair facility, where a preliminary examination confirmed that wing separation initiated somewhere in the trailing edge portion of the lower skin, probably at a fastener hole at the aft edge of the main thickness section of the plate. A number of segments from the lower skin of the port wing including this area were brought to NRL for detailed analysis of fatigue cracks around suspect fastener holes in this area.

Methodology: The pieces of fracture surface were first photographed to provide a record of the overall appearance of the important areas, with special attention to the vicinity of fastener holes, where fatigue or stress-corrosion cracks nearly always initiate in wing structures. After a thorough macroscopic examination, smaller pieces were cut where fatigue cracks appeared to have initiated, cleaned by rinsing in organic solvents (acetone, alcohol) then mounted for examination in a scanning electron microscope (SEM). Pieces cut from near the suspect fatigue areas were prepared for

metallographic examination, hardness testing, and compositional analysis by X-ray fluorescence. In some cases, it was necessary to use paint strippers (a mixture of organic solvents) in an ultrasonic cleaner to remove paint and other coatings which interfered with SEM examination. All SEM specimens were examined without metallization of the fracture surfaces. Any areas having signs of corrosion damage or deposits were handled with special care so that any residues could be chemically analyzed in the SEM.

Material Analysis: Metallographic examination indicated no abnormalities in the microstructure, which corresponded to 7075-T651. Chemical analysis using an x-ray fluorescence spectrometer showed a good match with 7075 aluminum alloy Standard Reference Material from the National Institute of Standards and Technology except that the zinc content was slightly high. The hardness was Rockwell B 88 which is within the expected range for this material.

Description of The Fracture: The fracture propagated perpendicular to the wing longitudinal axis, near the root or fuselage-wing transition area, **Fig. 1**. In the following description, the inboard fracture refers to the wing stub which remained with the fuselage, the outboard fracture denotes the mating fracture attached to the departed wing. **Fig. 2** is a sketch of the inboard fracture at the trailing edge of the lower skin plate, looking down on the fracture surface. The relatively thin aft portion (at right) is an extension tab of the main plate section which serves as an attachment point for the thin aerodynamic fairing which closes the trailing edge. Both holes B3 and A5 had small thumbnail fatigue cracks, **Figs. 3** and **4**, and the primary failure investigation laboratory concluded that the failure crack had initiated from one of these. However, preliminary stress analysis using simple fracture mechanics concepts showed very high stresses were needed to cause mechanical overload fracture from these small cracks, the largest of which, on the forward side of B3, was 1.14 mm deep. NRL was asked to make fatigue striation counts on the fatigue cracks at holes B3 and A5. While this work was in progress, NRL received a portion of the inboard fracture which included a region between holes B3 and C1 missing from materials previously received. Macroscopic examination showed that high-stress fatigue cracking had occurred between holes C1 and B3, and that the crack had propagated forward from hole C1 (partly missing and heat-damaged) to hole B3.

NRL requested and received the less-damaged outboard fracture of the thin aft extension tab containing hole C1. The fracture surfaces on either side of hole C1, **Fig. 5**, were difficult to identify macroscopically as fatigue, because of their surface texture, which was somewhat rougher than is usual for fatigue cracks. Examination in a high-resolution field-emission SEM identified scattered patches of fatigue striations, **Fig. 6**, obscured by burnishing caused by the two mating surfaces rubbing together, and by localized damage from small particles trapped in the crack. Fatigue striations continued aft from hole C1 about 5 mm, the remaining fracture being microvoid coalescence (MVC). Striations were observed up to 5.8 mm forward from C1, followed by MVC to a point 6 mm aft of the thickness transition from which point alternating bands of fatigue and MVC, **Figs. 2 & 3**, propagated into the aft side of hole B3. The initiation area in hole C1 showed no defects such as corrosion or metallurgical anomalies which might have contributed to early fatigue crack initiation. The appearance of the hole and the cracks was consistent with ordinary mechanical fatigue.

These discoveries changed the course of the investigation. By careful study of the small cracks in hole B3, and their relationship to the crack spreading forward from C1 to B3, it was proven that cracking initiating from C1 overran the cracks in B3. The striations at the terminus of the largest B3 crack were uniformly fine, **Fig. 7**, showing no acceleration at the fatigue-overload interface, only a stretch zone. All other cracks in

B3, and those on the aft side of A5, showed the same characteristics. The sequence of fracture on the aft side of B3 was complex; the crack from C1 broke into B3 through only half the plate thickness, then reinitiated from small fatigue cracks in the other half of the thickness and ran aft to complete the fracture aft of B3 (arrows, **Fig.2**). The plate section from the forward side of hole B3 to the aft side of hole A5 then fractured, and the crack apparently arrested temporarily in hole A5. Cracks in the forward side of hole A5 had very coarse striations, even near the the initiation edge, **Fig. 8**, and the hole bore in this area had numerous small gaping cracks indicative of high local stresses. Striations between 0.4 and 0.75 mm from the edge were mixed with MVC. Burnished MVC existed from 0.75 to 2.0 mm, suggesting a short burst of overload fracture followed by arrest for several load cycles before final fracture. This burnished MVC macroscopically resembled fatigue. The remainder of the wing fracture was overload, with no further indications of crack arrest.

Other Features: Hemispherical indents were found on both surfaces in the fracture surface regions (overload as well as fatigue) fore and aft of hole C1 in the tab, which considerably obscured the striations. The uniform size and smoothness of these indents and the fact that they could be matched on mating surfaces indicate that they were there before the mishap. The indents ranged in diameter from 30 to 60 μm, and were more numerous in the fracture surface aft of hole C1, becoming sparser and finally ceasing about 10.5 mm forward of hole C1. These indents were probably caused by glass beads used for stripping paint during tear-down and re-work of the aircraft, indicating, though not proving, that cracks then existed at C1.

Fatigue cracks were found later in many other fastener holes in the lower skin remote from the failure crack, but none apparently near critical size. One such crack, **Fig. 9**, was macroscopically identified as fatigue, but after considerable SEM study it was found to be entirely MVC, devoid of arrest markings, flattened and burnished to fatigue-like surface texture by repeated mutual rubbing of the mating crack surfaces, very much like the burnished MVC portion of the forward crack at hole A5 above. Evidently, an abnormally high local stress pulse "popped" open an MVC crack, which arrested spontaneously and never subsequently propagated.

Discussion and Conclusions: The failure-initiating fatigue cracks were ultimately located in the lower skin aft extension tab, which was not intended to carry any considerable stresses, and which for that reason was not carefully inspected during overhaul. Certainly cracks on either side of hole C1 as small as 2 mm, which would be through-thickness, should be inspectable by conventional techniques such as fluorescent penetrant, provided the fairing is removed. However, in the absence of a compelling motive, such as provided by the present findings, such comprehensive inspection would not routinely be done as part of overhaul.

The keys to properly evaluating the cause and locus of initiation were the suspicion that existing cracks in holes B3 and A5 were too small to have led to mechanical overload failure at any reasonable stress, the realization that the alternating bands of fatigue and overload were propagating forward toward hole B3, rather than aft away from the hole, and the possession of a SEM with exceptionally good resolution, with which to detect poorly defined striations in an area around hole C1 that did not macroscopically look very much like a fatigue crack. The area of hole C1 was originally overlooked in part because it was not considered to be in the main structural stress path of the lower skin plate. It is probable that a certain amount of structural analysis naivete on the part of NRL investigators assisted in the discovery of fatigue cracks in an area where none should have been found.

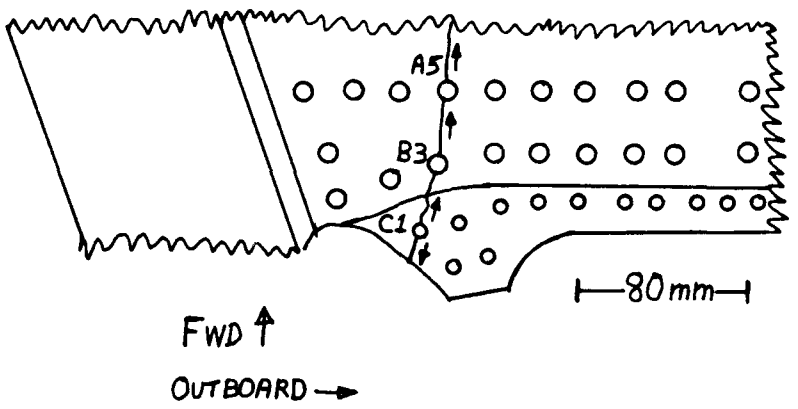

1. Sketch of portion of the lower skin where failure initiated, looking up from under the aircraft. The round circles are fastener holes, sizes exaggerated.

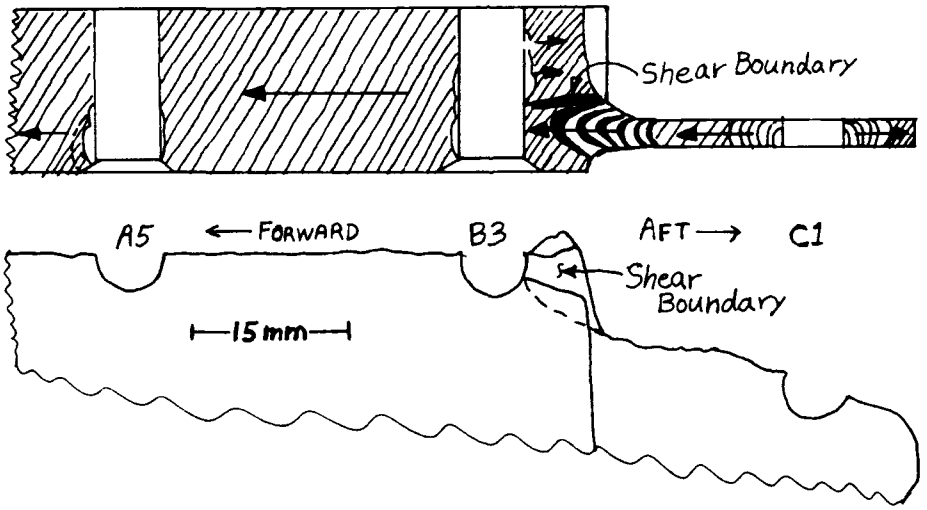

2. Sketch of the fracture surface in the origin area in plan (top) and profile (bottom). Failure crack initiated in hole C1, propagation directions are shown by arrows. Cross-hatching denotes MVC, other areas are fatigue. Dotted line at forward side, hole A5, indicates end of burnished MVC (see text).

3. Hole B3, showing small fatigue cracks (lighter strips at hole bore, upper right and lower left), alternating bands of fatigue (light) and MVC (dark) to right of hole. Arrows point to one fatigue band. Left = forward in all macrophotos.

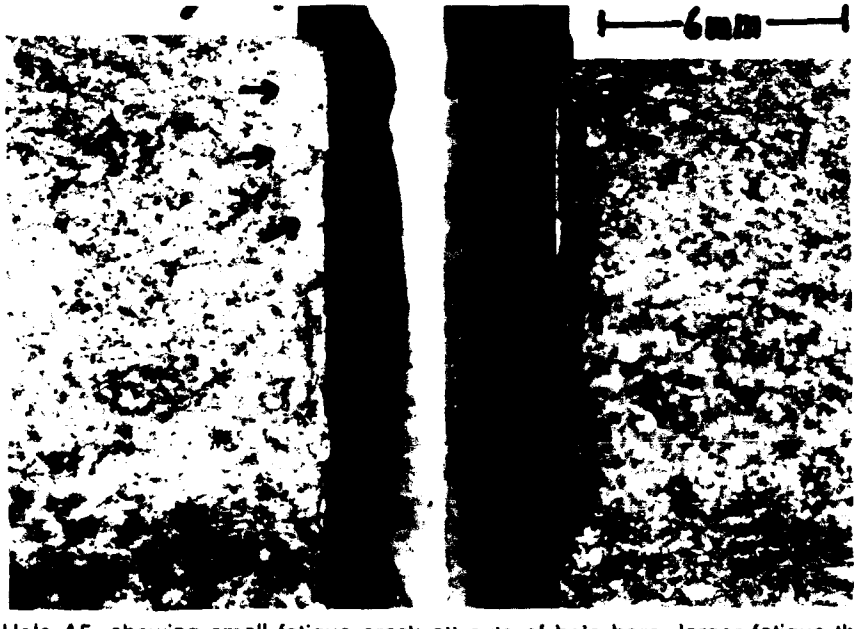

4. Hole A5, showing small fatigue crack at side of hole bore, larger fatigue-then-MVC crack forward, outlined by arrows. Final 2/3 of larger crack is burnished MVC (see text).

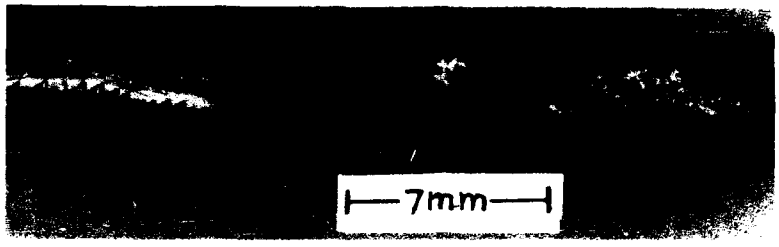

5. Hole C1, showing atypical appearance of fatigue areas, which extend 5 mm aft and 5.8 mm forward from hole. Part of the fracture surface forward of the hole is damaged. The forward hole bore surface has been upset by contact with the fastener.

6. SEM fractograph of rare undamaged patch of striations near forward edge of hole C1. Large arrow indicates macroscopic crack propagation direction in all fractographs.

7. Fine striations in the largest fatigue crack in hole B3, forward side, near hole bore.

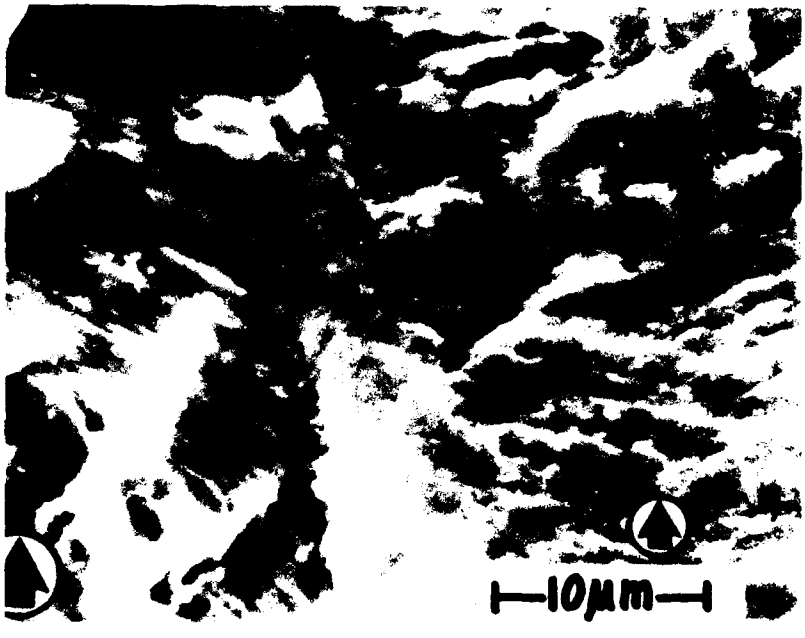

8. Coarse striations in forward side of hole A5, near hole bore. Compare with Fig. 7.

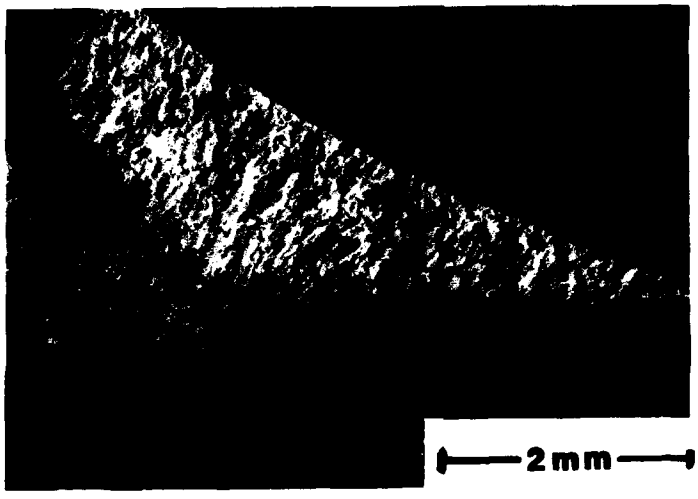

9. Fatigue-like crack found in a fastener hole remote from the fracture area, resulting from MVC pop-in which then arrested and became burnished by repeated rubbing of mating surfaces. Compare with Fig. 4.

DYNAMIC ANALYSIS OF A VERTICAL NUCLEAR WATER PUMP FOR ENHANCEMENT OF PUMP LIFE

By
E. J. Gunter
University of Virginia, Charlottesville
J. T. O'Brien
Philadelphia Electric Company
J. T. O'Brien, Jr.
J. Weil Company, Philadelphia, PA

ABSTRACT

This paper deals with the static and dynamic simulation of a vertical motor-pump system using the transfer matrix and the finite element methods on a microcomputer. This particular class of vertical motor water pump has experienced thermal cracking near the pump bearing bracket support. The object of the study was to examine the possibility that static and dynamical loads on the motor-pump system could increase the rate of crack propagation.

A critical speed analysis of the motor-pump system with casing effects was performed using the transfer matrix method. These mode shapes matched experimentally determined data. A finite element model was developed using MSC/PAL2 which gave excellent agreement with the transfer matrix analysis. Using the finite element model, the axial and torsional natural frequencies of the pump were also determined. The stresses at the bearing cartridge were analyzed under various combinations of axial, radial and torsional moments. It was concluded that the combined action of torsional and radial loading could enhance the rate of crack propagation observed in this class of pump.

BACKGROUND AND INTRODUCTION

Figure 1 represents a schematic diagram of a vertical water pump driven by a variable speed motor. This class of pump which has been in operation for over ten years has been experiencing cracks and shaft failure above the hydrostatic pump journal bearing. There is a large thermal gradient at this location which has led to thermal shaft cracking (*Kowal*). However, the theory of thermal shaft cracking has not been sufficient to explain the complete mechanical failure at this location. Attempts to redesign the seal to alleviate the thermal stress cracking problem has resulted in some pump lives being reduced by over 60%.

Vibration instrumentation have been placed on several of these pumps to determine if there are any vibrational modes of motion existing in the system (*Begian*). Figure 2 represents the location of various transducers placed upon the motor-pump system. Accelerometers have been placed upon the upper motor casing and displacement probes have been placed at the coupling to monitor the shaft motion.

Various spectra have been obtained on the pump under different conditions of speed and loading. Figure 3 represents the spectrum for start-up at (A) 387 RPM low speed, (B) 653 RPM, and at the operating speed range of (C) 1,183 RPM. The motor bearings in this system are plain journal bearings. In Figure A, half frequency oil film whirl is shown in the system. Also, a 5X is illustrated. As the pump increases in speed and the loading on the impeller increases, Figure B shows that the half frequency whirl diminishes but that there is substantial 5X excitation on the pump. As the speed of the rotor increases to 1,183 RPM, it is seen that the 5X excitation reduces by a factor of 3. The high value of the 5X excitation at 653 RPM is indicative of an excitation of a resonance frequency in this system.

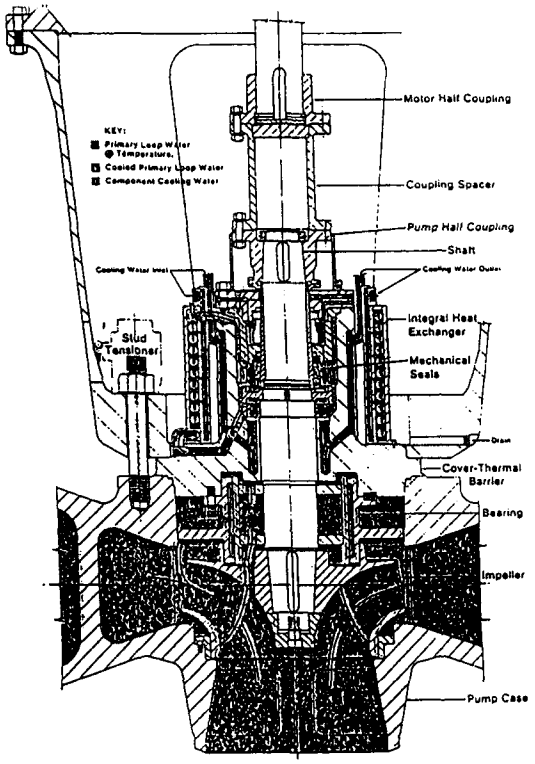

Fig. 1 Schematic Diagram of a Vertical Water Pump

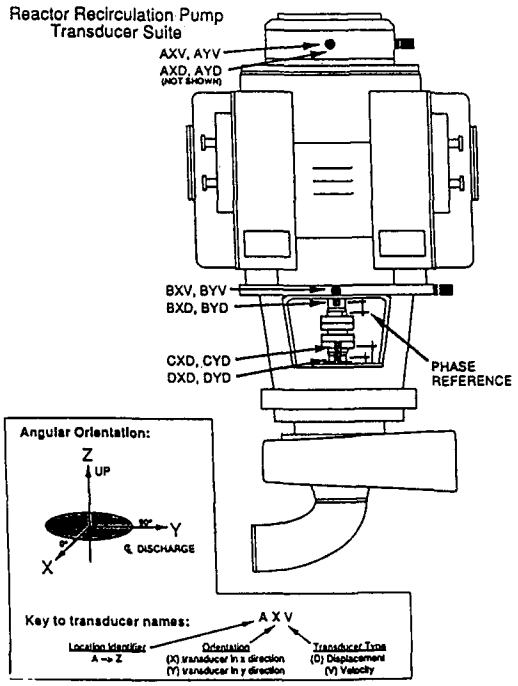

Fig. 2 Location of Various Transducers on Motor-Pump System

Figure 4 represents the amplitude at the shaft using 5X order tracking. From the shape of the amplitude response and the phase change, it is apparent that there is a significant resonant frequency in the rotor which is being excited by the 5X pulses from the impeller. One of the objectives of this study, therefore, was to model the motor-pump system to determine the nature of the resonant frequency and to see if it contributed to the crack propagation at the bearing.

Figure 5 represents the synchronous amplitude and phase of the motor up to 1,200 RPM. It is apparent from the synchronous amplitude and response that there is no rotor critical speed in the operating speed range. However, resonant frequencies on the motor casing were observed.

From the displacements measured at various transducer locations, estimates of the pump shaft deflection were made for 1X and 5X excitation (*Kowal*). For example, Figure 6 represents the extrapolated pump shaft mode shape at 1,250 RPM based on experimental data. Figure 7 represents the 5X pump shaft deflection at 640 RPM determined by a cubic spline fit. Figure 7 represents the estimated motor-pump mode shape based on the available experimental data.

The data obtained on this pump is rather remarkable in that the amplitude and phase for 5X excitation were recorded showing the obvious existence of a higher order resonance frequency in the motor-pump system which appears to be excited by the five bladed impeller. It has been conjectured that the thermal cracks are driven by some mechanical means. It was, therefore, the object of this study to determine if static or dynamic loading could be responsible for accelerating the cracks obtained in the pump shaft due to thermal cycling.

In this study, dynamic and static analyses were performed using state-of-the-art microcomputers.

LATERAL AND TORSIONAL CRITICAL SPEEDS OF MOTOR-PUMP SYSTEM

The first procedure in the dynamic analysis of a turbo-rotor is to compute the lateral critical speeds. The lateral critical speed analysis computes the undamped natural frequencies of the system (*Prohl*). In the original design of this system, the lateral and torsional critical speeds of the combined system were not investigated since they were assumed to be above the operating speed range of the system. However, because of the experimental evidence of 5X excitation of the system, it was considered necessary to compute both the lateral and the torsional critical speeds to at least 5 times the running speed.

The critical speeds were first computed using the transfer matrix method (*Gunter*). The motor was analyzed separately to determine its critical speeds. A simulation of the pump was developed to analyze its critical speeds, and then the system modes for the combined motor-pump configuration were computed.

The critical speed analysis using the transfer matrix method has several major advantages. It is very rapid and easy to perform on a turbo-rotor. From the analysis of the critical speeds, one can determine the kinetic and strain energy distributions in the system for the various modes. It is also possible to include foundation mass effects with the pump. The inclusion of foundation mass effects can significantly alter the critical speeds (*Kazao*). The transfer matrix method, however, has a major limitation in the complexity of the rotor and casing model that one is able to incorporate into the system.

In this phase of the study, the parametric study of the critical speeds of the motor-pump system were analyzed with various combinations of pump and motor weights. It was found that under certain circumstances, there could be two critical speeds of the system at close to the same frequency. It is therefore possible to miss the first two critical speeds of the system due to the nature of the search procedure for the undamped roots. Such a problem is not encountered with the finite element method.

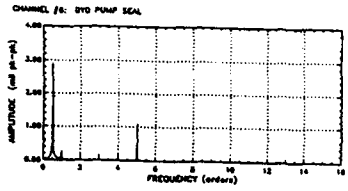

A: Shaft Vibration at 387 RPM Showing Large Half-Frequency Whirl Component

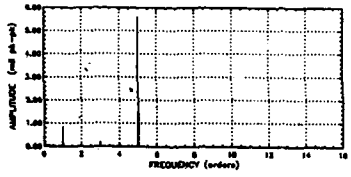

B: Shaft Vibration at 653 RPM Showing Large 5X Component

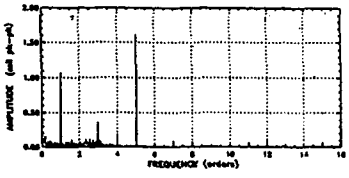

C: Shaft Vibration at 1183 RPM Showing Synchronous (1X)
and Reduced 5X Component

Fig. 3 Vibration Characteristics of Pump Seal at Various Speeds

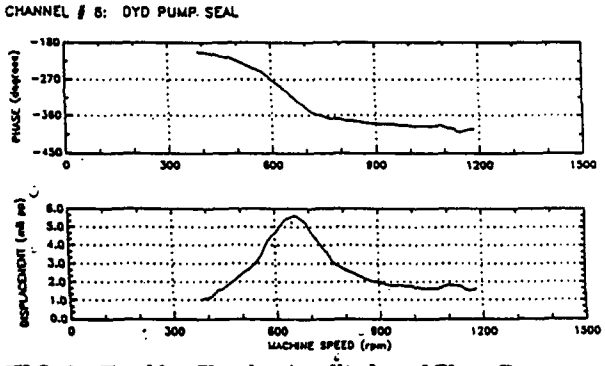

Fig. 4 5X Order Tracking Showing Amplitude and Phase Response at the Shaft

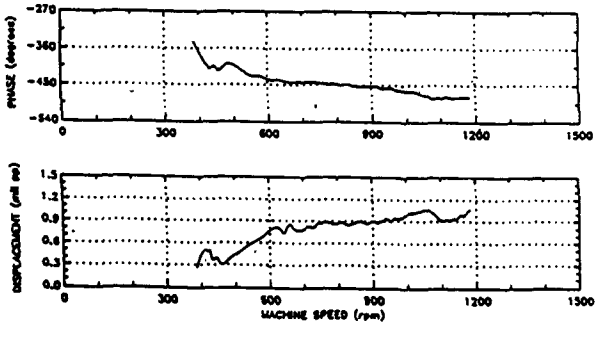

Fig. 5 Pump Startup Synchronous Amplitude and Phase

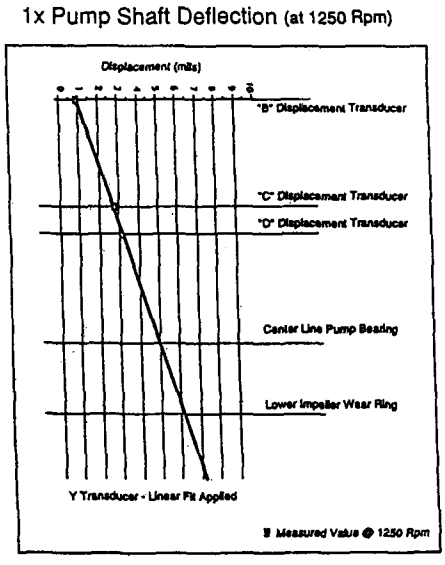

Fig. 6 Extrapolated Pump Shaft Mode Shape Based on Experimental Data

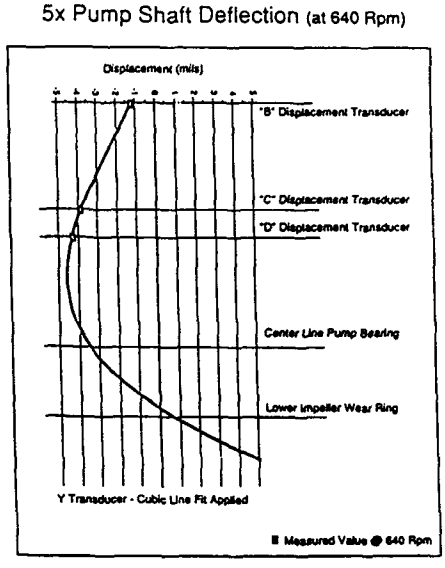

Fig. 7 5X Pump Shaft Deflection (at 640 RPM)

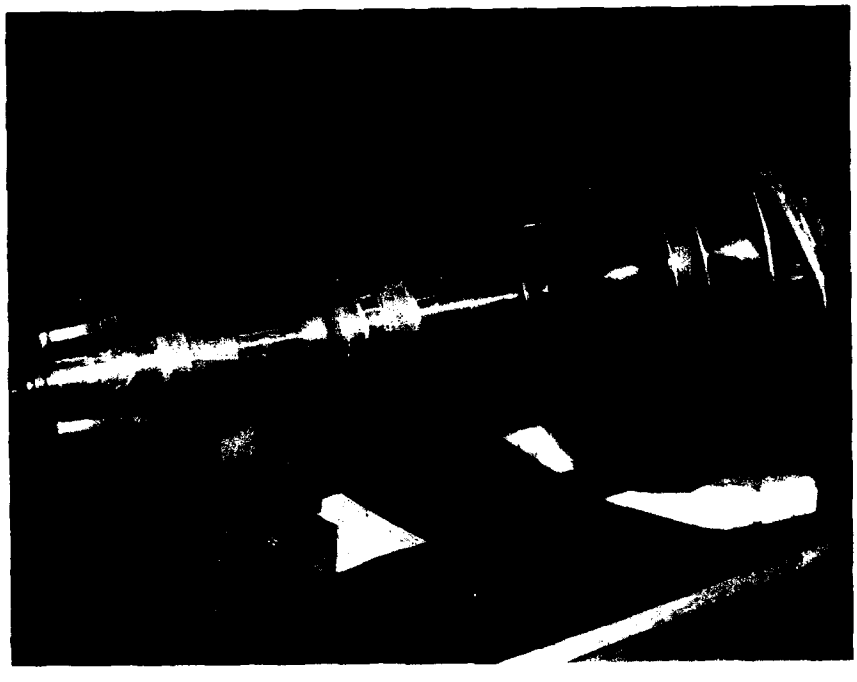

Fig. 8 Photograph of Pump

Critical Speed Analysis of Motor

A model was developed of the motor based on the manufacturer's drawings. The diameter and dimensions of the shaft were given along with the total rotor weight and the polar moment of inertia. The motor polar moment of inertia was given as I_p = 18,000 lb-ft^2 and the motor rotor weight was given as 12,600 lb.

The motor was developed as an eighteen station model. The motor windings, in general, are not assumed to contribute significantly to the shaft stiffness. The motor windings were approximated by attached disks with a density of 0.141 lb-in^3. The bearings were modeled by means of springs. The stiffness values of the springs matched the bearing stiffnesses. The actual motor bearings are plain cylindrical fluid film bearings.

The first motor critical speed is computed to be 2,254 RPM and the second critical is 8,378 RPM. The value of the first mode is very close to the listed motor manufacturer's first critical speed of 2,300 RPM. Therefore, it is considered that a reasonably accurate motor model has been generated. For the motor, it is seen that 58% of the strain energy is in the bending of the shaft and 41% of the strain energy is in the bearings. The motor polar and transverse moments of inertia have very little effect on the rotor first critical speed. The motor polar moment of inertia, however, is extremely important in order to correctly calculate the complete motor-pump torsional critical speeds. Since the gyroscopic energy in the motor is extremely small, this implies that the motor may be adequately modeled using finite element techniques as will be discussed in later sections. The finite element procedure on most microcomputers does not allow the input of gyroscopic matrices. The mainframe version of NASTRAN, of which PAL2 is a derivative, however, will allow the input of skew symmetric damping matrices which can simulate gyroscopic effects. However, for the case of the modeling of the motor with the PAL2 finite element technique, the gyroscopic effects for prediction of critical speeds is not essential. The proper treatment of disc gyroscopic effects in finite element analysis of rotors is presented by Ruhl in his PhD Dissertation in 1970.

Critical Speed Analysis of Pump

The second phase of the critical speed modeling consists of developing a critical speed model for the pump alone. From the manufacturer's drawings of the pump and its specified weights for the shaft and impeller, a three bearing model was constructed. The total weight of the pump is 2,600 lbs. Figure 8 is a photograph of the pump shaft. The pump is comprised of three components: the pump shaft, the bearing ring and the impeller itself. The bearing configuration consists of two rings attached to the basic shaft. The two rings support the outer cylinder which forms the surface for the hydrostatic pump bearing. At the end of the shaft is attached the 5 bladed impeller.

Figure 9 represents a schematic representation of the pump cross section. The pump model is comprised of 27 mass stations. At the left end of the shaft with the coupling, a bearing stiffness of 0.5E6 lb/in. was assumed to approximate the influence of the motor. At the pump bearing location, several models were considered. In the first model, the bearing was divided into two stations because of the length of the hydrostatic bearing. The length of the hydrostatic bearing is over 12 inches. Therefore, it was considered appropriate to consider the bearing distributed at two stations along the journal.

The assumed bearing stiffness values are 0.5E6 lb/in. This would make the total effective hydrostatic bearing stiffness equal to 1.0E6 lb/in. The pump manufacturer's stated stiffness for the hydrostatic bearing was between 0.7E6 lb/in. The first critical speed was found to be 3,289 RPM and the second critical speed to be 6,252 RPM.

Figure 10 represents the animated mode shape for the 1st critical speed. Note that the computed 1st critical speed of 3,289 RPM matches very well with the observed critical speed in the pump caused by

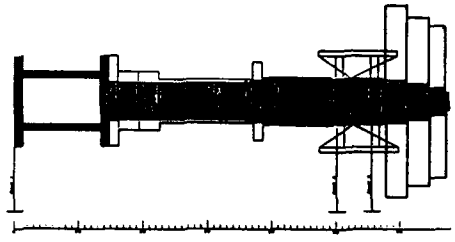

Fig. 9 Schematic Representation of Pump Cross Section

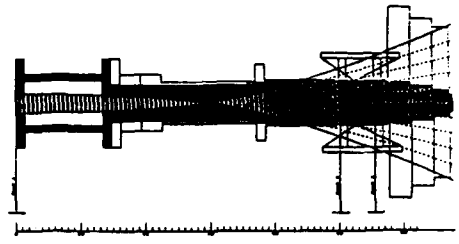

Fig. 10 Animated Mode Shape of First Critical Speed for Pump

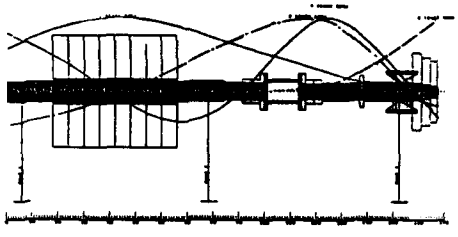

Fig. 11 Combined Motor-Pump Model with Mode Shapes

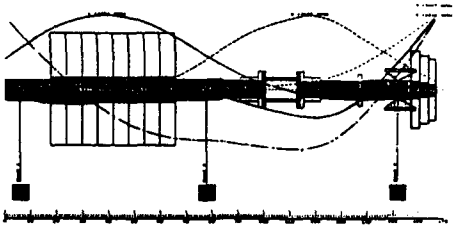

Fig. 12 Mode Shapes of Combined Motor-Pump Model with Foundation Effects

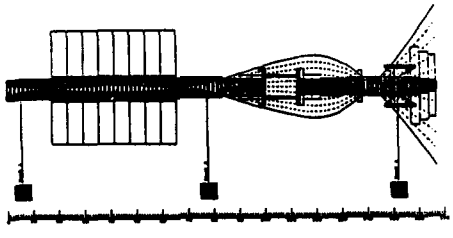

Fig. 13 Mode Shape of Fourth Critical Speed

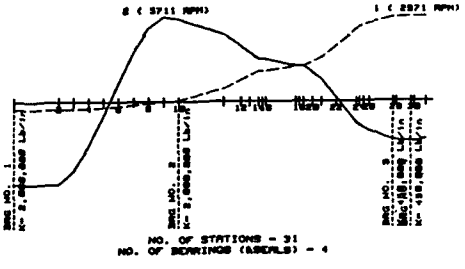

Fig. 14 Motor-Pump 1st and 2nd Torsional Modes at 2,971 CPM and 5,711 CPM

5X excitation. However, it should be emphasized that this model does not contain the motor characteristics or the motor-pump casing effects.

It is of interest to note that the strain energy of the assumed bearing at the motor end is only 2.4%. Therefore, the influence of the motor on the first critical speed has only a minimal effect. The hydrostatic pump bearing, which is divided into two sections has 28.4% and 52.7% of the strain energy distributed between them. Therefore, the total pump bearing strain energy is over 81%. Hence, the first pump model, considered without pump casing effects is highly dependent upon the total pump bearing stiffness. The pump bearing is a hydrostatic bearing design which is dependent upon the discharge pressure of the impeller. Therefore, the hydrostatic bearing stiffness may vary with speed due to the operating characteristics of the impeller.

In the pump critical speed analysis, the gyroscopic energy of the impeller is less than 7% for the first mode. For the speed range of operation assumed, and since the impeller is a mixed flow design in which the polar moment of inertia I_p is not much larger than the transverse moment of inertia I_t, the gyroscopic energy of the impeller is minimal.

Critical Speed Analysis of Combined Motor-Pump Without Foundation Effects

A combined motor-pump critical speed analysis was computed. In this model the hydrostatic bearing has been treated as one bearing to check the effects of just one bearing. Little difference was observed between the two models. Figure 11 represents the motor-pump critical speeds assuming the motor bearings have a stiffness of 0.5E6 lb/in. each and the pump bearing has a stiffness of 0.5E6 lb/in. The first critical speed is at 1,496 RPM and is predominantly motor motion as shown in Figure 11. The second critical speed is at 2,429 RPM; with the third and fourth criticals at 3,904 RPM and 6,888 RPM respectively.

For the first critical, it is seen that 34.4%, 42.5% and 0.1% of strain energy is distributed at the upper, lower motor bearings, and the pump bearing, respectively. This means that a significant amount of strain energy is concentrated at the two motor bearings, for the first critical speed. However, for the second critical at 2,429 RPM, it is observed that there has been a switch in the strain energy distribution. We now have a mere 0.2% strain energy in the upper motor bearing and practically no strain energy in the lower motor bearing, but a significant 83.3% of strain energy is found at the pump bearing. Hence, this mode is highly dependent upon the hydrostatic pump bearing characteristics. Similar to the first critical, the third critical follows a pattern of bearing strain energy with 22.2%, 34.2% and 5.7% strain energy being distributed among the upper and lower motor and pump bearing respectively. Therefore, in this combined model, a mode in the 3,600 RPM range may be achieved by low motor bearing effective stiffness.

Critical Speed Analysis of Combined Motor-Pump With Foundation Effects

In the preceding analysis, no influence of the motor or pump casings were taken into consideration. Vibration measurements of the motor casing indicated substantial casing motion. In this particular transfer matrix model, casing effects may be simulated by lumped masses acting at the bearing stations. In this system, the motor casing weighs 26,000 lbs. and the pump casing weighs 24,000 lbs. The vertical motor is attached to the foundation near the lower motor bearing. The pump casing is suspended from the motor casing by a webbed flange. In this particular phase of the study, casing weights were assumed acting at each of the two motor bearings, and a pump casing weight of 24,000 lbs. was assumed acting at the pump bearing station.

One of the advantages of the finite element model is that a more elaborate casing model may be incorporated in the system. It was found, however, that the lumped mass casing model gave considerable insight into the dynamical behavior of the system.

Since the lower motor bearing is firmly anchored in the foundation, a motor foundation stiffness of 8.0E6 lb/in. was assumed based on past experience, while the upper motor bearing foundation was assumed to be 4.0E6 lb/in. The resonant frequencies of the foundation are computed with the inclusion of bearing and foundation stiffness and are in the range of 2,762 RPM to 5,203 RPM. These foundation resonances will interact with the fundamental rotor critical speeds to form bifurcated or split critical speeds. In a bifurcated critical speed, a lower branch is obtained in which the rotor and foundation are in phase. A second branch is obtained in which the rotor and foundation are out of phase.

Figure 12 represents the motor-pump first five modes below 7,000 RPM. The 1st motor-pump mode is essentially a motor mode at 2,071 RPM. In this mode, the motor and foundation motion are in phase. The introduction of the motor casing masses cause only a slight reduction in the motor first critical speed. The pump has very little influence on this particular mode. This mode is well damped by the fluid film motor bearings and should not be excited either by 1X or 5X pump excitation. The second mode at 2,228 RPM is essentially an overhung cantilever pump mode. Note that the experimentally measured mode as shown in Figure 6 does not appear to correspond to the first pump mode.

Figure 13 represents the system 4th mode at 3,687 RPM. This mode is also in the same frequency range as that observed experimentally at the coupling. In this mode, over 64% of the system kinetic energy is associated with the pump impeller. The pump bearing has approximately 50% of the system strain energy, and the strain energy of the motor support is only 9%. There is a 20% kinetic energy associated with the pump casing. However, by including the pump casing in the model, the mode shape has considerable changed from the mode shape of the pump alone. The mode shape now looks very similar to the estimated mode shape shown in Figure 7 based on experimental data. It is impossible to generate a mode shape similar to that shown in Figure 7 unless the pump casing effects are included in the model. This model also indicates the importance of placing accelerometer or velocity pick-ups on the pump casing in order to monitor the casing motion.

From the study performed on the critical speed analysis of the motor-pump system, it is apparent that casing or foundation mass effects may play an important roll in determining the critical speeds and the mode shapes. Therefore, it is essential to instrument the motor-pump casing as well as the shaft for the determination of the complete system mode shapes. This situation of casing interactions with the rotor modes is well known for large turbine-generators and is normally taken into consideration by the manufacturers. The casing impedance characteristics may be determined experimentally by means of an exciter and an FFT analyzer. Impedance measurements of casings and foundations is now a standard procedure in industry. As a general rule, all rotating elements over 2,000 lbs. usually have casing or foundation effects associated with them.

Therefore, it is concluded that for the proper dynamical analysis of a large vertical motor-pump system, casing-foundation effects should also be taken into consideration.

Torsional Critical Speed Analysis

Torsional critical speeds were computed for the combined motor-pump system (*Colen-Gunter*). In the original design and analysis of this system, no torsional critical speeds were computed because it was felt that they would be above the operating speed range. From the experimental data, however, it was seen that there is a substantial 5X excitation due to the interaction of the 5 bladed impeller with the single discharge volute. Therefore, torsional pulsations can be generated in the pump and it is necessary to examine the torsional critical speeds up through 5 times the operating speed range.

The evaluation of the location of the torsional critical speeds is of particular importance, especially with this type of unit. A variable frequency motor is used in which a wide range of operating speeds can be achieved. There are many circumstances when the pump must operate at part flow with a reduced speed. It is extremely important not to operate near or at the vicinity of a torsional critical

speed as torsional stresses may be greatly amplified. Figure 14 represents the 1st two torsional critical speeds of the motor-pump at 2,971 CPM and 5,711 CPM.

It is apparent from the torsional analysis that the operating speed range of 1,000 to 1,200 RPM may be undesirable because of the possible excitation of a second torsional critical speed in the operating speed range. The motor has relatively little effect on the first torsional critical speed. However, the motor has a considerable influence on the second critical speed.

LATERAL, TORSIONAL AND AXIAL NATURAL FREQUENCIES USING FINITE ELEMENT METHODS

In this study, it was determined that the rotor critical speeds, or lateral natural frequencies, may be accurately computed using finite element techniques when the disc gyroscopic effects may be ignored. By ignoring the shaft and disca gyroscopic moments, rotor critical speed simulation may be reduced to lateral beam vibrations. The model is reduced to planar motion in the X-Y plane. Gyroscopic moments may be incorporated into the mainframe NASTRAN finite element code by means of skew symmetric damping matrices. This provision, however, has not been implemented yet on any finite element PC versions.

It should be emphasized that one of the major advantages of the finite element technique is that the same model may be used for lateral, torsional and axial modes of motion by changing the constraints of the system. Also, shaft material properties may be easily varied along the rotor by means of the material properties command.

Finite Element Analysis of Motor-Pump System with Foundation Effects

One of the powerful features of the finite element procedure is the ability to put in foundation structures of considerable complexity. This is one of the major drawbacks of the transfer matrix method. In order to represent the effect of the foundation, additional nodes must be included at each bearing location. Lumped masses are placed at the nodes to simulate the motor and pump casing masses. More complex three-dimensional casing models are to be investigated.

One must be very careful when developing a finite element model with springs in series. There is no lateral stiffness across the spring interface. Therefore, one must either zero out the displacements in the out-of-plane direction or add a constraining spring. In this model, three extra node points were introduced along the axis in line with the journal bearing nodes. Stiff springs of the order of 1.0E7 lb/in. were used to constrain the casing masses in the axial direction.

In order to calculate the natural frequencies of the system, there are a number of important constraints that must be applied to the model in order not to obtain a singular stiffness matrix. The first set of constraints corresponds to the ground nodes which are zeroed out. The second set of constraints refers to the assumption of planar modes in which the out-of-plane displacements and rotations are eliminated. A very subtle constraint that must be applied is to zero out all angular rotations at the intersection of the journal bearing at the foundation. Hence, the lumped mass of the casing contains no moments of inertia, and rotational degrees of freedom are not desired. In applying this final constraint, the modes for the combined motor-pump system with foundation effects were successfully calculated. Table 1 represents the first four motor-pump nodes with foundation effects in comparison to the values obtained by the transfer matrix method. The finite element model produced unusually good agreement with the critical speed model as the errors on all those were less than 2%. The mode shapes were also in excellent agreement. Figure 15 represents the motor-pump 4th natural frequency at N = 3,724 RPM with foundation effects.

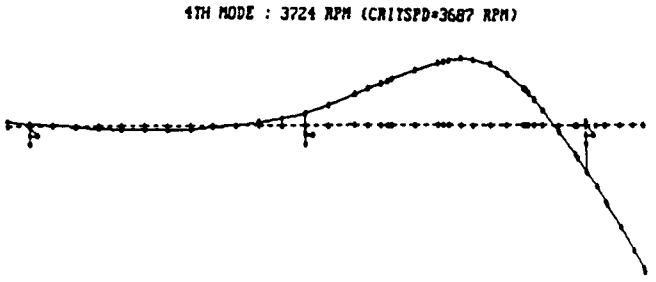

Fig. 15 Finite Element Mode Shape of First Natural Frequency (N_4 = 3,724 RPM) - Combined Model With Foundation

Mode	Transfer Matrix (RPM)	Finite Element Method (RPM)	% Error
1	2,071	2,037	1.6
2	2,228	2,248	-0.9
3	3,444	3,426	0.5
4	3,687	3,724	-1.0

Table 1 Comparison of Critical Speeds Using Transfer Matrix and Finite Element Method For Motor-Pump System With Foundation Effects

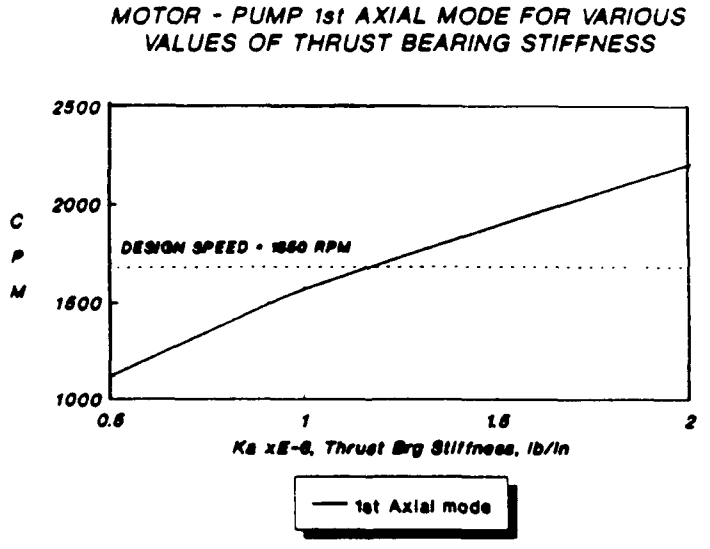

Fig. 16 Motor-Pump 1st Axial Mode for Various Values of Thrust Bearing Stiffness

Torsional Natural Frequencies of Motor-Pump System by Finite Element Method

The torsional analysis of a turbo-rotor using finite element techniques requires additional components to be added to the rotor model. In the earlier motor-pump models, the mass command was used to specify lumped masses. The finite element mass command in MSC/PAL2 may also be used to specify the principal moments of inertia of the body. The first principal moment of inertia for the X direction corresponds to the polar moment of inertia for the rotor. The polar moments of inertia were specified for the various components of the motor and pump based on calculated values of I_p from the critical speed program.

If one constrains the rotor to allow only angular motion along the axis of the shaft (i.e. the X direction), it is still not possible to calculate a torsional critical speed. The reason for this is that a singular stiffness matrix is encountered. To alleviate this problem, there are two procedures that may be used. One is to artificially constrain a node or angular rotation along the shaft and the second method is to attach a light torsional spring to the end of the shaft. If one knows beforehand, the node point at which zero angular displacement is obtained, then that node may be constrained. However, it is, in general, not desirable to constrain any nodes along the shaft as this will distort the mode shapes and the values of the torsional natural frequencies. The procedure finally arrived at to calculate the torsional natural frequencies was to connect a torsional spring to the first node point.

By attaching a light rotational spring, the stiffness matrix is no longer singular. This essentially eliminates the rigid body mode of zero frequency that is inherent in the system. At higher frequencies, the light torsional spring has no effect on the higher torsional modes.

The second and third critical speeds were computed to be 44.39 and 96.09 Hz. respectively. These modes are in error by only 4.2% and 1.4% for the second mode and third modes computed by the Holzer method. The 2nd torsional mode is strongly affected by the diameter assumed at the motor center. If, for example, an effective larger shaft diameter is assumed, then the second mode would increase higher than 5,765 CPM. The improvement of the second mode to above 5,700 RPM is significant because of the 5X pump excitation throughout the operating speed range. It would be highly undesirable to have any torsional modes between the vicinity of 5,000 and 8,000 CPM because of the possibility of excitation with the variable speed drive system.

Axial Natural Frequencies of Motor-Pump System by Finite Element Method

Although this model has been developed for lateral and torsional modal analysis, it is of interest to note that the axial modes of motion may be easily determined by unconstraining the axial displacements. Axial modes are normally not a problem with most turbo-rotors but should be taken into consideration with long multispan turbine-generators and large vertical motor-pumps. The length and weight of this system is of significant magnitude to warrant investigation of the axial modes.

In order to determine the axial modes of motions, the system is constrained in all of the degrees of freedom except the axial coordinates. An additional ground node was placed near the thrust bearing. An axial spring, representing the thrust bearing, was then connected to the thrust bearing. The first four axial modes were calculated for a range of thrust bearing stiffnesses. Figure 16 represents the motor-pump first axial mode for various values of thrust bearing stiffness. It is seen that, for a thrust bearing stiffness of approximately 1.2E6 lb/in., the first axial mode is at the design operating speed. This implies that there may be the existence of an axial or "pogo" mode. The axial or pogo mode may be significant in motor-pump systems with rolling element bearings because of the lack of inherent damping in the system.

From this analysis, it is concluded that instrumentation should be mounted on the coupling to monitor the axial motion of the shaft.

DYNAMIC SIMULATION OF MOTOR-PUMP SYSTEM WITH 5X EXCITATION USING FINITE ELEMENT TECHNIQUES

One of the significant vibrational characteristics of the vertical motor-pump system was the discovery that the pumps have a 5X excitation which could excite a system resonance frequency at approximately 3,400 CPM with the pump running at 680 RPM. By means of a tracking filter, the amplitude and phase for several positions along the coupling were recorded as shown in Figure 4. Since the impeller is a 5 bladed design a 5 times running frequency excitation is generated in the system. One of the system unknowns is the magnitude of the 5X forcing function that the pump may generate

One of the capabilities of the MSC/PAL2 finite element program is the ability to determine the forced response of the system with a dynamic excitation. A harmonic exciting force of 1,000 lb acting at the impeller was applied for a frequency range of 40 to 75 Hz. One of the other essential elements, in order to correctly calculate the dynamic response, is the amount of damping acting at the various bearings. In the finite element program, only one of the principal components of damping may be applied (no bearing cross coupling effects). For the case of the upper fluid film motor bearing, eight bearing stiffness and damping coefficients were generated. These coefficients can further be reduced to 4 synchronous stiffness and damping coefficients corresponding to the X-Y planes. A nominal value of bearing stiffness of 2.0E6 lb/in. and damping of 8.0E3 lb-sec/in. for the motor bearings was assumed. It was found that there could be a considerable variation in the assumed motor bearing characteristics without appreciably affecting the results.

The characteristics of the hydrostatic bearing were furnished by the pump manufacturer and the stiffness was computed to vary between 0.7E6 and 0.9E6 lb/in. The hydrostatic pump damping for the bearing was computed by the manufacturer to be less than 30 lb-sec/in. This unusually low damping value is similar to what would be encountered with a rolling element bearing. The total effective damping at the impeller-bearing location was determined to be considerable higher.

One of the significant experimental plots is the phase associated with the 5X excitation. The rate of change of the phase curve is directly related to the amount of damping in the system. In particular for this mode, the amount of damping at the bearing-impeller region directly affects the slope of the phase curve. A wide range of response curves was generated for various damping values. A value of damping of 200 lb-sec/in. produced a response phase curve similar to the phase angle observed in the experimental data.

Figure 17 represents the harmonic response of the impeller simulating 5X excitation assuming a dynamic load of 1,000 lbs. Curve A represents the end of the impeller and Curve C represents the coupling location monitored. The impeller shows an amplitude of over 40 mils. Rubbing of the outer impeller wear ring seal has been experienced and seal clearances there have been opened up to over 100 mils. The coupling amplitude is approximately 4 mils radial or 8 mils peak to peak. Since the observed amplitude at the coupling may vary between 3.5 to 5 mils peak to peak, it is estimated that the dynamic loading on the shaft caused by the 5X excitation is of the order of 500 to 800 lbs. This value of loading by itself is not sufficient to account for shaft cracking. There is very little amplitude observed at the motor bearings which is consistent with the undamped mode shape for the frequency of 3,687 RPM as shown in Figure 17.

The generated response of amplitude and phase for the motor-pump represent the system transfer function. It was seen that the impeller and coupling are 180^{o} out of phase. this phase relationship is the same as that observed in the critical speed mode shape data. It is of interest to compare the relative magnitudes of the impeller and coupling responses. The ratio of impeller to coupling response is approximately 10 to 1. Therefore, if the experimental amplitude on the coupling is determined to be between 4 to 5 mils, then the impeller motion may be assumed to be 10 times larger, between 40 to 50 mils.

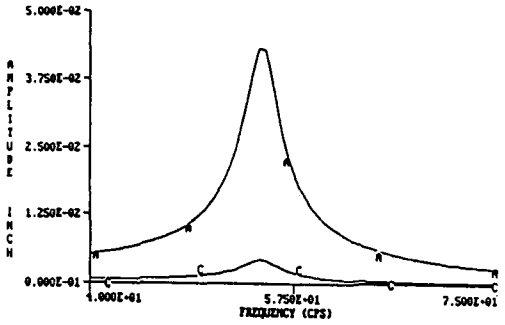

Fig. 17 Lateral Response of Impeller and Coupling with a Simulated 5X Excitation from 40 to 75 Hz 1,000 Lb. Dynamic Excitation

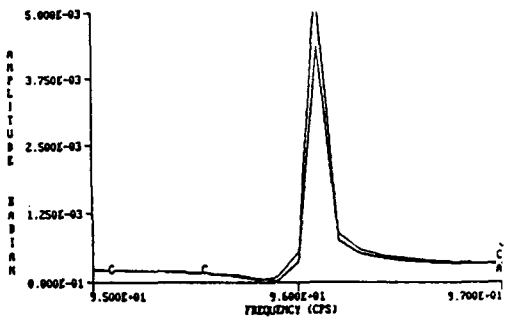

Fig. 18 Torsional Response of Motor Pump System from 95 to 97 Hz

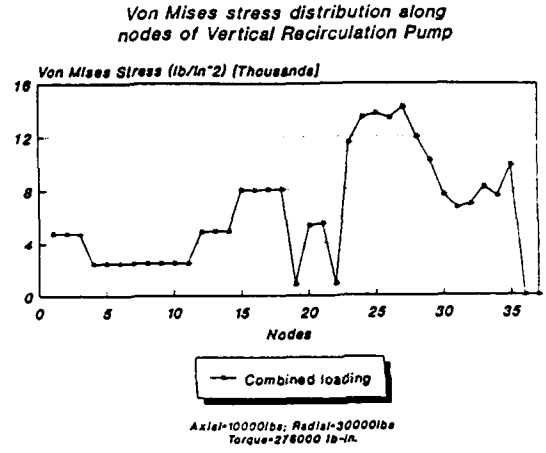

Fig. 19 Von Mises Stress Distribution for Combined Loading

Load	Value	Stress At Cracked Region (psi)	Type of Stress
5X Radial	1,000 lb	300-500	Alternating Mises
Axial	20,000 lb	580	Von Mises
Dynamic Axial	20,000 lb	600	Alternating Mises
Radial	30,000 lb	5,200	Alternating Mises
Steady State Torque	276,000 lb-in	8,500	Von Mises
Dynamic Torsional	30,000 lb-in	27,000	Alternating Mises

Table 2 Comparison of Stresses At Cracked Region Due To Various Types of Static and Dynamic Loads

The complete finite element motor-pump transfer function analysis on a 386 class computer operating at 25 MHz required only 5 minutes to perform. One powerful advantage of working with finite elements on a microcomputer is that the binary files may be stored after the analysis is completed. This allows one to rapidly review and replot the computed data without requiring a rerun.

STRESSES IN SHAFT DUE TO STATIC AND DYNAMIC LOADING

The vertical recirculation pump has various types of static and dynamic loads acting upon it. On the motor, there is the magnetic pull of the field and the rotor unbalance. These forces have relatively little effect on the impeller. On the rotor, there is the gravitational weight of the system acting downward. The impeller has a net thrust upward due to the hydraulic axial load. This load may be as high as 20,000 lbs. There are several types of forces that may act on the impeller. The first type is rotor unbalance due to mechanical unbalance in the wheel. A large hydraulic synchronous loading may also be generated in the impeller by a nonuniformly filled impeller passage. The second type of loading is the nonsynchronous 5X excitation due to the pump blade passing frequency. A more serious type of load, however, is the hydraulic radial loading that may exist in a single discharge volute when it is operated off of BEP (Best Efficiency Point). This may generate a large radial loading. The presence of a radial load vector acting on the impeller will lead to alternating stresses in the shaft.

Although this effect has been known for over 50 years, it is difficult to quantify with a new pump design. The radial load factor must be determined experimentally. There have been a number of instances in the petrochemical industry where single discharge volutes have led to shaft failure because of the excessive loading developed when operating away from BEP (best efficiency point).

Another type of mechanical shaft loading that should be considered for vertical motor pumps is the steady state and dynamic torques that may exist in the system. Since horsepower of the motor is over 7,000 HP, this creates a steady state torque of 276,000 lb/in. acting at the impeller. Of concern also is the possibility of the 5X excitation causing a dynamic fluctuating torque which could excite the motor-pump 2nd torsional resonance speed. Even a small value of fluctuating torque near the resonant frequency could be greatly magnified. Therefore, in addition to radial static and dynamic loading, static and dynamic torsional effects should also be considered acting on the motor-pump system. The magnitude of the dynamic torque is extremely difficult to estimate and requires experimental measurements on the shaft.

Shaft Stresses Due to Steady-State Loads

The shaft stresses were calculated with various combinations of steady state radial and axial loading and torsional moments. One of the advantages of the finite element method is that the same model may be used to calculate static deflections and stresses that are used in the critical speed and dynamics model. The stresses on the shaft were computed first with the individual load components and then the total stress distribution was computed adding the various combinations of loading on the impeller. The first loading distribution that was considered was that of axial loading on the shaft. It was seen that even large axial loads of 20,000 lbs. at most cause only 700 psi stress in the shaft. At the crack location, there is a stress of approximately 600 psi only. Therefore, the steady-state stress caused by axial loading is minimal.

The Von Mises shaft stress corresponding to radial loads of 15,000 and 30,000 lbs. was computed. For this pump, the bearing cartridge was assumed to contribute to the load path. This generates an abrupt change in stress at node 35. The radial loading then could generate a stress of 5,000 psi at the crack location depending upon the assumed value of radial loading. It is of interest to note that much higher stress occurs at node 27 which is just beyond the coupling. However, cracking is not encountered at this location as this region is not in a nuclear environment and is operational in air. Hence, the endurance life of the material should be significantly higher at the coupling area than adjacent to the bearing cartridge.

Shaft Stresses with Dynamic Axial Loading

The first axial or pogo mode was determined to be at or near the design operating speed and the stresses generated due to an oscillating axial loading were computed. For the case of a rolling element thrust bearing with no damping in the axial direction, the response at resonance would be excessive.

The action of the fluid film thrust bearing provides a considerable amount of damping in the axial direction. The axial response was computed with the incorporation of damping of 2,000 lb-sec/in. which is representative of the damping magnitude encountered with this class of thrust bearing. The sinusoidal axial mode will be approximately 3.5 mils per 1,000 lb. of axial excitation force. When damping is incorporated into the calculation of the dynamic axial response, this value is reduced by a factor of 10. Therefore, dynamical axial stresses may be relatively insignificant in comparison to the radial and torsional stresses. However, it is important to note that many failures of motor-pump systems of this size have been encountered when using rolling element thrust bearings rather than tilting pad kingsbury thrust bearings. The lack of damping of the rolling element bearing may cause premature failure in the presence of an axial or a pogo mode at running speed.

Shaft Stresses with Torsional Moment

With synchronous and variable speed drive motor systems, there is always a concern of instantaneous dynamic torques being applied to the system. For example, with a synchronous motor under 10% voltage reduction, a pulsating torque of 10 times steady state torque can sometimes be achieved. This can cause catastrophic effects on gear box driven machinery. Since the pump produces a 5X excitation, there will be some dynamic torque existing in the system and it may have a considerable effect on the stresses.

Another source of dynamic torsional excitation on the pump could be the excitation of the motor pump second torsional critical speed under variable speed operating conditions. A pulsating torque value of approximately 10% of the steady state torque, 30,000 lb/in. was applied to the rotor system. The response of the shaft over a frequency range of 60 Hz to 130 Hz was investigated.

Figure 18 represents the torsional response near the crack due to a sinusoidal oscillation of 30,000 lb/in. At the frequency of approximately 96 Hz, it is seen that a sharp torsional resonance is encountered. This implies that, with a variable speed motor, it is possible to transverse this region causing excessive torsional stresses. The shear stress at node 35 is approximately 14,000 psi at the second torsional resonance, with an oscillating torque of 30,000 lb/in.

There may exist a torsional stress concentration of over 4 at the abrupt change in cross section. Therefore, the total effective torsional stress encountered at node 35 may be well over 50,000 psi. This would be a more than sufficient stress level to cause propagation of the thermal cracks.

Combined Loading

A Von Mises stress distribution was produced with a combined loading of axial, radial and steady state torque as shown in Figure 19. Figure 19 shows that there is a dramatic increase in the stress at node 35 which corresponds to the crack vicinity. This combined stress is of the order of 10,000 lb/in^2. If there are additional dynamical torsional moments applied to the shaft, this stress may increase significantly. It is therefore apparent that the mechanical loading in the vicinity of the thermally induced cracks may aggravate the situation over a long period of time. With the influence of stress concentration factors due to abrupt shaft sectional change, notch and surface grooving in the seal vicinity, these act as stress concentration factors which enhance the effect of the stress distribution. In addition to these factors, the endurance life of the material is reduced by operating under neutron bombardment. It appears that up to 80% of the endurance life of the material may be reduced by the

operating conditions. Therefore, even relatively moderate stresses of the magnitude shown here may be of sufficient magnitude to cause the long term failure as experienced in this class of pump.

DISCUSSION AND CONCLUSIONS

It was the object of this investigation to see if there is a possibility that mechanical loading of various types could be responsible for crack propagation as observed in this class of variable speed motor-pumps. There indeed appears to be a strong possibility that combinations of unidirectional radial and static and dynamic torsional loading of the impeller may substantially contribute to the crack growth initiated by thermal gradients at the seal area near the bearing.

Table 2 represents a summary table of the stresses near the pump crack region generated by the various types of loads assumed acting on the impeller. The first loading shown is the dynamical 5X excitation of 1,000 lbs. The actual 5X excitation forcing function is estimated to be below this value. The alternating Von Mises stresses are between 300 to 500 psi depending upon the operating speed. The 5X excitation should not be of serious concern.

The next level of stresses shown are the values of stress caused by static and dynamic axial excitation. Although the shaft may be operating on an axial resonance mode, the damping of the thrust bearing should control the motion and axial stresses, for even large axial dynamical loads. This would not be the case if a rolling element thrust bearing were employed on the motor.

The third class of loading investigated are the effects of the radial loading. The radial loading acting on the shaft is unidirectional and hence the shaft may act as a fatigue testing machine. The assumed value of 30,000 lb radial loading produces an alternating Von Mises stress of 5,200 psi near the crack area. This value of loading is substantially higher than what was estimated by the pump manufacturer. Further strain gauge testing is required to verify the magnitude of the radial load when operating off of BEP.

The fourth class of loading shown in Table 2 are the stresses due to steady state and dynamic 5X excitation torque. Due to the possible existence of a second torsional critical speed near 5 times running speed, small dynamic torques could cause large stresses when the rotor speed corresponds to this speed range. The shear stress concentration factor of over 4 at the pump-bearing sectional change would greatly exacerbate the situation.

In the design of the bearing cartridge for this pump, there is an abrupt change in cross section and there are several factors which are stress raisers acting in the system. These stress factors can magnify the stresses at this location. It is also apparent that the endurance limit of the material operating in water in a neutron rich environment is considerable reduced over the endurance life of the material when operating in air. Although there are higher stress areas in the shaft such as near the coupling location, the combination of stress concentration factors and reduced endurance life of material near the bearing cartridge may be responsible for crack growth.

Attempts to redesign the thermal seal in order to improve shaft life have, in certain circumstances, exacerbated the situation. Pump life, on the average, has been approximately 10 years with this class of design (90,000 hrs.). With one of the seal redesigns, the shaft life was reduced to 30,000 hrs.

One of the important conclusions of this research is that there may exist a second torsional critical speed in the system which could be excited by the impeller 5X excitation. It was found that steady state and dynamic torques on the pump may have a significant effect on the overall stress. Because of the significance of the existence of a second torsional critical speed, instrumentation should be placed on one of these pumps to examine the principal and shear stresses under various operating conditions.

There are a number of design changes which may be introduced into the motor-pump system to alleviate the stresses induced by the various mechanical loads. One substantial design change would be to alleviate the magnitude of the radial loading on the impeller. There are two procedures that could be performed here. One would be to round the tip of the impeller blades or reduce the impeller diameter slightly. This is permissible since the impeller has excess capacity. The other procedure would be to increase the diameter of the volute tongue. This would increase the net clearance between the impeller and the discharge volute tongue. The 5X excitation would be reduced along with any dynamical 5X torsional excitation, and the radial loading would also be reduced when operating away from BEP.

It is concluded that the cracking experienced with this class of pump may not be simply attributed to thermal effects alone, and that the combined static and dynamic stresses encountered during variable speed operations may indeed contribute to crack propagation.

BIBLIOGRAPHY

Beeston, J. M. and Brinkman, C. R., "Axial Fatigue of Irradiated Stainless Steels Tested at Elevated Temperatures," *Irradiation Effects on Structured Alloys for Nuclear REactor Applications,* ASTM STP 484, 1970.

Bently, D. E., "Vibration Monitoring Techniques and Shaft Crack Detection of Reactor Coolant Pumps and Recirculation Pumps," Reactor Coolant Pump and Recirculation Pump Monitoring Workshop, 1988.

Brinkman, C. R., et. al., "Influence of Irradiation on the Creep/Fatigue Behavior of Several Austenitic Stainless Steels and Incoloy 800 to 700^{O}C," *Effect of Radiation on Substructure and Mechanical Properties of Metals and Alloys,* ASTM STP 529, 1973.

Colen, R. B., and Gunter, E. J., "Undamped Torsional Critical Speed Analysis of Rotor Systems - A manual for Use with Computer Program CRITSPD," Report No. UVA/643078/MAE81/105, June 1981.

Forrest, P. G., *Fatigue of Metals,* Pergamon Press, London, 1962.

Fuchs, H. O., Stephens, R.I., *Metal Fatigue in Engineering,* John Wiley, 1980.

Gunter, E. J., Gaston, C. G., "CRITSPD-PC User's Manual" August, 1987.

Huber, K. A., "Considerations for Primary Reactor Pump Monitoring Systems," EPRI Workshop, 1988.

Jackson, Charles and Ingram, James H., "Centerfugal Pump Mechanical Performance, Instrumentation, and Diagnostics," *Pump Handbook,* McGraw-Hill, 1986.

Kowal, M. G. and O'Brien, J. T., "Monitoring for Shaft Cracks on Reactor Recirculation Pumps," *Sound and Vibration,* 1989.

Maleev, V. L. and Hartman, J. B., *Machine Design,* International Textbook Company, 1954.

Potts, Frank J. and Oler, Walter J., *Finite Element Applications With Microcomputers,* Prentice Hall, 1989.

Zienkiewicz, O. C., *The Finite Element Method,* McGraw-Hill, 1977.

AN INVESTIGATION INTO THE FAILURES OF TURBO BLOWER ROTOR SHAFTS

D. MOREHOUSE*, J. PORTER*, M. BRAUSS**

*Defence Research Establishment Atlantic, P.O. Box 1012 Dartmouth, Nova Scotia, Canada, B2Y 3Z7
**Proto Manufacturing Ltd., 2175 Solar Crescent, Oldcastle, Ontario, Canada, N0R 1L0

ABSTRACT: Recurring failures of Y100 Turbo Blower Rotor shafts used in some Canadian destroyer propulsion systems prompted an investigation by the Defence Research Establishment Atlantic (DREA) to determine the probable cause. Although a number of the failures could be attributed to mechanical fitting problems, a large percentage of rotors distorted excessively for unknown reasons. This study focussed on identifying possible metallurgical damage which may have occurred as a result of the hot spot repair process employed to straighten previously bent shafts. X-ray diffraction surface residual stress measurements were made on damaged shafts in order to detect residual stress anomalies. When the hot spot repair procedure for straightening shafts or beams is applied properly, a tensile residual strain is induced at the hot spot center which draws the component straight. The zone of tensile strain extends to the edge of the hot spot whereupon a low compressive residual strain is present. The turbo blower rotor shafts examined by DREA, however, exhibited compressive residual stresses in the center of the hot spot repaired areas combined with adjacent high tensile stresses in the surrounding zones. Microstructural investigation revealed that the improperly repaired hot spot areas had hardnesses in excess of 40 Rc and martensitic microstructures. In contrast, properly executed repairs exhibited hardnesses less than 30 Rc. These high hardness martensitic microstructures could limit the life of the shaft through the time and temperature dependant normalization of the hot spot residual stress states, with attendant shaft distortion.

KEY WORDS: Residual stress; turbo blower rotor shaft; thermal straightening; x-ray diffraction

HISTORY OF Y100 TURBO BLOWER FAILURES: Y100 turbo blowers first entered service in the mid 1950's in the Canadian St. Laurent Class frigates and were later installed in all the Canadian Y100 steam destroyers. At present 34 turbo blowers are in service on 17 Canadian warships. The turbo blowers provide combustion air for the two Y100 boilers in each vessel. The single stage axial flow impeller is driven by a two row curtis wheel turbine through single reduction gearing. At maximum output, with superheated steam at 440 degrees C(825 degrees F) and 3800 kPa(550 psi), the turbine turns at 13600 RPM, subsequently turning the impellor at 4750 RPM producing 1840 cubic meters(65000 cubic feet) of air per minute. Although a large number of turbo blower failures had occurred over the years (156 between 1971 and 1988), it was not until the latest series of failures (26 in an 18 month period commencing in 1987), that serious concerns were raised with regard to the reliability of the system. The turbo blower failures appeared to occur quite randomly; for example, at times of steady state operation, low power maneuvering, intermediate or high speeds, during full power trials or in early stages of basin trials. Previous investigations revolved around the steam line support arrangements, operational procedures and installation misalignments. However, rotors were still failing even when these factors were carefully watched. The sole common factor to all failures was the bending of the turbo blower turbine rotor shafts resulting in damage to steam labyrinths, oil baffles and bearings. When these shafts were removed they would exhibit an axial shaft deflection of 0.025 to 0.178 mm(0.001 to 0.007 inches) in the vicinity of the steam labyrinths.

DREA's Dockyard Laboratory was contacted to conduct a failure investigation on several of these turbo blower rotor shafts which had bent in service. The investigation was hampered initially as the shafts could not be sectioned or in any way further damaged as attempts were to be made to salvage and repair these shafts for future service. It was noted that a high percentage of these shafts had undergone a hot spot straightening process during earlier repairs and as such the present investigation focussed on assessing the shaft material in these areas.

The hot spot repair procedure is one in which a previously bent shaft is thermally straightened by rapidly applying concentrated heat to a localized spot on the shaft corresponding to the apex of the bend. Initially, as the spot is heated, the bend in the shaft will increase due to local thermal expansion. The cooler surrounding shaft material will resist the bending effect due to the localized expansion of the hot spot, and as the highly heated spot loses its strength, local plastic deformation (or crushing) of the spot occurs. The resisting moment in the cooler shaft material returns the shaft to its shape prior to treatment.

At this time the heat source is removed and the subsequent rapid cooling of the spot sets up high tensile residual stresses on the shaft surface in the hot spot region, which draw the shaft straight. Re-hot spotting the same location on a shaft a second time will not result in further straightening.
Straightening of a severely bent shaft can be accomplished, however, by hot spotting adjacent locations where the combined tensile residual stress fields would interact to draw the shaft straight. A properly applied hot spot should not contain hardnesses greater than that of the original shaft material [1].

The primary difficulty associated with the hot spot procedure is the risk of applying excessive heat which could result in the surpassing of the material's transformation temperature, whereupon rapid cooling would result in the formation of an undesirable phase. In the specific case of the Y100 turbo blower rotor shafts (steels with varying amounts of alloys of chrome, nickel, molybdenum, vanadium) the transformation temperatures would be in the vicinity of 800 to 830 degrees C(1472 to 1526 degrees F) [1]. Hot spot repairs are limited to the shaft material adjacent to both sides of the turbine wheel. The operator applies the flame until the 2.54 cm(1 inch) diameter spot has attained the annealing color temperature which indicates that he is below the transformation temperature. An oxygen-propane torch provides the heat input. The torch to surface distance and the application time (seconds) are critical variables to effect a proper hot spot procedure. Ensuring that excessive heat has not been applied is extremely difficult due to the rapid heating rate in the localized spot and the narrow temperature window between that temperature required to cause the desired repair and that resulting in undesirable phase transformation. Hardness measurements conducted showed that the original hardnesses of the shafts were in the range of 15 to 20 Rockwell "C" while the centers of the hot spots were in the range of 35 to 45 on the Rockwell "C" scale.

X-RAY DIFFRACTION DETERMINATION OF RESIDUAL STRESS:
All examinations of the shaft had to be non-destructive in nature as the shafts were considered repairable. It was decided to conduct a non-destructive residual stress survey across several hot spot repairs in order to search for any unusual anomalies. In principle, if a component with a known residual stress distribution has failed, it can be examined for residual stress anomalies which may have contributed to the failure. The x-ray diffraction residual stress method was selected to conduct this survey.

X-ray diffraction allows direct measurement of surface residual strain by the measurement of the elastic distention in the atomic lattice spacings of the material.

In crystalline materials, the lattice spacings (the distance between planes of atoms) are a function of the material and the stresses present at the point of measurement in the structure. By measuring the diffraction of x-rays on the sample surface and applying Bragg's law, strain is measured from which stress can be determined. In effect, the crystalline structure itself acts as the smallest possible strain gauge. As such, a significant advantage of the x-ray diffraction residual stress measurement technique is the precision of measurements possible. This is particularly important for structures with high surface residual stress gradients. As well, apart from a very shallow electropolishing of the sample surface, this method is completely non-destructive. This technique is described in detail in Reference 2.

EXPERIMENTAL PROCEDURE: X-ray diffraction residual stress measurements were made on three Y100 turbo blower rotor shafts. The first shaft examined was straight and showed no evidence of prior hot spot thermal straightening. The second shaft had recently failed in service but had not yet been hot spot repaired. The third shaft had previously failed in service and had been recently thermally straightened. This shaft contained two adjacent hot spots.

The shaft surfaces fore and aft of the turbine wheel were lightly sanded with emery paper to remove the oxide layers. A 15% nitric acid and 85% methanol etching solution was applied to the surfaces in order to highlight the hot spot locations as seen in Figure 1.

A residual strain survey around the circumference of each shaft was conducted using the CANMET/Proto Stress Analyser, as seen in Figure 2, and the Denver X-Ray Stress Analyser x-ray diffraction apparatus. Apertures of 1 mm by 5 mm(0.04 by 0.2 inches) and 1 mm by 3 mm(0.04 by 0.12 inches) were used with $CrK\alpha_1$ radiation. Exposure times were 3 seconds. The Miller Index used was [211], "2θ" was 156.1 degrees and the original lattice spacing "d_0" was 1.1702 Angstroms. Variations of the lattice spacings such as that caused by the effects of carbon concentration are considered insignificant in relation to the lattice strains produced by residual stresses. Axial and circumferential strain measurements were taken at each location. Measurements were made on the shaft surfaces following electropolishing to a depth of 0.025 mm(0.001 inch) below the surface.

EXPERIMENTAL RESULTS: Residual stress measurements determined for the straight unrepaired shaft indicated a mean axial stress and circumferential stress of -68.9 MPa(-10 ksi).

Figure 3 shows the residual stress profile as a function of circumferential position. Measurements made on the bent but unrepaired shaft surfaces indicated similar residual stress profiles with a mean residual stress of -131 MPa(-19 ksi). Axial and circumferential residual stress values for the recently straightened shaft containing two adjacent hot spots are depicted in Figures 4 and 5 respectively. Whereas high tensile residual stresses were expected at the center of the hot spots, high compressive residual stresses of -150 MPa(-22 ksi) axially and -375 MPa(-54 ksi) circumferentially were observed. Peak tensile residual stresses of +400 MPa(+58 ksi) axially and +500 MPa(+75 ksi) circumferentially, corresponding to the hot spot periphery positions, were also noted. The surface stress gradients were very steep.

MICROSTRUCTURAL INVESTIGATION: The hardness survey showed that the hot spot procedure was not being conducted properly on the turbo blower shafts. X-ray diffraction measurements on these hot spots showed that significant stresses were localizied in these areas. The presence of high compressive residual stresses in the hot spot centers, surrounded by high tensile residual stresses at the periphery of the hot spots, indicated a volumetric expansion which is associated with an undesirable phase transformation. This presents a picture of a tensile ring of residual stresses that are pulling a shaft straight as well as containing the expanded volume of material.

The repaired shafts were reportedly subjected to a "thermal stability" test after a hot spot repair process [3]. This was carried out at a temperature of 480 degrees C after which measurements were made to ensure that no detrimential axial shaft deflections had occurred. The recently hot spot straightened shaft that was assessed during this study had been returned as an operational ready unit. However, the high hardnesses and the significantly high stress states observed in the hot spot repaired areas were cause for concern. These hot spot regions were adjacent to the turbine wheel which is subjected to 440 degree C steam during turbine operation.

The significance of the x-ray diffraction results and the implications associated with the occurence of an undesirable phase transformation finally resulted in permission being granted to destructively examine one of the non-repairable rotor shafts containing hot spots.

A representative microstructure in an area remote from a hot spot repair is shown in Figure 6. The microstructure at the center of a hot spot repair is seen in Figure 7.

This metallographic examination confirmed that martensite had been formed during the hot spot repair process.

The problem with martensite is that it is a highly stressed phase that will relax depending on time and associated temperatures. This tempering relaxes the stresses through the precipitation of carbides [4]. The change of stress state in the martensite and its volumetric reduction [5] would also effect a change in the overall balancing stresses in the shaft.

CONCLUSIONS: An x-ray diffraction residual stress survey was conducted on several Y100 turbo blower rotor shafts in various conditions. Measurements obtained revealed high residual stresses in the hot spot repaired regions of the shafts. Subsequent destructive microstrutural investigations on hot spot regions revealed the presence of martensite. This confirmed that the shafts had been overheated during the hot spot straightening procedures. In service these turbo blower rotor shafts see temperatures that lead to the tempering of the martensitic microstructures and a change in the balance of the residual stresses present. The probability of subsequent shaft distortion due to the residual stress imbalance is therefore very significant. Consequently, other mechanical shaft straightening procedures have been adopted.

REFERENCES:

1. "Flame Straightening of Turbine Rotors", Engineering Department Report, NEI-APE Ltd - W.H.Allen, Bedford, England, Feb. 1965.

2. B.D. Cullity, The Elements of X-Ray Diffraction, 2nd Edition, Addison-Wesley, Reading Massachusetts, USA, 1978.

3. W.H. Whiting, personal communication, NEI-APE Ltd - W.H. Allen, Bedford, England, 17 October 1988.

4. William T.Lankford,Jr.,et al. The Making, Shaping and Treating of Steels, Tenth Edition, Association of Iron and Steel Engineers, Pittsburgh, Pennsylvania, 1985.

5. Anvil Kumar Sinah, Ferrous Physical Metallurgy, Butterworth, Stoneham, MA, USA, 1989.

Figure 1: Y100 Turbo Blower Rotor Containing a Hot Spot Repair (dark circular area near turbine wheel)

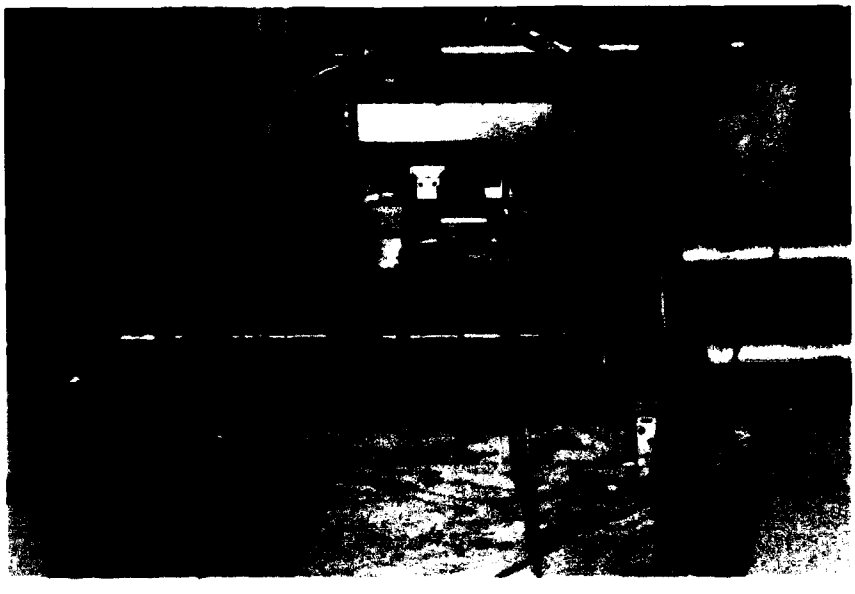

Figure 2: CANMET/Proto Stress Analyser Measuring Residual Strain on a Turbo Blower Shaft

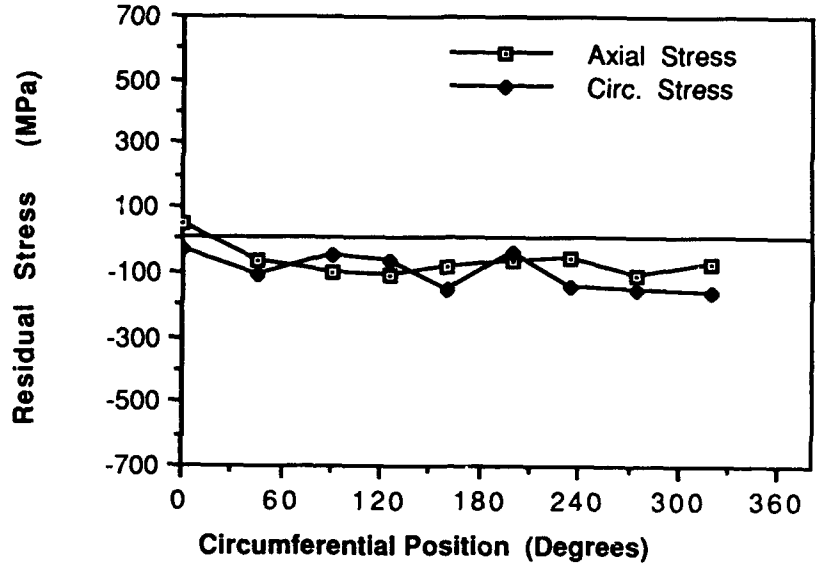

Figure 3: Residual Stress Profiles Around the Circumference of an Unrepaired Turbo Blower Rotor Shaft

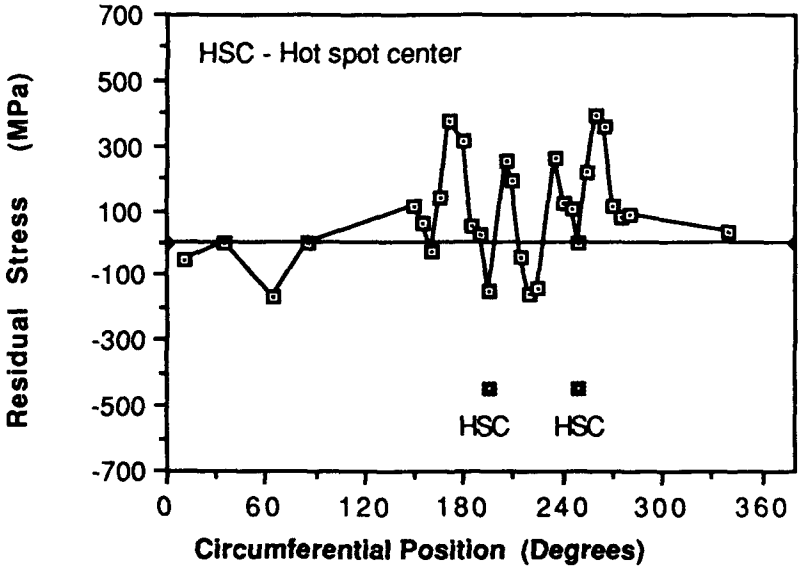

Figure 4: Axial Residual Stress Profile Around the Circumference of a Turbo Blower Rotor Shaft Containing Two Hot Spots

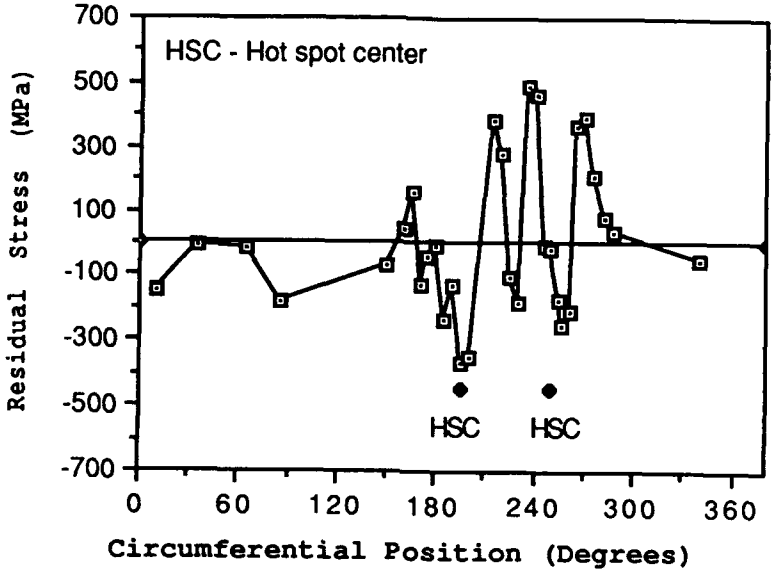

Figure 5: Circumferential Residual Stress Profile Around the Circumference of a Turbo Blower Rotor Shaft Containing Two Hot Spot Repairs.

Figure 6: Unaltered Microstructure of a Turbo Blower Rotor Shaft Showing Ferrite and Pearlite (500 X)

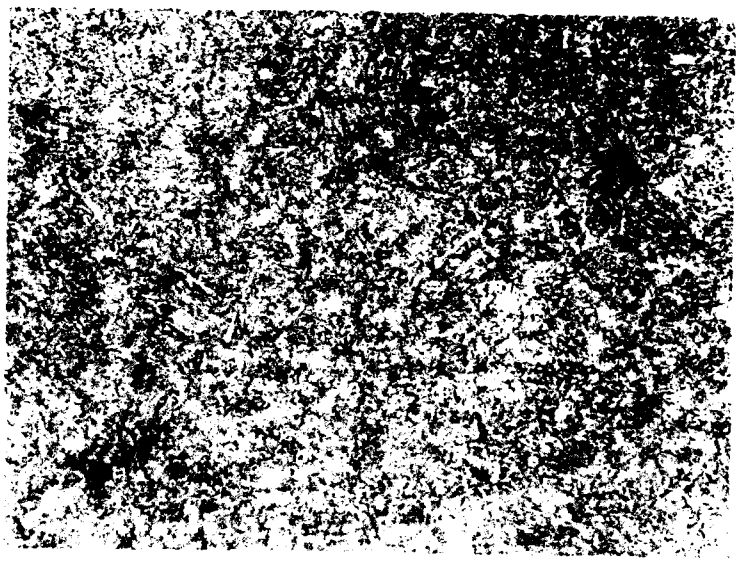

Figure 7: Turbo Blower Hot Spot Microstructure Showing a Tempered Martensite (500 X)

EVALUATION OF A UNIQUE FAILURE OF MAIN REINFORCEMENT IN BUILDING V-90 NAVAL AIR REWORK FACILITY NAVAL AIR STATION NORFOLK, VIRGINIA

John J. Cecilio
Naval Facilities Engineering Command
Alexandria, Virginia 22332-2300

Abstract: NARF Naval Air Station Norfolk building V-90 is a column free, high bay hangar structure which is 160 feet wide and 360 feet long. Building V-90 was constructed in 1943 and originally served as an aircraft hangar. The structure consists of a concrete shell spanning to arch frames spaced 40 feet on center. Approximately 40% of the main connections of the structure indicated serious structural damage, cracks greater than 1/2 inch wide and almost 50% of the main top reinforcement fractured. Current state-of-the-art technology of fracture mechanics, diagnosis and failure analysis was used in the evaluation of the failure.

Key Words: Failure analysis; fracture mechanics; stress corrosion; hydrogen assisted cracking

Basic Data: Building V-90 was built in 1943. It is a column free structure 160 feet wide and 360 feet long, with hangar doors at each end and with a low bay lean-to structure on each side along the length of the building. The building served originally as an aircraft hangar. At the time of the failure investigation it was functioning as a jet engine repair shop and storage area. The building was designed to handle various weight handling equipment, including four bridge crane runways with multiple bridges and five ton hoists and trolleys. A 25 ton fixed hoist is also located near each end of the building. The estimated replacement cost for the building is $6,000,000 not including demolition/disposal cost.

Background: The building is a high bay structural system consisting of a concrete shell spanning to arch frames spaced at 40 feet on center. See Figures 1 and 2 for a simplified sketch of the building. The building is divided into 80 foot segments by expansion joints at alternate midspans of the roof shells, which leave segments of twin arches.

The arch frame can be described as having three distinct components--arch, knee and column. These three parts are designed to act as a unit. An arch derives its strength from its ability to carry compression. This can only be accomplished if it has solid, unyielding supports. Building V-90 obtains this support from the frame action developed in the knees that induce moments in both column and arch. Heavy reinforcing steel was provided to resist

these bending moments and compression forces at the knee connection. The outer reinforcement in the knee connections carried the maximum stress and had failed. Approximately 40% of the knees indicated serious structural damage, which consisted of cracks up to 1/2 inch wide and almost half of the outer reinforcement bar broken. The rebars failed at different times over a long period of time.

The roof shell was in good condition. The columns below the knee location were in excellent condition. However, the arches, being exposed and unprotected for over 40 years, showed signs of deterioration such as localized cracking, spalling and pockets of weathered (soft) concrete.

Findings: A structural element fails when it is subjected to forces greater than its capacity to resist them. Reinforced concrete derives its ability to resist loads by combining concrete's natural strength in compression with steel's great strength in tension. To work properly, these materials must have other properties besides strength. Most notably, rebars must be properly bonded to the concrete (anchorage) and must possess the ability to stretch elastically so stresses can equalize (ductility). To insure that proper materials are used, so that assumed behavior does in fact exist, various building codes have established criteria that sets limits on chemical and mechanical properties. The codes also specify ways to design, fabricate and install concrete structures for the same reason.

When these rules are violated, undesirable consequences can result, ranging from unsightly cracking and concrete deterioration to total collapse. In a structure which is over 40 years old, determining which if any of these rules may have been violated is difficult at best. While some areas such as material chemical composition, strength and geometry can still be evaluated and determined, other defects such as improper techniques of construction are almost impossible to detect conclusively.

An inspection of the fractured reinforcement in place indicated that the displacement of the broken ends away from one another varied from less than 1/16 up to 3 inches. The displacement was primarily along the bars longitudinal axis but was to some degree lateral with the upper break moving towards the interior of the hangar relative to the lower break surface. The cast impressions of unbroken rebars were found in the concrete beneath the broken reinforcement rebars, indicating that the rebars were not broken at the time the concrete hardened (Figure 3).

Figure 4 is an example of the overall concrete cracking pattern at the corners which contained broken rebars. Cracks radiated from the corners and are made visible macroscopically by redeposition of (probably) calcium carbonate into layers. The thin outermost layer of this redeposited accretion was brown and contained iron (determined by X-ray fluorescence spectroscopy) whereas the inner layers were white and did not contain iron. The presence of iron on the last deposition of calcium carbonate at these cracks indicated

the dissolution of rebars, by rusting, at least in the later stages of the concrete cracking.

A section of the broken rebar was removed for closer inspection and evaluation at Naval Research Laboratory (NRL). The fracture surface was covered with heavy deposits which readily dissolved in diluted acetic acid and was probably calcium carbonate. The fractured surfaces were cleaned with inhibited HCl and found to be deeply pitted and rusted. No fine scale fracture surface marking could be found to indicate the failure mechanism.

Inspection indicated that the lower portion of the fracture was more heavily pitted from corrosion than the top. This condition was common on all of the broken rebars. The redeposited calcium carbonate and the deep rust beneath this layer indicated that the rebars had been broken for a long time.

This rebar was sectioned for hardness measurements and microscopy. The hardness tests indicated that the microstructure in the bent regions of the rebar had a Rockwell "B" 83.5 and the straight section a Rockwell "B" 75.6. This would indicate that the rebars were bent while cold. Microhardness measurements across the thickness of the rebars are shown on Figure 5 where it can be seen that the hardnesses were greater at the edges of the bent region. This again would support that the rebars were bent while cold.

Charpy V-Notch tests were conducted over a range of temperatures as shown in Figure 6. Values of 6 ft. lbs. at room temperature and 4 ft. lbs. at 32 degree F show the extreme brittleness of the steel rebar at the bend.

Early in July 1986 while the contractor was removing concrete around a knee containing broken rebars, another rebar broke when the contractor hit it with a hammer. This rebar was removed and sent to NRL for evaluation. Only slightly rusted, this rebar indicated cleavage patterns and chevron patterns providing a fracture origin on the inside of the bend (see Figure 7). Of even greater interest was the presence of other cracks in this rebar parallel to the main fracture surface.

The square rebars visible on the middle layer are bent to the same radius as the failed bars; however, these bars carried less load initially and were not vulnerable to abuse during construction and subsequent corrosion due to rain water penetration. The outer surface of the concrete arch beam would be more subject to hot/cold cycles (i.e., thermal fatigue) which would be a minor contributing factor to the failure. This could help explain why the other bars haven't failed similar to the outer layer bars.

Another possible cause could be, over-jacking of the ties at the column footings during the original construction, could have caused the original failure. Each arch beam was designed to be tied at the column footing level with four 1-9/16 inch diameter high strength rods using a preload force of 102,000 pounds. The effect of this is very difficult to quantify, since so much depends on the construction

sequence and the indeterminate resistance of the foundations already in place, when actual tensioning of the rods was done.

Blast effects on the roof from an explosion near Building V-90 in the middle 1940s was also investigated. It was possible that it could have started the failure. According to verbal reports, a torpedo was dropped from a transport wagon causing an explosion that extensively damaged other buildings in the surrounding area. This possibility was ruled out, since the location of knees containing failed bars was not consistent.

Other buildings that were erected at or about the same time were inspected. No other buildings inspected indicated any reinforcement rebar failure.

Conclusions (Causes of Failure):

1. Failure occurred after the concrete had hardened.

2. Failure of all but one rebar occurred long before the inspection.

3. The fracture surface of the rebar which failed in 1986 indicated that failure occurred by a hydrogen embrittlement or stress-corrosion cracking mechanism (HAC/SCC).

4. The other failed rebars were severely corroded but had generally flat fracture surfaces with no necking evident, suggesting that they also failed by HAC/SCC.

5. Contributory factors which cause HAC/SCC include:

a. Deterioration of the concrete allowed moisture to enter and produce a hydrogen-generating corrosion cell.

b. Cold-forming of the bars provided residual tensile stresses approaching the yield stress; over-jacking or blast effects may have contributed additional sustained loading.

c. These conditions persisted for an extended period of time, permitting development of an occluded corrosion cell, crack initiation, and crack propagation to failure.

6. The loads from the failed rebars transferred to the rest of the structure which also showed evidence of deterioration. The building was determined to be unsafe and was closed.

Acknowledgements: The author wishes to acknowledge the support and guidance of Dr. Cedric Beachem, Dr. Robert Bayles of the Naval Research Laboratory and Mr. V. R. Donnally, Structural Engineer from the Naval Facilities Engineering Command, Atlantic Division located in Norfolk, Virginia.

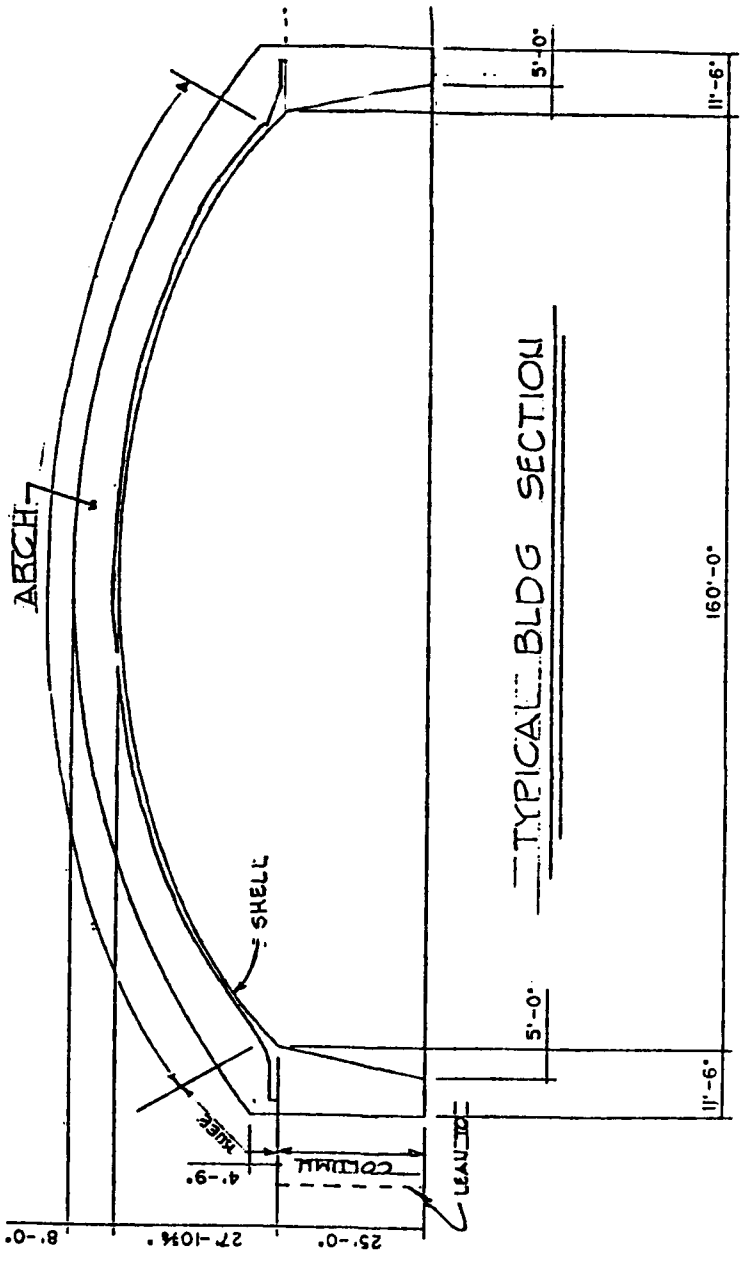
ARCH
SHELL
KNEE
COLUMN
LEAN-TO
TYPICAL BLDG SECTION
5'-0"
11'-6"
160'-0"
5'-0"
11'-6"
4'-9"
25'-0"
27'-10¾"
8'-0"

FIG. 1

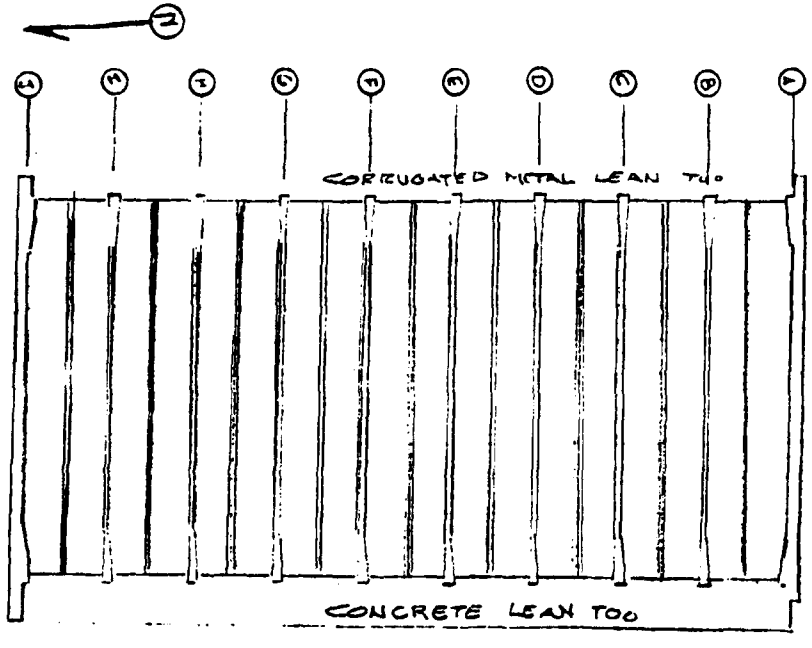

PLAN - BLDG V90

TABLE - SHOWING DAMAGED BARS		
	East Damaged Rebar - Outer Layer	West Damaged Rebar - Outer Layer
A		
B		
C	3	5
D	9	
E		
F		
G	7	9
H		
I	9	8
J		

DESIGN STEEL:

INNER LAYER 4
MIDDLE LAYER 8
OUTER LAYER 10

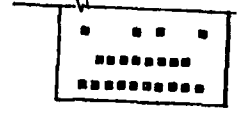

TOTAL = 22
1¼" SQ
BARS

SECT @ KNEE

SKETCH - PLAN VIEW OF BLDG V-90 AND SUMMARY OF KNOWN DAMAGED REINFORCING

FIG. 2

Figure 3

Figure 4

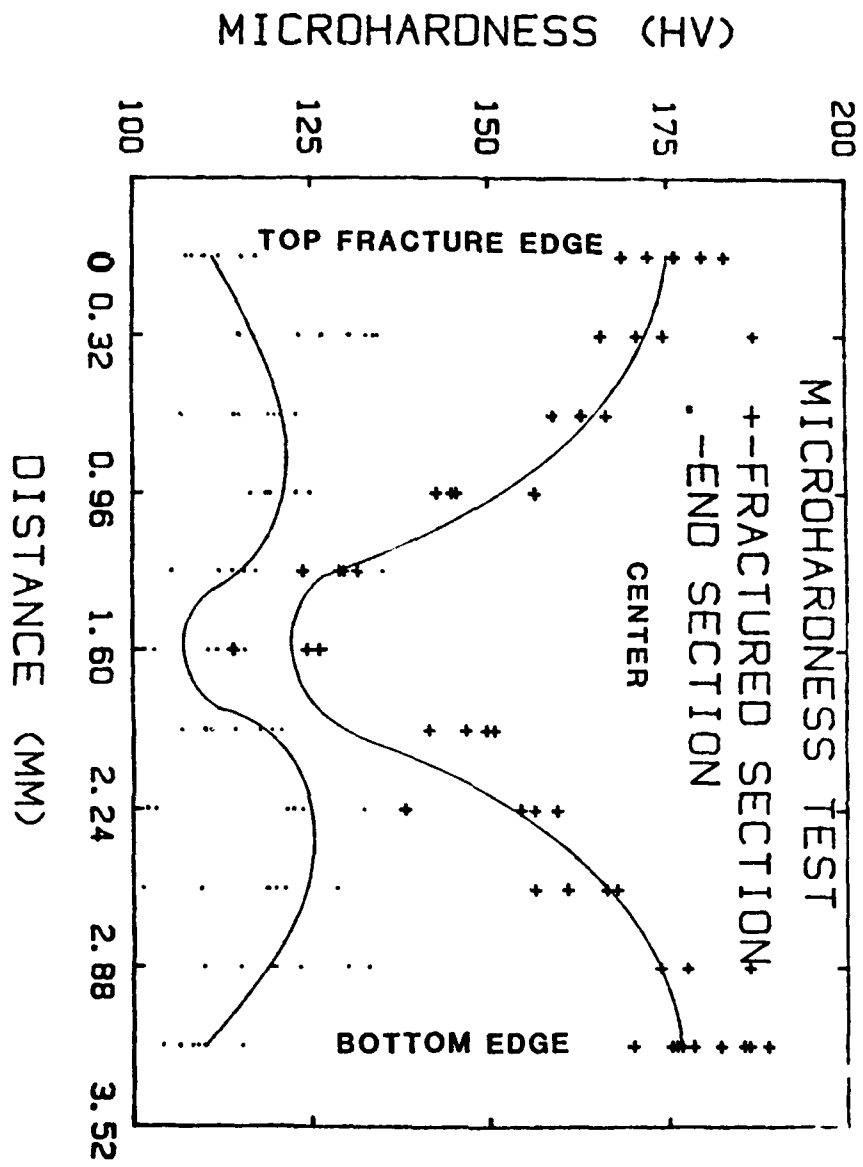

Figure 5 - Variation of hardness across the thickness of the bar

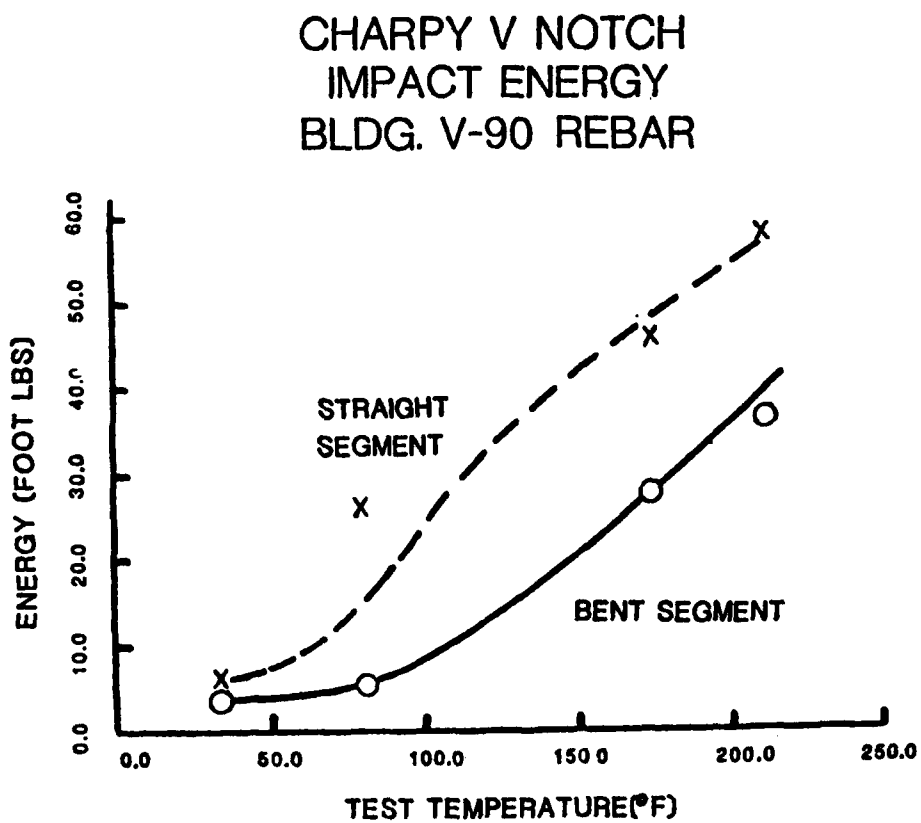
CHARPY V NOTCH
IMPACT ENERGY
BLDG. V-90 REBAR
ENERGY (FOOT LBS)
0.0
10.0
20.0
30.0
40.0
50.0
60.0
STRAIGHT
SEGMENT
BENT SEGMENT
0.0
50.0
100.0
150.0
200.0
250.0
TEST TEMPERATURE(°F)

Figure 6

Figure 7

APPENDIX

MFPG PUBLICATIONS

Both printed and microfiche copies of the following MFPG publications (1-12) whose catalog numbers start with either "AD" or "COM" may be obtained from the National Technical Information Service (NTIS).

NTIS
5285 Port Royal Road
Springfield, Virginia 22161

1. Glossary of Terms ..... AD 721 354

2. Proceedings of Meeting Nos. 1-9 (set of five) ..... AD 721 359

   Meeting Nos. 1-5 Papers and discussion on Failure Analysis and Control

   Meeting No. 6 "Detection, Diagnosis and Prognosis" December 6, 1968

   Meeting No. 7 "Failure Mechanisms as Identified with Helicopter Transmissions" March 27, 1969

   Meeting No. 8 "Critical Failure Problem Areas in the Aircraft Gas Turbine Engine" June 25-26, 1969

   Meeting No. 9 "Potential for Reduction of Mechanical Failure through Design Methodology" November 5-6, 1969

3. Proceedings of Meeting No. 10 ..... AD 721 912
   "Vibration Analysis Systems"
   January 21-22, 1970

4. Proceedings of Meeting No. 11 ..... AD 724 475
   "Failure Mechanisms: Fatigue"
   April 7-8, 1970

5. Proceedings of Meeting No. 12 ..... AD 721 913
   "Identification and Prevention of Mechanical Failures in Internal Combustion Engines"
   July 8-9, 1970

6. Proceedings of Meeting No. 13 ..... AD 724 637
   "Standards as a Design Tool in Surface Specification for Mechanical Components and Structures"
   October 19-20, 1970

7. Proceedings of Meeting No. 14 ..... AD 721 355
   "Advances in Decision-Making Processes in Detection, Diagnosis and Prognosis"
   January 25-26, 1971

8. Proceedings of Meeting No. 15 ..... AD 725 200
"Failure Mechanisms: Corrosion"
April 14-15, 1971

9. Proceedings of Meeting No. 16 ..... AD 738 855
"Mechanical Failure Prevention through Lubricating Oil Analysis"
November 2-4, 1971

10. Proceedings of Meeting No. 17 ..... AD 750 411
"Effects of Environment upon Mechanical Failures, Mechanisms and Detection"
April 25-27, 1972

11. Proceedings of Meeting No. 18 ..... AD 772 082
"Detection, Diagnosis and Prognosis"
November 8-10, 1972

12. Proceedings of Meeting No. 19 (NBS SP 394)..... COM-74-50523
"The Role of Cavitation in Mechanical Failures"
October 31-November 2, 1973

Printed copies of the following publications may be obtained from the U.S. Government Printing Office.

Superintendent of Documents
U.S. Government Printing Office
Washington, DC 20402

Microfiche copies of these publications may be obtained from the NTIS.

13. Proceedings of Meeting No. 20 (NBS SP 423).... SN003-003-01451-6
"Mechanical Failure - Definition of the Problem"
May 8-10, 1974

14. Proceedings of Meeting No. 21 (NBS SP 433).... SN003-003-01639-0
"Success by Design: Progress through Failure Analysis"
November 7-8, 1974

15. Proceedings of Meeting No. 22 (NBS SP 436).... SN003-003-01556-3
"Detection, Diagnosis and Prognosis"
April 23-25, 1975

16. Proceedings of Meeting No. 23 (NBS SP 452).... SN003-003-01664-1
"The Role of Coatings in the Prevention of Mechanical Failures"
October 29-31, 1975

17. Proceedings of Meeting No. 24 (NBS SP 468).... SN003-003-01760-4
"Prevention of Failures in Coal Conversion Systems"
April 21-24, 1976

18. Proceedings of Meeting No. 25 (NBS SP 487) SN003-003-01829-5
"Engineering Design"
November 3-5, 1976

19. Proceedings of Meeting No. 26 (NBS SP 494) ... SN0003-003-01844-9
"Detection, Diagnosis and Prognosis"
May 17-19, 1977

20. Proceedings of Meeting No. 27 (NBS SP 514) SN003-003-01935-6
"Product Durability and Life"
November 1-3, 1977

21. Proceedings of Meeting No. 28 (NBS SP 547) SN003-003-02083-4
"Detection, Diagnosis and Prognosis"
November 28-30, 1978

22. Proceedings of Meeting No. 29 (NBS SP 563) SN003-003-02120-2
"Advanced Composites"
May 23-25, 1979

23. Proceedings of Meeting No. 30 (NBS SP 584) SN003-003-02272-1
"Joint Conference on Measurements and
Standards for Recycled Oil/Systems
Performance and Durability"
October 23-26, 1979

24. Proceedings of Meeting No. 31 (NBS SP 621) SN003-003-02428-7
"Failure Prevention in Ground
Transportation Systems"
April 22-24, 1980

25. Proceedings of Meeting No. 32 (NBS SP 622) SN003-003-02361-2
"Detection, Diagnosis and Prognosis:
Contribution to the Energy Challenge"
October 7-9, 1980

26. Proceedings of Meeting No. 33 (NBS SP 640) SN003-003-02425-2
"Innovation for Maintenance
Technology Improvements"
April 21-23, 1981

27. Proceedings of Meeting No. 34 (NBS SP 652) SN003-003-02488-1
"Damage Prevention in the
Transportation Environment"
October 21-23, 1981

Printed copies of the following MFPG publications are available from Cambridge University Press, 110 Midland Ave., Port Chester, NY 10573

28. Proceedings of Meeting No. 35
"Time Dependent Failure Mechanisms
and Assessment Methodologies"
April 20-22, 1982

29. Proceedings of Meeting No. 36
"Technology Advances in Engineering and Their Impact on Detection, Diagnosis and Prognosis Methods"
December 6-10, 1982

30. Proceedings of Meeting No. 37
"Mechanical Properties, Performance and Failure Modes of Coatings"
May 10-12, 1983

Note: The proceedings of meeting no. 38 were not published because of the format of the meeting.

31. Proceedings of Meeting No. 39
"Failure Mechanisms in High Performance Materials"
May 1-3. 1984

32. Proceedings of Meeting No. 40
"Use of New Technology to Improve Mechanical Readiness, Reliability and Maintainability"
April 16-18, 1985

33. Proceedings of Meeting No. 41
"Detection, Diagnosis and Prognosis of Rotating Machinery to Improve Reliability, Maintainability, and Readiness through the Application of New and Innovative Techniques"
October 28-30, 1986

The proceedings of meeting nos. 42 and 43 are in press.

34. Proceedings of Meeting No. 42
"Technology Innovation - Key to international Competitiveness"
September 15-17, 1987

35. Proceedings of Meeting No. 43
"Advanced Technology in Failure Prevention"
October 3-6, 1988

Printed copies of the following MFPG publications are available from The Vibration Institute, 6262 S. Kingery Highway, Suite 212, Willowbrook, IL 60514

36. Proceedings of Meeting No. 44
"Current Practices and Trends in Mechanical Failure Prevention"
April 3-5, 1990

SECURITY CLASSIFICATION OF THIS PAGE

REPORT DOCUMENTATION PAGE

1a REPORT SECURITY CLASSIFICATION Unclassified	1b RESTRICTIVE MARKINGS None
2a SECURITY CLASSIFICATION AUTHORITY	3 DISTRIBUTION/AVAILABILITY OF REPORT Unclassified/Unlimited
2b DECLASSIFICATION/DOWNGRADING SCHEDULE	
4 PERFORMING ORGANIZATION REPORT NUMBER(S) MFPG-45	5 MONITORING ORGANIZATION REPORT NUMBER(S)
6a NAME OF PERFORMING ORGANIZATION Vibration Institute 6b OFFICE SYMBOL (If applicable)	7a NAME OF MONITORING ORGANIZATION Office of Naval Research
6c ADDRESS (City, State, and ZIP Code) 6262 S. Kingery Hwy. Willowbrook, IL 60514	7b ADDRESS (City, State, and ZIP Code) Arlington, VA 22217-5000
8a NAME OF FUNDING/SPONSORING ORGANIZATION Office of Naval Research 8b OFFICE SYMBOL (If applicable)	9 PROCUREMENT INSTRUMENT IDENTIFICATION NUMBER
8c ADDRESS (City, State, and ZIP Code) Arlington, VA 22217-5000	10 SOURCE OF FUNDING NUMBERS PROGRAM ELEMENT NO. / PROJECT NO. / TASK NO / WORK UNIT ACCESSION NO.

11 TITLE (Include Security Classification)
Focus on Mechanical Failures: Mechanisms and Detection

12 PERSONAL AUTHOR(S)
Compiled by Henry C. Pusey and Sallie C. Pusey

13a TYPE OF REPORT	13b TIME COVERED	14 DATE OF REPORT (Year, Month, Day)	15 PAGE COUNT
	FROM 91/1/1 TO 91/4/9	91/4/9	362

16 SUPPLEMENTARY NOTATION

17 COSATI CODES			18 SUBJECT TERMS (Continue on reverse if necessary and identify by block number)
FIELD	GROUP	SUB-GROUP	Rotating equipment, reciprocating machinery, motors, detection diagnosis, prognosis, failure mechanisms, failure analysis, gearbox, durability, materials.

19 ABSTRACT (Continue on reverse if necessary and identify by block number)

This document is the proceedings of the 45th Meeting of the Mechanical Failures Prevention Group (MFPG) which was held at Annapolis, MD on April 9-11, 1991. The proceedings contains featured papers on failure analysis and prevention and condition-based maintenance. Session papers on detection, diagnosis and prognosis; failure mechanisms; expert systems; failures in composites; failures in metals; diagnostics of reciprocating machinery; valve diagnostics; and case histories of systems failure analyses.

20 DISTRIBUTION/AVAILABILITY OF ABSTRACT	21 ABSTRACT SECURITY CLASSIFICATION
☒ UNCLASSIFIED/UNLIMITED ☐ SAME AS RPT ☐ DTIC USERS	
22a NAME OF RESPONSIBLE INDIVIDUAL Peter Schmidt	22b TELEPHONE (Include Area Code) (202) 696-4410 / 22c OFFICE SYMBOL

DD FORM 1473, 84 MAR 83 APR edition may be used until exhausted
All other editions are obsolete

SECURITY CLASSIFICATION OF THIS PAGE

GPO U.S. Government Printing Office